A SEDIMENTOLOGICAL AND MICROPALEONTOLOGICAL STUDY OF QUATERNARY SECTIONS OF CORES FROM THE NEW ZEALAND SECTOR OF THE SOUTHERN OCEAN

A thesis submitted in partial fulfilment
of the requirements for the
Degree of
Master of Science (Technology)
in
Earth Sciences
at the
University of Waikato

by

Jon Mackie

UNIVERSITY OF WAIKATO

1998

Abstract

The Southern Ocean lies between the Subtropical Front (STF) at about 45°S latitude and the continental landmass of Antarctica. It plays an important role in global climatic and oceanic circulation patterns, and is responsible for production of most water characteristics below the thermocline. The New Zealand sector of the Southern Ocean (NZSSO) is situated in a unique position to study past changes in oceanic circulation and climate from the record preserved in deep-sea sediment cores. Using piston cores collected from water depths of 461-5100 m by *USNS Eltanin* during 1968-1972, a sedimentological, micropaleontological, and stable oxygen and carbon isotope study, including some radiocarbon dating, has been conducted on the upper 1 m of sediment in 12 cores spanning a latitudinal transect from 52°S to 61°S south of New Zealand. The transect crosses the modern position of the Subantarctic Front (SAF) at ~56°S and extends as far as the Antarctic Polar Front (AAPF) at ~63°S.

The study has shown the NZSSO cores must be viewed as two subgroups. The cores are divided at the SAF into a northern subgroup (north of the SAF) and a southern subgroup (south of the SAF) on the basis of sedimentary lithologies, textures, composition and depositional histories. The northern cores are located in the vicinity of the southern margin of Campbell Plateau and are all highly calcareous (~95%), being composed of planktic and benthic foraminifera and nannofossils with minimal terrigenous material content. The northern cores include two textural facies controlled by the dominant biogenic sediment. Facies A, a muddy sand, is dominated by the Subantarctic foraminiferal assemblage of *Globigerina bulloides, Neogloboquadrina pachyderma* (sinstral and dextral), *Globigerinita* spp., *Globorotalia inflata* and *Globorotalia truncatulinoides.* Facies B, a sandy mud, is dominated by calcareous nannofossils, especially *Emiliania huxley, Coccolithus* spp., and *Calcidiscus* spp.

The southern subgroup of cores lies in the Southwest Pacific Basin and are dominated by biogenic siliceous material and common (11-27%) terrigenous material. They belong to Facies C, a sandy silt, composed mainly of silt-sized frustules of diatoms and nassellaria radiolaria and terrigenous material (quartz, plagioclase feldspars, biotite and muscovite). Where calcareous material exists south of the SAF it is composed of an Antarctic foraminiferal assemblage involving *Neogloboquadrina pachyderma* (sinstral), *Globigerina bulloides* and *Globorotalia inflata.* All foraminifera of the Antarctic assemblage show evidence of dissolution. The northern subgroup of cores lies in an average water depth of 1200 m, while south of the SAF the average water depth of the cores is 4700 m. The lysocline for the NZSSO is determined at ~3200-4100 m, with a carbonate compensation depth (CCD) of 4800 m. Any calcareous material south of the

SAF is actively being affected by dissolution which biases the sedimentary record of the southern subgroup of cores to dissolution resistant organisms (diatoms and radiolaria) and terrigenous material.

The stable isotope records for the northern NZSSO cores show only a 0.8‰ shift between inferred glacial and interglacial conditions. Smoothing of the record may be due to bioturbation and/or to extensive sediment reworking by bottom currents, forming rather condensed sedimentary records, especially during glacial periods. Oxygen isotope stages back to stage 5 have been suggested in one core (36-42); this places the Last Glacial - Holocene transition at ~7 cm, stage 2/3 boundary at ~21 cm, stage 3/4 boundary at ~65 cm, and a possible stage 4/5 boundary at ~95 cm downcore. The position of the Last Glacial and stage 2/3 boundary are confirmed by radiometric dates obtained from the same northern core: 19,120 +/- 110 yrs BP at 10 cm downcore and 23,900 yrs +/- 200 yrs BP at 20 cm downcore. Faunal changes in the benthic foraminifera occur near the glacial-interglacial transitions from *Globocassidulina subglobosa*-dominated during glacial periods to common *Epistominella exigua* during interglacials. Textural facies also show changes near these transitions, with Facies A characterising glacial periods and Facies B during interglacial periods. Associated with changes in texture are colour changes which allow the correlation of the glacial-interglacial transitions across many of the northern cores. The Last Glacial situation cannot be determined uniquely for the southern subgroup of cores as they have, to varying degrees, experienced extensive erosion and reworking during the Late Quaternary or earlier.

Collectively, the data suggest there has not been significant change in oceanic paleoenvironmental conditions north of the SAF, immediately south of New Zealand, between glacial and interglacial periods. This could be because the topographic high marking the southern edge of the Campbell Plateau has essentially fixed the SAF, irrespective of oceanic climatic conditions. The topographic lock would be further enhanced by sea level drops of ~120 m during glacial periods. In contrast, east and west of New Zealand in open water conditions evidence from other studies indicates major northward shifts in the position of both the SAF and the AAPF. The limited variation downcore in the abundances of sinistrally coiled *Neogloboquadrina pachyderma,* the small shifts in the stable oxygen isotope record, and the lack of change in faunal assemblages together suggest that ranges in the sea surface temperature change between glacial and interglacial periods at higher latitudes were probably not so severe as at intermediate latitudes. Due to the relatively small temperature changes between glacial and interglacial conditions at higher latitudes the faunal and isotopic indicators may only record extreme events.

Acknowledgements

I would sincerely like to thank the following for the support and encouragement that I received during this study.

My appreciation goes out to my supervisor, Professor Cam Nelson, for proposing this study, and for his continued ideas, advice, guidance and tolerance. Special thanks for arranging a cruise with New Zealand Oceanographic Institute; it added spice to the duller moments of microscope work!

I would also like to extend my grateful thanks to Dr Lionel Carter at the New Zealand Oceanographic Institute (NZOI) for his helpful comments in the course of this study, and especially for allowing me to participate on NZOI research cruise 3034, and to gain first hand invaluable knowledge about marine geoscience research at sea.

Thanks go to Helen Neil (now NZOI; formerly University of Waikato) for much of the initial preparation of samples and for discussions about results along the way. Penny Cooke (University of Waikato) assisted greatly with general day-to-day questions about equipment, procedures and identification of foraminiferal specimens. Also Martin Crundwell (University of Waikato) assisted with identification of the benthic foraminifera. Steve Cooke (University of Waikato) kept the mass spectrometer going and helped with queries about the raw isotopic data. Barry O'Conner (University of Auckland) is thanked for help with the identification of the radiolaria. Thanks also to Alf Harris (MIRINZ, Ruakura) for assistance with SEM work, Renat Radosinsky (University of Waikato) for assistance with XRD analysis, and the other technicians of the Department of Earth Sciences, University of Waikato, for general help.

To the scientists and crew whom I accompanied aboard the *R.V. Tangaroa*, on research cruise 3034, thank you for making my first voyage to sea a stimulating and enjoyable one.

To my family, without whose support I would not have made it this far, a big thanks. Time to start doing!

Abstract

The Southern Ocean lies between the Subtropical Front (STF) at about 45°S latitude and the continental landmass of Antarctica. It plays an important role in global climatic and oceanic circulation patterns, and is responsible for production of most water characteristics below the thermocline. The New Zealand sector of the Southern Ocean (NZSSO) is situated in a unique position to study past changes in oceanic circulation and climate from the record preserved in deep-sea sediment cores. Using piston cores collected from water depths of 461-5100 m by *USNS Eltanin* during 1968-1972, a sedimentological, micropaleontological, and stable oxygen and carbon isotope study, including some radiocarbon dating, has been conducted on the upper 1 m of sediment in 12 cores spanning a latitudinal transect from 52°S to 61°S south of New Zealand. The transect crosses the modern position of the Subantarctic Front (SAF) at ~56°S and extends as far as the Antarctic Polar Front (AAPF) at ~63°S.

The study has shown the NZSSO cores must be viewed as two subgroups. The cores are divided at the SAF into a northern subgroup (north of the SAF) and a southern subgroup (south of the SAF) on the basis of sedimentary lithologies, textures, composition and depositional histories. The northern cores are located in the vicinity of the southern margin of Campbell Plateau and are all highly calcareous (~95%), being composed of planktic and benthic foraminifera and nannofossils with minimal terrigenous material content. The northern cores include two textural facies controlled by the dominant biogenic sediment. Facies A, a muddy sand, is dominated by the Subantarctic foraminiferal assemblage of *Globigerina bulloides, Neogloboquadrina pachyderma* (sinstral and dextral), *Globigerinita* spp., *Globorotalia inflata* and *Globorotalia truncatulinoides.* Facies B, a sandy mud, is dominated by calcareous nannofossils, especially *Emiliania huxley, Coccolithus* spp., and *Calcidiscus* spp.

The southern subgroup of cores lies in the Southwest Pacific Basin and are dominated by biogenic siliceous material and common (11-27%) terrigenous material. They belong to Facies C, a sandy silt, composed mainly of silt-sized frustules of diatoms and nassellaria radiolaria and terrigenous material (quartz, plagioclase feldspars, biotite and muscovite). Where calcareous material exists south of the SAF it is composed of an Antarctic foraminiferal assemblage involving *Neogloboquadrina pachyderma* (sinstral), *Globigerina bulloides* and *Globorotalia inflata.* All foraminifera of the Antarctic assemblage show evidence of dissolution. The northern subgroup of cores lies in an average water depth of 1200 m, while south of the SAF the average water depth of the cores is 4700 m. The lysocline for the NZSSO is determined at ~3200-4100 m, with a carbonate compensation depth (CCD) of 4800 m. Any calcareous material south of the

SAF is actively being affected by dissolution which biases the sedimentary record of the southern subgroup of cores to dissolution resistant organisms (diatoms and radiolaria) and terrigenous material.

The stable isotope records for the northern NZSSO cores show only a 0.8‰ shift between inferred glacial and interglacial conditions. Smoothing of the record may be due to bioturbation and/or to extensive sediment reworking by bottom currents, forming rather condensed sedimentary records, especially during glacial periods. Oxygen isotope stages back to stage 5 have been suggested in one core (36-42); this places the Last Glacial - Holocene transition at ~7 cm, stage 2/3 boundary at ~21 cm, stage 3/4 boundary at ~65 cm, and a possible stage 4/5 boundary at ~95 cm downcore. The position of the Last Glacial and stage 2/3 boundary are confirmed by radiometric dates obtained from the same northern core: 19,120 +/- 110 yrs BP at 10 cm downcore and 23,900 yrs +/- 200 yrs BP at 20 cm downcore. Faunal changes in the benthic foraminifera occur near the glacial-interglacial transitions from *Globocassidulina subglobosa*-dominated during glacial periods to common *Epistominella exigua* during interglacials. Textural facies also show changes near these transitions, with Facies A characterising glacial periods and Facies B during interglacial periods. Associated with changes in texture are colour changes which allow the correlation of the glacial-interglacial transitions across many of the northern cores. The Last Glacial situation cannot be determined uniquely for the southern subgroup of cores as they have, to varying degrees, experienced extensive erosion and reworking during the Late Quaternary or earlier.

Collectively, the data suggest there has not been significant change in oceanic paleoenvironmental conditions north of the SAF, immediately south of New Zealand, between glacial and interglacial periods. This could be because the topographic high marking the southern edge of the Campbell Plateau has essentially fixed the SAF, irrespective of oceanic climatic conditions. The topographic lock would be further enhanced by sea level drops of ~120 m during glacial periods. In contrast, east and west of New Zealand in open water conditions evidence from other studies indicates major northward shifts in the position of both the SAF and the AAPF. The limited variation downcore in the abundances of sinistrally coiled *Neogloboquadrina pachyderma,* the small shifts in the stable oxygen isotope record, and the lack of change in faunal assemblages together suggest that ranges in the sea surface temperature change between glacial and interglacial periods at higher latitudes were probably not so severe as at intermediate latitudes. Due to the relatively small temperature changes between glacial and interglacial conditions at higher latitudes the faunal and isotopic indicators may only record extreme events.

Acknowledgements

I would sincerely like to thank the following for the support and encouragement that I received during this study.

My appreciation goes out to my supervisor, Professor Cam Nelson, for proposing this study, and for his continued ideas, advice, guidance and tolerance. Special thanks for arranging a cruise with New Zealand Oceanographic Institute; it added spice to the duller moments of microscope work!

I would also like to extend my grateful thanks to Dr Lionel Carter at the New Zealand Oceanographic Institute (NZOI) for his helpful comments in the course of this study, and especially for allowing me to participate on NZOI research cruise 3034, and to gain first hand invaluable knowledge about marine geoscience research at sea.

Thanks go to Helen Neil (now NZOI; formerly University of Waikato) for much of the initial preparation of samples and for discussions about results along the way. Penny Cooke (University of Waikato) assisted greatly with general day-to-day questions about equipment, procedures and identification of foraminiferal specimens. Also Martin Crundwell (University of Waikato) assisted with identification of the benthic foraminifera. Steve Cooke (University of Waikato) kept the mass spectrometer going and helped with queries about the raw isotopic data. Barry O'Conner (University of Auckland) is thanked for help with the identification of the radiolaria. Thanks also to Alf Harris (MIRINZ, Ruakura) for assistance with SEM work, Renat Radosinsky (University of Waikato) for assistance with XRD analysis, and the other technicians of the Department of Earth Sciences, University of Waikato, for general help.

To the scientists and crew whom I accompanied aboard the *R.V. Tangaroa*, on research cruise 3034, thank you for making my first voyage to sea a stimulating and enjoyable one.

To my family, without whose support I would not have made it this far, a big thanks. Time to start doing!

Table of Contents

List of Figures

List of Tables

List of Plates

Chapter One:

Southern Ocean and Environmental Setting

Chapter One: Table of Contents

1.1 Southern Ocean

The Southern Ocean (Fig. 1.1A) lies between about 45°S latitude, the approximate position of the modern Subtropical Convergence Zone, and the continental landmass of Antarctica (Gordon, 1975a, 1977; Kennett, 1982). Understanding the history of oceanic processes within the Southern Ocean is dominantly achieved through the study of deep-sea cores, which register variations in sedimentary, microfossil and geochemical signals. These changes in signal monitor changes in climate, and in oceanographic and environmental properties of the Southern Ocean (Hendy, 1995).

In comparison to mid- to high-latitude seas in the northern hemisphere, where coverage of cores is extensive, the Southern Ocean has few cores. The past decade has seen a realisation that the Southern Ocean plays an important role in global ocean circulation and climate change, and notably it receives signals from all the world's major oceans. Southern Ocean processes are responsible for production of most of the water characteristics below the main thermocline of the world's oceans (Gordon, 1988). Realisation of the importance the Southern Ocean has lead to projects such as the Ocean Drilling Program (ODP) drilling proposal 441, which focuses on the evolution of circum-Antarctic and Southwest Pacific Ocean current systems (Carter *et al.,* 1996a), and past Deep-Sea Drilling Program (DSDP) and ODP research cruises (Table 1.1). Studies by institutions and individual researchers continue to grow alongside these large joint research projects and add to our understanding of the Southern Ocean.

Table 1.1 DSDP and ODP Cruises Within or Adjacent to the Southern Ocean

Cruises	Year	Cruise Sector
DSDP Leg 26	1972	Durban (South Africa) - Fremantle (Australia)
DSDP Leg 28	1972-73	Fremantle (Australia) - Christchurch (New Zealand)
DSDP Leg 29	1973	Lyttleton (New Zealand) - Wellington (New Zealand)
DSDP Leg 35	1974	Callao (Peru) - Ushuaia (Argentina)
DSDP Leg 90	1983	Noumea (New Caledonia) - Wellington (New Zealand)
ODP Leg 113	1986-87	Weddell Sea (Antarctica)
ODP Leg 114	1987	Sub-Antarctic; South Atlantic
ODP Leg 119	1987-88	Kerguelen Plateau and Prydz Bay
ODP Leg 120	1988	Kerguelen Plateau

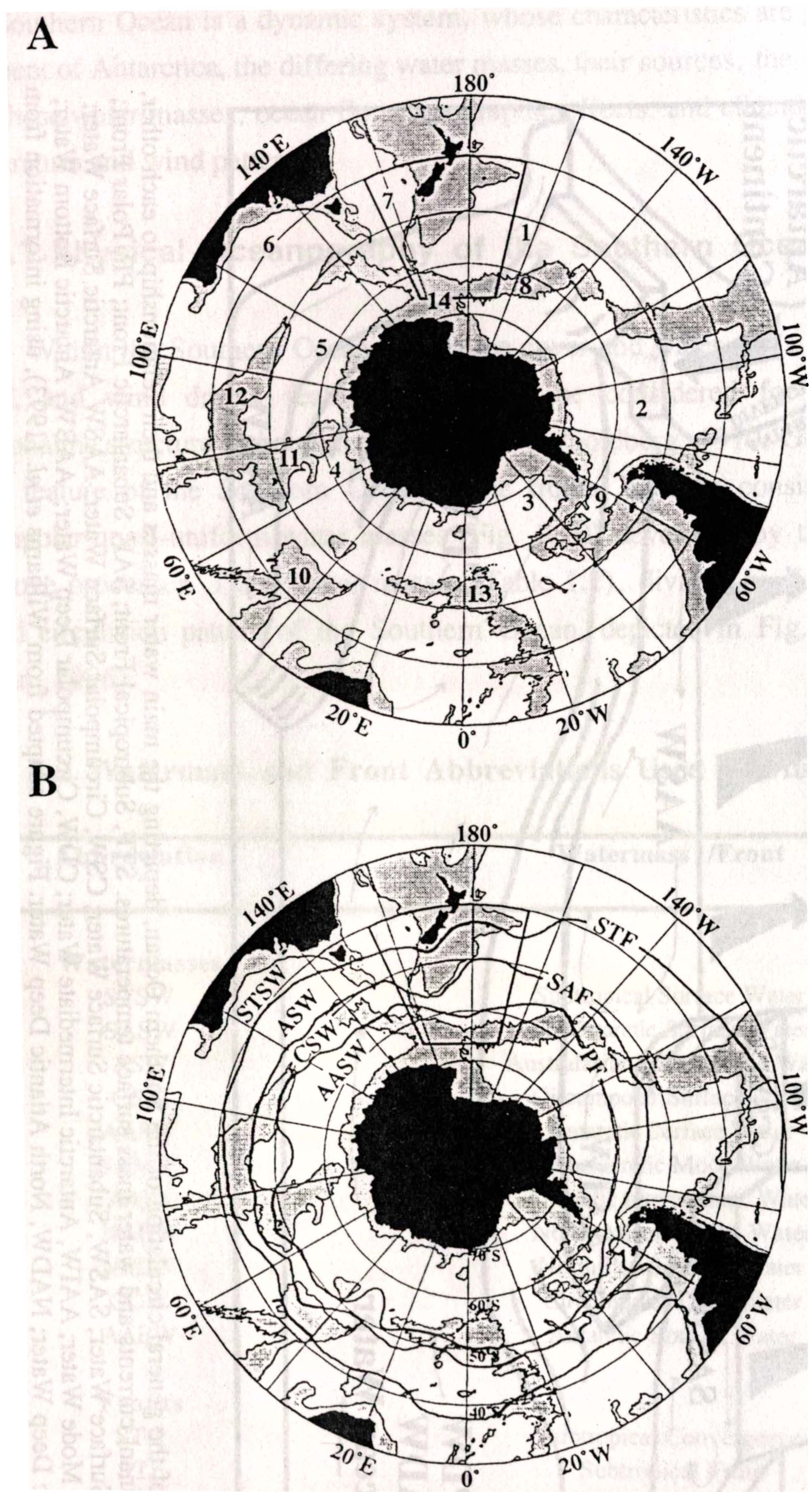

Fig. 1.1 (A) Simplified bathymetry of the Southern Ocean, shaded areas are above 3500 m water depth. The numbers refer to Table 1.3. #14 is the Balleny Plateau. (B) Dominant fronts of the Southern Ocean and the intervening surface water masses. STF, Subtropical Front; SAF, Subantarctic Front; AAPF Antarctic Polar Front; STSW, Subtropical Surface Water; ASW, Australasian Subantarctic Water; CSW, Circumpolar Surface Water; AASW, Antarctic Surface Water. Figure adapted from Orsi *et al.* (1995), using information from Gordon *et.al.* (1978) and Belkin & Gordon (1996).

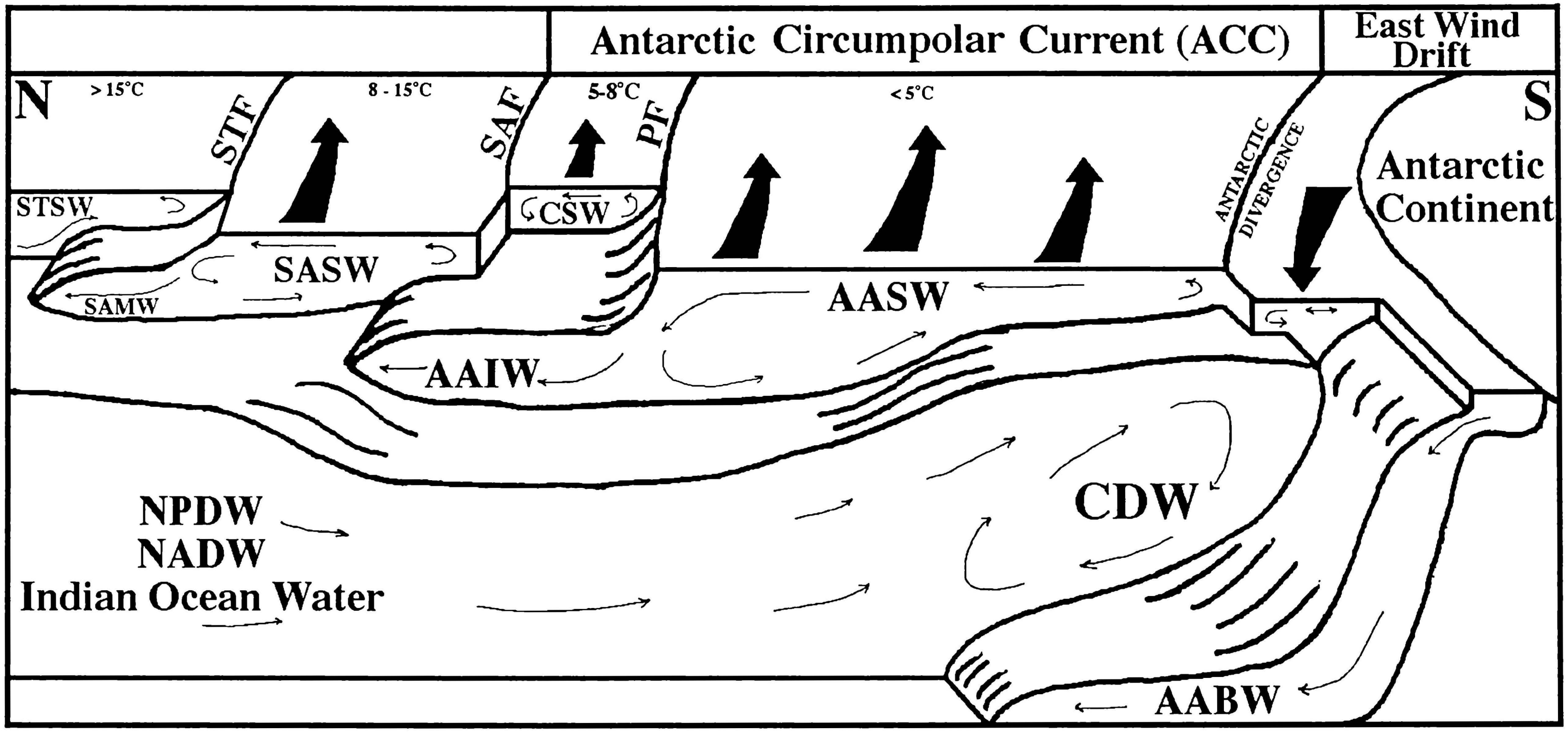

Fig. 1.2 Schematic diagram of the general circulation of the Southern Ocean, depicting the main water masses and their relationship to each other, flow directions, dominant currents and water mass surface temperatures. STF, Subtropical Front; SAF, Subantarctic Front; PF, Polar Front; STSW, Subtropical Surface Water; SASW, Subantarctic Surface Water; CSW, Circumpolar Surface Water; AASW Antarctic Surface Water; SAMW, Subantarctic Mode Water; AAIW, Antarctic Intermediate Water; CDW, Circumpolar Deep Water; AABW, Antarctic Bottom Water; NPDW, North Pacific Deep Water; NADW, North Atlantic Deep Water. Figure adapted from Williams *et al.* (1993), using information from Gordon (1988) and Heath (1981).

The Southern Ocean is a dynamic system, whose characteristics are governed by the continent of Antarctica, the differing water masses, their sources, the fronts associated with these water masses, ocean floor topographic effects, and climatic effects such as temperature and wind patterns.

1.1.1 Physical Oceanography of the Southern Ocean

Within the Southern Ocean the sea-ice cover and water mass modification are linked, and wind driven features must also be considered for their effect on thermohaline structure and circulation (Gordon & Goldberg, 1970; Gordon, 1988). A major feature of the Southern Ocean is the frontal banding consisting of several circumpolar quasi-uniform water masses (Fig. 1.1B) developed by the interaction of the above processes. These water masses (Table 1.2), divided by fronts, set up the general circulation pattern of the Southern Ocean, depicted in Fig. 1.2 (Belkin & Gordon, 1996).

Table 1.2 Watermass and Front Abbreviations Used in Study

Abbreviation	Watermass /Front
Watermasses	
STSW	Subtropical Surface Water
SASW	Subantarctic Surface Water
ASW	Australasian Subantarctic Water
CSW	Circumpolar Surface water
AASW	Antarctic Surface Water
SAMW	Subantarctic Mode Water
AAIW	Antarctic Intermediate Water
NADW	North Atlantic Deep Water
NPDW	North Pacific Deep Water
CDW	Circumpolar Deep Water
AABW	Antarctic Bottom Water
Fronts	
STC	Subtropical Convergence
STF	Subtropical Front
SAF	Subantarctic Front
AAC	Antarctic Convergence
AAPF	Antarctic Polar Front
Currents	
ACC	Antarctic Circumpolar Current

Warm, highly saline, low oxygenated North Pacific Deep Water (NPDW) and North Atlantic Deep Water (NADW) have a component of flow towards the south, which becomes integrated into the Circumpolar Deep Water (CDW). The CDW upwells into the near-surface to form two different water masses that are cold and have a high dissolved oxygen content (Gordon & Goldberg, 1970). One remains at the surface, known as Antarctic Surface Water (AASW); the second water mass sinks to form Antarctic Bottom Water (AABW). The predominant sites of AABW formation are in the Weddell Sea and Ross Sea. It's formation is associated with the production of sea-ice, or the interaction of water with the bottom of floating ice shelves along the continental margins of Antarctica (Gordon & Goldberg, 1970).

The AASW extends with uniform properties from the Antarctic Polar Front (AAPF) to the continental margins of Antarctica. Close to the continental margins of Antarctica the AASW is split by a semi-continuous frontal band around Antarctica, known as the Antarctic Divergence. The Antarctic Divergence is the shearing zone between the eastward flowing Antarctic Circumpolar Current (ACC) and the westward flowing Eastwind Drift (Fig. 1.2) (Gordon & Goldberg, 1970; Orsi *et al.,* 1995).

To the north the AASW ends abruptly at the Antarctic Convergence, or AAPF, at latitudes between 50°S and 62°S, where it sinks below less dense Circumpolar Surface Water (CSW), and contributes to the formation of the Antarctic Intermediate Water (AAIW), which flows northward (Gordon & Goldberg, 1970). The CSW is bounded to the north by the Subantarctic Front (SAF), which separates CSW from the Subantarctic Surface Water (SASW), which in turn is bounded by the Subtropical Convergence (STC) or Subtropical Front (STF) (Belkin & Gordon, 1996). SASW sinks below the warmer less dense Subtropical Surface Water which lies to the north of the STF to form a subsurface tongue of Subantarctic Mode Water (SAMW) (Fig. 1.2). SAMW occurs as a thick subsurface (c. 300-700 m) layer of nearly isothermal water (McCartney, 1977; Heath, 1985).

The northward flow of the AASW, the associated AAIW, and the AABW (Fig. 1.2) is compensated for by southward flowing CDW. The CDW also contains quantities of relatively highly saline NADW, which enters the circumpolar flow in the southern Atlantic, and NPDW, which enters the CDW in the Southwest Pacific. Both NADW and NPDW are completely integrated into the CDW on flowing eastwards, due to the Antarctic Circumpolar Current (ACC) (Gordon & Goldberg, 1970).

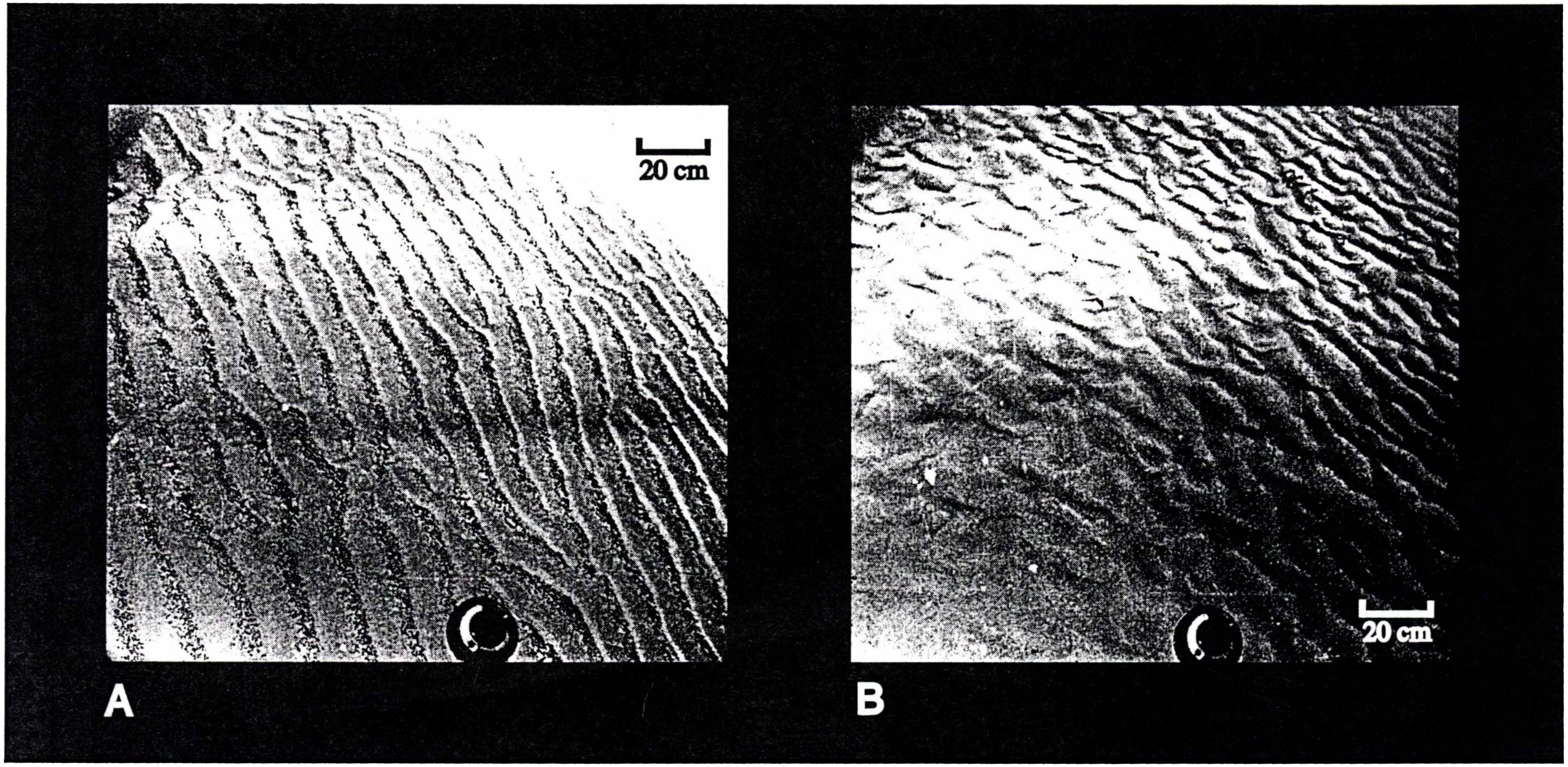

Plate 1.1 *USNS Eltanin* Cruise 36, ship station 50, camera station 42, water depth 2955. Both (A) and (B) show evidence of rippled bedforms that would require current velocities of at least 15-20 cm/sec. (A) shows concentrations of ferruginous material in the lee of the ripples. These photographs were taken on the southern margin of the Campbell Plateau, lying near the the cores in this study from north of the modern SAF. Source Jacobs *et al.*, 1970.

1.1.2 Antarctic Circumpolar Current

The ACC is a current which is superimposed on the above circulation, affecting all major water masses within its boundaries, which are to the north the SAF and to the south the Antarctic Divergence. The current has a surface velocity of generally less than 25 cm/sec, transporting between 233-240 x 10^6 m^3/sec (Gordon, 1971). Within Drake Passage surface currents in excess of 75 cm/sec are common, with bottom currents calculated in excess of 10 cm/sec transporting a volume of 218 x 10^6 m^3/sec (Goodell *et al.*, 1973). Photographic evidence (Plate 1.1) of megaripples in sand-sized sediments across the Pacific-Antarctic Ridge, and even at depth across the Southeast Pacific Basin and through Drake Passage, attest to bottom currents approaching 50 cm/sec (Goodell *et al.*, 1973).

The strong westerly wind field situated over 45°-55°S is predominantly responsible for circumpolar circulation (large amounts of momentum are transferred to the Southern Ocean by the westerly winds), with the maximum westerlies situated in close proximity to the ACC (Fig. 1.1B) (Kennett, 1982; Morrow *et al.,* 1992; McGlone *et al.,* 1994). The wind field produces Ekman divergence (upwelling) south of the ACC, while north of the ACC sinking (Ekman convergence) is associated with the formation of AAIW (Gordon, 1988). The ACC has a significant northward flow component in surface and bottom waters, and a southward component in intermediate water bodies; the northward movement of the surface water is due to Coriolis effect, the wind stress forming Ekman spirals and the higher density Antarctic water moving into less dense northern waters (Kennett, 1982).

Due to the distribution of land masses (Fig. 1.1A) the ACC is a unique link that connects all major oceans, and whose path is firmly controlled by major bottom ridges (Gordon *et al.,* 1978; Gordon, 1988; Orsi *et al.,* 1995). The SAF marks the northern boundary, while the southern boundary is defined by the sharp termination of the poleward extent of the CDW (Fig. 1.2). These boundaries are characterised by large horizontal shear, forming cyclonic circulation gyres on the northern and southern margins of the ACC (Orsi *et al.,* 1995). The energetic eddies are vertically coherent over a depth range 1000 - 5000 m, have horizontal scales exceeding 60 km, and are important in carrying heat polewards and momentum northwards away from the ACC (Bryden & Heath, 1985; Morrow *et al.,* 1992). South of the ACC, close to the Antarctic continent, the prevailing easterly wind drives the surface waters westwards. This current, the East Wind Drift, does not completely encircle the Antarctic continent as it is constricted at Drake Passage (Kennett, 1982).

1.1.3 Topography of the Southern Ocean

The Southern Ocean is a system of deep abyssal basins divided by high topographic features such as mid-ocean ridges and oceanic plateaus (Fig. 1.1A; Table 1.3) set around the continental landmass of Antarctica (Gordon & Goldberg, 1970; Gordon *et al.*, 1978; Gordon, 1988; Orsi *et al.*, 1995).

Table 1.3 Dominant Topographic Features of the Southern Ocean

Southern Ocean Basins (>3500m)	Dividing Barriers
Southwest Pacific Basin (1)	
Southeast Pacific Basin (2)	Pacific-Antarctic Ridge (8)
Weddell Abyssal Plain (3)	Drake Passage / South Scotia Ridge (9)
Enderby Abyssal Plain (4)	Southwest Indian Ridge (10)
Australian-Antarctic Basin (5)	Kerguelen Plateau (11)
South Australian Basin (6)	Southeast Indian Ridge (12)
Tasman Abyssal Plain (7)	Atlantic Ridge (13)

(Numbers in brackets refer to topographical features on Fig. 1.1A)

Topographic features such as sea mounts, smaller plateaus/ridges and subantarctic islands are numerous. Southern Ocean circulation is channelled via these topographic features into certain paths. Deep cold bottom waters (AABW), due to their density, are restricted to the basins and, as a result of Coriolis forces, these currents dominantly flow along the western side of the basins, often termed Deep Western Boundary Currents (DWBC) (Kennett, 1982).

Major bottom ridges firmly control the path of the ACC. As the ACC flows eastwards it undergoes latitudinal shifts related to bottom topographic effects, with northward migration over a shallowing seafloor and southward shifts over deepening seafloor. Poleward shifts occur across the Southwest Indian Ridge and through the fracture zones in the Pacific-Antarctic Ridge. Constriction of the ACC through Drake Passage greatly intensifies it's flow (Gordon *et al.*, 1978; Orsi *et al.*, 1995). The East Wind Drift current is affected by the large coastal embayments of Antarctic, notably Weddell Sea and Ross Sea, forming large cyclonic gyres (Gordon, 1971). The controlling and amplifying effect that topography has on current flow patterns means that topography is also a contributing factor to sedimentation patterns in the Southern Ocean.

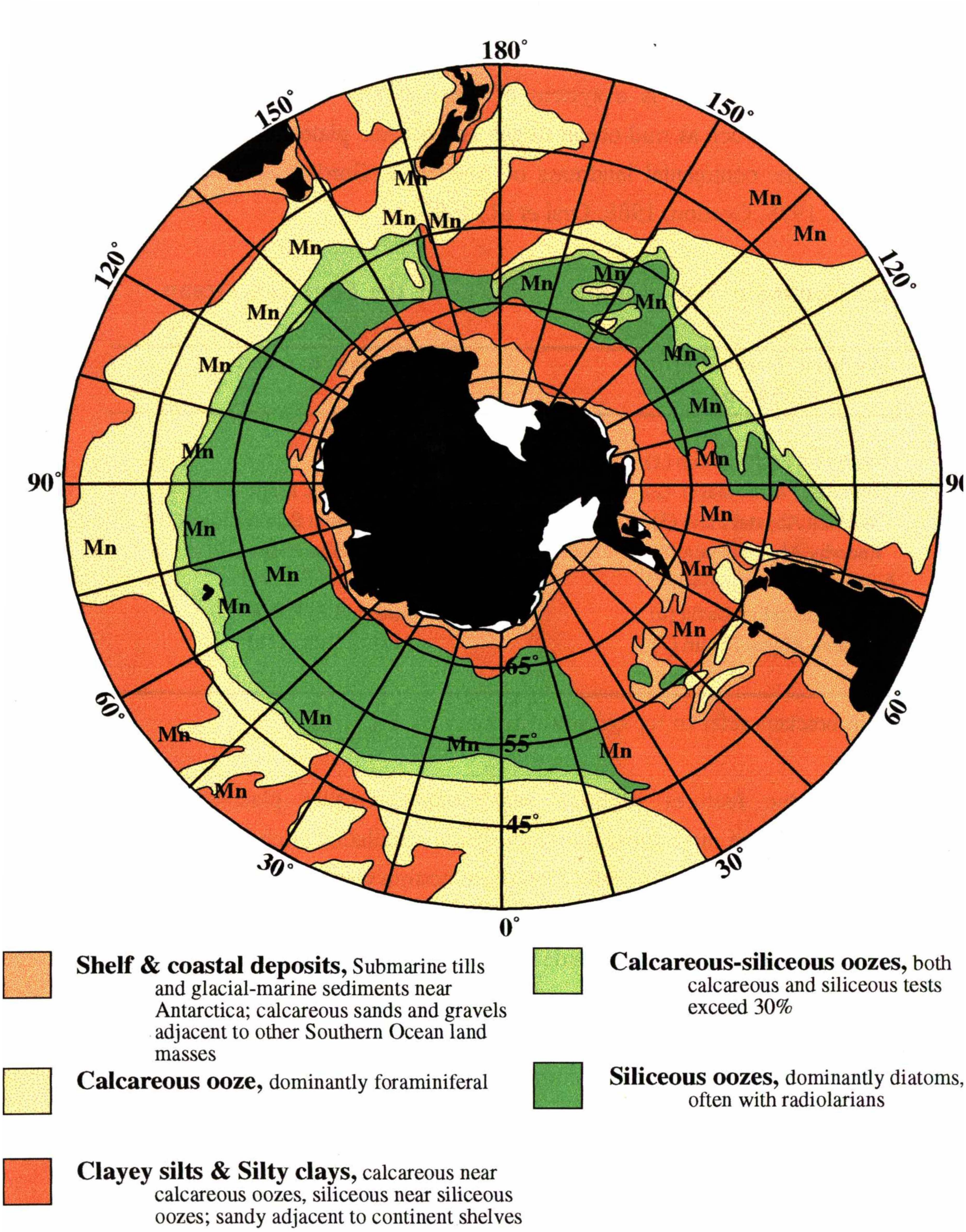

Fig. 1.3 Southern Ocean Sediments. Mn denotes areas where manganese nodule concentrations occur. Adapted from Goodell *et al.* (1973).

1.1.4 Sediments of the Southern Ocean

The broad sedimentation patterns and sediment types follow the zonal climate belts and can be divided into five broad groups (Fig. 1.3). Antarctic coastal sediments consist of undifferentiated deposits of submarine glacial till, gravels, sands and biogenic deposits. They occupy the inner Antarctic continental shelf and have a coarse fraction with abundant pebble/sand granules which are angular, faceted and striated. Clay minerals within the fine fraction are dominated by crystalline chlorite and illite (Goodell *et al.*, 1973). The tills often merge laterally with sands and gravels where winnowing has occurred. Often in regions of little terrigenous input the sediments consist of an interlocking mat of siliceous sponge spicules mixed with whole and fragmented calcareous benthic foraminifera (Lisitzin, 1972; Goodell *et al.*, 1973).

The outer continental shelf (Fig. 1.3), slope and rise region off Antarctica is dominated by Glacial-Marine Sediments. These sediments are classified as having 30% sand with common angular and faceted pebbles. The quartz sands show chatter marks imposed by glaciations (Krinsley & Takahashi, 1962). Clays within the glacial-marine sediments are dominated by crystalline chlorite and illite, with abundant smectites. On the outer shelf, slope and rise beneath the Antarctic Divergence, planktic foraminifera raise the $CaCO_3$ content to 10-20%; northwards, the glacial-marine sediments merge with sandy silts (Goodell *et al.*, 1973).

The glacial-marine deposits are ringed by silts which represent a transition between the coarser glacial-marine deposits and the pelagic clays of the abyssal sea floor (Goodell *et al.*, 1973), reflecting the decrease in ice-rafted terrigenous material away from the continent (although the northern limit of ice-rafted debris lies near the SAF). Within the silts, neither siliceous nor calcareous biogenic components exceed 10%, and clay minerals are dominated by chlorite and illite except in regions of local volcanism where smectite is abundant. These silts dominate the sediments in Drake Passage, West Scotia Sea and Weddell Sea, and form bands across the South Indian Basin and Southeast Pacific Basin; northwards the clayey silts merge with pelagic silty clays (Goodell *et al.*, 1973).

Silty clay sediments contain between 5-10% sand-sized clasts, and both siliceous and calcareous tests are less than 10%. The fine fraction is dominated by crystalline chlorite and illite, with smectite abundant in regions of local volcanism. Zeolites are present in the fine fraction, predominantly clinoptilolite and phillipsite. The silty clays can include occasional ice-rafted debris and ferromanganese nodules. These silty clays form a ribbon in the South Indian Basin, but extend up to 400 km across the Southeast Pacific Basin and are found in the Weddell Sea, Southwest Pacific Basin, Tasman and South Australian Basins (Fig. 1.3). Northwards these silty clays merge with biogenic oozes (Goodell *et al.*, 1973).

Other than glacial-marine deposits, siliceous oozes characterise the sediments of the Southern Ocean and dominate the abyssal depths of the major basins (Fig. 1.3). Siliceous sediments are dominantly composed of opaline frustules of diatoms of silt size, with locally important regions of radiolarian- and dinoflagellate-rich sediments (Lisitzin, 1972; Florida State University, 1973). The fine-grained fraction contains large amounts of terrigenous material, predominantly chlorite and illite with variable amounts of quartz, plagioclase feldspar and amphibole. The zeolites phillipsite and clinoptilolite are present in region of volcanism (Goodell *et al.*, 1973). A sand fraction comprises only about 10% of the ooze and consists of ice-rafted debris, micro-ferromanganese nodules and various biogenic particles (Florida State University, 1973).

The siliceous oozes become progressively more calcareous towards the Antarctic Convergence. The zone where both siliceous and calcareous material comprises greater than 30% of the sediment lies in a 200-300 km-wide belt on the northern margins of the Antarctic abyssal basins, beneath the AAC, across the Kerguelen Plateau and Macquarie Ridge (Goodell *et al.*, 1973). North of this region sediments are dominated by pelagic silty clays or biogenic calcareous oozes. The calcareous biogenic components are dominantly planktic foraminifera (e.g., *Neogloboquadrina* spp., *Globigerina* spp. and *Globorotalia* spp.), with abyssal zones containing a mix of pelagic red silty clays and carbonate ooze (Lisitzin, 1972). Excluding the ice-rafted sediments close to the continent of Antarctic, the sediments within the Southern Ocean are mud-dominated, though sediments range texturally from mud (< 63 μm) to coarse sand (> 150 μm).

Sedimentation rates vary within the Southern Ocean and within individual basins, ranging from 0.2-2.5 cm/ky (Kennett, 1982). Where the ACC interacts with a mid-ocean ridge system, very low sedimentation rates (0.3 cm/ky) are characteristic (Watkins and Kennett, 1971). On the Antarctic continental rise, glacial-marine sediment accumulates at a rate of 2.5 cm/ky (Goodell *et al.*, 1973). In comparison, the Southwest Pacific Basin has depositional rates for pelagic silty clays between 0.2-0.5 cm/ky (Goodell *et al.*, 1973; Schmitz *et al.*, 1986).

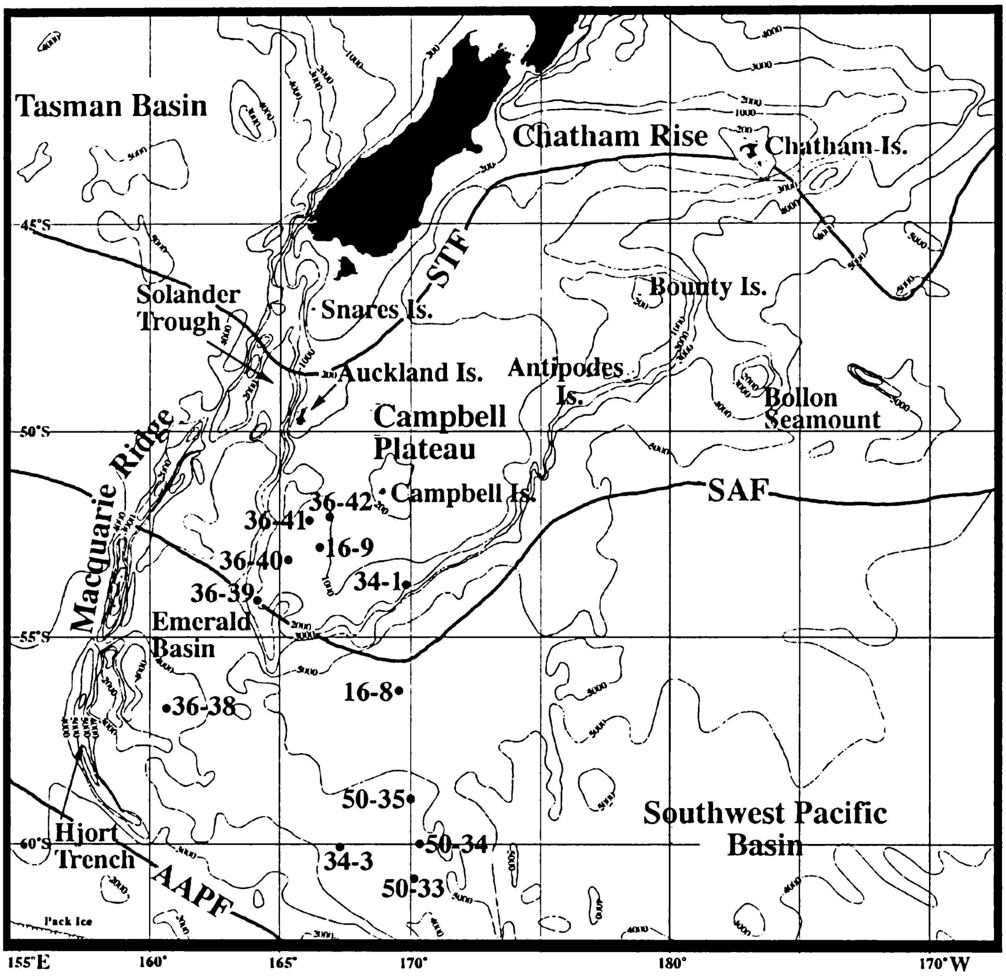

Fig. 1.4 New Zealand sector of the Southern Ocean (NZSSO), showing the main geomorphic features and the location of the NZSSO cores used in this study. Bathymetry in metres. STF, Subtropical Front; SAF, Subantarctic Front and AAPF Antarctic Polar Front. Positions of the oceanic fronts from Gordon (1975b), Heath (1981, 1985) and Belkin & Gordon (1996). Figure adapted from Admiralty Charts (1994).

The major differences to this pattern are related to changes in topographic features and currents. Topographic highs such as mid-ocean ridges and plateaus tend to have carbonate sediments, or a calcareous/siliceous mix, a trend extending south to latitudes of 65°S. At shallower depths calcareous oozes predominate, the topographic highs keeping the carbonate sediments above the Carbonate Compensation Depth (CCD), which lies ~4700 m depth in the Southern Ocean (Lisitzin, 1972). Cold deep water below 4000 m is especially corrosive. These topographic highs often have high current velocities over their surfaces, which reduce sedimentation rates, winnow fine material and produce scour features. Other regions of high current velocity are beneath DWBC, where sediments often show scouring and winnowing, and typically comprise coarse-grained terrigenous material (Ovenshine *et al.*, 1973; Carter & McCave, 1994; Carter & McCave, 1997). In certain regions of the Southern Ocean authigenic minerals are important, in particular manganese nodules (Fig. 1.3). Regions where manganese nodules cover between 75-100% of the seafloor include the central sector of Drake Passage, Southeast Pacific Basin, Southwest Pacific Basin, South Tasman Sea and Pacific-Atlantic Ridge. These regions are all associated with low sedimentation rates and high bottom current velocities beneath the ACC (Glasby, 1976). Manganese nodules require these conditions to prevent the accreting nodules from being smothered, while local submarine volcanism is probably also important, allowing oxides of iron, manganese, and other elements to be incorporated into sediments (Goodell *et al.*, 1973; Watkins & Kennett, 1977).

1.2 New Zealand Sector of Southern Ocean

The New Zealand sector of the Southern Ocean (abbreviated hereafter as NZSSO), sometimes loosely included in the name Southwest Pacific, is very important to the Southern Ocean and the Earth as a whole. For this study the New Zealand sector is defined as that part of the Southern Ocean which lies between longitudes 165° W and 155° E, with the STF used as the northern limit (Fig. 1.4). The New Zealand sector is important because the New Zealand continental landmass deflects the ACC southwards, and the region makes a major contribution to global climates by transportation of heat through the various surface and subsurface water masses (Gordon, 1972).

Circulation of cold deep water is one of the controlling factors of the Earth's climate. With 40% of cold deep water entering the world's ocean through the Southwest Pacific as a Deep Western Boundary Current (DWBC) which is linked with the ACC, the Southwest Pacific is the largest single contributor of cold deep ocean water (Carter *et al.*, 1996a). The DWBC is the largest boundary flow (20 Sv) in the world's oceans, transporting significant amounts of heat and nutrients into the Pacific Ocean Basin (Warren, 1981). Another important feature is that the New Zealand continental landmass is one of the globes prominent sediment sources, accounting for about 2% of the annual suspended fluvial input into the oceans and about 9% of the annual input into South Pacific (Carter & McCave, 1997).

1.2.1 Topographic Features of the New Zealand Sector

The NZSSO is a region where there is a constriction and deflection of the ACC, due primarily to the system of ridges within the region. The Tasman Abyssal Basin is separated from the Emerald Basin and Southwest Pacific Basin by the Macquarie Ridge which extends to approximately 58°S (Fig. 1.4) (Summerhayes, 1969). Oblique collision of Australian and Pacific plates has structurally formed a trench-transform-trench system, the southern extent of which is the Macquarie Ridge and associated trenches. These formed through crustal flexure and shortening associated with the underthrusting Australian plate. Macquarie Island, the highest point of the ridge, is a calc-alkaline island arc volcano (Summerhayes, 1969; Carter & McCave, 1997).

Macquarie Ridge and the southern Balleny Plateau form a barrier to free zonal flow of the ACC. With an average depth of nearly 1000 m, the ridge is broken by east-west trending passages north and south of Macquarie Island. These passages funnel the ACC, the most important, a 890 km-wide passage between 57°-65°S, reaching depths over 2000 m (Gordon, 1972; Rodman & Gordon, 1982).

The Campbell Plateau (Fig. 1.4) is a major topographic feature of the New Zealand sector. It forms a large, upstanding part of the continental borderland of New Zealand, and is well defined by the 2000 m bathymetric contour. The plateau is composed of sedimentary and metamorphic rocks, and has a low relief due to peneplanation and marine erosion by transgressive seas during the early Tertiary. Situated on the Campbell Plateau is a number of Subantarctic islands of predominantly alkali volcanic origin (Fig. 1.4), including Auckland Islands, Campbell Island, and Antipodes Islands. The Bounty Islands are formed entirely from biotite granite, and Snares Islands are composed of gneissic muscovite granite (Summerhayes, 1969).

To the north, and separated from the Campbell Plateau by the Bounty Trough, is the Chatham Rise (Fig. 1.4), again part of New Zealand's continental borderland. Chatham Rise forms a 1300 km-long east-west trending submarine barrier, which has a 200-400 m deep rise crest, and acts as a barrier to oceanographic water mass transport (Fenner *et al.*, 1992).

1.2.2 Physical Oceanography of the New Zealand Sector

The NZSSO (Fig. 1.4) is characterised by the following water masses: the surface (cool) Subtropical Water (STW) and Australasian Subantarctic Water (ASW), Circumpolar Surface Water (CSW), and Antarctic Surface Water (AASW), and the sub-surface Subantarctic Mode Water (SAMW), Antarctic Intermediate Water (AAIW), North Atlantic Deep Water (NADW), Circumpolar Deep Water (CDW) and North Pacific Deep Water (NPDW) which flows south, east of Louisville Seamounts (Carter & McCave, 1994). Antarctic Bottom Water (AABW) is absent in the Southwest Pacific Basin, due to the East Pacific Rise / Pacific-Antarctic Ridge preventing the AABW formed in the Ross Sea from entering the basin. The water masses above are characterised predominantly on their temperature and salinity (Table 1.4) (Houltman, 1967; Gordon *et al.,* 1977; Heath, 1985; Nelson *et al.*, 1993a; Williams *et al.,* 1993; Carter & McCave, 1994; Belkin & Gordon, 1996). The circulation pattern is very similar to that previously described more generally for the Southern Ocean in Fig. 1.2, although in the NZSSO the STSW is renamed (cool) STW and the SASW is known as Australasian Subantarctic Water (ASW)

Table 1.4 Major Water Masses and Fronts of the Southwest Pacific

Water Mass	Abbr.	Depth (m)	Density (σt)	Salinity (‰)	Temp (°C)	Silica
(Cool) Subtropical Water	STW	Surface			>15	
Subtropical Front	STF		Separates STW from ASW at 15 °C summer isotherm			
Australasian Subantarctic Water	ASW	Surface			8->15	
Subantarctic Front	SAF		Separates ASW from CSW at 8 °C summer isotherm			
Circumpolar Surface Water	CSW	Surface			5->8	
Subantarctic Surface Water	SASW	Surface				
Antarctic Polar Front	AAPF		Separates CSW from AASW , with icebergs (<5°C)			
Antarctic Surface Water	AASW	Surface				
Thermocline water		0 - 400		34.42 - 34.90	7.00 - 11.00	
Subantarctic Mode Water	SAMW	400 - 600	26.80 - 27.20	34.00 - 34.20	6.00 - 10.00	Very low
Antarctic Intermediate Water	AAIW	600 - 1450	27.20 - 27.35	34.36-34.50	3.20 - 7.00	
North Pacific Deep Water	NPDW	1450 - 2550		34.50 - 34.67	1.80 - 3.20	
North Atlantic Deep Water	NADW	2900 - 3800	37.00 - 45.93	34.71 - 34.73	0.90 - 1.60	High
Upper Circumpolar Deep Water	$CPDW_{(u)}$	2550 - 2900	36.50 - 37.00	34.50 - 34.70	1.60 - 1.80	
Lower Circumpolar Deep Water (1)	$LCPDW_{(1)}$	2900 - 3800	37.00 - 45.93	34.70 - 34.75	0.90 - 1.60	High
Lower Circumpolar Deep Water (2)	$LCPDW_{(2)}$	> 3800	45.93 - 46.00	< 34.71	0.55 - 0.90	High
Antarctic Bottom Water	AABW		General term for cold water of Antarctic origin which spreads north into major ocean basins.			
Antarctic Circumpolar Current	ACC	0 - seafloor	various			

(Table adapted from Carter *et al.*, 1996b).

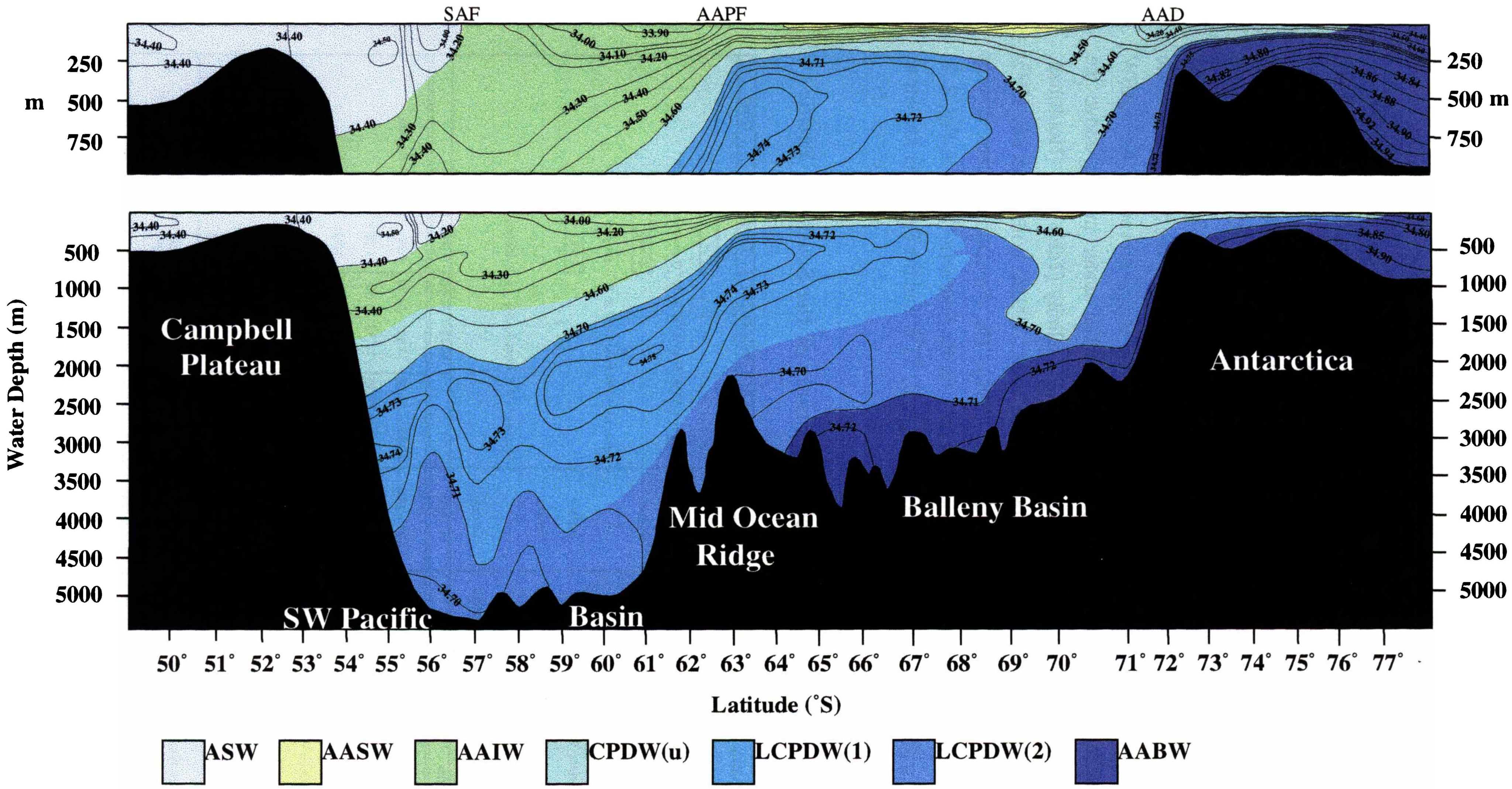

Fig. 1.5 Water masses in the New Zealand sector of the Southern Ocean. Cross-section runs along 170° E and is adapted from Gordon *et al.* (1982). Abbreviations for water masses and fronts are in Table 1.4, AAD is the Antarctic Divergence. Salinity data from Gordon (1975b).

Table 1.4 shows how water masses in the Southwest Pacific are defined. The fronts represent boundaries across which there are rapid spatial changes in water mass properties (Fig. 1.5). The two main surface water masses immediately off New Zealand have separate sources; the STW is derived from southwards flow of the East Cape Current supplied across the Tasman Sea from the East Australian Current, which in turn is fed from the westwards flowing South Equatorial Current. The cooler ASW is derived from water driven north by the flow of the ACC (Heath, 1985). Presently the Campbell Plateau is washed mainly by AAIW. Below this occurs the Circumpolar Deep Water, which is divided into two parts, the $CPDW_{(U)}$ (34.50-34.70‰) and LCDW. The later is further divided in two, $LCPDW_{(1)}$ being characterised by a salinity maximum of 34.74‰. This high salinity core within the $LCDW_{(1)}$ is the signature of the NADW; $LCPDW_{(2)}$ has a salinity of <34.71‰ and lies below the less dense higher saline $LCPDW_{(1)}$ (Fenner *et al.*, 1992; Carter & McCave, 1994; Carter & McCave, 1997). These physical oceanographic trends are seen in Fig. 1.5, which depicts the spatial relationships between the water masses in the NZSSO.

Flow of the ACC in the NZSSO shows a deviation from the normal pattern of flow, deflecting southward south of New Zealand despite shallowing of the seafloor. Southern deflection of the ACC to pass south of the Macquarie Ridge has the effect of carrying ASW characteristics to latitudes nearly 10° further south than is ordinarily the case (Gordon, 1972).

The deep water from Antarctica and southern Indian Ocean enters the Southwest Pacific at Macquarie Ridge and southernmost Campbell Plateau by passing through the Balleny Fracture Zone (Fig. 1.1) which transects the Southeast Indian Ridge (Rodman & Gordon, 1982; Carter & McCave, 1997). DWBC encounters the steep topography of the Macquarie Ridge and Campbell Plateau, and contacts with the ACC. The ACC-DWBC is coupled by transfer of kinetic energy from the ACC to the DWBC by transient eddies that spall off the southern tip of Macquarie Ridge (Gordon, 1972; Morrow *et al.*, 1982). Another coupling mechanism is the direct transfer of momentum from the ACC to the DWBC (Gordon, 1975a; Carter & McCave, 1997).

As the ACC-DWBC encounters Macquarie Ridge the flow body is diverted around the southern reaches of Macquarie Ridge, although streams of flow pass through passages north and south of Macquarie Island (Gordon, 1972). Constriction of the flow generates high geostrophic velocities of 30-40 cm/sec. On the northeastern side of Macquarie Ridge the main ACC-DWBC flow again merges with the flows that passed through the ridge. This coupled flow is topographically intensified on the subantarctic slope of Campbell Plateau, reaching flow velocities of 29 cm/sec

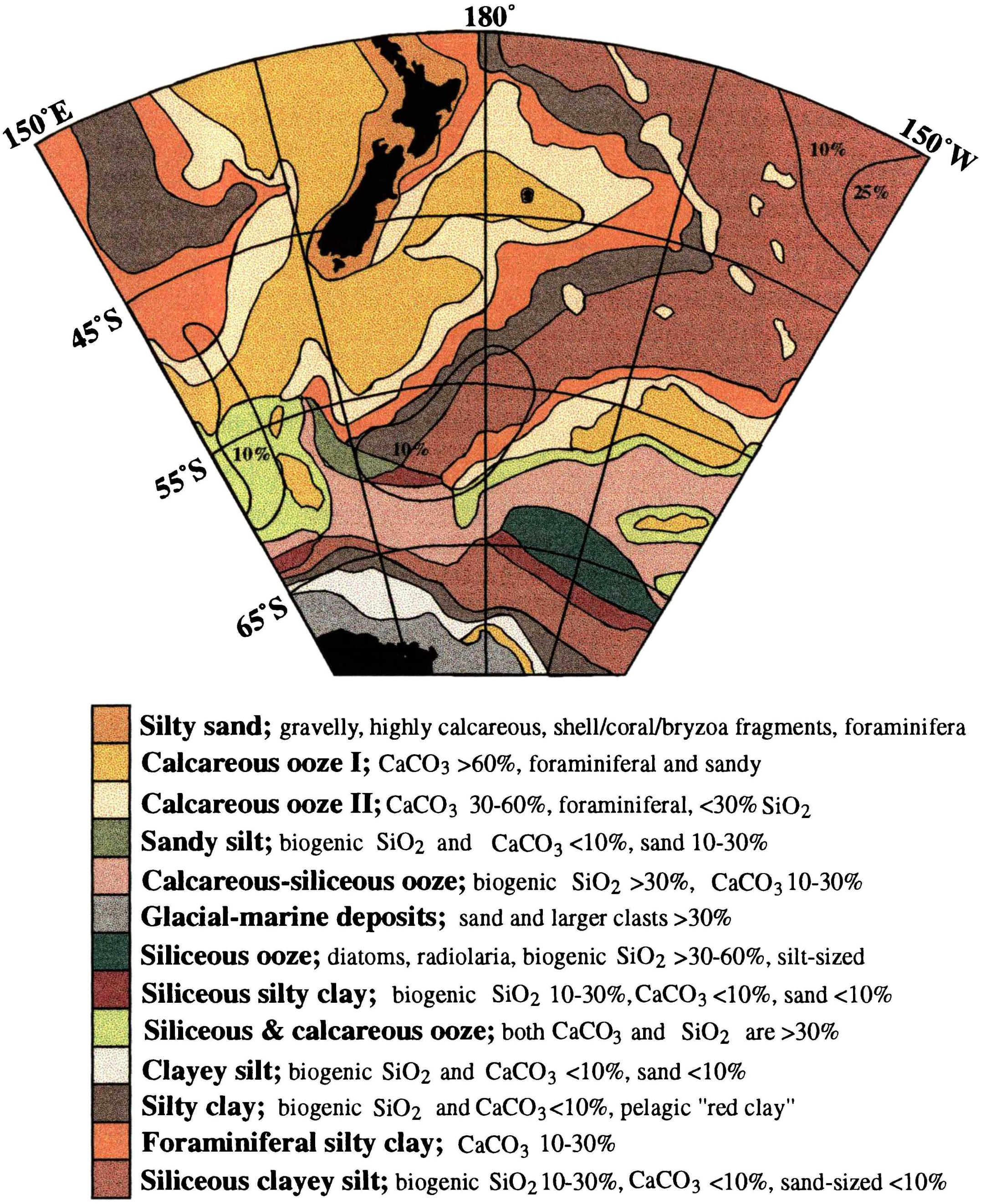

Fig. 1.6 Sediments of the New Zealand sector of the Southern Ocean. Contours with percentage values indicate surface coverage of the seafloor in manganese nodules. Adapted from Goodell *et al.* (1973).

(Gordon, 1975a; Carter & McCave, 1997). ACC-DWBC follows the margin of the Campbell Plateau until south of the Bounty Trough (56°S) where the SAF (the acknowledged northern boundary of the ACC) diverts to the east. The DWBC continues northeast as a wide, slower flow (Carter & McCave, 1997).

1.2.3 Sediments of the New Zealand Sector

The Southwest Pacific Basin sediments are dominated by clayey silts and silty clays, with a belt of siliceous ooze (Fig. 1.6) (Lisitzin, 1972; Florida State University, 1973; Goodell *et al.*, 1973). The oozes contain varying amounts of manganese micro-nodules, sponge spicules and terrigenous material, dominantly mica; moving northwards in the abyssal basin sediments change to diatomaceous clays / oozes and silty clays (Florida State University, 1973).

Sediments off the southeastern margin of Campbell Plateau associated with the DWBC at depths > 4500 m are terrigenous rich (quartz and plagioclase feldspars dominate), due to the corrosive conditions under the currents which allow for the increased dissolution of biogenic material. Because current velocities here reach 30-40 cm/sec, the dominant textural size is coarse sand to sandy gravel. Winnowing of the finer, less dense biogenic material occurs, leaving highly spherical polished grains that often have ferro-manganese coatings, seen as black or dark brown scale on the terrigenous grains. These sediments are interpreted as winnowed lag deposits formed through erosion of Tertiary deposits by vigorous DWBC action (Ovenshine, 1973; Carter & McCave, 1997; Carter *et al.,* 1996b).

Sediments at DSDP Site 594 (Fig. 3.6), situated on the southern flank of Chatham Rise, at mid-bathyal depth (1204 m), show changes in colour, composition and texture related to glacial and interglacial periods (Nelson *et al.,* 1993a). During glacial periods the sediments are greenish grey, dominated by silt and mud, and terrigenous input is high. Foraminifera become rare, and radiolarians and diatoms are more abundant, which is reflected in the lower carbonate percentage (typically 5-20%) and lower abundance of sand-sized fraction. Interglacial sediments are distinguished by bluish grey colour, an increase in sand fraction, and lower terrigenous inputs. The carbonate percentage increases to 30-60%, related to the greater abundance of calcareous nannofossils and foraminifera (Nelson *et al.,* 1993a).

Campbell Plateau is predominantly covered by a *Globigerina / Neogloboquadrina* ooze mix, a white fine-grained ooze consisting of 50-60% foraminifera. The remainder of this ooze comprises siliceous biogenic material

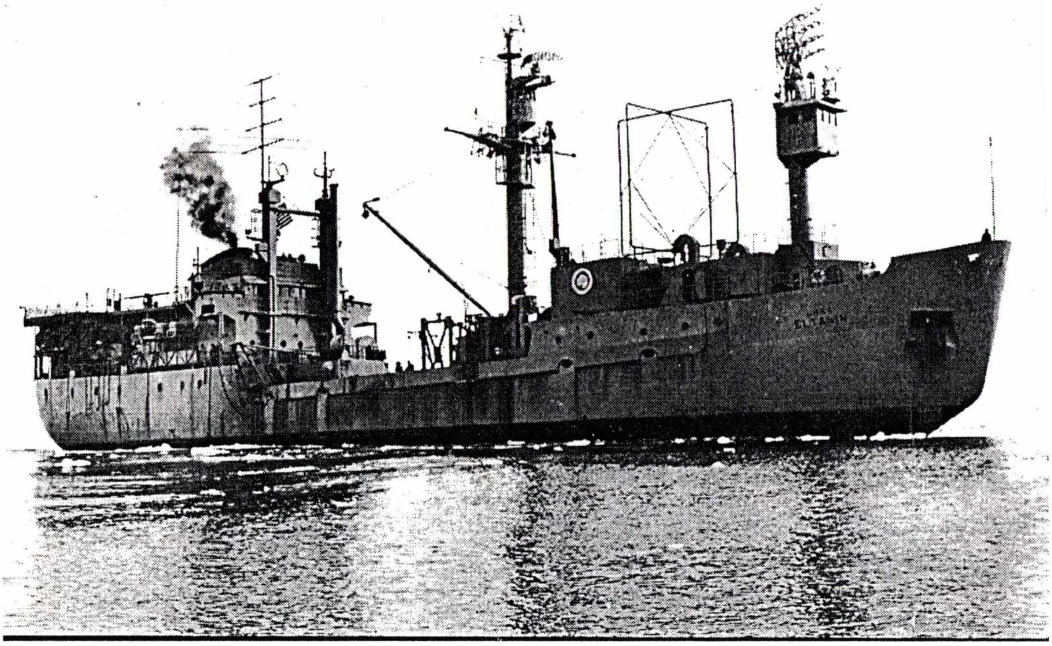

Fig. 1.7 The *USNS Eltanin* (World.Wide.Web, 1997).

(radiolaria and sponge spicules), terrigenous material (quartz, biotite and volcanic rock fragments) and authigenic minerals (manganese nodules, glauconite and phosphate nodules), as well as other calcareous organisms (coccoliths, nannofossils). Carbonate percentages range from 65-100% (Summerhayes, 1969; Lisitzin, 1972).

The subantarctic island shelves and the New Zealand southern shelf are dominated by coarse bryozoan and molluscan skeletal sands averaging 90% $CaCO_3$ and including rare authigenic minerals. The amount of non-carbonate material in these shelf carbonate sediments is low (Summerhayes, 1969; Nelson *et al.*, 1988).

1.3 *USNS Eltanin* History

In 1960, the United States National Science Foundation (NSF), through its Office of Polar Programs, established a curatorial and research centre, the Antarctic Research Facility (ARF), to house marine sediment cores. The facility is an adjunct of the Department of Geology at Florida State University. The Antarctic Research Facility was designed specifically as a national repository for geological materials collected in polar regions, being originally responsible for the analysis of Antarctic continental shelf deposits collected through the US Navy Hydrographic Office, using US Coast Guard icebreakers. The facility from 1968-72 became responsible for the curation of marine sediments collected by the research vessel *USNS Eltanin* (Fig. 1.7). This vessel embarked on a marine geology coring program, which involved a systematic multi-disciplinary survey of some 80% of the Southern Ocean between 35°S and the Antarctic continent (World.Wide.Web, 1997). Collections from the cruises of the *USNS Eltanin* expeditions during its circum-antarctic surveys are mostly limited to the study of the Quaternary because the coring device used rarely penetrated more than 20 m sub-bottom depth (Kennett, 1982).

1.3.1 Core Selection

Data for this study comes from the analysis of twelve NZSSO cores collected south of New Zealand (Fig. 1.4). These cores (Table 1.5) were selected so as to provide a rough north-south trending transect from 52°S to 61°S, so traversing the main oceanographic fronts in the NZSSO. Samples were requested from only the top 1 m of the cores listed in Table 1.5. Samples of the twelve cores were received at 10 cm spacing down core.

Table 1.5 Core Location and Water Depth

Core #	Latitude	Longitude	Water depth (m)	Core length (cm)
36-42	51° 55.7'S	167° 08.0'E	461	607
36-41	51° 56.7'S	166° 23.2'E	1051	304
16-9	52° 25'S	166° 44'E	1052	563
36-40	52° 56.4'S	165° 24.3'E	783	320
34-1	53° 55.4'S	169° 59.2'E	1041	612
36-39	54° 02.4'S	164° 25.7'E	2999	113
16-8	56° 08'S	169° 42'E	5117	314
36-38	56° 28.0'S	161° 45.5'E	4129	1209
50-35	58° 59.3'S	170° 02.6'E	5024	1094
50-34	60° 00.0'S	170° 09.8'E	4863	1014
34-3	60° 01.5'S	167° 20.9'E	4517	564
50-33	61° 05.1'S	170° 03.8'E	4550	1132

The cores were collected between the years 1968-1972 using a standard piston corer developed by Kullenberg in 1947 (Kennett, 1982), the corer consisting of a tight-fitting piston inside a core barrel. The piston is held at or near the sediment-water interface during penetration of the barrel, so creating a suction which holds the sediment column in place while at the same time reducing internal wall friction, and increasing the length of core obtainable (Kennett, 1982).

1.4 Main Aims of Study

The main aims of this study were as follows:

♦ For selected cores to establish downcore records of various sedimentological (textural components, carbonate percentages and terrigenous percentages), micropaleontological and stable oxygen and carbon isotope parameters. From these data an attempt would be made to determine the following information:

- The position of the transition between Last Glacial and the Holocene in the NZSSO cores, and thus the sedimentary characteristics pertaining during contrasting glacial and interglacial conditions.

- The position of the oceanic fronts within the NZSSO during the Last Glacial period and what, if any, shift occurred in these fronts between then and the present interglacial. In particular, the question of whether or not the SAF was topographically controlled and restrained in its position between glacial and interglacial periods is considered, a situation which has been suggested for the STF off eastern New Zealand (Heath, 1981; Fenner *et al.*, 1992; Nelson *et al.*, 1993a).

1.5 Personal Shipboard Experience

While not involved in the collection of the *USNS Eltanin* cores, I was very fortunate to have the opportunity of joining a research cruise aboard *R.V. Tangaroa* run by New Zealand Oceanographic Institute (NZOI) of National Institute for Atmospheric and Water (NIWA) from 10-28 February 1997 off southeastern New Zealand. This research cruise 3034, titled Pacific Gateway - Paleoceanography, had two primary objectives:

- Objective 1. A series of sites designated SWPAC numbers, were to be surveyed by multichannel airgun seismic system, by piston or Kasten core collections, by underwater camera observations, and by water sampling. In addition an Acoustic Doppler Current Profiler (ADCP) was to be run to provide a current velocity field for the upper 300 m. The SWPAC sites were to be surveyed to provide subsurface information for upcoming the Ocean Drilling Programme (ODP) 181 cruise in August-September 1998.

- Objective 2. To determine the history of the northward movement of Antarctic Intermediate Water (AAIW) and Subantarctic surface water across Campbell Plateau since the Last Glacial Maximum or earlier. A series of cores on a latitudinal transect was planned to monitor the northward incursion of AAIW and overlying waters.

These two primary, as well as three secondary objectives were achieved, with all ODP sites having seismic surveys completed and cores obtained where necessary to expand on the seismic data. The transect of cores to observe the AAIW trends was also successfully completed with a total of 13 cores collected. A summary report for research cruise 3034 is included as Appendix 1 (Carter, 1997).

The particular aspects of research cruise 3034 for which I had gained personal experience were with watch keeping of the multichannel airgun seismic system and the 12kHz and 3.5kHz sounder profilers. This involved every 10-15 minutes recording the depth and ship's position on underway sounder logs and multichannel seismic logs when operating, and the recalibration of recorders when profiles rapidly moved across the recorder due to extreme changes in submarine topography. Watch keeping also involved checking the array eel and airgun mooring lines and checking the operation of the compressor for the airgun.

I also gained much experience with the coring programme onboard *R.V. Tangaroa.* The coring was mainly done using a Kasten corer with a 4 m barrel, retrieving ~2-3 m of sediment on a regular basis (the corer failed in consolidated or sandy substrates, because of tilting on it's side). Through active participation I learnt the handling of core deployment/retrieval under calm to gale-force sea conditions that were experienced on the cruise. Once the corer had been retrieved and disassembled, the exposed sediment was described. The onboard processing of a core involved scraping the core down to expose a clean surface to describe. Once a full description (colour, texture, composition, boundaries, and other features) was completed, subsamples were taken, flat tray slabs were removed for X-ray analysis of the core to observe any structures in the sediment, conduits were removed for archival purposes, wet bulk density tubes were taken, and core top sediment was bagged for later study. The final phase involved cleaning the Kasten corer and resetting it for redeployment.

1.6 Format of Thesis

Following the foregoing general introduction and review of the Southern Ocean and the New Zealand Sector of the Southern Ocean (NZSSO), Chapter 2 reports the methods used to obtain the various sedimentological, micropaleontological and stable isotope data for the cores. Chapter 3 will discuss core stratigraphy, based on both original *USNS Eltanin* descriptions and personal observations from this study. Whether there is possible points of correlation between cores based on broad lithological properties and colour marked boundaries is considered. The subsequent chapters begin to look at the cores in greater detail, considering their different sedimentary characteristics. Chapter 4 describes textural features, and discusses variation in textural characteristics and classes with latitude and water depth. Chapter 5 describes the composition of the sediments, including their carbonate content, terrigenous composition and broad biogenic components. A detailed analysis of the biogenic components is given in Chapter 6, which describes faunal variations and their implications. In association with the micropaleontological results, Chapter 7 discusses the stable oxygen and carbon isotopic records for selected NZSSO cores. Chapter 8 attempts to meld the observations into a history of the NZSSO during the transition from the Last Glacial to the Holocene.

Chapter Two:

Methodology

Chapter Two: Table of Contents

2.1 Micropaleontological Sample Preparation

2.1.1 Cleaning and Pretreatment of Samples

Samples obtained at 10 cm intervals from the top 1 m of the piston cores listed in Table 1.5 were cleaned and prepared for further study, using standard procedures adopted at the University of Waikato for the preparation of core samples.

These samples were oven dried for 24 h at 35°C, then cooled to room temperature in a desiccator. Cooled samples were weighed to four decimal places, determining the bulk sample weight. Weighed samples were transferred to a labelled 50 ml conical flask and 40 ml of buffer solution (pH ~ 9.4, 4g $NaHCO_3$ + 1g Na_2CO_3 in 20 l of distilled water) added and left to stand. The buffer solution is used so that dissolution of calcareous microfossils does not occur, and it also helps to deflocculate mud aggregates.

Samples are then washed across a 63 μm Tyler screen with buffer solution, and the collected mud is allowed to settle, and then stored for later analysis. Sand collected on the 63 μm mesh is rewashed by returning it to the conical flask with distilled water, and placing the flask in a sonic bath for 10 sec; the above rewashing process is repeated approximately five times. Rewashed sand is washed onto filter paper with distilled water and left to air dry.

2.1.2 Textural Determination

Clean sand is dry sieved over 125 μm sieve to obtain 63-125 μm (fine sand) and >125 μm (coarse sand) fractions. These sand fractions are then weighed and recorded to four decimal places (Appendix 2). The coarse sand fraction was later resieved over a 150 μm sieve to obtain the >150 μm fraction which was used for isotope pickings and micropaleontological census. The percentage of mud, fine sand (63-150 μm) and coarse sand (>150 μm) was recalculated (Appendix 3).

To determine the mud content, the mud fraction (<63 μm) is washed into large measuring cylinders and made up to 500 ml with buffer solution ($NaCO_3$ / Na_2HCO_3). The contents of the measuring flasks are then mixed to reach homogeneity and a 20 ml aliquot is removed and deposited onto a pre-weighted filter paper. Once the 20 ml sample has drained the filter paper is oven dried overnight, at 105°C. The filter paper is then reweighed and the amount of mud on the filter paper determined. This value is then multiplied by the dilution factor to determine the weight of mud in the original sample (Appendix 2).

2.1.3 Carbonate Determination

Small amounts (slightly more than required, to allow for water loss) of bulk sample are placed in aluminium tins and dried for 24 h at 105°C. Dried samples are crushed, and between 0.05 and 0.06g is removed and the weight recorded; these smaller samples are used for carbonate determination.

The crushed and weighed samples are then added to 20 ml of HCl of a known concentration and back titrated against NaOH also of known concentration. The volume titrated (NaOH) is then used in the following equation to determine the percentage carbonate:

$$CaCO_3\ \% = \frac{\text{vol. NaOH} * [\text{NaOH}]}{2} \quad \frac{10.009}{\text{weight of sample}}$$

These titrations were performed using a Metler DL40RC Automatic Titrator; each sample run was accompanied by samples of four standards containing 80%, 50%, 30% and 10% carbonate. The standards did not appear to drift, so it was assumed that the results (Appendix 2) obtained for the carbonate analysis were acceptable.

2.2 Micropaleontological Census Procedure

2.2.1 Sample Splitting

Determination of the microfossil population in the samples obtained from the twelve *USNS Eltanin* cores required the splitting of the coarse sand fraction (>150 μm) into sub-samples. Workers such as Kennett (1970) and Griggs *et al.* (1983) have shown that the sample split produced is representative of the whole population. Many workers recommend the use of a micro-splitter to take an unbiased split of approximately 300 specimens. A sub-sample size is acceptable on the assumption that if a given species represents 1% of the whole population then there is a 95% certainty of that species being in the sub-sample split, if the split taken is random.

The coarse sand fraction (>150 μm) was used for the micropaleontological census study. The selected sample is split down until a sub-sample containing approximately 300 individual specimens is obtained. Often a sub-sample split ranged from 300-500 individual specimens; no samples split were under 300 individual specimens.

2.2.2 Sample Mounting

The sub-sample splits of approximately 300-500 specimens were mounted on micropaleontological slides (60 grid slides). The specimens were identified to genus and/or species level. All cores had samples mounted at intervals of 20 cm; for cores 36-42, 34-1, 36-38 and 50-34 analyses were conducted at 10 cm intervals to provide higher resolution results.

2.3 Semi-quantitative Micropaleontological Study

The fine sand (63-150 μm) samples from the four cores (36-42, 34-1, 36-38 and 50-34) analysed at intervals of 10 cm, underwent a semi-quantitative study in which a random split of the fine sand was distributed over a 60 grid micropaleontological slide. The particle material which fell into certain boxes was counted and recorded to genus and/or species level.

2.4 Malvern Mastersizer Laser Particle Sizer

2.4.1 Theory of Malvern Laser Particle Sizer

A narrow beam of monochromatic light from a Helium-Neon Laser (650 nm wavelength, with a maximum diameter of 18 mm) is passed through a suspension containing particulate samples and the diffracted light from the particles is focused onto a detector, which senses the angular distribution of scattered light energy (McCave *et al.,* 1986; Singer *et al.,* 1988). A lens (Fig. 2.1) placed between the illuminated sample with the detector at it's focal point, focuses the undiffracted light to a point at the centre and leaves only the surrounding diffraction pattern; this pattern is not affected by particle movement through the beam. Therefore a flow of particles can pass through the beam and generate a stable diffraction pattern (McCave *et al.,* 1986).

This diffraction pattern is the essential data that is analysed to produce a size distribution. The fraction of light scattered is the sum of the individual particle contributions; the scattered light is typically measured and integrated over the time the particle takes to move through the beam. Particles in the suspension are not sized individually and counted, instead the laser beam is large at the point of measurement and many thousands of particles are simultaneously illuminated. Particle size is determined on the principle of the equivalent sphere; only one shape, a sphere, can be described in three dimensions with one number (i.e. stating that a particle is a 50 μm sphere fully describes the particle). The laser sizer measures some property of an unknown particle and assumes this refers to a sphere of a volume equivalent to that of the measured particle (Rawle, 1994).

2.4.2 Operational Set-up of Malvern Laser Sizer

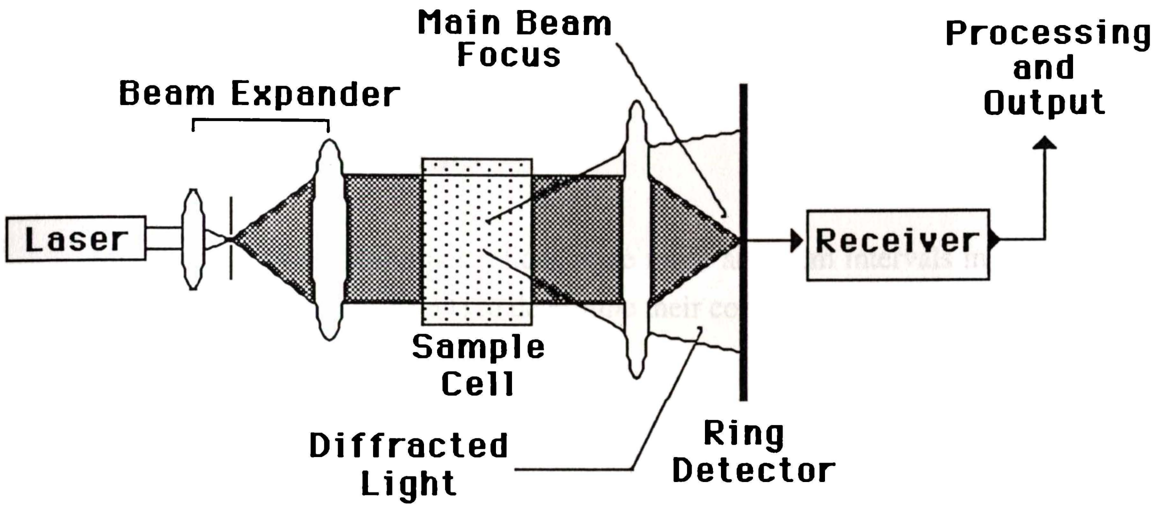

Fig. 2.1 Schematic diagram showing the arrangement of the Malvern Laser Particle Sizer (From McCave *et al.,* 1986).

The Malvern Laser Sizer set-up involves a laser source, beam expander, sample chamber, focusing lens and ring detector with associated electronics, and a systems computer which runs measurement control and data storage (Fig. 2.1). The size range detected by the laser sizer depends on the focal length of the focusing lens. The laser sizer can measure particle sizes between 0.5 - 900 μm. There are three focusing lens (63, 100 and 300 mm) which can be changed depending on the range of particle sizes in the samples: the 63 mm lens range is 1.2 - 118 μm, 100 mm lens 1.9 - 188 μm, and the 300 mm lens 5.8 to detection limit (McCave *et al.,* 1986). Since the diffraction pattern is not affected by the movement of particles through the beam the flow rate can be high, which allows the analysis of a sample to be completed rapidly; full printout can be obtained in five minutes. The step in the process which is rate determining is cleaning the sample cell after each sample run. Approximately 40 samples can be run per day (McCave *et al.,* 1986).

2.4.3 Operational Method of Malvern Laser Sizer

Mud samples (stored in buffer solution) were prepared for the laser sizer by stirring the mud into a homogenous suspension. Using a pipette, 0.5 to 1 g of sample was extracted and dispersed into the sample bath with the sample pump and stirrer all operating reasonably vigorously. The sample was then sonicated for 10 secs. The amount of sample dispersed was dependent upon the obscuration value, which ideally should be between 18-25%. Once the sample was in the sample cell (Fig. 2.1) the sample was analysed. On completion, the sample cell was drained and flushed clean at least two times to ensure no sample particles remain. This process was then repeated for each proceeding sample.

2.5 Smear Slide Analysis

Mud fraction (< 63 μm) smear slides were made at 10 cm intervals in selected cores (36-42, 34-1, 36-38 and 50-34) to determine their composition (qualitative study of biogenic vs. terrigenous components).

Using a spatula, a small amount of mud was obtained, and was mixed with a drop of water on a standard glass slide until the sediment and water were smeared into a thin film. The slide was then dried on a hot plate (using a low temperature). When the slurry was dry, a film of Araldite glue was placed over the sediment and covered with a glass cover slip, care being taken to exclude air bubbles. The slide was then placed on a hotplate at 60°C for 3 h to cure the glue. Once the glue had cured the slide was ready for viewing, under a petrographic microscope.

2.6 Isotopic Analysis of Core Material

2.6.1 Sample Collection

A stable oxygen and carbon isotopic analysis was undertaken on samples from three cores (36-42, 34-1 and 36-38). These cores were chosen for isotopic analysis due to their proximity to major oceanographic fronts and the availability of sinistral (s) *Neogloboquadrina pachyderma* within the samples analysed; an additional factor for analysing core 36-38 was that it contains abundant populations of both siliceous and calcareous biogenic organisms. The >150 μm (coarse sand) fraction at 10 cm intervals was picked and placed on a slide, ~40 *Neogloboquadrina pachyderma* (s) were picked for analysis. Where possible, larger *Neogloboquadrina pachyderma* (s) were taken to reduce the inclusion of juvenile foraminifera.

2.6.2 Sample Preparation

Picked samples were removed from the slide, placed in small bottles and immersed in methanol. The bottles were placed in a sonic bath for 10 secs to remove organic and fine material from the tests. Picked samples from core 36-38 were found to disintegrate when placed in the sonic bath, and so this procedure was not used for this core. The methanol, dissolved organic materials and disaggregated fine matter from the foraminiferal tests were removed from the small bottles using a syringe.

Cleaned *Neogloboquadrina pachyderma* (s) were placed in small glass vials for roasting, under a vacuum of ~ 1 Hg µm. The samples were baked at 375 °C for 3-4 h; roasting was done overnight, allowing the sample to cool under vacuum as well.

2.6.3 Sample Analysis

Samples were analysed on a Europa Scientific Geo 20-20 mass spectrometer, using "Blue-box" preparation method of CO_2. The oven (Blue-box), which was maintained at a constant 70 °C, housed a reaction vessel in which the sample was placed and suspended below a reservoir of 100% orthophosphoric acid. Samples were reacted with the acid for 20 min; all reactions had to occur at a constant temperature so that the reaction rate was constant, allowing no fractionation of the CO_2 gas being produced from the reaction vessel (Hendy, 1995). The CO_2 from the oven was passed through a water trap and a cold trap before entering the first cold finger on the Europa 20-20. CO_2 gas was transferred to the mass spectrometer as quickly as possible to prevent fractionation.

Three standard samples were analysed at the start of a run to check the calibration of the mass spectrometer. The standard used was Toilet Seat Standard (TSS); the standard supplied by Dr I. Friedman (USGS) was originally a marble toilet seat from the Smithsonian Institute before it became the standard NBS-19 (Hendy, 1995). The precision of the standards are $O^{18} \pm 0.05$ ‰ vpdb and $C^{13} \pm 0.01$ ‰ vpdb.

2.7 X-Ray Diffraction Analysis of Cores

2.7.1 XRD Slide Preparation

The samples from cores 36-42, 34-1, 36-38 and 50-34 were taken at 10 cm intervals for preparation of XRD slides. The slides were prepared for bulk sedimentological analysis. Samples were made into a thick slurry which was applied to glass slides by pipette. Once the slurry was evenly distributed (glass should not be exposed so the x-rays will diffract off the sediment surface), the slide was left to air dry over night. The slow drying allowed clay minerals to preferentially settle on their flat faces, thereby increasing the peak intensities of the clays.

2.7.2 XRD Analysis

Smear slide samples for X-ray diffraction were scanned from 3-40° 2Ø min^{-1}, using the setting: speed at 0.05, chart speed at 10 $mm.min^{-1}$, range at $5x10^{-3}$, T.C at 2.0, slit spacing at 0.2, voltage at approximately 34 kV, and current at about 26 mA.

At the start of every run a set of two quartz standards were run between 20°-21° 2Ø, and had to show a peak height of 6.5 units at 20.8°; it was found that the quartz standard peak was consistently displaced by 0.3° 2Ø, so that a small correction in peak position was applied to all samples.

2.8 Scanning Electron Microscope (SEM) Analysis

SEM analysis of the mud fraction was undertaken on three cores (36-42, 50-34 and 36-38) and on picked foraminifera and radiolaria from the >150 µm fraction. The SEM stubs of the mud fraction were prepared by placing a very small amount of the mud fraction onto the graphite sticker of the stub, then adding a drop of water to smear the mud into a thin film. The stubs were then allowed to dry overnight, before being sputter coated with platinum. Coated stubs were then observed under the SEM, and photographs taken of dominant sedimentary features. Picked foraminifera and radiolaria were mounted on the graphite sticker with the aperture of the foraminifera facing upwards.

Chapter Three:

USNS Eltanin Core Lithostratigraphy

Chapter Three: Table of Contents

3.1 Introduction

This chapter highlights general lithostratigraphic properties of the NZSSO cores (Table. 1.5) in this study, briefly commenting on particular lithological properties of interest. It collates and summarises lithostratigraphic information, such as dominant sediment types, colour and other lithologic features, noted in three *USNS Eltanin* Core Descriptions (Goodell, 1968; Florida State Univerity, 1971, 1973) and combines these with personal observations of the core sediments. Water depths vary greatly with core location, ranging from outer shelf on the Campbell Plateau to abyssal in the Southwest Pacific Basin (Fig. 3.1). An attempt is made to compare and contrast the broad similarities and differences between the cores of this study and those from other studies. Core logs are summarised on Fig. 3.2 which for convenience appears as an extended foldout on page 37

3.2 NZSSO Core Lithostratigraphy

3.2.1 Core 36-42 (Campbell Plateau, 52°S, 461 m)

The sediment is composed of sandy foraminiferal ooze (Fig. 3.2A), containing molluscan fragments (ranging to gravel size) and bryozoa throughout the 1 m length, indicative of the outer shelf to upper bathyal depth of the core (Figs. 3.1 and 3.3). The dominant lithology does not change downcore, although two boundaries are noted, marked by distinct colour changes. From 0-16 cm is greyish olive sandy foraminiferal ooze, containing sponge spicules, echinoderm spines and glauconite. The sharp base of this upper unit corresponds to a colour change to greyish white, and higher carbonate values. This greyish white foraminiferal ooze extends from 16-65 cm and has a gradational lower boundary into olive grey foraminiferal ooze (65 cm to base), with shell fragments and bryozoa with minor amounts of echinoderm spines. All three units are highly calcareous, with very good microfossil preservation.

3.2.2 Core 36-41 (Campbell Plateau, 52°S, 951 m)

The core sediment is a sandy foraminiferal ooze that is mottled to greyish white, highly calcareous and has good preservation of microfossils (Fig. 3.2B). No lithologic boundaries are detected in the top 1 m of this core. Core 36-41 lies close to core 36-42 (Fig. 3.3), but is at greater depth (i.e. mid-bathyal). Rare ice-rafted debris is present.

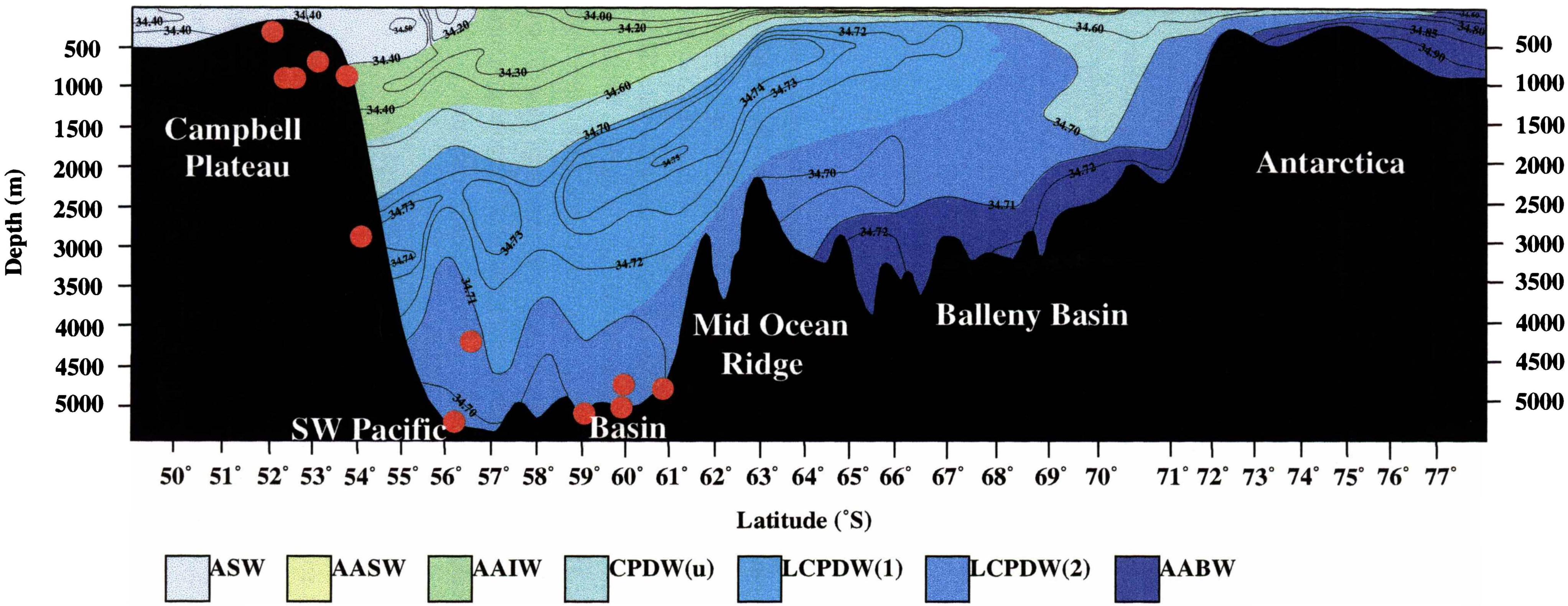

Fig. 3.1 Cross-section shown in Fig. 1.5 with superimposed positions of the NZSSO cores in this study. The majority of the cores in fact lie just to the east of this transect profile along 170˚E (see Fig. 1.4). Figure adapted from Gordon *et al.* (1982).

3.2.3 Core 16-9 (Campbell Plateau, 52.5°S, 1052 m)

The top 1 m of this core is a sandy foraminiferal ooze, with good preservation of microfossils, lying at mid-bathyal depths. The core involves two units separated by a sharp colour boundary at 20 cm. The upper unit is a highly calcareous olive grey sandy foraminiferal ooze, while the lower unit is a greyish white clayey foraminiferal ooze with a higher carbonate content. The lower unit is broken at 85 and 90 cm by two inclined stripes (at 30° to the horizontal) of bluish grey stiff clay (Fig. 3.2C).

3.2.4 Core 36-40 (Southern Campbell Plateau, 53°S 783 m)

This upper bathyal depth core is a continuous light yellow brown sandy foraminiferal ooze (Fig. 3.2D) with mollascan fragments, echinoderm spines, radiolaria and bryozoa, in decreasing order of abundance downcore. The core sediment is highly calcareous with microfossils well preserved.

3.2.5 Core 34-1 (Campbell Plateau margin, 54°S, 1041 m)

The top metre of this core is highly calcareous sandy foraminiferal ooze, from a mid-bathyal depth. The preservation of microfossils is good. The core comprises three colour units (Fig. 3.2E). The upper unit, from 0-18 cm is a light grey foraminiferal ooze with occasional radiolaria. It has a sharp base at 18 cm across which the colour changes to a light greyish yellow foraminiferal ooze (18-58 cm), more mud, and with scattered remains of echinoderm spines, sponge spicules and radiolaria. At 58 cm a gradational boundary leads into a light grey foraminiferal ooze (58 cm to core base), with occasional radiolaria.

3.2.6 Core 36-39 (Southern Campbell Plateau, 54°S, 2999 m)

Of the 50 cm of the core obtained the lithology is highly calcareous clayey foraminiferal ooze, from a lower bathyal depth, with good preservation of microfossils. One colour change (Fig. 3.2F) occurs at 18 cm. The upper unit (0-18 cm) is a white foraminiferal ooze with occasional echinoderm spines and radiolaria, and some micronodules of manganese. Across the boundary at 18 cm the colour changes to a greyish yellow, and micronodules of manganese remain present. The boundary appears to represent a change in texture, with decreasing mud and increasing sand downcore, and a decrease in fragmentation as well.

3.2.7 Core 16-8 (Southwest Pacific Basin, 56°S, 5117 m)

Core 16-8 lies at abyssal depth, and is dominantly a sandy silt (biogenic SiO_2, $CaCO_3$ <10%, sand 10-30%). There is very poor preservation of calcareous biogenic material, but good preservation of siliceous biogenic material (Fig. 3.2G). Three colour changes occur down core. From 0-51 cm is a dark reddish brown terrigenous sandy silt (dominated by quartz and plagioclase feldspars) with abundant siliceous biogenic material and sparse calcic planktic and benthic foraminifera. At 4-9, 32 and 48 cm micromanganese nodules are abundant. From 51-89 cm the colour changes to a greyish yellow brown, but with little apparent change in sediment type. Burrowing associated is with the colour boundary. The final 11 cm of core is olive coloured sandy silt.

3.2.8 Core 36-38 (South Emerald Basin, 56.5°S, 4129 m)

The entire top metre of core 36-38 is a greyish olive mud with abundant sponge spicules containing scattered remains of radiolaria, diatoms and foraminifera, in decreasing order of abundance. The core contains biogenic SiO_2 >30%, a $CaCO_3$ content of 10-30%, and sand 10-20%. It comes from an abyssal depth, and while preservation of siliceous material is good, that of calcareous material is moderate to poor. Heavy minerals are conspicuous throughout the core (Fig. 3.2H).

3.2.9 Core 50-35 (Southwest Pacific Basin, 59°S, 5025 m)

Core 50-35 has two lithologies, sandy diatomaceous ooze and muddy diatomaceous ooze, seperated by gradational colour boundaries (Fig. 3.2I). The sediments have no carbonate material and good preservation of siliceous biogenic components. The upper unit of sandy diatomaceous ooze (0-69 cm), with radiolaria and mud in decreasing order of abundance, and is bounded by a basal gradational boundary. The colour of this unit is mottled yellowish brown to olive yellow. It's lower boundary is gradational into a sponge spicule bearing unit whose colour is mottled from brown to olive. This unit is bounded at the base by another gradational boundary at 83 cm across which the lithology changes to muddy diatomaceous ooze with abundant radiolaria (Fig. 3.2I). This lowest unit is mottled olive to brown.

3.2.10 Core 50-34 (Southwest Pacific Basin, 60°S, 4863 m)

Two lithologies dominate downcore: a diatomaceous ooze (0-80 cm) changing to a muddy sand diatomaceous ooze (>80 cm) near the base of the core (Fig. 3.2J). There is good preservation of biosiliceous material, insignificant calcium carbonate is present (< 2%) and the terrigenous content increases downcore. From 0-80 cm is a diatom ooze containing scattered concentrations of radiolaria and sponge spicules, along with mica and micronodules of manganese. This 80 cm thick unit is divided in three by gradational boundaries at 18, 28 and 44 cm marked by colour changes; the dominant colours are olive inter-mottled with a lighter yellow olive (Fig. 3.2J). At 80 cm lies a gradational boundary across which the lithology changes to a muddy sand diatomaceous ooze, with abundant radiolaria. This lowest unit is greyish yellow brown.

3.2.11 Core 34-3 (Southwest Pacfic Basin, 60°S, 4517 m)

Core 34-3 lies at abyssal depths (Fig. 3.3). Two lithologies are present in the top 1 m of core, radiolarian ooze and spicule/radiolarian ooze, with good preservation of biogenic siliceous material. Colour changes alternate down core from dark olive to a lighter grey olive (Fig. 3.2K), these colour changes occur across gradational boundaries. 0-40 cm is a radiolarian ooze with scattered remains of sponge spicules and diatoms in decreasing order of abundance downcore. Units between 40-50 cm and 50-60 cm are a sandy radiolarian ooze with local concentrations sponge spicules, and increased terrigenous material downcore. The distinguishing feature between these two units is a colour change from greyish olive to dark olive across a gradational boundary at 50 cm. From 60-70 cm is an olive radiolarian ooze containing sponge spicules and scattered diatoms. Terrigenous material influx to the sediment decreases downcore. From 70-80 cm a darker black olive radiolarian ooze, with sediment type and texture very similar to overlying units (Fig. 3.2K), terrigenous material influx continues to decrease. A gradational boundary at 80 cm leads into a greyish olive sandy radiolarian ooze (80-90 cm) with scattered sponge spicules and diatoms, and increased amounts of terrigenous material. Between 90-100 cm the core material changes to a spicule / radiolarian ooze with scattered diatoms.

3.2.12 Core 50-33 (Southwest Pacfic Basin, 61°S, 4550 m)

The core contains two lithologies, a dominant muddy diatomaceous ooze, and a gravelly mud ooze (Fig. 3.2L). There is very poor preservation of calcareous biogenic

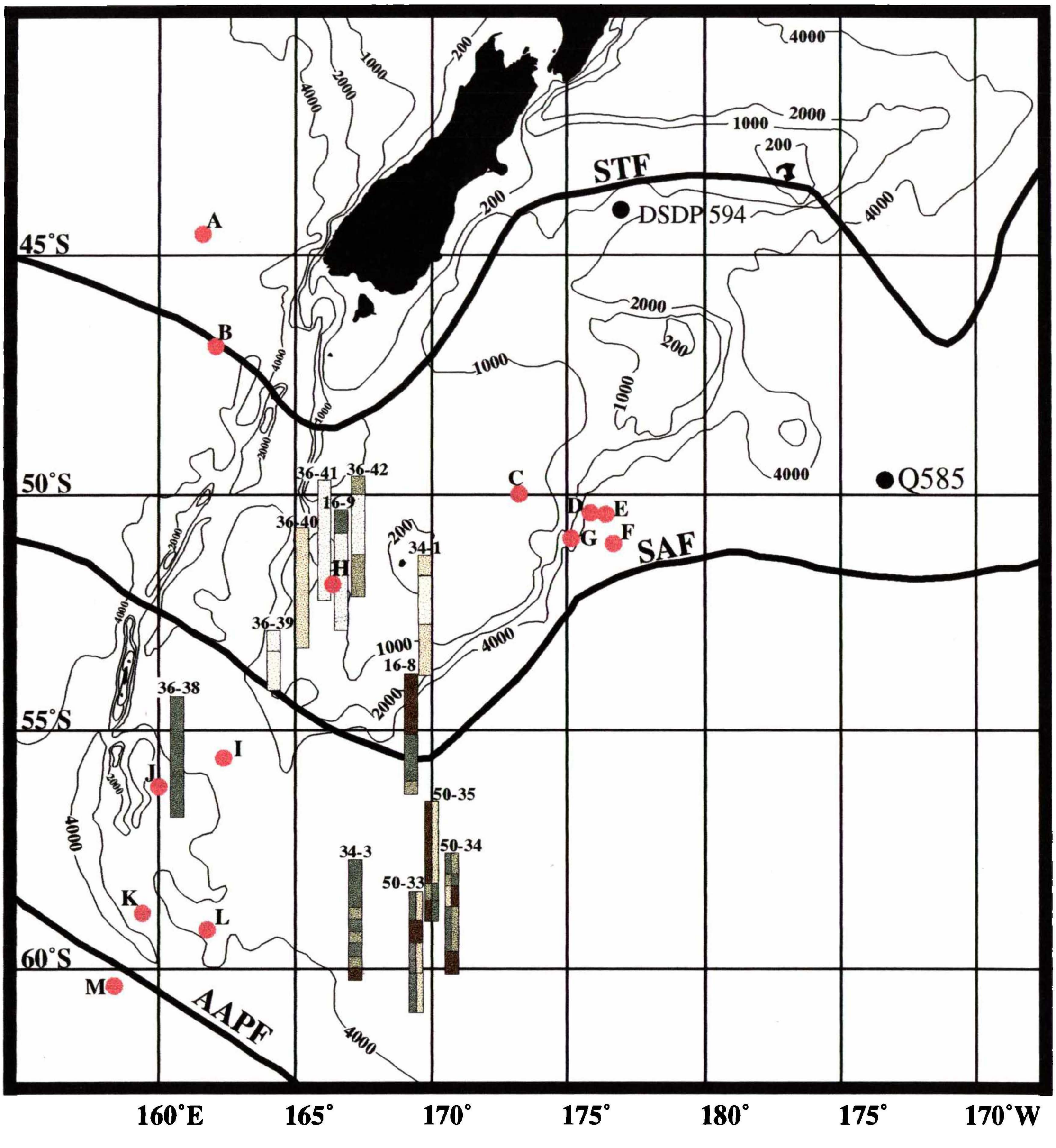

Fig. 3.3 Location of NZSSO cores in relation to major oceanic fronts in the NZSSO. Cores north of the SAF commonly have correlatable colour boundaries; those south of the SAF, however show little intercore similarity. The base of the depicted cores represents their position. Labeled red points refer to core lithostratigraphies of other regional cores in Fig. 3.4. Bathymetry in metres.

material, only the core top surface contains calcareous biogenic material which is dominated by sinistrally coiled *Neogloboquadrina pachyderma* and calcareous fragments. All calcareous material shows signs of dissolution, and below the core top the calcium carbonate percentage drops from 13% to < 1%. Biosiliceous material is well preserved. From 0-24 cm is a reddish brown mottled with dull yellow orange muddy diatomaceous ooze, containing radiolaria, terrigenous material and foraminifera, in decreasing order of abundance. The unit has a gradational lower boundary into a reddish brown gravelly mud ooze, with abundant radiolaria, diatoms and heavy minerals. This in turn has a gradational base (43 cm), and from 43-67 cm the lithology returns to reddish brown mottled with dull yellow orange muddy diatomaceous ooze containing abundant heavy minerals. Another gradational boundary occurs at 67 cm into a muddy diatomaceous ooze containing micronodules of manganese and abundant heavy minerals that is mottled between dull yellowish brown and dull yellow orange and continues to the base of the described core.

3.3 Relationships to Other NZSSO Cores

The main similarities between the NZSSO cores of this study and other previously described cores from the region (Fig. 3.4; Appendix 4) are the relationships that exist between core lithology, core latitude, core depth and the local/regional environmental conditions.

- Cores on the Campbell Plateau are calcareous (foraminifera, nannofossils, mollusca fragments, and echinoderm fragments), whereas those beyond the plateau and south of 50°S latitude tend to be siliceous, and dominated by diatoms and radiolaria. Exceptions to this include cores Elt 36-36 and Elt 36-37 which have units where calcareous foraminiferal oozes dominate (Fig. 3.4 K and M). This probably relates to their positions on the topographic high of Balleny Plateau (Fig. 1.1A, #14), where calcareous material may be preserved above the lysocline (c. 3600-4100 m) and carbonate compensation depth (~4700 m) (Lisitzin, 1972), or locally $CaCO_3$ can exceed 80% where benthic foraminifera and sponge spicules form an interlocking weave (Goodell *et al.*, 1973). The upper unit of core 50-33, the southernmost core of this study, contains planktic foraminifera at a depth of 5000 m. At this depth calcareous material should have been removed by dissolution from the sediment. The preservation of calcareous sediments at this depth may be due to an absence of cold, carbon dioxide-rich AABW washing over the site as the Southeast Indian Ridge prevents the corrosive AABW from entering the Southwest Pacific Basin (Fig. 1.5) (Berger, 1968; Rodman & Gordon, 1982).

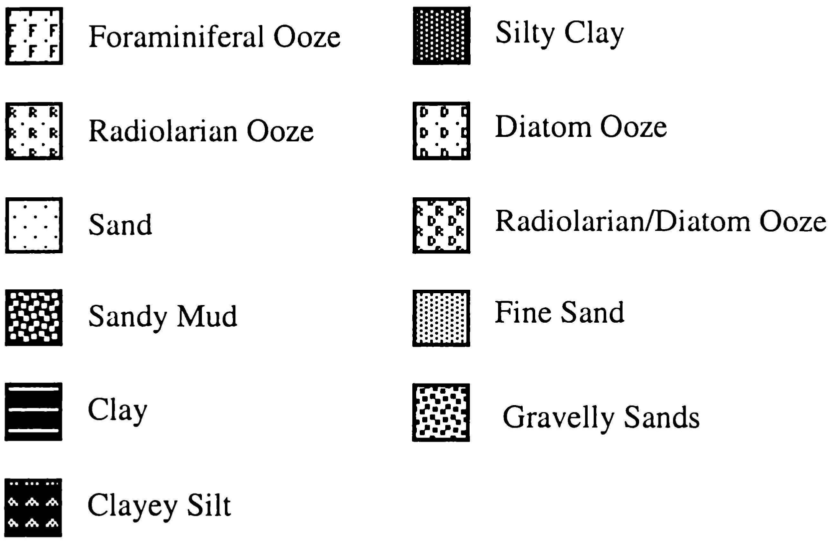

Legend for Fig. 3.4 Core lithologies.

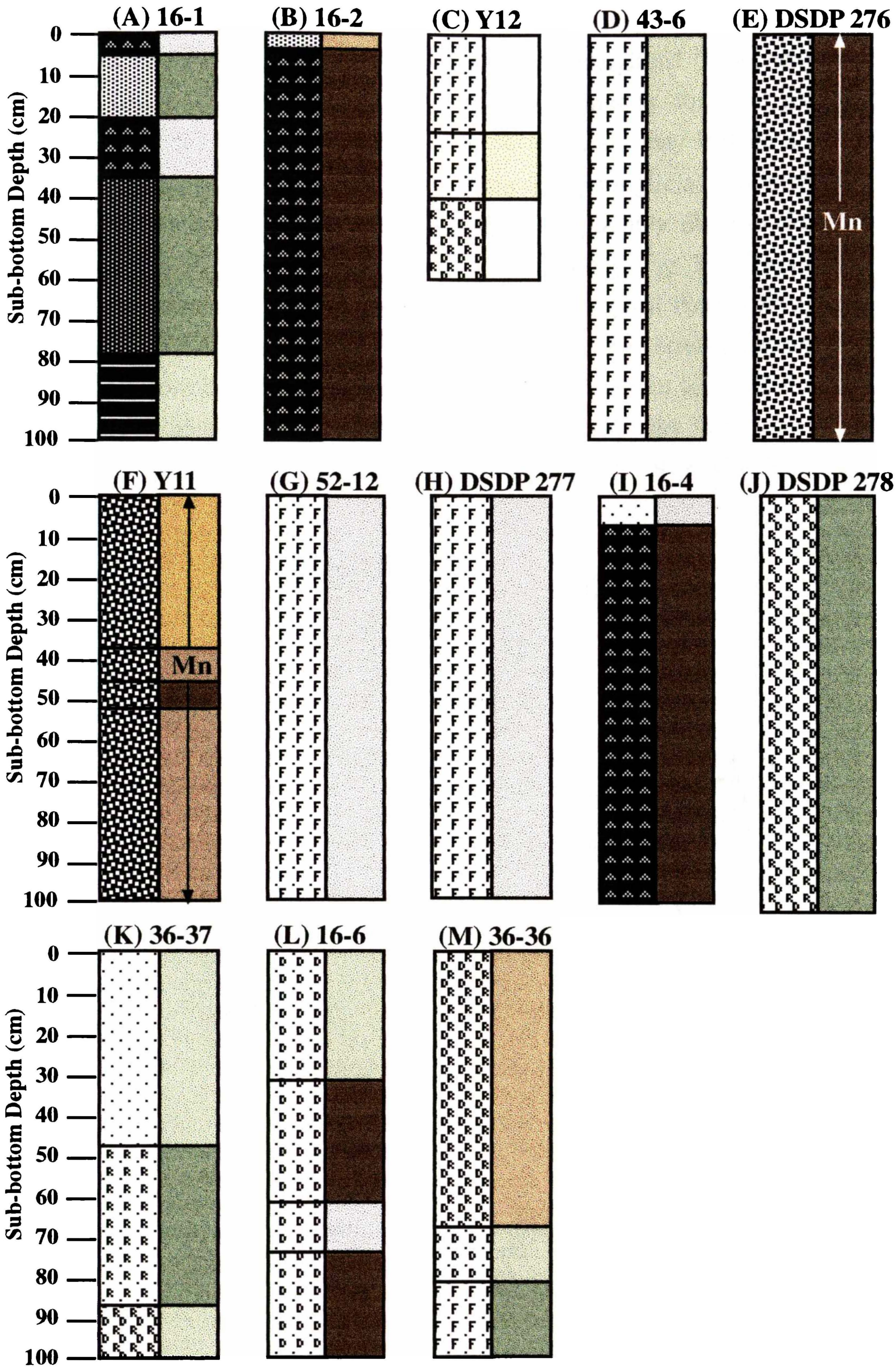

Fig. 3.4 Other sediment cores from the NZSSO region, showing dominant lithologies and associated colour changes. Core positions are shown in Fig. 3.3. The colours used in this figure are an attempt to reproduce described colours from the core descriptions (Appendix 4). Cores E and F show manganese (Mn) nodules throughout the core length.

- Core Y12 (SWPAC 6B, Fig. 3.4C) shows a colour change between 15-25 cm attributed to the transition between glacial stage 2 and interglacial (Holocene) stage 1 (Carter, 1997). There appears to be no obvious change in dominant sediment type across this colour boundary. Thus other cores locally may include a colour change at a similar depth that represents the transition from glacial into interglacial sedimentation patterns, as observed in cores Elt 16-1, possibly Elt 16-6 (Fig. 3.4 A and L), and in 36-42, 16-9, 36-39 and 34-1 of this study (Fig. 3.5). This allows a degree of correlation between cores that lie on the Campbell Plateau (Fig. 3.3). Cores that lie off the Plateau and south of the SAF cannot be correlated to northern cores using colour boundaries or lithologies due to a dominant biogenic sediment type and depositional changes, as well as extensive erosion and reworking of the sediments (Heezen & Hollister, 1964; Waktins & Kennett, 1972; Goodell *et al.*, 1973)

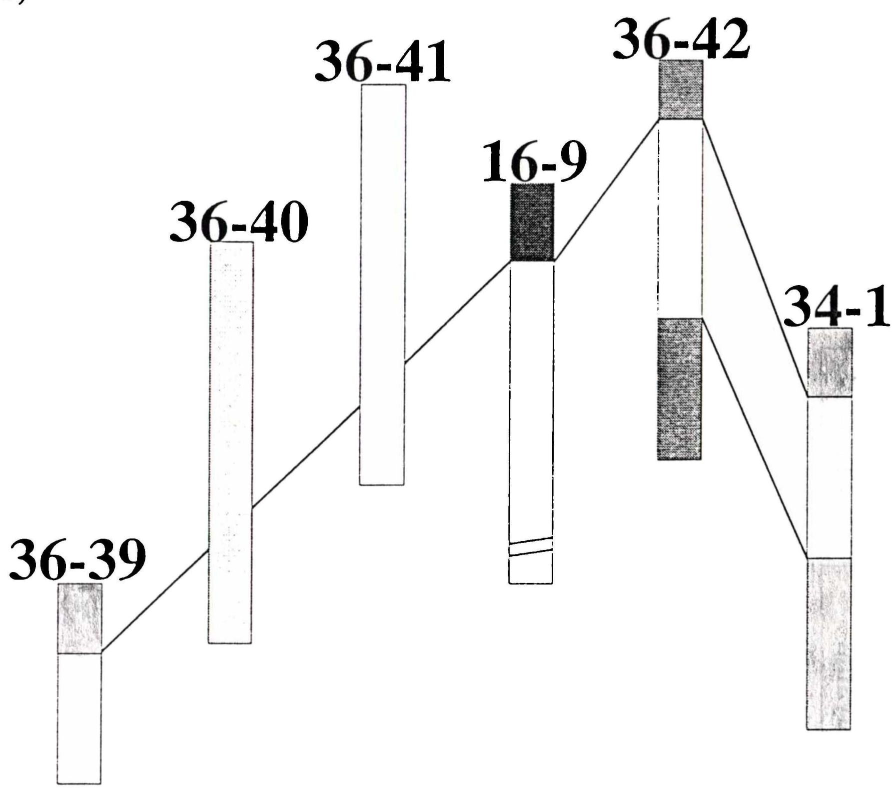

Fig. 3.5 Shows the correlation between four of the northern NZSSO cores of this study, based on colour changes downcore. Though cores 36-41 and 36-40 do not show colour changes, correlation can be made due to textural changes (see Section 4.3)

- Many cores show evidence of low sedimentation rates through the presence of manganese-rich sands and micro-nodules and of glauconite (Plate 3.1 A-C). Manganese-bearing material dominates the surface sediments of cores in areas washed by fast moving currents, such as cores 16-8, Y11 (Fig. 3.4F) and DSDP 276 (beneath DWBC, Fig. 3.4E), and cores situated in deep water (3000-4700 m)

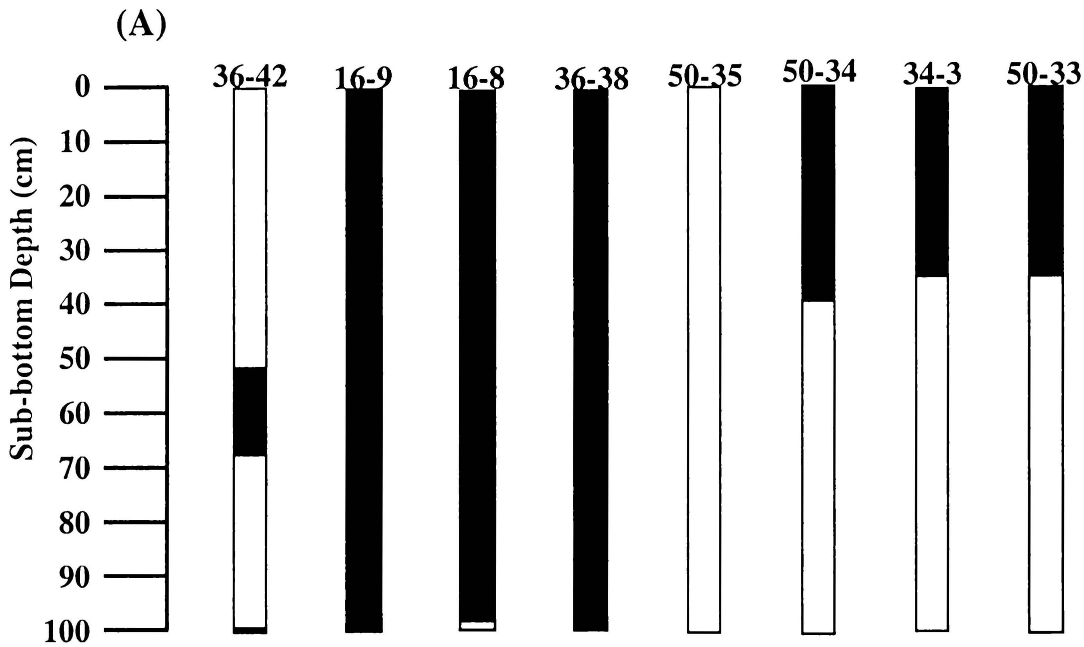

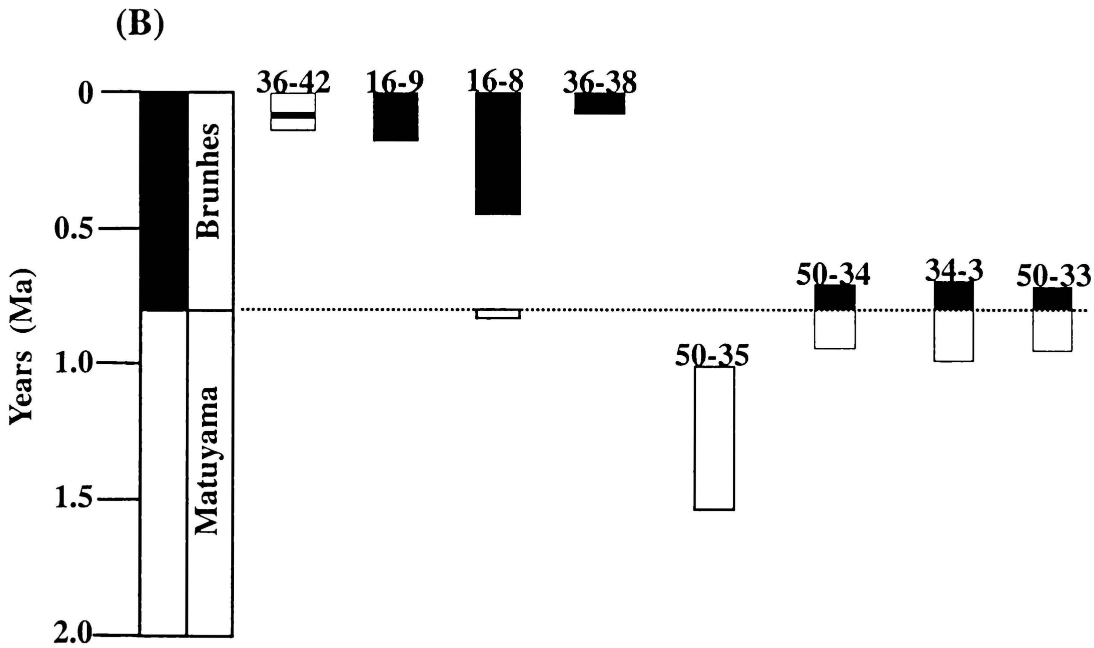

Fig. 3.6 (A) Paleomagnetic polarities for selected cores as a function of depth below the top of each core. Black areas represent times of normal polarity and open areas shows intervals of reversed polarity. (B) Shows assigned time ranges. Adapted from Watkins and Kennett (1972), Ledbetter *et al.* (1983), and Osborn *et al.* (1983).

beneath the ACC (i.e., Elt 36-37, Elt 36-35, Elt 36-36, Elt 16-1, Elt 16-2, Elt 16-4, Elt 16-6, 34-3, 50-34 and 50-35) (Glasby, 1976; Watkins & Kennett, 1977).

- Some of the cores mentioned above (34-3, 50-34, 50-35, 36-37, 16-4 and 16-6) show evidence of surface erosion and winnowing, forming hiatuses in the sediment record. Paleomagnetic (accompanied by biostratigraphic) dating of the sediments suggests cores within Emerald Basin, Southeast Indian Basin, and the western sector of the central junction between the Southeast Indian Ridge and Pacific-Antarctic Ridge are missing Brunhes sediment younger than about 0.6 Ma (Fig. 3.6). During the Brunhes (0-0.78 Ma) the abundances of erosional hiatuses decreases, suggesting a decrease in the intensity of ACC (and/or ACC-DWBC coupled) or CPDW (Osborn *et al.,* 1983).

These hiatuses in the sedimentary record result from either: (1) a lack of deposition through complete reduction in biogenic productivity. This is unlikely due to the moderate to high productivity of the subantarctic watermasses (Bradford, 1980 a/b). (2) The removal of sediment on a regional extent (Watkins & Kennett, 1972). The three sources of evidence for the removal of sediment by sea-bottom current activity comes from bottom current velocity measurements, sea-bottom photographs and sedimentology. Currents greater than 15 cm/sec are needed for the erosion of noncohesive particles of fine sand and finer sizes and may be effective on coarser sand-sized fractions (Heezen & Hollister, 1964).

Current speeds of 10-50 cm/sec have been recorded in the region, sufficient to mobilise cohesionless sediment (Gordon, 1971; Goodell *et al.,* 1973). Bottom photographs of rippled seafloor (e.g. Plate 1.1) corroborates the measured velocities. Areas of Brunhes sedimentation are dominated by lower velocity currents. The sedimentology of the scoured regions is dominated by a coarser, higher density fraction (Watkins & Kennett, 1972). Sites of extensive erosion in the NZSSO are found in the south Emerald Basin and Southwest Pacific Basin. This contrasts with cores from the Tasman Basin, Southeast Indian Ridge, Campbell Plateau and Antarctic Continental Rise, where Brunhes or Brunhes and upper Matuyama sediments are widespread (Fig. 3.7) (Goodell & Watkins, 1968; Watkins & Kennett, 1972; Watkins & Kennett, 1977; Osborn *et al.,* 1983).

- DSDP 276 and Y11 (Fig. 3.4 E and F) lie in the Campbell Drift region (along the slope margin of Campbell Plateau), and have a dominantly gravelly, sandy silt texture, with ferro-manganese varnish coating the sand grains which are very well rounded (Ovenshine *et al.,* 1973). Little biogenic sediment, calcareous or siliceous,

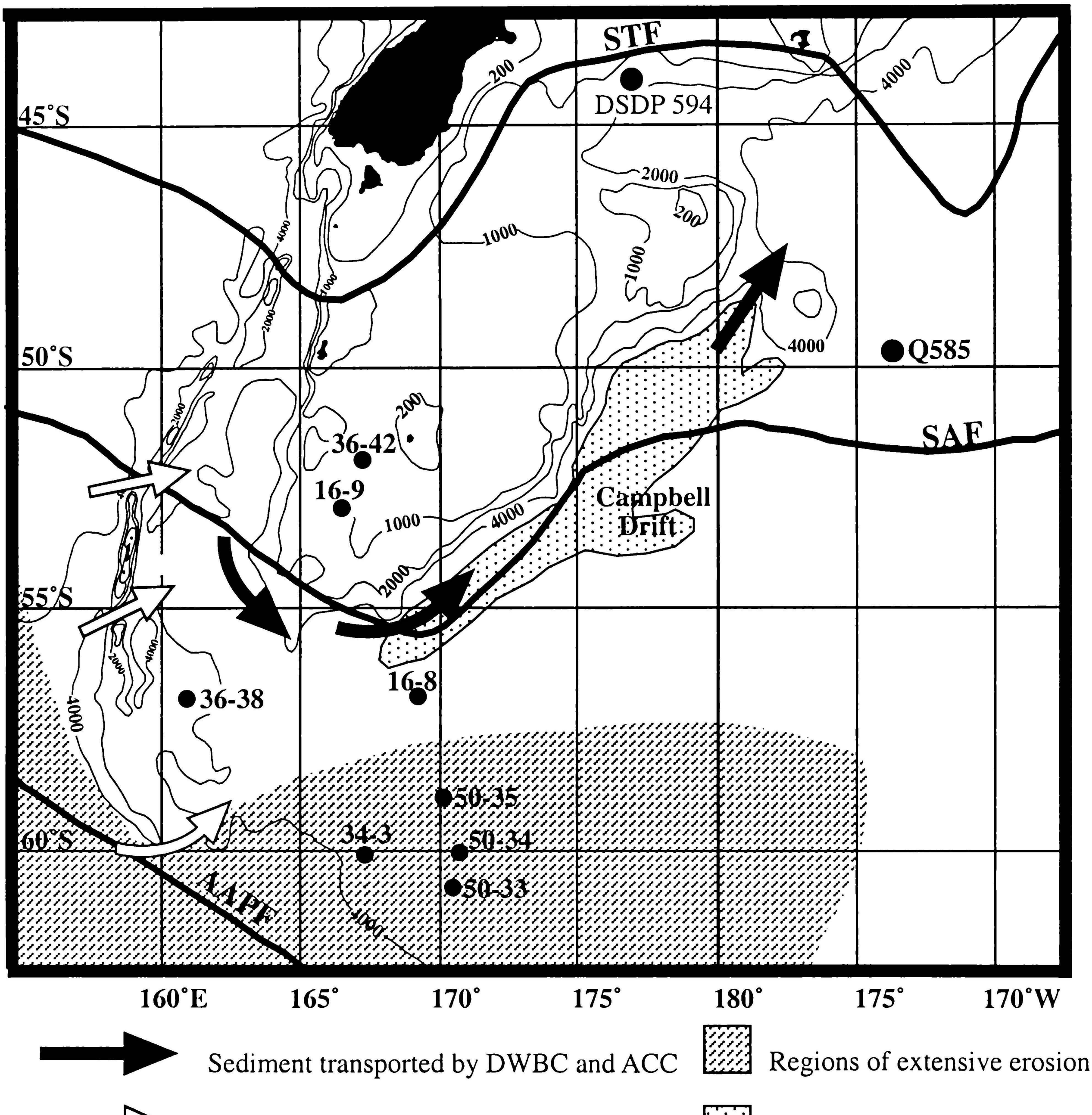

Fig. 3.7 Flow directions and sediment transport paths of the coupled DWBC + ACC (from Carter *et al.,* 1996a/b), and areas of extensive (paleo)erosion based on paleomagnetic age distributions in cores from the southern NZSSO(from Watkins and Kennett, 1972, 1977; Osborn *et al.,* 1983). Core Q585, is a NZOI coreused for later discussion as is DSDP site 594.

is associated with these drift sediments, and any biogenic material present is typically fragmented, the calcareous material being affected moreso than the siliceous. Core 16-8 lies on the southern edge of the Campbell Drift (Fig. 3.7) and has similar sedimentary types and textures as those described for DSDP 276 and Y11. NZSSO core 16-8 contains a high proportion of coarse rock and biogenic debris throughout, which is strongly abraded and thus certainly reworked, which is constructing a accretionary deep-sea sand (Carter & McCave, 1997).

3.4 Summary

From the lithostratigraphic evidence of the studied NZSSO cores and other cores from the region, the NZSSO cores can be divided into two subsets. A northern group lying north of the SAF and on the southern margins of the Campbell Plateau, and a southern subset lying south of the SAF in the south Emerald Basin and Southwest Pacifc Basin.

The northern NZSSO cores can often be correlated on the basis of colour marked boundaries, lithology and sedimentary textures. The southern subset of NZSSO cores, due to variations in seafloor erosion and depositional history between cores, cannot readily be interrelated and correlated. Cores 50-34, 34-3, and 50-33 possibly exhibit similar trends as their paleomagnetic stratigraphy is similar. However, it is abundantly clear that rapid changes in environmental conditions at the seabed alter the resulting sedimentological records over relatively short distances in the NZSSO.

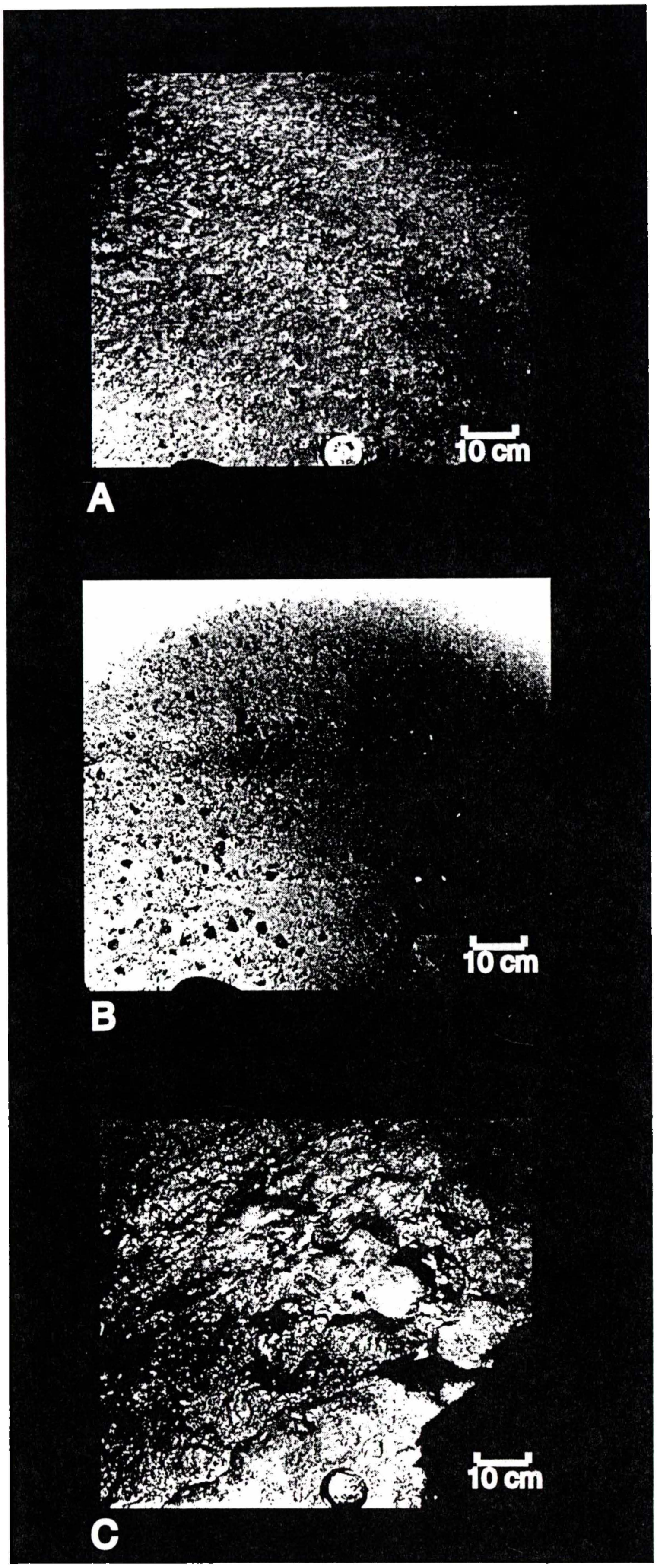

Plate 3.1 Manganese micronodules and nodules (A/B) are present over large areas of the Southwest Pacific Ocean. Nodules grow from direct precipitation from seawater, in areas becoming solid sheets plating the seafloor (C). The photographs were taken from the region of extensive erosion depicted in Fig. 3.6, near the southern NZSSO cores (34-1, 50-33, 50-34 and 50-35). Source Jacobs *et al.*, 1970.

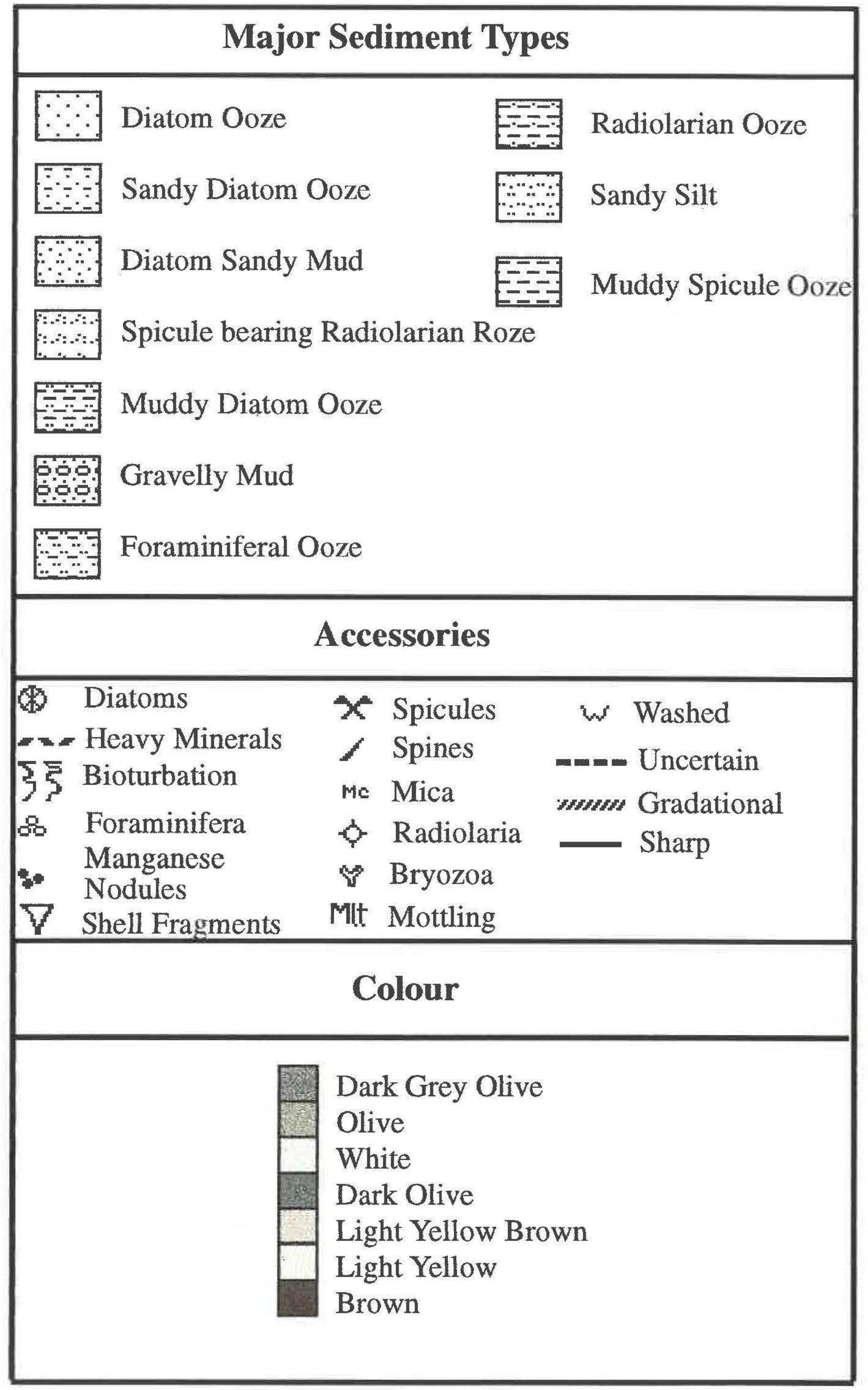

Legend for Fig. 3.2 Lithostratigraphic Columns

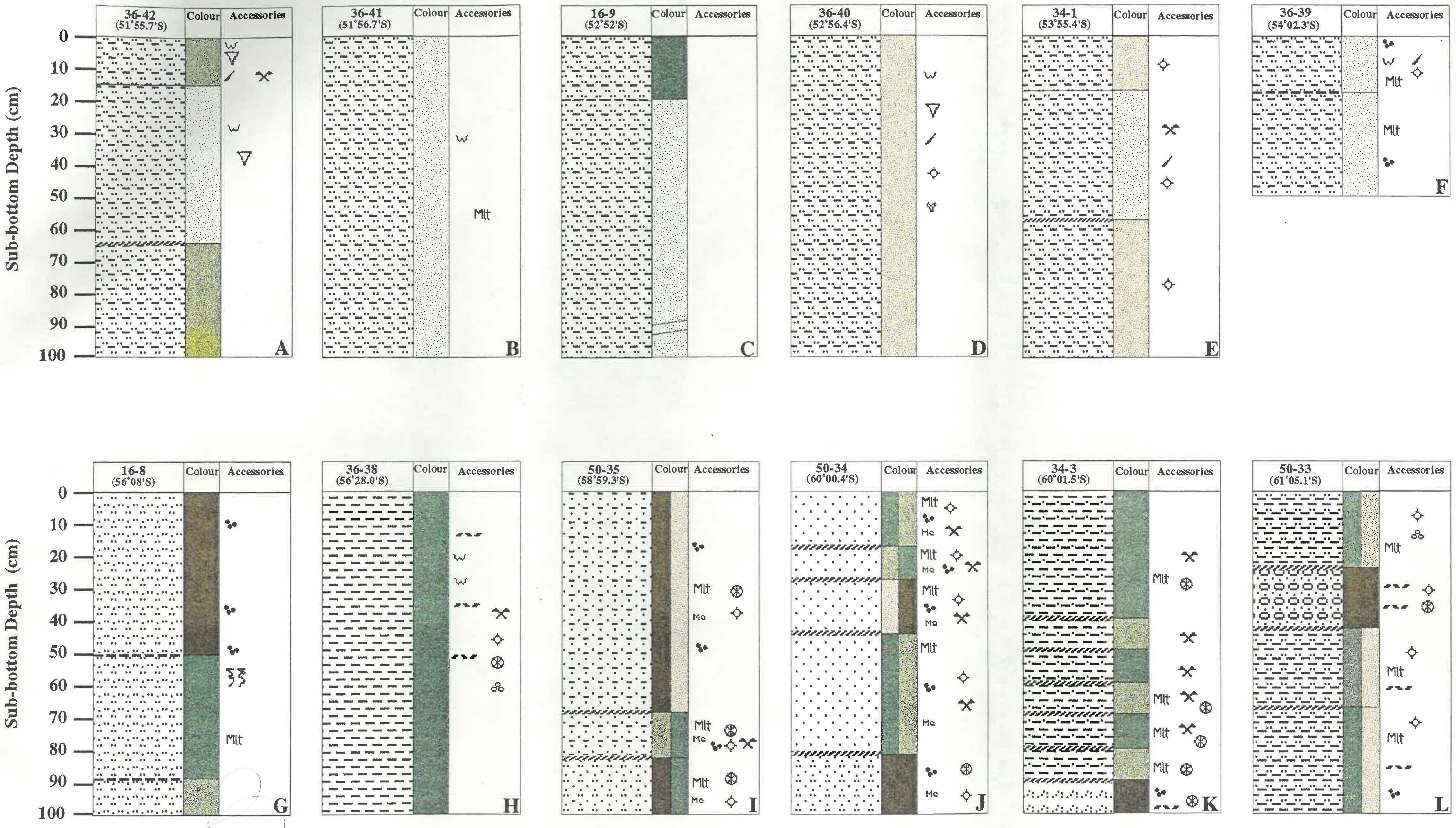

Fig. 3.2 Lithostratigraphic columns, compiled from *USNS Eltanin* Core Descriptions (Goodell, 1967; Florida State University, 1971, 1973) and personal observations.

Chapter Four:

Textural Characteristics of Cores

Chapter Four: ***Table of Contents***

4.1 Introduction

This chapter describes important trends within the sediment textural data, and what dominant textural characteristics can be determined based on core location, depth, and surrounding topographical features. The textural data were obtained by a combination of sieving and the use of a Malvern laser-sizer particle sizer. The main textural size classes determined were mud (<63 μm), fine sand (63-125 μm) and coarse sand (>125 μm) (Appendix 2). For micropaleontological and stable isotopic studies the fine and coarse sand were resieved over a 150 μm mesh to give revised fine sand (63-150 μm) and coarse sand (>150 μm) fractions (Appendix 3). The down core textural trends are summarised in Figs. 4.1 and 4.2. The latter (resieved/revised data) is used to discuss textural trends within each core.

The mud textural component (< 63 μm) has been analysed on the Malvern instrument to determine the silt (Z, 4-63 μm) and clay (C, < 4 μm) size classes within the broad mud textural class. The silt and clay textural classes derived from the mud component were recombined with the sieved sand textural classes to produce three bulk sediment textural classes, sand (S, > 63 μm), silt (Z, 4-63 μm) and clay (C, < 4 μm). These are used to discuss the textural implications and characteristics of the NZSSO cores of this study.

Gravel-sized material is absent from samples except in cores 36-38 and 16-8, where it is a minor fraction and often not represented in sample splits. Accordingly, it is noted in the bulk sample characteristics in Section 5.3 only.

4.2 Textural Classification

The bulk texture for the NZSSO cores, using the recombined data (sieved and laser sizer), was determined using the ternary plots (Fig. 4.3) of Folk (1968) and Lewis & McConchie (1994).

The texture of bulk sediments from the NZSSO cores lies in four of the textural classes outlined in Fig. 4.3. The three dominant textural classes are sandy mud, muddy sand and sandy silt, while a slight overlap exists into silty sand forming the fourth minor textural class (Fig. 4.4). The NZSSO cores in this study are divided by the SAF into a northern (north of the SAF) and a southern subset (south of the SAF) (Figs. 1.4 and 3.3). The bulk textural data for the two subsets are shown in Fig. 4.5 A and B.

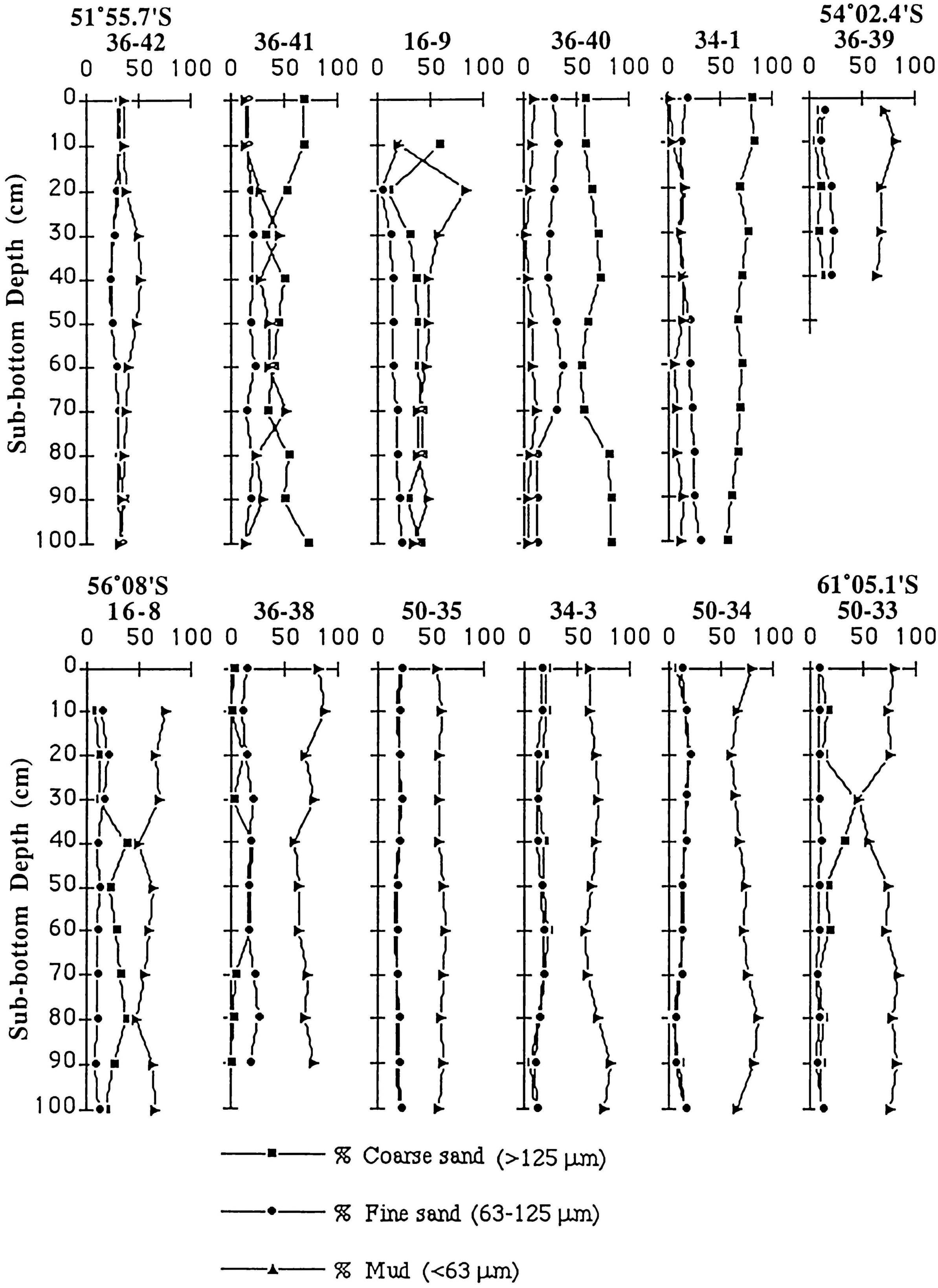

Fig. 4.1 Textural curves for NZSSO cores, compiled from data tabulated in Appendix 2.

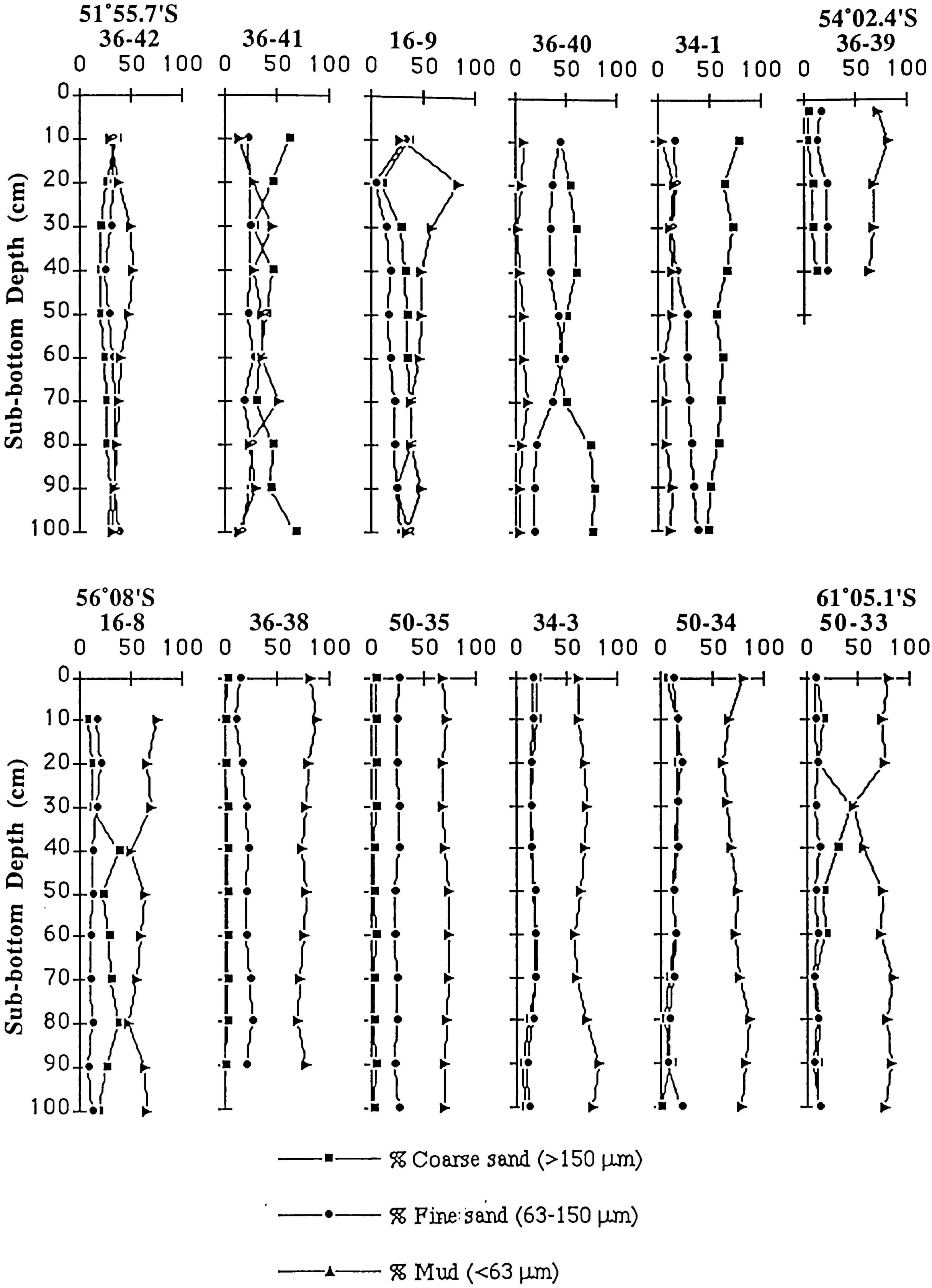

Fig. 4.2 Textural curves for NZSSO cores, compiled from resieved data (Appendix 3) using 150 µm as the boundary between fine and coarse sands.

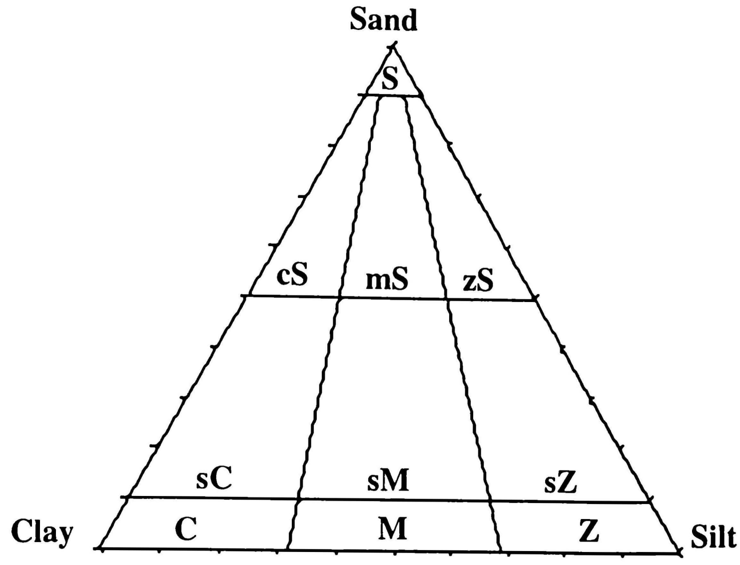

Fig. 4.3 Textural classification used for the NZSSO cores. S, sand; cS, clayey sand; mS, muddy sand; zS, silty sand; sC, sandy clay; sM, sandy mud; sZ, sandy silt; C, clay; M, mud; Z, silt. From Folk (1968).

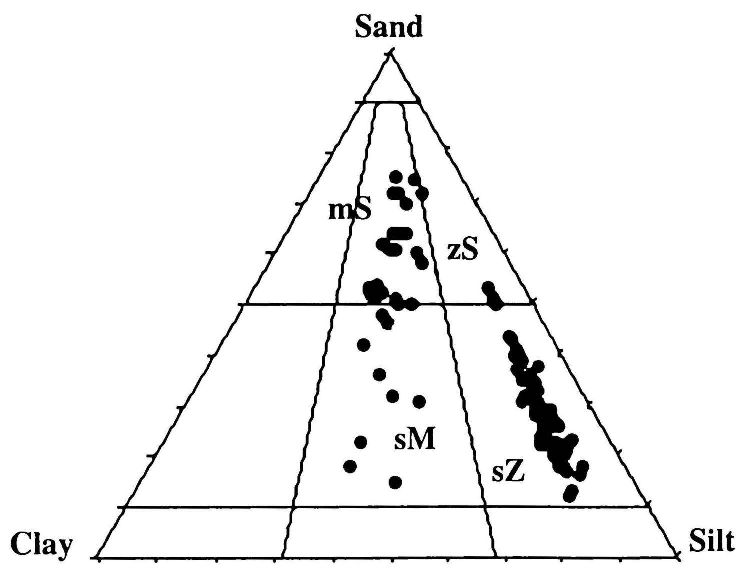

Fig. 4.4 Textural classes of the bulk sediment samples from NZSSO cores. Data from Appendix 3 and laser sizer data.

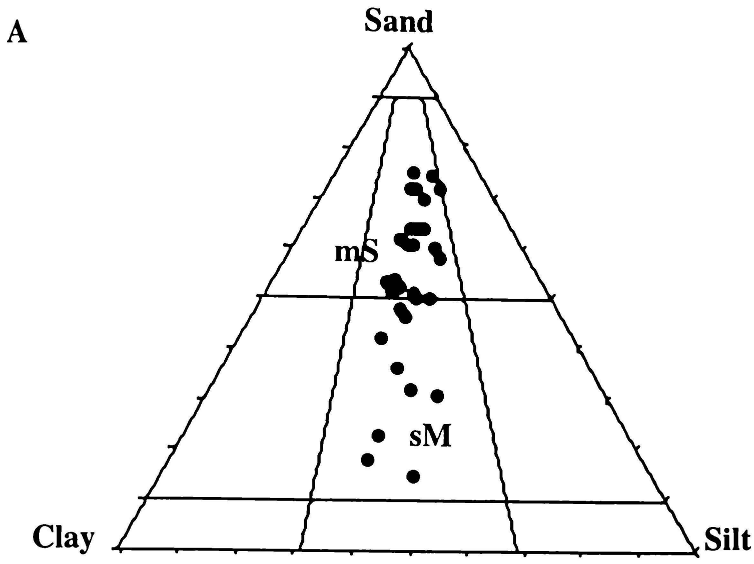

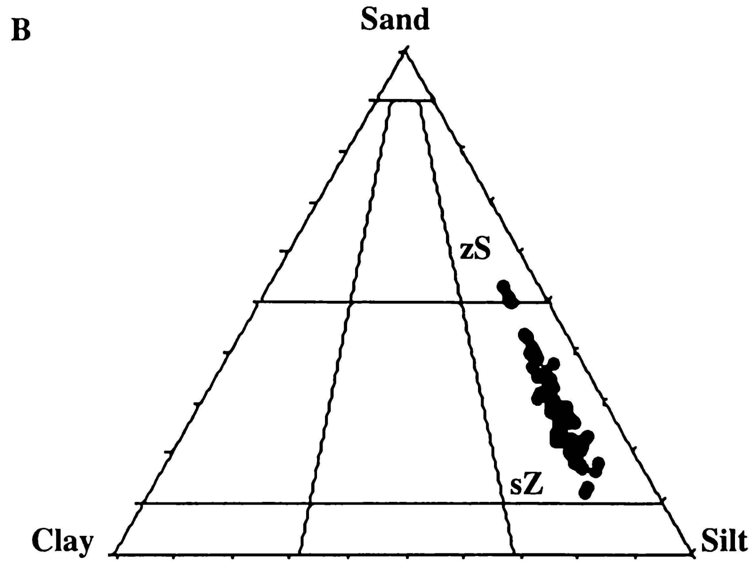

Fig. 4.5 Textural classes of samples from the northern (A) and southern (B) subsets of NZSSO cores. Data from Appendix 3 and laser sizer data.

These plots show there is a strong relationship between geographic location and texture. Samples from north of the SAF are sandy muds and muddy sands, while samples in the southern locations are sandy silts. This is emphasised by plotting the mean sand, silt and clay abundances for cores against their latitude (Fig. 4.6 A-C). The mean percentage trends of the bulk texture show that both sand and clay become less abundant south of ~56°S, the modern position of the SAF in NZSSO, while the silt content rapidly increases beyond this latitude.

From the three textural classes, and from data that will be presented in Chapters 5 and 6, three sediment facies are developed (Fig. 4.7). Facies A comprises the muddy sand textural class, Facies B is sandy mud, and Facies C is sandy silt.

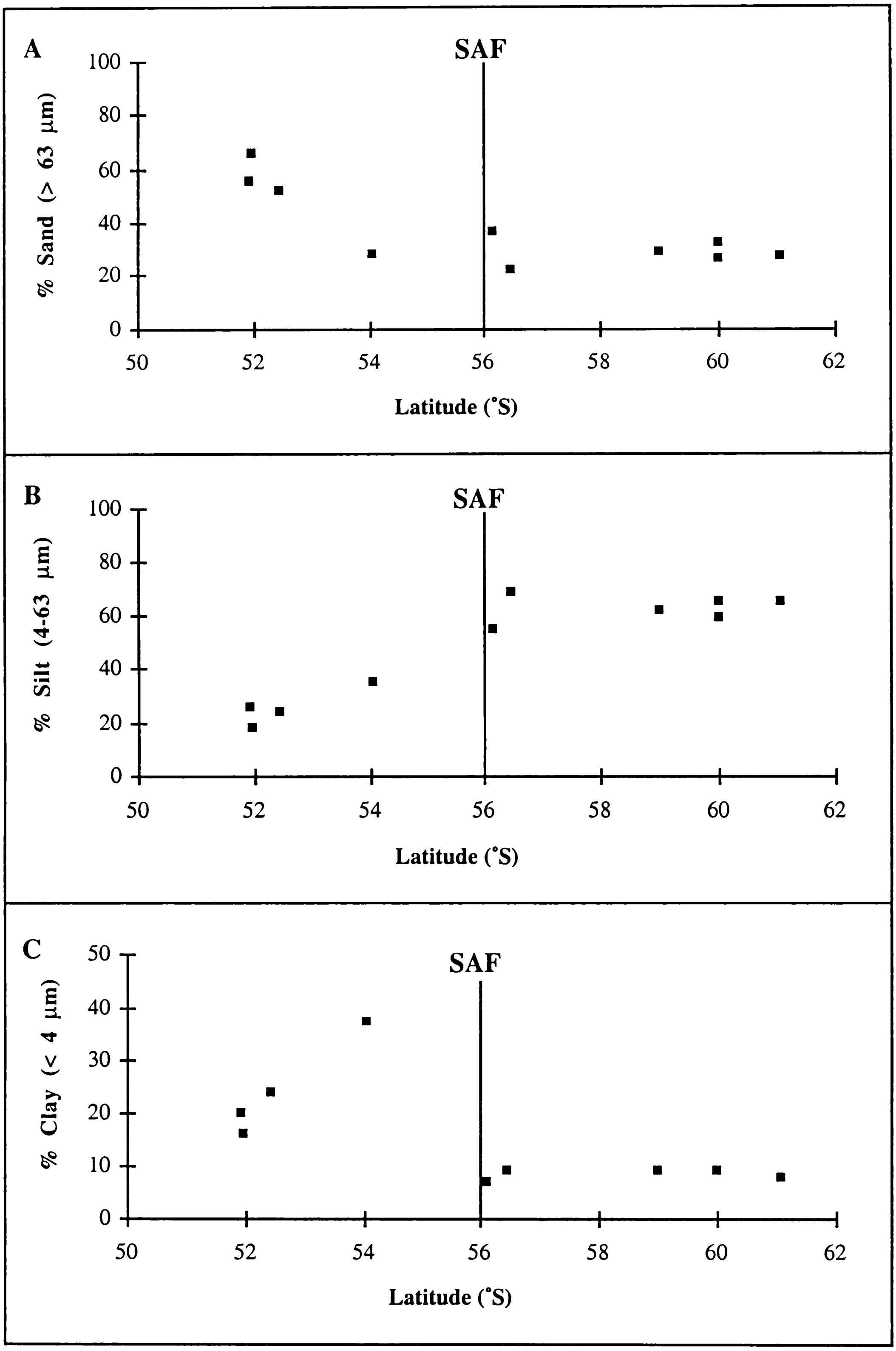

Fig. 4.6 Mean percentage of sand (> 63 µm)(A), silt (4-63 µm)(B) and clay (<4 µm) (C) in NZSSO core samples versus core latitude. Recombined data from Appendix 3 and laser sizer data..

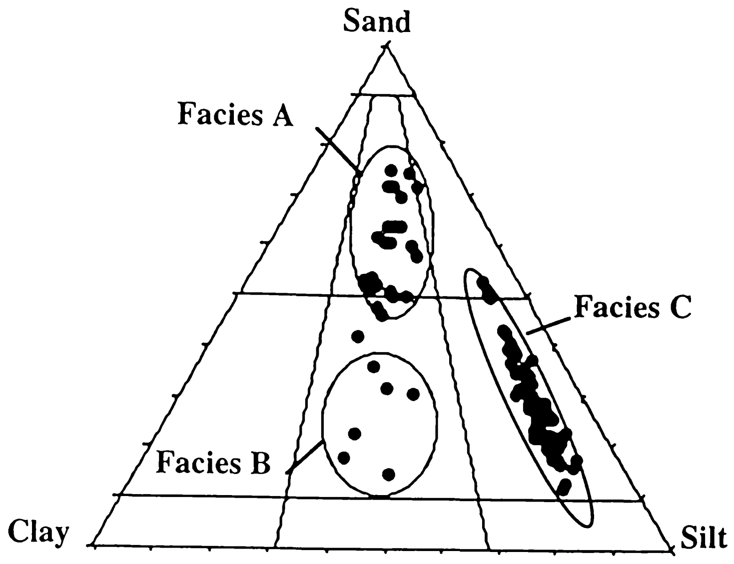

Fig. 4.7 Textural facies for NZSSO core samples. Facies A, muddy sand; Facies B, sandy mud; and Facies C, sandy silt. Data from Appendix 3 and laser sizer data.

Facies A and B constitute the northern subgroup of cores and Facies C the southern subgroup (cf. Fig. 4.5 A and B). Chapters 5 and 6 present evidence that shows that terrigenous material is rare to absent in the northern subgroup, and sedimentary textures are dominantly of biological origin. Facies A (muddy sand) are sediments composed mainly of calcareous planktic and benthic foraminifera; Facies B (sandy mud) is dominated by calcareous nannofossils; and Facies C (sandy silts), forming the southern subgroup, comprises sediments composed mainly of siliceous diatoms, nassellarian radiolaria and silt-sized terrigenous material. Table 4.1 summarises these facies associations.

Table 4.1 Facies Associations for Bulk Texture of NZSSO Cores

Facies	Textural classes	Dominant sediment composition
Facies A	muddy sand	Planktic and benthic foraminifera
Facies B	sandy mud	Calcareous nannofossils
Facies C	sandy silt	Diatoms, radiolaria and terrigenous material

4.3 Facies Correlation With Textural Core Logs

The textural facies can be superimposed onto the textural core logs (Fig. 4.8). For the northern cores there is an alternation downcore between Facies A and Facies

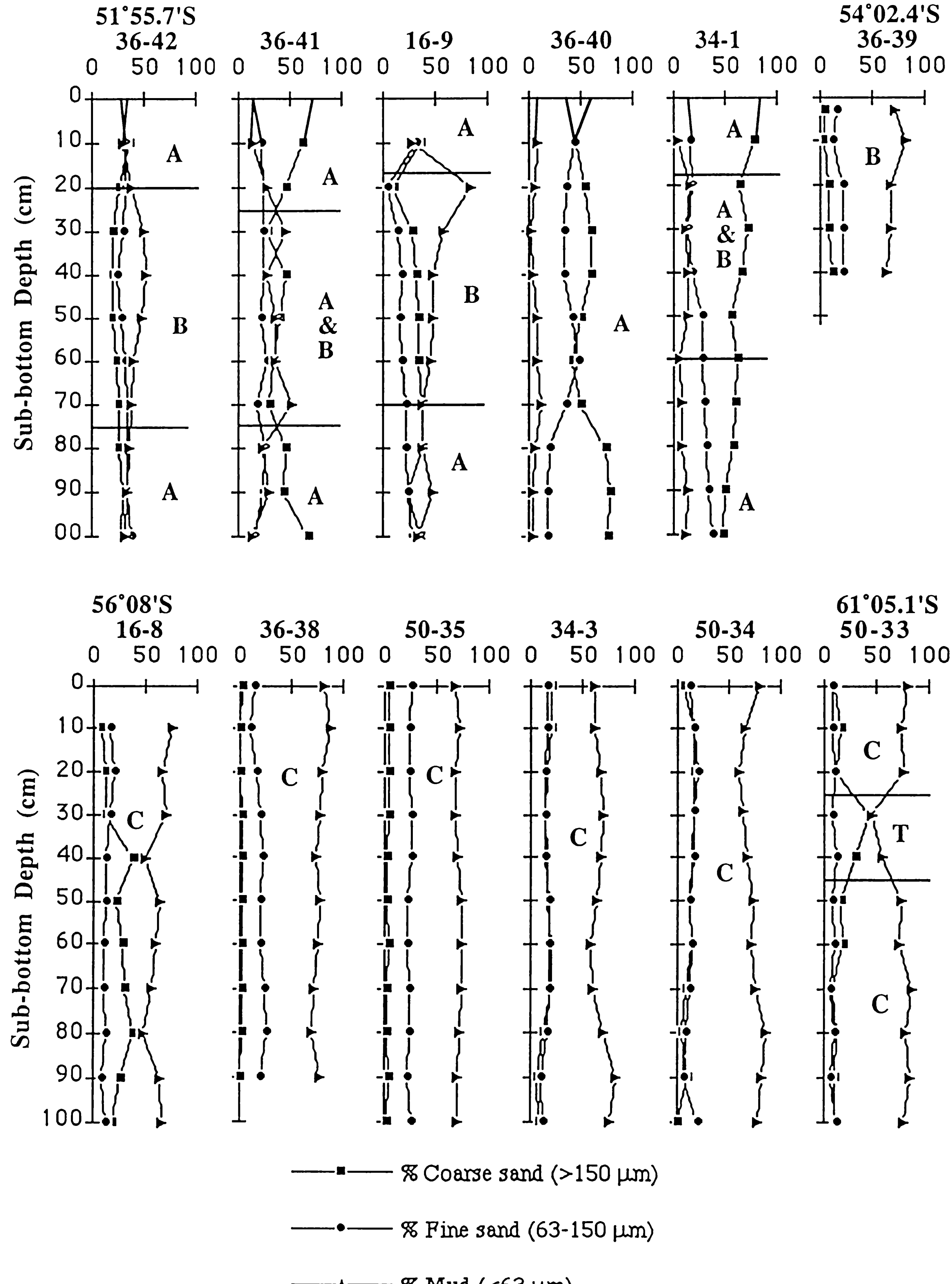

Fig. 4.8 Textural records for the NZSSO cores, with textural facies zones superimposed. A, Facies A; B, Facies B; C, Facies C; and T, Terrigenous. Compiled from Appendix 3 and laser sizer data.

B. Facies A lies between the core top and ~20 cm downcore, and occurs across four cores (36-42, 36-41, 16-9 and 34-1). The base of this upper Facies A zone corresponds with a colour change in cores 36-42, 16-9, 34-1 and 36-39 (Fig. 3.2). From the colour marked boundary at ~20 cm the record shows a change to Facies B. This zone extends downcore ~50 cm, and the mud (clay) size content increases associated with an increase in calcareous nannofossils. In cores 36-41 and 34-1 there is also an increase in clay-sized particles associated with the passage from Facies A into Facies B, although sand-sized material remains abundant; the texture represents a variant involving both Facies A and B. The base of Facies B zone lies between 60-75 cm downcore in four northern cores (36-42, 36-41, 16-9 and 34-1). This base represents a transition from Facies B back into a lower Facies A, and corresponds with another colour change across a gradational boundary (Fig. 3.2).

Two cores are exceptions to the above general pattern. Core 36-40 shows only Facies A for the full metre length of the core, and short-core 36-39, which has a colour boundary at ~18 cm (Fig. 3.2F), involves only Facies B throughout.

A feature of the northern subgroup is that the boundary between Facies B and the lower Facies A at ~60-75 cm downcore becomes shallower with increasing latitude (Table 4.2). The upper Facies A/B boundary may also exhibit this trend.

Table 4.2 Facies A/B Boundary Depth for Northern NZSSO Cores

Core	Latitude	Upper Facies A/B Boundary	Lower Facies A/B Boundary
36-42	51°55.7'S	~20	~75
36-41	51°56.7'S	~20	~70
16-9	52°25'S	~10	~70
34-1	53°55.4'S	~10	~60

Regional and global changes in climate and oceanic circulation are often represented by changes in textural facies and sediment composition. On this basis, the shallowing of facies boundaries downcore (Table 4.2) could indicate changes in biogenic sedimentation patterns. As latitude increases the core positions approach the SAF and sea surface temperatures decreases. The changes in the facies boundaries could be registering the approach of the SAF and a transition between sediments north of the SAF on the southern margins of the Campbell Plateau to sediments south of the SAF. Changes in sedimentation patterns across the SAF are discussed in Chapter 5 and 6.

The southern subgroup of cores shows only Facies C in the logs (Fig. 4.8). South of the modern SAF position there are a number of colour-change boundaries (Fig. 3.2), yet the textural records show very little variation downcore, particularly in cores 36-38, 50-35, 34-3 and 50-34. This indicates that the colour changes relate to some property other than texture, possibly compositional changes or watermass geochemical changes effecting oxidation and/or reduction of the sediments. Only NZSSO core 50-33 shows any textural variation downcore: Facies C extends from the core top to ~25 cm, then is sharply replaced by a terrigenous-dominated zone (T) which extends to ~45 cm downcore, after which Facies C again dominates. These textural changes are represented by colour boundaries. The terrigenous zone (T) represents an input of very coarse sand to gravel.

4.4 Interpretation of Facies and Textural Trends

- Using mean data, there are strong relationships between textural components (S, Z, and C) and latitude (Fig. 4.6) and water depth (Fig. 4.9). The textural shifts are related to changes in sediment composition. North of the SAF a change from sand-dominated to clay-rich sediments is associated with a change from sediments rich in planktic and benthic foraminiferal tests (Facies A) to sediments rich in calcareous nannofossils (Facies B) (cf. Nelson *et al.,* 1993a).

- South of the SAF little variation in texture is recorded and there is only one dominant facies, Facies C. Two cores (50-33 and 16-8) show some significant shifts, with increasing coarse sand and decreasing mud (Fig. 4.2). The decrease in mud fraction is associated with a decrease in silt content of samples, which suggests a decrease in the abundance of diatoms and radiolaria due to dilution by an increased flux of terrigenous material. Core 16-8 lies on the southern limit of the Campbell Drift along the lower slope margin of Campbell Plateau. An increase in coarse sand terrigenous material may indicate an intensification of paleocurrents winnowing seafloor sediments or an increased sedimentation of coarse sand-sized terrigenous material into the sediment drift in the past.

- The inferred sea-ice limit during the Last Glacial Maximum (LGM) possibly lay over the southern NZSSO core sites (Fig. 4.10). This suggests that an age structure could be determined for core 50-33 (i.e. LGM position is recorded by the terrigenous increase ~24 cm downcore). However, the paleomagnetic stratigraphy (Fig. 3.6) for core 50-33 suggests that the top 0.6 Ma or so of sedimentary record is lost. Paleomagnetic data from Ledbetter *et al.* (1983) places the terrigenous

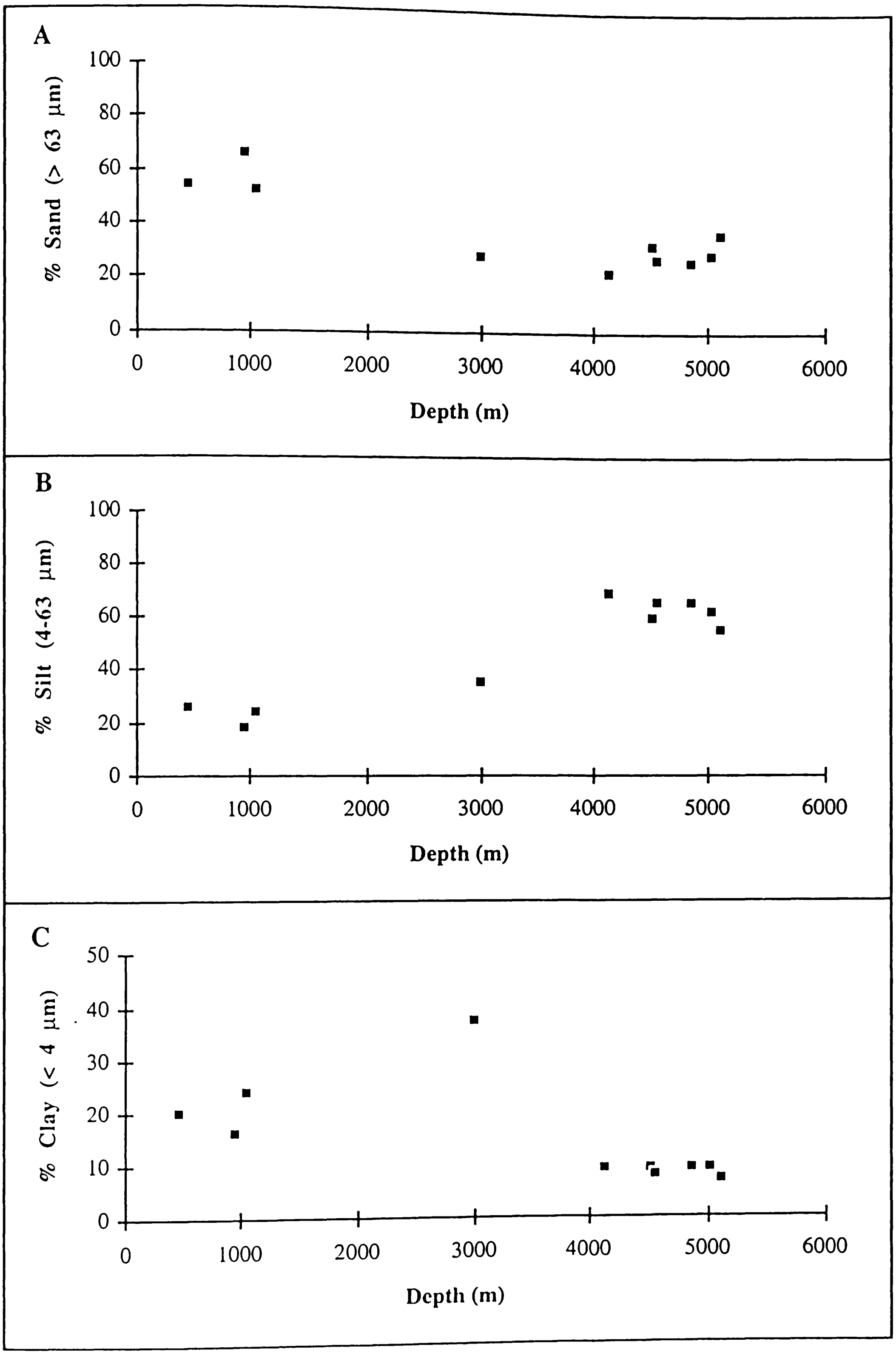

Fig. 4.9 Variation in mean percentage of textural size classes with water depth for the NZSSO cores. Data from Appendix 3 and laser sizer data.

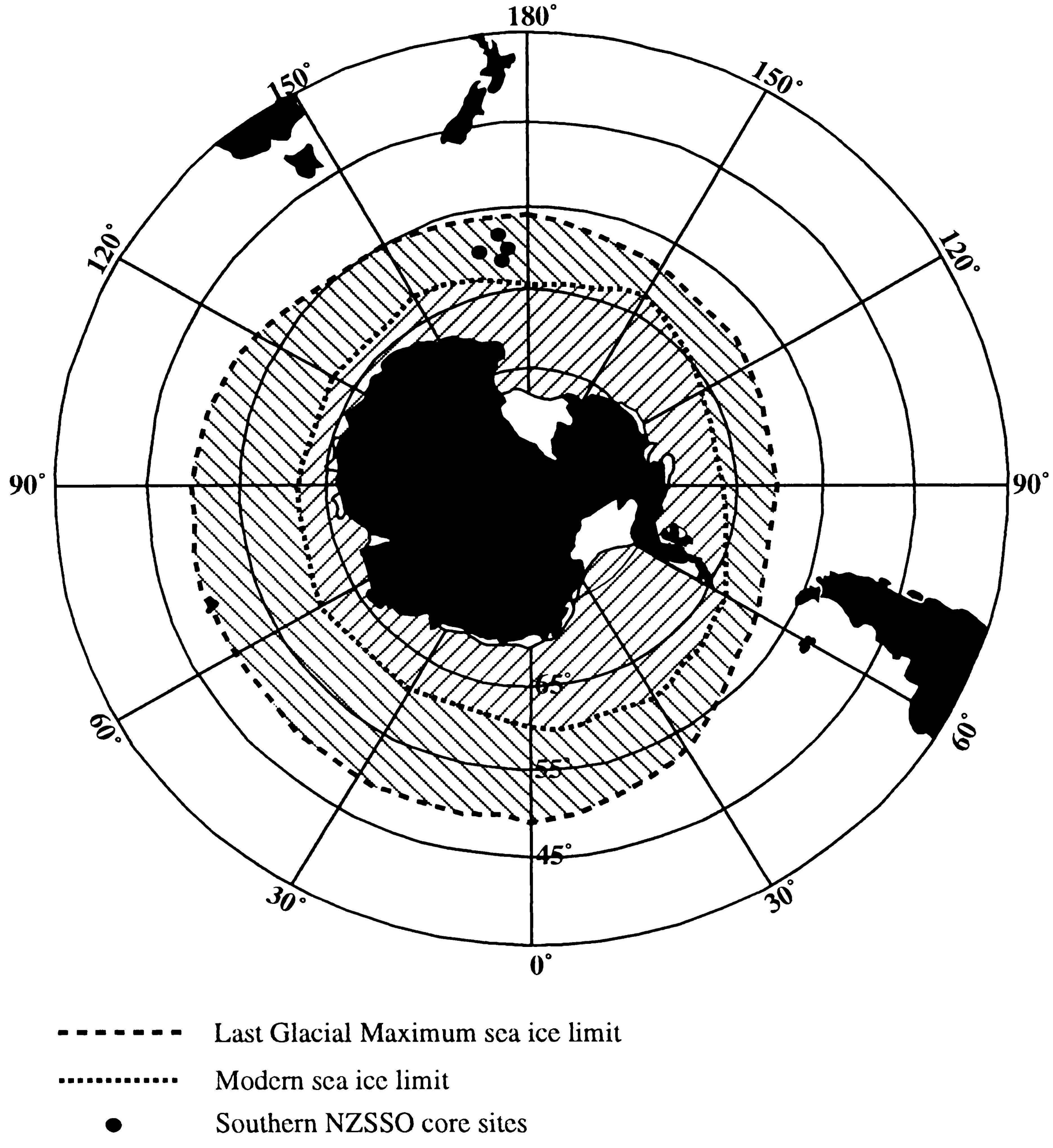

Fig. 4.10 Map of the Southern Ocean showing inferred sea ice limit during the Last Glacial Maximum and modern sea ice limits. Adapted from Climap Project Members (1981) and Heusser (1989).

influx during the mid-Pleistocene, possibly during glacial period oxygen isotope stage 16. Fig. 3.2L shows the sediment over the interval of coarse sand increase becomes a gravelly mud (Facies T in Fig. 4.8), and it contains an increased abundance of identifiable ice-rafted debris.

- Silt abundance increases with water depth in the NZSSO cores (Fig. 4.9). In the shallower cores from north of the SAF the sand fraction is dominated by the tests of planktic and benthic foraminifera. South of the SAF this biogenic material is rare to absent from the sediment, due to dissolution and habitat ranges of planktic and benthic species (Section 5.4). As water depth increases the abundance of clay-sized particles decreases associated with loss of calcareous nannofossils due to dissolution.

  The increase in silt sizes with water depth represents the residual sediment, below the lysocline and calcium carbonate compensation depth, composed of dissolution resistant diatom and finer nassellarian radiolarian material. Due to the position of the deeper cores south of the SAF, the predominant sediment inputs are silt-sized. The dominant source of sand-sized material comes from the deposition of ice-rafted debris, which is evident in core 50-33 where the coarse sand peaks to ~48% (Fig. 4.2). The rapid decrease in clay-size sediment and increase in silt-sized material occurs between 3000-4000 m for the NZSSO cores. This rapid textural change indicates rapid changes from Facies A and B above 3000 m depth to Facies C below ~3300 m.

- Silt and clay abundance in the NZSSO cores has a strong relationship with latitude, the higher the latitude the greater the abundance of silt within the sediments (Fig. 4.6). This results from a decrease in clay-sized particles. The SAF is clearly defined by this relationship; all cores south of 56°S (where the SAF reaches the highest latitude as it is diverted along the southern margin of the Campbell Plateau) are silt-dominated.

4.5 Type Cores for Northern and Southern NZSSO

The above textural information for the NZSSO cores is summarised in Fig. 4.11. Northern cores north of the SAF contain Facies A to ~20 cm downcore followed by a sharp boundary into Facies B to from 60-75 cm, after which a gradational boundary leads into a lower Facies A which continues to the core base. The boundaries that divide the facies are colour marked.

Southern cores, south of the SAF, typically contain only Facies C. Colour changes downcore are not necessarily associated with facies changes. NZSSO core 50-33 shows a gravelly mud terrigenous-rich layer at ~24 cm downcore which represents both a facies and colour change, involving an increase in terrigenous material due to ice rafting.

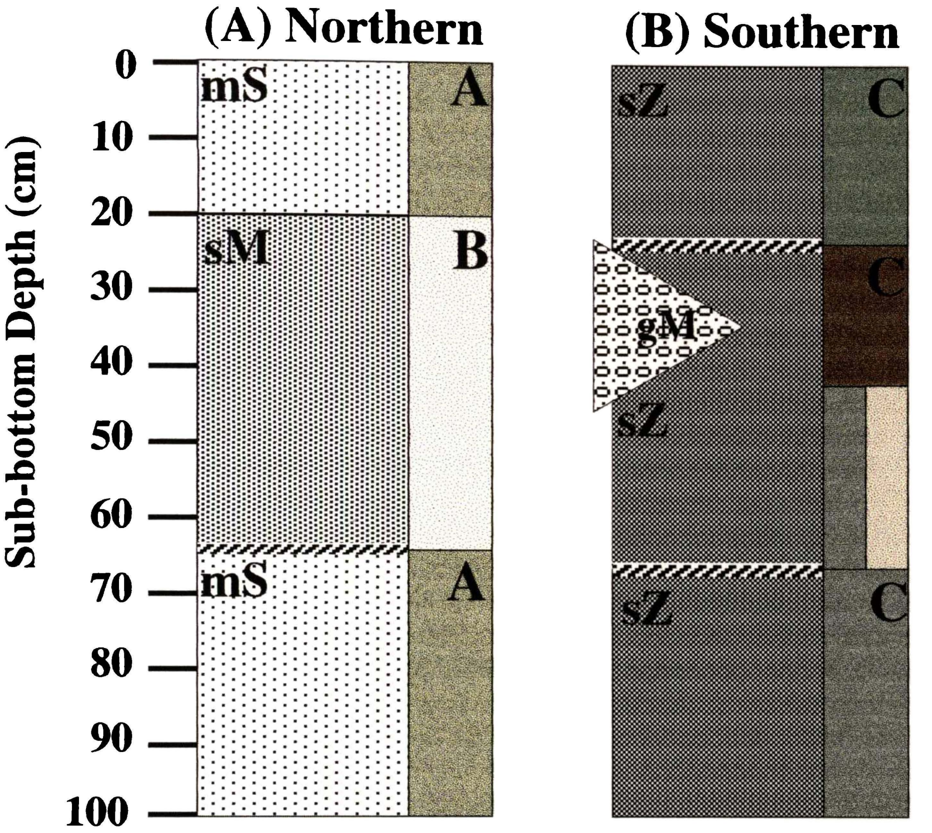

Fig. 4.11 Idealised sediment textural and facies relationships typical of NZSSO cores from north (A) and south (B) of the SAF. mS, muddy sand; sM, sandy mud; sZ, sandy silt; gM gravelly mud. A, B and C refer to Facies in Table 4.1. The two boundary types associated with the cores are: a sharp boundary at ~20 cm downcore in northern (A) cores and a gradational boundary ~25 cm downcore in the southern (B) cores. Colours approximate the actual colour code values in the core log descriptions.

Chapter Five:

Bulk Compositional Characteristics of Cores

Chapter Five: Table of Contents

5.1 Introduction

The compositional characteristics (Table 5.1) of the NZSSO cores ($CaCO_3$ content, major biogenic components and terrigenous material) are influenced by a number of factors. The dominant influences are latitude and topography since these determine the effects of watermass temperatures and current speeds across the ocean-sediment interface and the depths at which sediments lie. This chapter highlights the different sediment components and what trends develop from these compositional components for the NZSSO. Broad compositional changes occurring in the NZSSO cores are highlighted in Table 5.1.

Table 5.1 Coarse Sand (> 150 μm) Characteristics and Bulk Carbonate

Core	Depth (m)	CaCO3 %	Terrigenous %	Dominant Biogenic Components (Order of Abundance)
36-42	461	86-95	< 0.5	Forams>moll frags>spicules>echin spines
36-41	951	94-100	0.0	Forams
16-9	1052	87-100	< 0.5	Forams
36-40	783	93-100	0.0	Forams>moll frags>echin spine>bryozoa
34-1	1041	93-98	0.0	Forams>echin spine>rads
36-39	2999	95-99	< 1.5	Forams>echin spine>rads
16-8	5117	0.0-4	40-80	Sand>silt >rads>forams
36-38	4129	10-18	5-11	Spicules>rads >dia>forams
50-35	5024	< 1.0	8-12	(Muddy) dia>rads>sand
50-34	4863	< 1.0	6-21	Dia>rads>spicules>sand
34-3	4517	0.5-1.5	5-13	Rads>dia>spicules
50-33	4550	0.0-13	4-27	(Muddy) dia-rads>sand-gravel

Forams - planktic and benthic combined; Moll - mollusca; Echin - echinoderms; Rads - radiolaria; Dia - diatoms. Data from Goodell (1968) and Florida State University, (1971, 1973) in Appendices 2 and 5.

5.2 Carbonate Content of Bulk Samples

$CaCO_3$ trends clearly show northern cores 36-42 (52°S) to 36-39 (54°S) have a high $CaCO_3$ content (Fig. 5.1), which falls dramatically south of the modern SAF at ~56°S in the NZSSO (Fig. 5.2). Cores north of the modern SAF with high $CaCO_3$ values show little variation downcore; cores 36-42 and 16-9 show increasing $CaCO_3$ percentage from core top to 20-30 cm downcore, 87-95% and 87-99% respectively. Cores 34-1 and 36-39 show insignificant increases between 10-20 cm. Another expected trend is the decrease in $CaCO_3$ abundances with water depth (Fig. 5.3). Lisitzin (1972) states the CCD for the South Pacific is ~4700 m. However, NZSSO

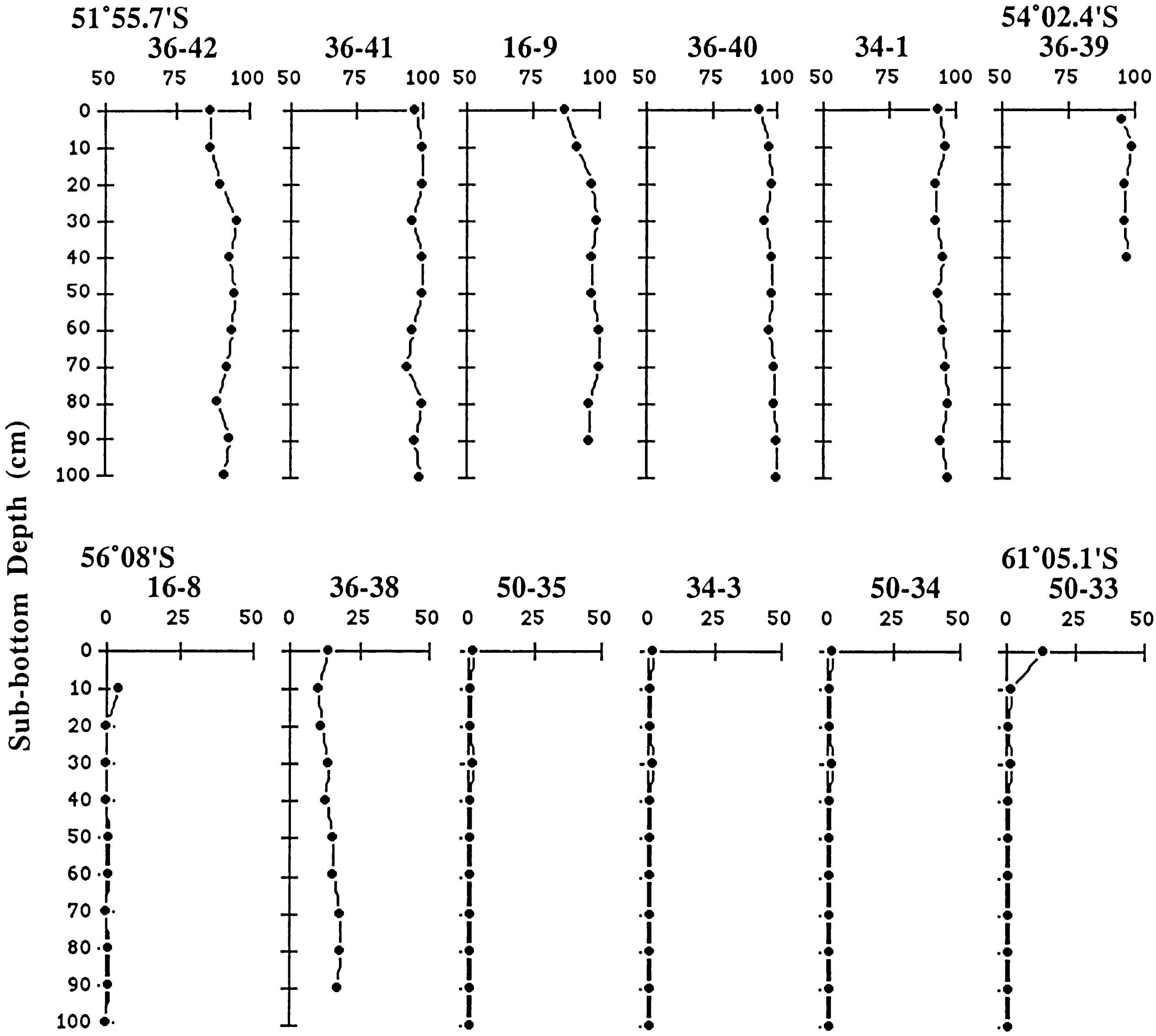

Fig. 5.1 Carbonate records (% $CaCO_3$) for the NZSSO cores. Data from Appendix 2.

core data show that calcareous sediments are surviving to depths of ~5000 m, suggesting perhaps a greater depth for the CCD (see Section 6.9.2).

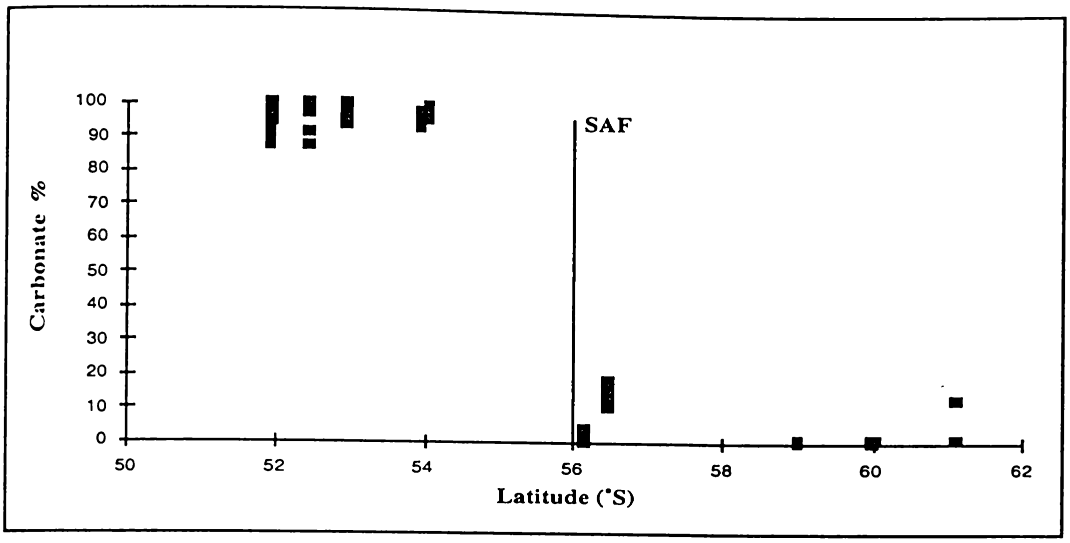

Fig. 5.2 $CaCO_3$ percentages plotted against latitude (°S) for the NZSSO cores. Data from Appendix 2.

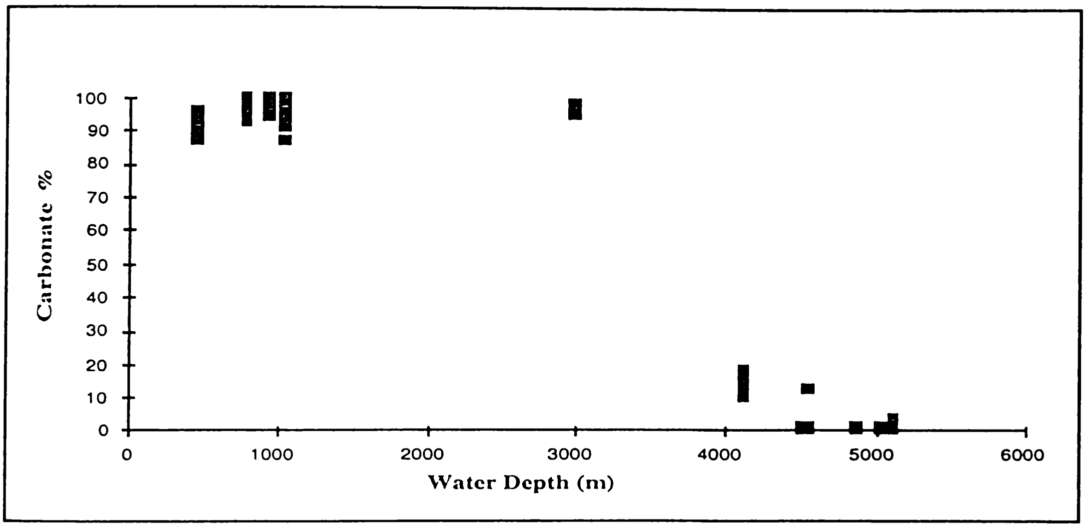

Fig. 5.3 $CaCO_3$ percentages plotted against water depth for the NZSSO cores. Data from Appendix 2.

$CaCO_3$ material in the NZSSO sediments is biologic in origin. $CaCO_3$ in the coarse sand and fine sand fractions originates mainly from planktic and benthic foraminifera; in the shallower water cores (e.g. 36-42 and 36-40), molluscan fragments and echinoderm spines also introduce carbonate to the sediment. Calcareous components in the mud fraction are due to nannofossils.

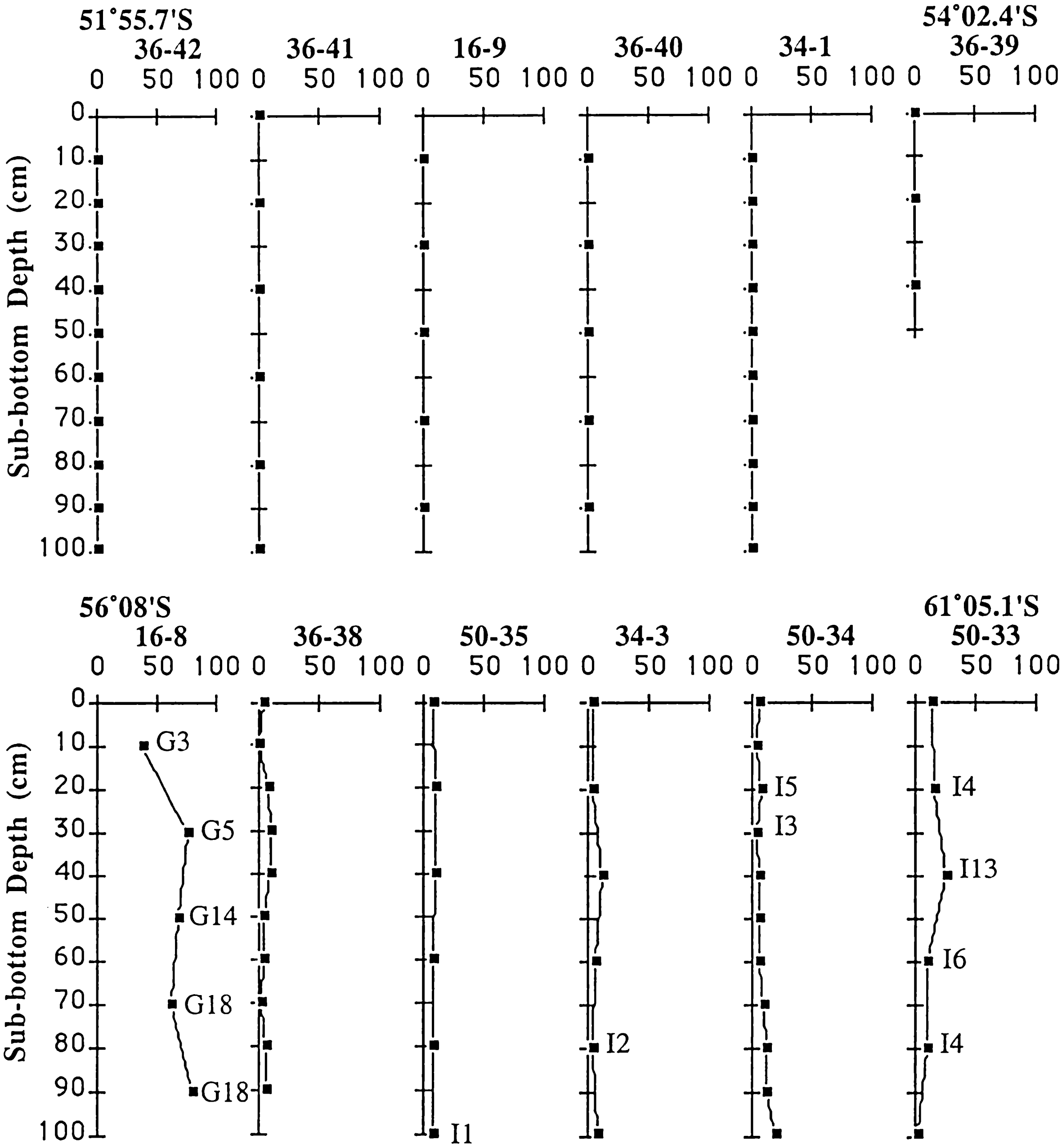

Fig. 5.4 Terrigenous material percentages for the coarse sand fraction of NZSSO cores. I indicates ice-rafted debris, G indicates terrigenous particles of gravel size, and the number indicates the number of that type counted. Data from Appendix 5.

5.3 Terrigenous Components

5.3.1 Terrigenous Abundances and Spatial Variations

NZSSO cores north of the modern SAF contain only trace amounts (<1%) of terrigenous material in the coarse sand fraction. The percentage abundance of terrigenous material rapidly increases south of the modern SAF (at ~56°S), in particular the occurrence of ice-rafted debris (Fig. 5.4).

The southern cores 16-8 to 50-33 show significant variation in coarse sand terrigenous patterns between cores (Fig. 5.4). Core 16-8 has the highest terrigenous content which increases downcore from ~40% of coarse sand at the top of the core to ~80% at core base. Associated with this increase in terrigenous percentage is the occurrence of gravel-sized (> 2 mm) material downcore, possibly associated with intensification of currents beneath a coupled ACC-DWBC. All terrigenous grains at this NZSSO site show evidence of previous fluvial reworking, and are well rounded with a ferro-manganese scale coating (Margolis & Krinsley, 1971; Ovenshine *et al.*, 1973; Carter *et al*., 1996a; Carter & McCave, 1997).

NZSSO cores 36-38 and 34-3 show terrigenous increases downcore of ~10% from 20 and 30 cm respectively; the increases are seen over a ~50 cm core section, before decreasing. Two outsized ice-rafted debris (IRD) fragments were found in core 34-3 at 80 cm depth downcore; the IRD comprised angular felsic rock fragments. These outsized terrigenous fragments were identified as IRD due to their size and angular nature.

Core 50-35 shows insignificant variation downcore, with coarse sand terrigenous components constituting ~10% of the sediment. Core 50-34 shows a steady increase in terrigenous material downcore, from ~5% at core top to ~21% at core base; 20-30 cm downcore an influx of IRD occurs. NZSSO core 50-33 shows terrigenous percentages increase downcore to ~27% at 40 cm, followed by a rapid decrease to the core base; the point of maximum terrigenous content is marked by the highest numbers of IRD (Fig. 5.4).

A semi-quantitative investigation was undertaken on the fine sand fraction of four cores (36-42, 34-1, 36-38 and 50-34) (Fig. 5.5). These cores displayed similar trends to those depicted in Fig. 5.4 for the coarse sand fraction. Cores 36-42 and 34-1, from north of the modern SAF, contained only trace amounts of terrigenous material (< 1%) (Appendix 6).

Terrigenous material in the fine sand fraction of core 36-38 comprises a greater percentage of the sediment than in the coarse sand fraction. Terrigenous material in the fine sand fraction ranges from 8-32% (Fig. 5.5; Appendix 6.3) in comparison to the coarse sand where terrigenous components constitutes between 1-12% of the sediment (Fig. 5.4; Appendix 5.8). Trends downcore of the fine sand fraction show an increase in terrigenous abundance between 20-70 cm (Fig. 5.5), which reflects the trend in the coarse sand fraction (Fig. 5.4). Core 50-34 contains greater terrigenous percentages in the fine sand fraction (7-48%), in comparison to the coarse sand fraction (5-21%). The downcore trends of the fine sand fraction (Fig. 5.5) reflect trends in the coarse sand fraction, showing a spike in terrigenous abundances at 20 cm. This corresponds to an increase in terrigenous material and ice-rafted debris in the coarse sand fraction (Figs. 5.4 and 5.5).

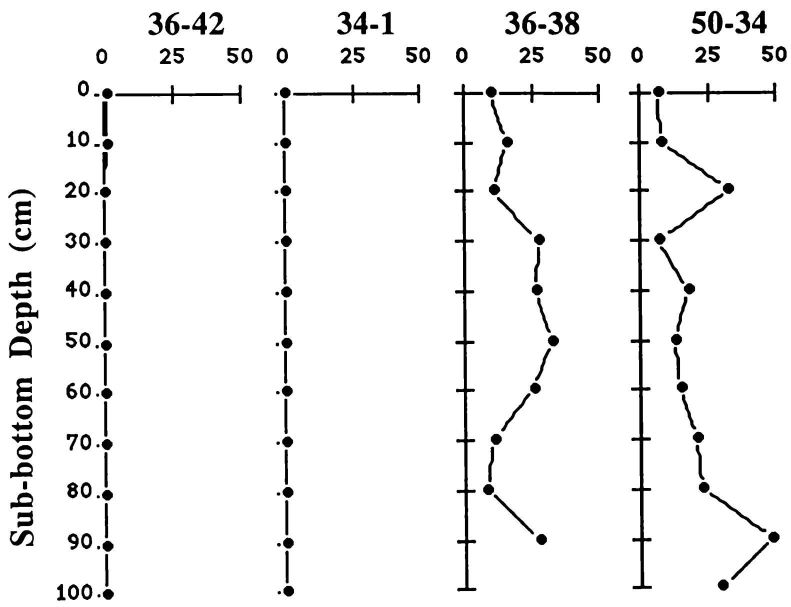

Fig. 5.5 Semi-quantitative census percentage records for terrigenous material in the fine sand fraction of the NZSSO cores. Data from Appendix 6.

The southward increase in terrigenous abundance (Fig. 5.6) shows an anomaly at ~56 °S (core 16-8) with terrigenous abundances ranging between 40-80 %. Core 16-8 lies at the southern margin of Campbell Drift (Fig. 3.6), a region of medium to coarse sand and possibly sandy gravel formed from the winnowing of Tertiary deposits (Ovenshine *et al.,* 1973). In the study area (52-61°S) the percentage of terrigenous material in the coarse sand fraction increases in abundance with depth (Fig. 5.7).

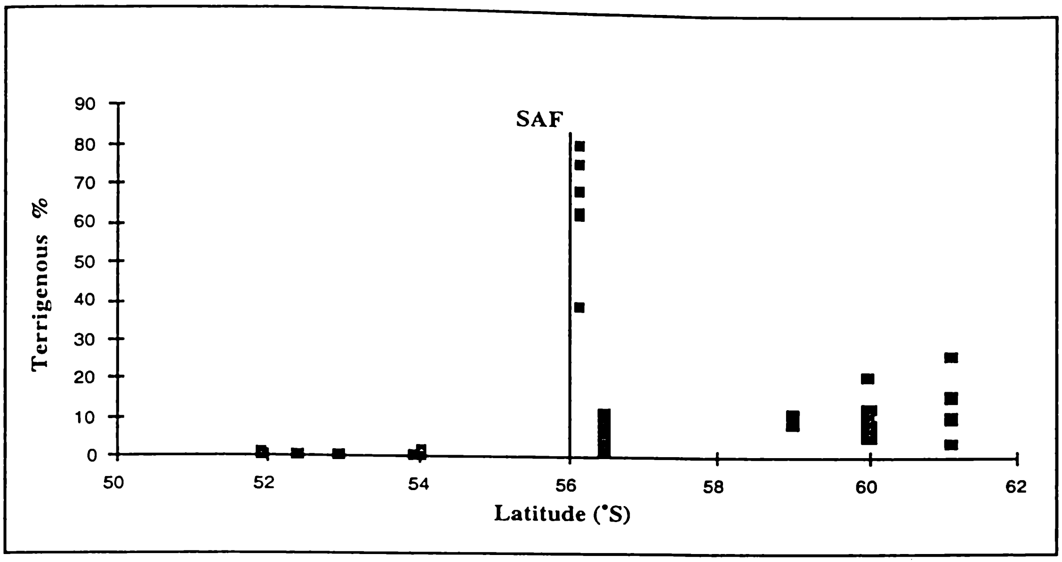

Fig. 5.6 Terrigenous percentages (> 150 μm) plotted against latitude (°S) for NZSSO cores. Data from Appendix 5.

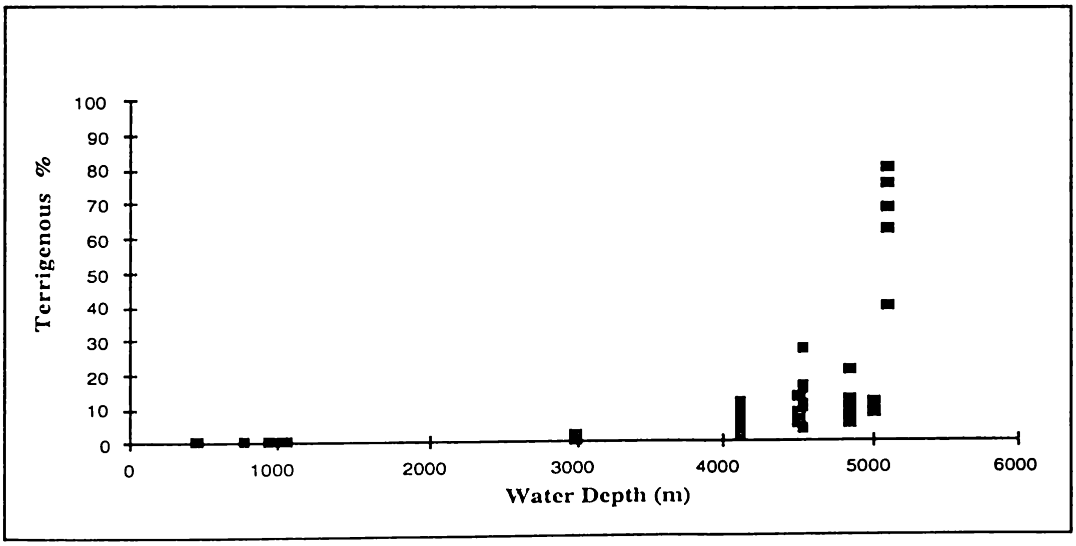

Fig. 5.7 Terrigenous percentages (> 150 μm) plotted against water depth (m) for NZSSO cores. Data from Appendix 5.

An attempt was made to see if a reciprocal relationship existed between the $CaCO_3$ and terrigenous record as used by Nelson *et al.* (1993a) off southeastern New Zealand to show an increase in terrigenous material in the hemipelagic sediment associated with the glacials. However, the presence of biogenic silica distorted any such relationship in the NZSSO core samples, and no reliable results were achieved.

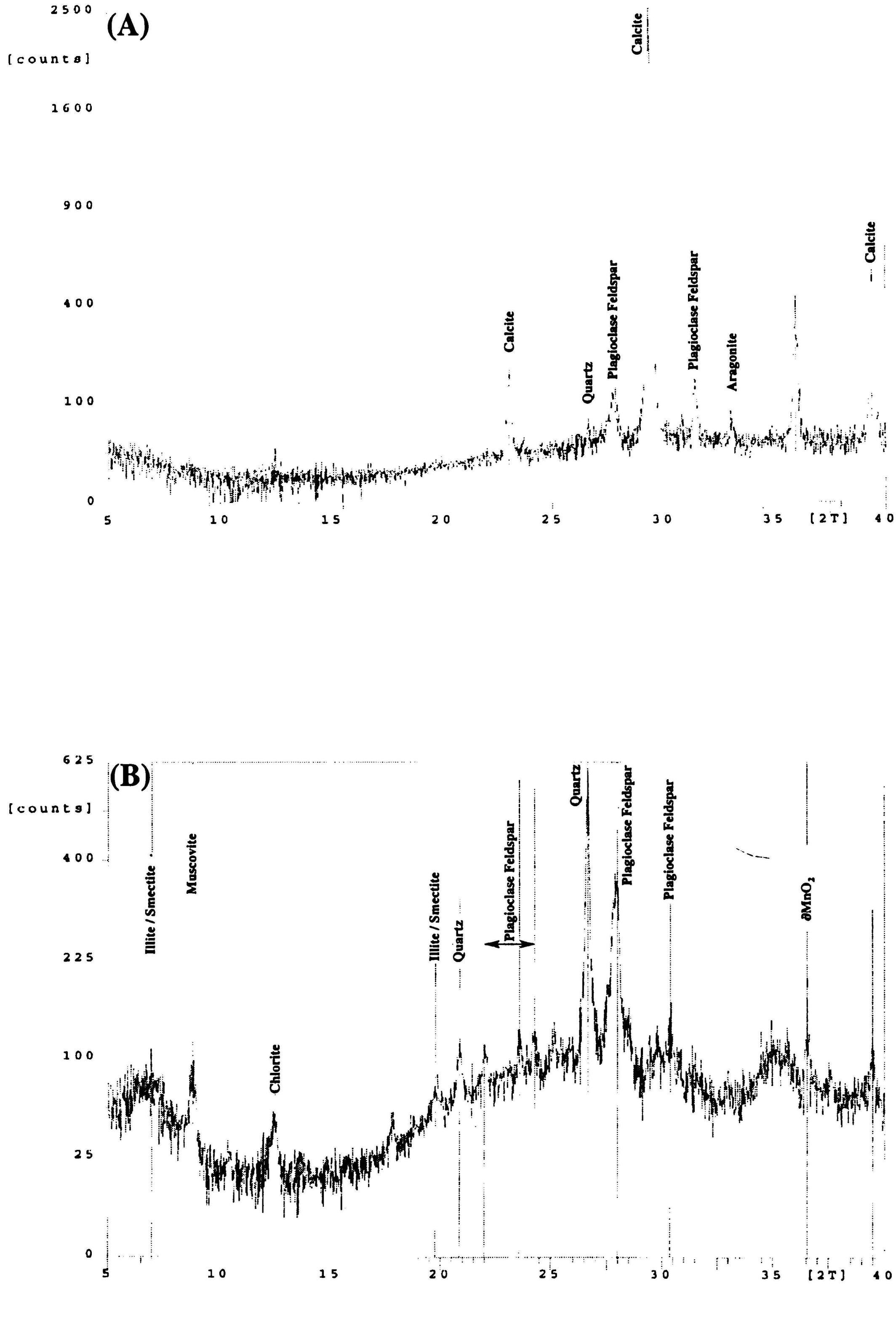

Fig. 5.8 (A) NZSSO core 36-42, XRD profile of sample from 60 cm down core. (B) NZSSO core 50-34, XRD profile of sample from 10 cm down core. The doming of the 50-34 background trace is due to a high concentration of amorphous silica from diatoms and radiolarian fragments.

5.3.2 Terrigenous Material Composition

From petrographic studies of whole grain mounts, terrigenous components were found to be dominantly quartz and plagioclase feldspars, dominantly in the coarse and fine sand fractions, with ice-rafted debris containing whole angular felsic rock fragments ranging to gravel size.

The determination of terrigenous composition of the mud fraction was achieved by two methods: smear slide and X-ray diffraction (XRD) analysis. The mud fraction from four NZSSO cores was analysed (36-42, 34-1, 36-38 and 50-33). Smear slide analysis showed core 36-42 contained glauconite in the top 20 cm, which decreased in abundance downcore. Mica was present throughout the 1m length of core, with heavy minerals present at 60 and 80 cm. Core 34-1 contains only trace amounts of glauconite and mica at 20 and 80 cm. Core 36-38 has mica and heavy minerals predominantly throughout the 1m length, but with only trace amounts between 10-30 cm depth downcore. Core 50-34 contains abundant mica and trace amounts of heavy minerals throughout the 1m core (Table 5.2).

Table 5.2 Smear Slide Analysis

Depth (cm)	36-42	34-1	36-38	50-34
0	glauc, mica		mica, hvy min	mica, hvy min
10	glauc, mica		mica, hvy min	mica, hvy min
20	glauc, mica	mica	mica, hvy min	mica, hvy min
30	mica		mica, hvy min	mica, hvy min
40	mica		mica, hvy min	mica, hvy min
50	mica		mica, hvy min	mica, hvy min
60	mica, hvy min		mica, hvy min	mica, hvy min
70	mica		mica, hvy min	mica, hvy min
80	mica, hvy min	mica	mica, hvy min	mica, hvy min
90	mica		mica, hvy min	mica, hvy min
100	mica		mica, hvy min	mica, hvy min

(glauc - glauconite; hvy min - heavy minerals)

XRD analysis (Fig. 5.8 A and B) of these four cores (Table 5.3) shows that the dominant terrigenous material is quartz and minerals of the plagioclase feldspar series, with mica (muscovite and biotite) being abundant in many cores. The XRD analysis also confirms the presence of clay minerals, mainly chlorite, illite and smectite formed from the weathering and decomposition of micas and feldspars. XRD analysis detected

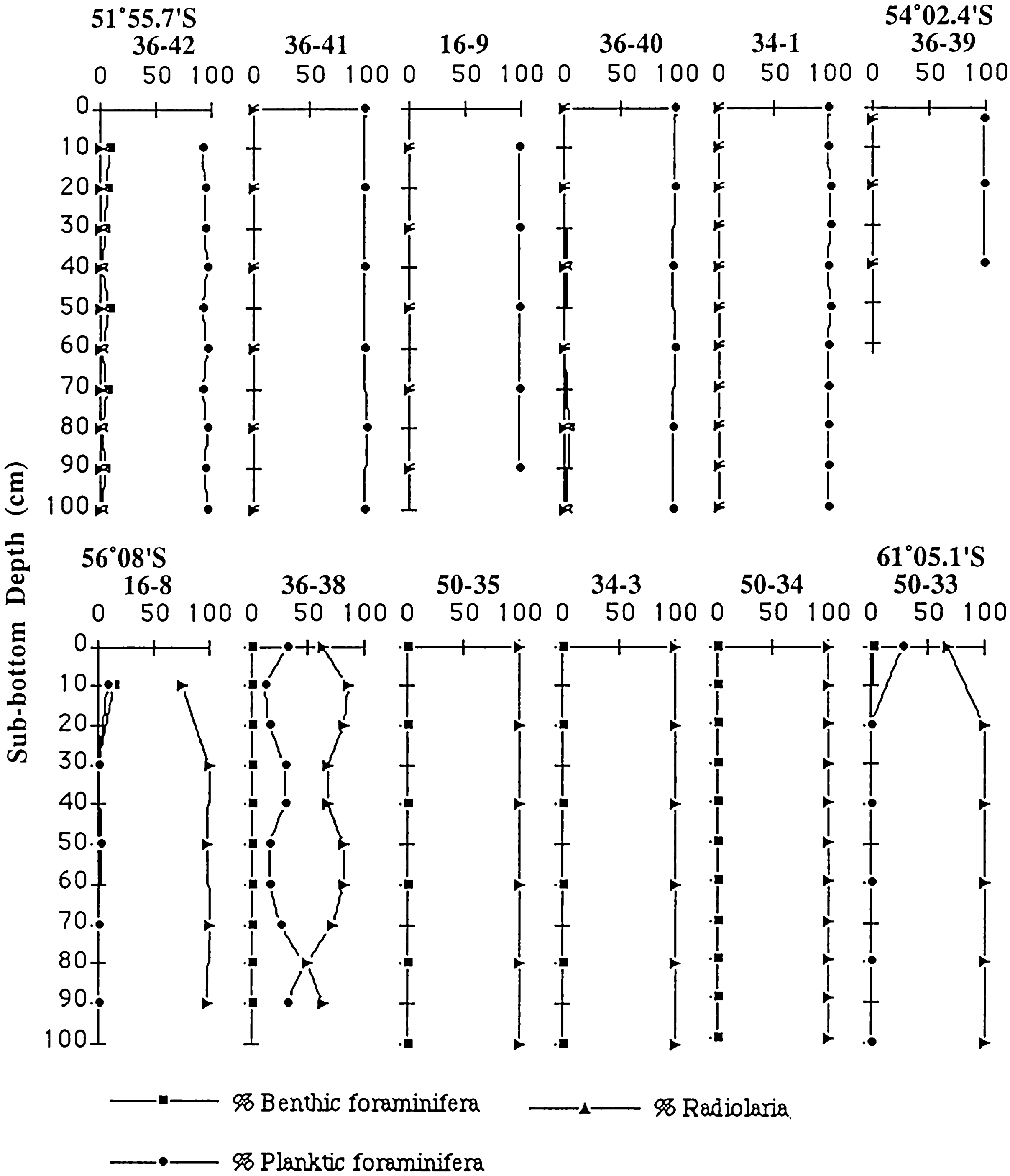

Fig. 5.9 Broad biogenic constituents from the coarse sand fraction (> 150 μm) of the NZSSO cores. Data from Appendix 5.

the zeolite phillipsite in the northern core of 36-42. However, no other zeolites were found in the four cores analysed, despite the fact that clinoptilolite might have been expected in the deeper finer sediments (Goodell *et al.*, 1973).

Table 5.3 Mud Fraction Terrigenous Composition of NZSSO Cores from XRD Analysis

Core	Clay	Minerals & Rock Fragments	Other
36-42	Illite	Quartz, Plagioclase Feldspars, Mica, Nepheline, Phillipsite	
34-1		Quartz, Plagioclase Feldspars	
36-38	Chlorite, Illite, Smectite	Quartz, Plagioclase Feldspars, Mica, Nepheline	MnO_2, Pyrite
50-34	Chlorite, Illite, Smectite	Quartz, Plagioclase Feldspars, Mica	MnO_2, Pyrite

(Tabulated from Appendix 7)

XRD analysis reveals that in the deeper cores 36-38 and 50-34, manganese and pyrite constitute an important part of the authigenic material. Manganese-bearing minerals often form a scale over the terrigenous sand grains.

5.4 Biogenic Composition

5.4.1 Biogenic Composition of the Sand Fraction

Biogenic components of the coarse sand fraction of sediments in the NZSSO cores are shown in Fig. 5.9. Again the modern SAF boundary marks a strong change in the dominant sediment composition (Table 5.1). Sediment changes across the SAF at ~56°S from northern foraminiferal-dominated sediment to southern diatom- and/or radiolarian-dominated. Planktic foraminifera dominate the biogenic components of the coarse sand-sized sediment, ranging between 85-99% abundance in all cores north of the modern SAF. Radiolaria are absent from the coarse sand fraction in the northern cores. The benthic foraminifera comprise a very small component of the biogenic material, ranging from 0-2% on average. Two cores from north of the modern SAF have significant percentages of benthic foraminifera. Core 36-42 has abundances ranging from 3-8%, with benthic foraminifera decreasing in abundance downcore from

~8% at the core top to ~3% at 40 cm, while further downcore abundances fluctuate between ~3-~7% (Fig. 5.9). Core 36-40 has benthic foraminiferal abundances between ~1-~5%, with abundances averaging ~1% with peaks at 40 cm of ~3%, 80 cm of ~5% and 100 cm of ~4%.

South of the modern SAF the cores are radiolarian-dominated in the coarse sand fraction; within cores 50-35, 34-3 and 50-34 calcareous planktic and benthic foraminifera are rare to absent. Cores 16-8 and 50-33 show an increase in planktic and benthic foraminiferal content up core, from 30 cm and 20 cm respectively. Core 36-38 has insignificant amounts of benthic foraminifera, but has planktic foraminifera ranging in abundance from ~13% to ~48%, forming an inverse relationship with the dominant radiolarians (Fig. 5.9). Increases in planktic foraminifera occur between 20 and 50 cm downcore to ~31%, and again between 70 and 90 cm with an abundance of ~48%.

Semi-quantitative analysis of the fine sand fraction of four cores showed similar patterns to those expressed in the coarse sand fraction (Fig. 5.10). Core 36-42 shows an overall trend of decreasing benthic foraminifera, ranging from ~10% abundance at the core top to ~2% at the base. Planktic foraminifera represent ~90-98% of the biogenic population. Radiolaria are absent from the fine sand fraction of this core. Core 34-1 shows a greater percentage range of benthic foraminifera in the fine sand fraction (0-~8%) compared to the coarse sand fraction (0-~1.5%). Radiolaria are absent from core 34-1.

The fine sand fraction of the radiolarian-dominated core 36-38 does not exhibit similar biogenic patterns to the coarse sand fraction. The fine sand fraction is less calcareous due to the planktic foraminiferal abundances dropping to between 0-~3% (cS ~13-~48%). However, benthic foraminiferal abundances increase from 0 to ~2% at 30 cm and continues downcore at this value. In core 36-38 diatoms are observed in the fine sand fraction for the first time of any of the NZSSO cores. The fine sand fraction of core 36-38 is dominantly composed of radiolaria (65-83%) and diatoms (15-35%). The diatoms and radiolaria have an inverse relationship downcore, the diatoms decreasing in percentage abundance from ~32 to ~17% between 0-30 cm. From 30 cm diatom percentages increase to ~35% at core base. Radiolaria show shifts of similar magnitude over the same intervals (Fig. 5.10).

Core 50-34 contains no planktic or benthic foraminifera in the fine sand fraction. Biogenic material is dominated by radiolaria and diatoms, and there is little variation downcore, with radiolaria ranging in abundance between 84-98% and diatoms from 2-16%. Two small shifts occur downcore between 0-30 cm and 80-100 cm, over which the diatoms decrease in abundance by ~14% and radiolaria gain ~14%.

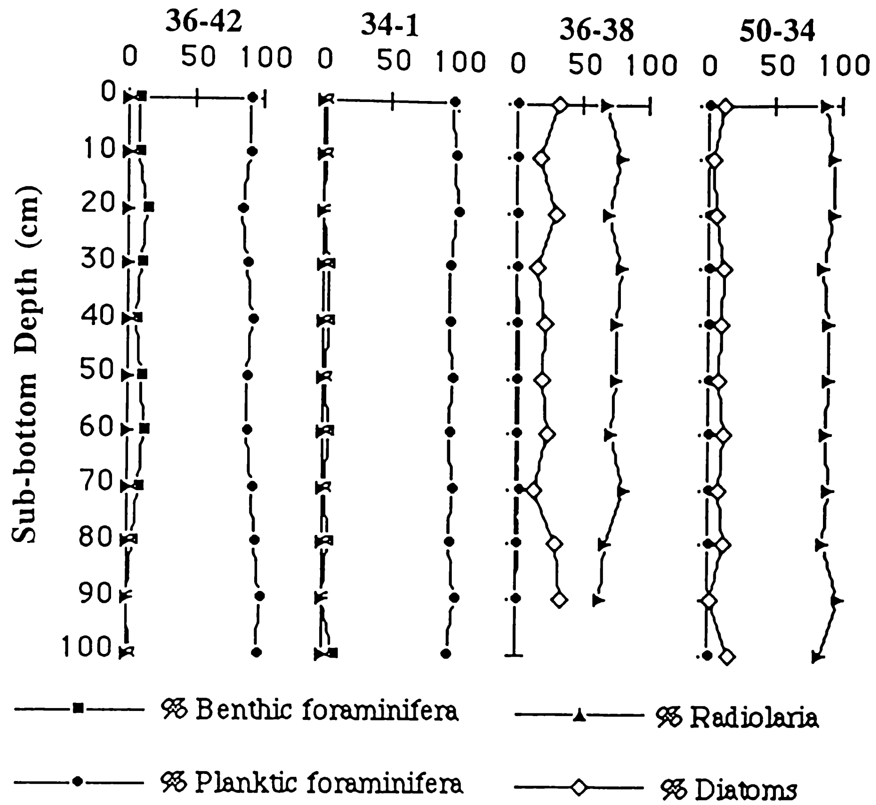

Fig. 5.10 Semi-quantitative analysis of the dominant biogenic trends in the fine sand fraction of selected NZSSO core samples. Data from Appendix 6.

5.4.1 Biogenic Composition of the Mud Fraction

Smear slide analysis of the mud fraction for samples from core 36-42 reveals the biogenic material is composed dominantly of juvenile foraminifera, foraminiferal fragments, molluscan fragments, and occasional sponge spicules and echinoderm spines, all within a presumably nannofossil-rich matrix. Sample slides of Core 34-1 show juvenile foraminifera, foraminiferal fragments, and scattered remains of echinoderm spines, sponge spicules and radiolaria in decreasing order of abundance within a micrite matrix. Radiolaria increase in abundance downcore from 60 cm.

Sample from Core 36-38 is dominated by siliceous material, mainly sponge spicules, radiolaria and diatoms, with occasional scattered juvenile foraminiferal and foraminifera fragments within a clayey mud matrix. Core 50-34 is clearly dominated by diatoms, radiolaria and radiolarian fragments, with conspicuous sponge spicules.

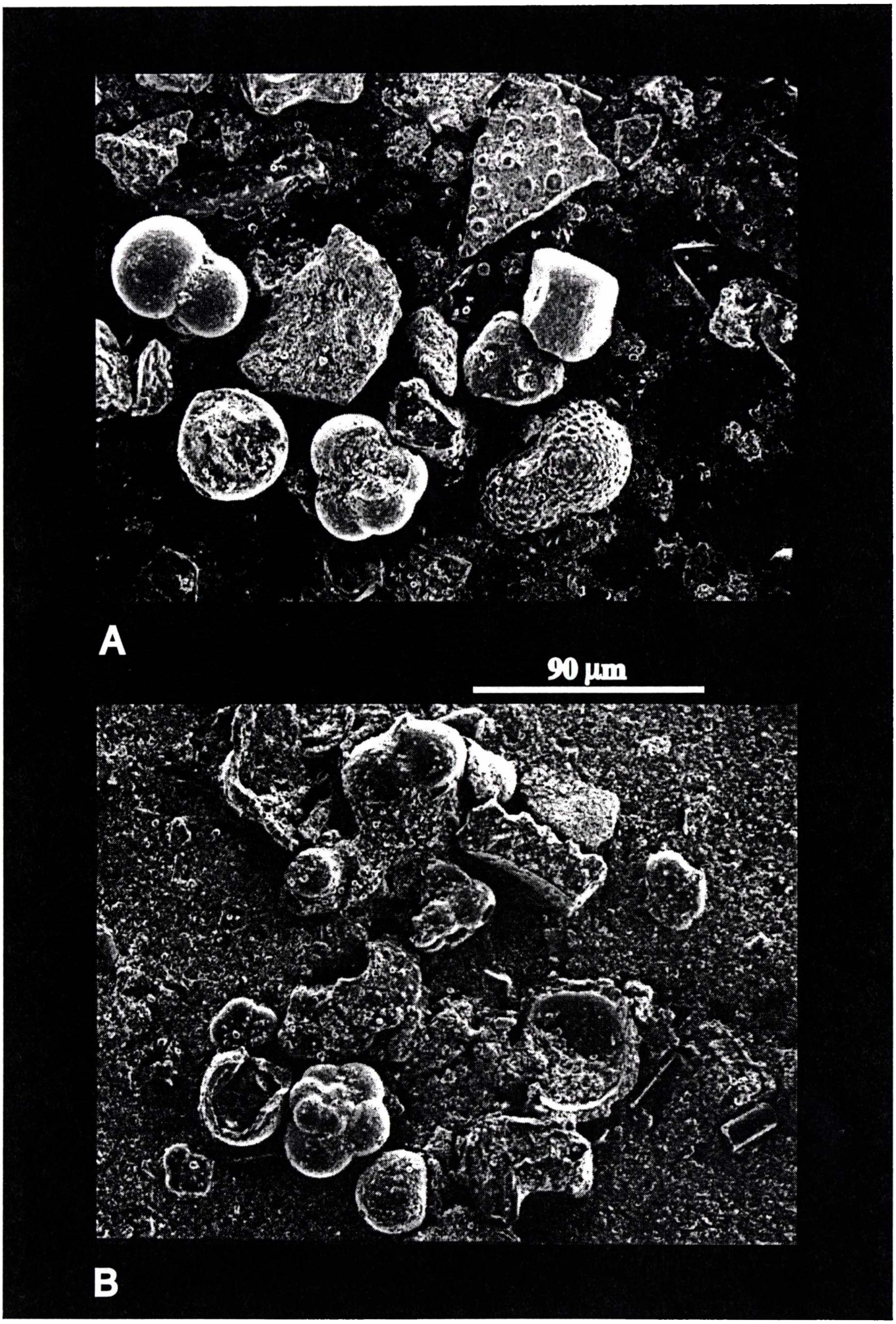

Plate 5.1 (1) NZSSO core 36-42, sample from 10 cm downcore, x 200; (2) NZSSO core 36-42, sample from 20 cm downcore, x200. Note the significant increase in the abundance of fine material in the sample at 20 cm, across the colour boundary at 16 cm downcore, composed predominantly of calcareous nannofossils.

SEM stubs of the mud fraction from cores 36-42 and 50-34 at 10 and 20 cm, and core 36-38 at 40 and 50 cm downcore were prepared and SEM photographs taken. Core samples (10 and 20 cm) from 36-42 were taken across a colour boundary which was believed to represent the transition from Last Glacial conditions into present interglacial Holocene conditions. Core 36-42 and 50-34 were chosen as they represent typical cores north and south of the SAF.

The sample from 10 cm in Core 36-42 shows that the mud fraction is composed of juvenile foraminifera, foraminiferal fragments, and terrigenous material set in a matrix of micrite and calcareous nannofossils (Plate 5.1A). Plate 5.1B is a sample at 20 cm from core 36-42, below the colour boundary at 16 cm. A compositional change is seen across the boundary: juvenile foraminifera, foraminiferal fragments, and terrigenous material all decrease in abundance, while the quantity of nannofossils increases significantly.

Samples at 10 and 20 cm downcore Core 50-34 (see Plate 6.4) are dominated by clean diatoms, diatom fragments and radiolarian fragments, while sponge spicule fragments are also present, as are assorted unidentified spines. The SEM photographs do not appear to give a representative description of the southern cores; no terrigenous material is clearly evident in the SEM images, yet XRD analysis reveals the presence of quartz, plagioclase feldspars and clays. Another distinguishing feature of the mud fraction from cores south of the SAF is that the sediment is predominantly finer.

5.5 Summary

The compositional characteristics of the twelve NZSSO cores used in this study are strongly divided into two groups by SAF and by topographical variations. The northern group, north of the SAF and lying on the southern margins of the Campbell Plateau, have an average water depth of 1215 m. The southern group south of the SAF and lying in the Southwest Pacific Basin, have an average water depth of 4700 m.

The carbonate values (Fig. 5.1) reflect this immense difference in depositional environments. The northern group averages 95% carbonate, and the calcium carbonate is biogenic in origin. The sand-sized sediments are predominantly planktic and benthic foraminifera with local concentrations of molluscan and echinoderm fragments; this comprises Facies A (Section 4.2, Table 4.1). Some cores have moderate clay content, due to higher concentrations of nannofossils (Facies B). Terrigenous material is rare to absent. What terrigenous material there is comprises mainly present is mica (muscovite and biotite) and (in core 36-42) authigenic glauconite.

The southern group averages < 1% carbonate, with the exception of core 36-38 which ranges from 10-18%. The dramatic fall in carbonate across the SAF (Fig. 5.2) is due to a change in the dominant biogenic sediment type, from calcareous tests to siliceous diatoms and radiolaria. These siliceous organisms dominate the fine sand to silt-size fraction (Facies C). The greater average depth of the southern cores allows the loss of carbonate through dissolution. Terrigenous material becomes common, quartz and plagioclase feldspars dominating. A greater percentage of the terrigenous material is represented in the fine sand and silt-sized fraction (Facies C). However, ice-rafted debris occurs in increasing amount in higher latitudes, particularly in core 50-33. Gravel is present in core 16-8, part of a reworked accretionary drift system. The southern cores also contain clay minerals, notably crystalline chlorite, illite and smectite, and authigenic pyrite and ferro-manganese deposits.

Chapter Six:

Micropaleontology

Chapter Six: ***Table of Contents***

6.1 Introduction

Micropaleontological studies on twelve cores from the New Zealand sector of the Southern Ocean (NZSSO) show abrupt spatial variations in faunal assemblages southwards from 52°S across the SAF to 61°S. These transformations of the faunal assemblages record changes in watermass temperature, density structure, and nutrient content, and the effects of dissolution and currents in the differing depositional environments of the NZSSO (Parker & Berger, 1971; Nelson *et al.*, 1993a; Weaver *et al.*, 1997). The faunal assemblages are readily related to oceanic fronts which control the latitudinal distributions of these assemblages within the Southern Ocean (Parker & Berger, 1971).

The >150 µm fraction (coarse sand) was used for the quantitative study of the foraminiferal and radiolarian populations, as recommended by other workers (e.g. Vella *et al.*, 1975; Griggs *et al.*, 1983); this was also supplemented by a semi-quantitative census undertaken on four cores in the 63-150 µm fraction (fine sand). Diatom assemblages of the cores south of the SAF were determined from smear slide analysis and Scanning Electron Microscope (SEM) of the mud fraction. To complete a micropaleontological investigation of the twelve NZSSO cores, a SEM analysis was used to identify nannofossils within the mud fraction.

6.2 Taxonomy and Species Identification

Microfossil composition was determined for the top metre of core for the twelve cores (Table 1.5) with a sample interval of 20 cm, except for cores 36-42, 34-1, 36-38 and 50-34 where 10 cm intervals were used to provide higher resolution. Species were identified using diagrams and photographs from various authors. Planktic and benthic foraminifera were identified using Baker (1960), Bandy *et al.* (1971), Echols (1971), Kennett & Srinivasan (1983), Jenkins & Srinivasan (1986), Kurihara & Kennett (1986), and Collen (1995). Radiolaria were identified from fine sand Chen (1975), Nigrini & Moore (1979) and Lombari & Boden (1985). Diatoms were identified using Abbott (1973), McCollum (1975) and Ceisielski (1986). Nannofossil identification was from Geitzenauer (1969), Edwards & Perch-Neilsen (1975) and Edwards (pers. commun., 1997).

A full species list is given in Appendix 5 for the planktic and benthic foraminifera and radiolaria in the coarse sand fraction census. The coarse sand fraction includes 10 planktic and 36 benthic foraminiferal species, and 16 radiolaria species.

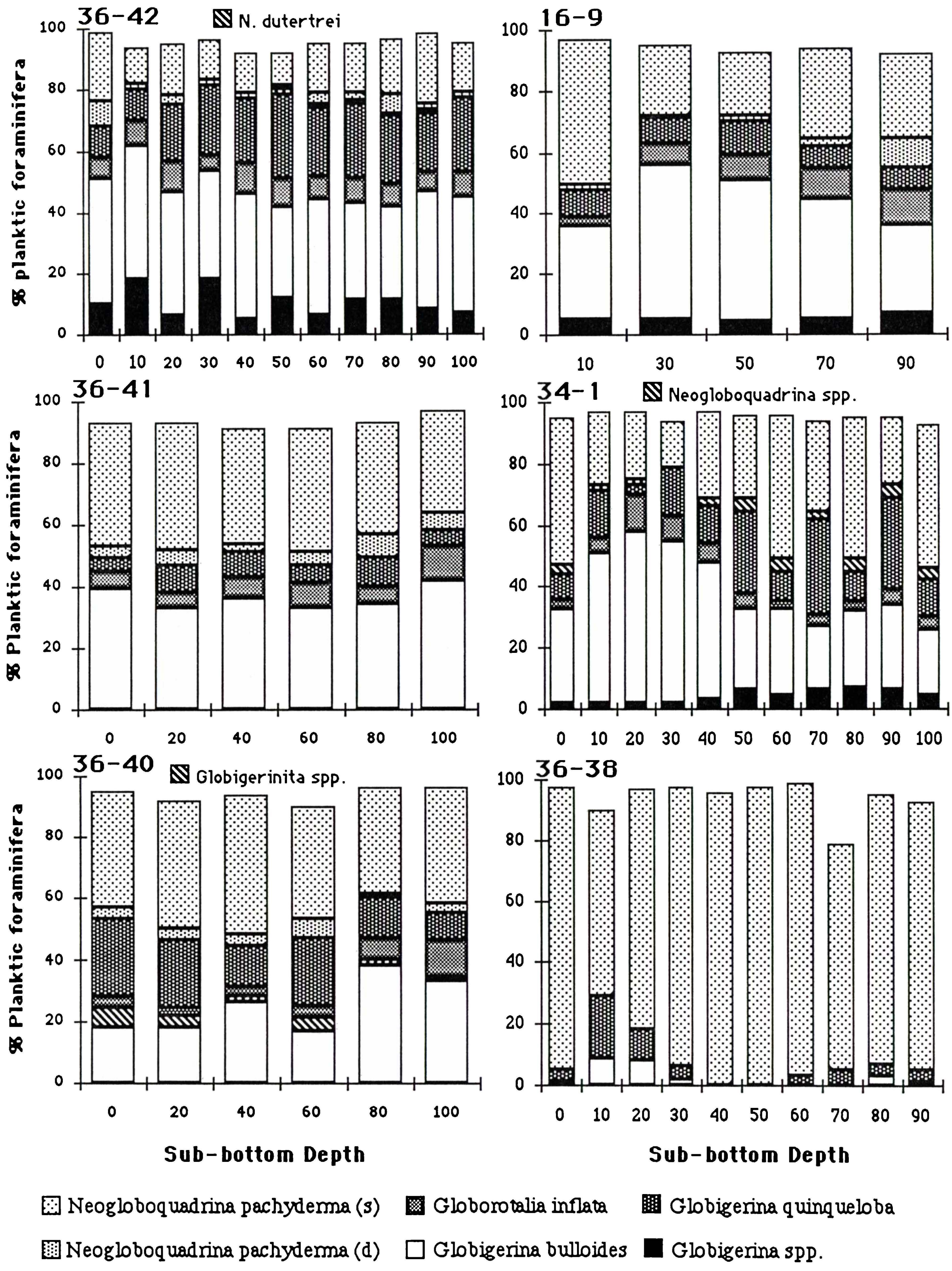

Fig. 6.1 Planktic foraminiferal abundances and trends for common species found in NZSSO cores. Data from Appendix 5.

The semi-quantitative study of the fine sand fraction revealed no additional foraminiferal species, but 21 radiolarian species were observed, 7 more than in the coarse sand fraction. Figs. 5.8 and 5.9 indicate the broad biogenic patterns for the microfossil assemblages. Diatoms and calcareous nannofossils are dominantly limited to the mud fraction.

6.3 Planktic Foraminiferal Assemblages

Nine planktic foraminiferal species were distinguished in the census undertaken on the coarse sand fraction, three of which form a significant proportion of the foraminiferal population (Table 6.1), namely *Globigerina bulloides, Globigerina quinqueloba,* and *Neogloboquadrina pachyderma*, both sinistral and dextral forms (Plate 6.1; Appendix 5). All these species are present in most samples (Fig. 6.1). For many of the *Globigerina* foraminifera present in the census population of the coarse sand fraction it was not possible to positively distinguish species; these indeterminate *Globigerina* are assigned to a *Gg.* spp. column in Table 6.1.

Table 6.1 Common Planktic Foraminiferal Species

Samples	Gg.(spp)	Gg.b	Ga.(spp)	Gr.s	Gr.i	Gr.t	Gg.q	N.d	N.p(d)	N.p(s)
36-42										
0	10	41	2	x	7	3	10	x	8	23
10	18	44	3	x	8	3	10	x	2	12
20	6	41	2	x	10	3	18	x	3	17
30	18	36	2	x	5	2	22	x	2	13
40	5	41	3	1	10	4	21	x	2	13
50	12	30	4	1	9	2	27	2	1	11
60	6	38	3	x	8	2	22	1	4	16
70	11	32	2	2	8	1	24	1	3	16
80	11	31	2	1	7	1	22	1	6	18
90	8	39	1	x	6	1	19	1	2	23
100	7	38	3	x	8	2	24	x	2	16
36-41										
0	1	39	2	x	6	3	4	x	4	40
20	1	33	3	x	5	1	9	x	5	41
40	3	36	5	x	7	1	8	1	3	37
60	2	33	5	x	8	1	6	x	4	40
80	1	34	4	x	6	1	9	x	8	36
100	1	42	2	x	11	x	5	x	6	33
16-9										
10	5	31	3	x	3		9	x	2	47
30	5	51	1	x	7	3	8	x	1	23
50	4	47	4	x	8	2	11	x	2	21
70	5	40	3	x	10	3	7	x	2	30
90	7	29	4	1	12	2	7	x	9	28

(continued over)

Table 6.1 Cont.

Samples	Gg.(spp)	Gg.b	Ga.(spp)	Gr.s	Gr.i	Gr.t	Gg.q	N.d	N.p(d)	N.p(s)
36-40										
0	4	18	6	x	4	1	25	x	4	38
20	6	18	4	x	2	1	22	x	4	42
40	5	26	2	x	3	1	13	x	4	46
60	7	17	4	x	4	1	22	x	6	37
80	x	38	2	x	7	2	13	x	1	35
100	x	33	1	x	12	2	9	x	3	38
34-1										
0	2	31	2	x	3	x	8	3	1	48
10	2	49	2	1	5	1	15	2	x	24
20	2	56	1	x	12	1	3	2	1	22
30	2	53	3	x	8	2	16	x	x	15
40	3	45	2	x	6	2	12	3	x	28
50	6	27	2	x	5	x	26	5	1	27
60	4	29	2	x	2	x	10	4	1	47
70	6	21	5	x	4	1	31	2	1	30
80	7	25	4	x	3	1	10	4	1	46
90	6	28	2	x	5	1	30	4	1	22
100	4	22	3	x	4		12	4	2	47
36-39										
3	3	24	6	x	12	2	4	x	3	45
20	4	23	11	x	28	2	5	x	7	19
40	2	22	7	x	13	2	11	x	7	36
16-8										
10	32	x	x	x	78	x	x	x	x	x
30	x	x	x	x	x	x	x	x	x	x
50	x	x	x	x	x	x	x	x	x	100
70	x	x	x	x	x	x	x	x	x	x
90	x	x	x	x	100	x	x	x	x	x
36-38										
0	2	1	x	x	x	x	4	x	x	93
10	x	9	x	x	4	x	20	4	x	61
20	3	8	x	x	x	x	10	x	x	79
30	1	2	x	x	x	x	4	x	x	92
40	4	x	x	x	x	x	x	x	x	96
50	x	x	x	x	x	x	x	x	2	98
60	1	x	x	x	x	x	3	x	x	96
70	2	x	x	x	x	x	5	x	4	74
80	2	3	1	x	x	x	4	x	2	88
90	1	1	x	x	x	1	4	x	2	88
100	x	x	x	x	x	x	x	x	x	x
50-33										
0	1	6	x	x	9	x	x	x	x	82

Common planktic foraminiferal species given as a percentage of the planktic population. *Globigerina* species *(Gg.* spp.*)*, *Globigerina bulloides* (*Gg. b*), *Globigerina quinqueloba (Gg. q)*, *Globigerinita* species *(Ga.* spp.*)*, *Globorotalia inflata (Gr. i)*, *Globorotalia truncatulinoides (Gr. t)*, *Globorotalia cf. scitula (Gr. s)*, *Neogloboquadrina dutertrei (N. d)*, *Neogloboquadrina pachyderma (N. p)* sinistral (s) and dextral (d). x = <1% of population. *Orbulina universa* is not tabulated as it consistently represents <1% of the planktic foraminiferal population.

Kennett (1970) found that Southern Ocean cores are characterised by alternations of cold water and warm water faunas. The cold water faunas are dominated by sinistrally coiled *Neogloboquadrina pachyderma* and the warmer faunas composed of dextral coiling *Neogloboquadrina pachyderma*, *Globorotalia inflata*, *Globigerina quinqueloba*, *Globigerina bulloides*, *Globigerinita* spp. and *Globorotalia truncatulinoides*, with *Orbulina universa* becoming more abundant northwards towards subtropical water.

Parker & Berger (1971), using cluster analyses, named two assemblages for the Southern Ocean (I and K) that were separated by the Antarctic Convergence (AAPF) at ~56°S. Later salinity and temperature determinations by Gordon (1975b) showed this to be the approximate position of the SAF in the NZSSO due to the poleward shift of oceanic fronts because of the extension of the New Zealand continental landmass into high latitudes (Fig. 1.1B). Parker & Berger's (1971) cores came dominantly from east of the NZSSO where open ocean conditions allow a more northward position of the SAF and AAPF.

The faunal assemblage north of the Antarctic Convergence was characterised by *Globigerinita glutinata*, *Orbulina universa*, *Globorotalia truncatulinoides*, *Globorotalia inflata*, *Neogloboquadrina dutertrei*, *Globigerina bulloides*, *Neogloboquadrina pachyderma* and *Globigerina quinqueloba*. The fauna south of the Antarctic Convergence was dominated by *Neogloboquadrina pachyderma*, *Globigerina bulloides* and *Globorotalia inflata*. These findings are in agreement with those of Kennett (1970).

Griggs *et al.* (1983), studying two cores (Q200 and Q217) in the Bounty Trough, found that the faunal assemblage of the northern subantarctic watermass was dominated by *Globigerina bulloides*, *Globorotalia inflata*, *Globorotalia truncatulinoides* and *Neogloboquadrina pachyderma* (both dextral and sinistral coiling forms). Interglacial sediments contain higher numbers of *Globigerina bulloides* and dextral *Neogloboquadrina pachyderma* and glacial periods were marked by sinistral *Neogloboquadrina pachyderma* increases.

Based on evidence from this study and previous studies the planktic foraminiferal fauna can be divided into two faunal assemblages, an Antarctic (Table 6.2) and a Subantarctic group (Table 6.3). In the NZSSO the two assemblages are sharply divided at ~56°S, the approximate position of the modern SAF.

Table 6.2 Antarctic Planktic Foraminiferal Assemblage

Globigerina bulloides	*Globigerina quinqueloba*
Neogloboquadrina pachyderma (s)	*Globorotalia inflata*

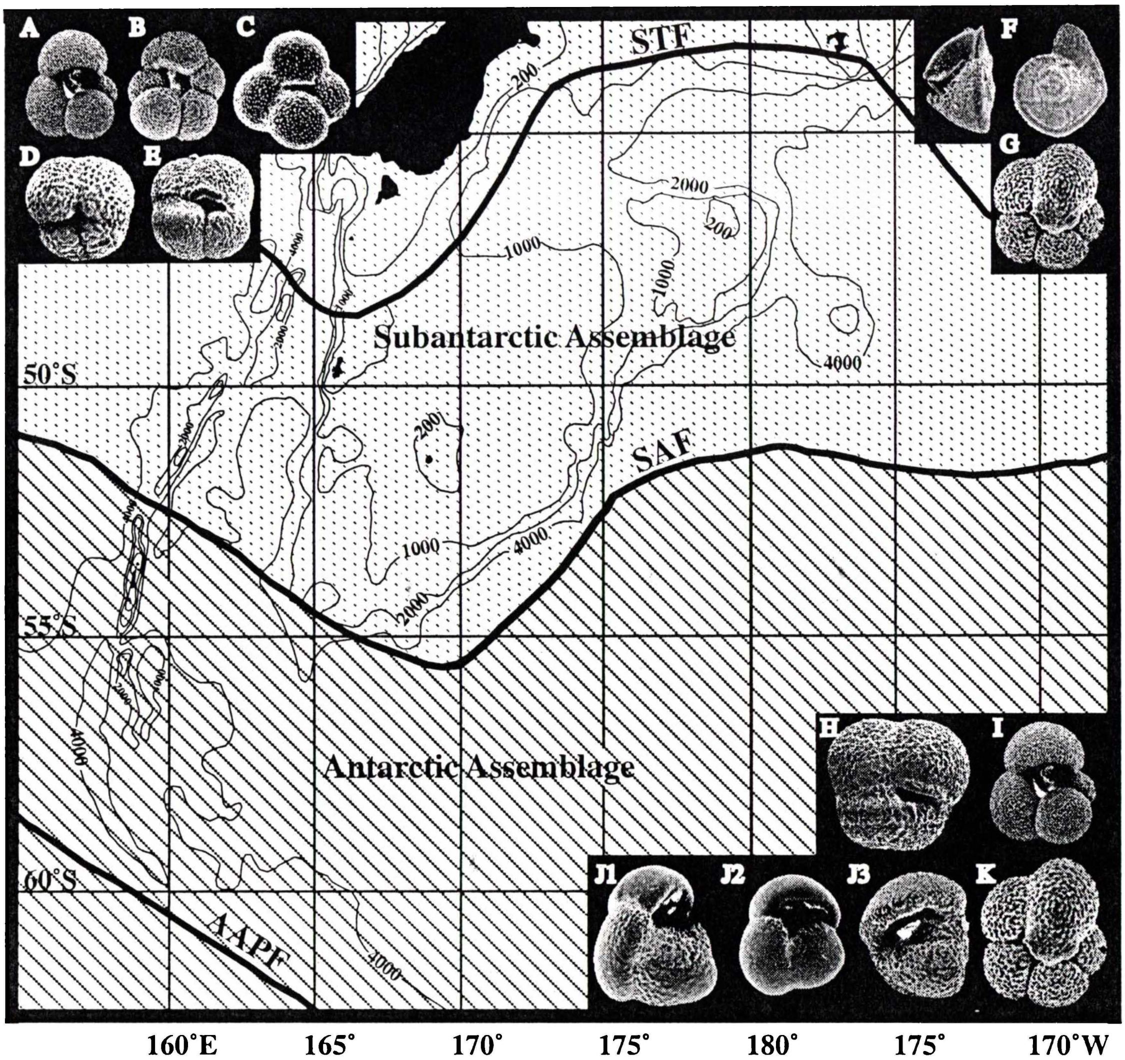

Fig. 6.2 Planktic foraminiferal assemblage in the NZSSO. The Subantarctic Assemblage comprises (A) *Globigerina bulloides,* (B) *Neogloboquadrina dutertrei,* (C) *Globigerinita* spp., (D) *Neogloboquadrina pachyderma* (dextral), (E) *Neogloboquadrina pachyderma* (sinstral), (F) *Globorotalia truncatulinoides,* (G) *Globigerina quinqueloba.* South of the SAF the Antarctic Assemblage is dominated by four species: (H) *Neogloboquadrina pachyderma* (sinstral), (I) *Globigerina bulloides,* (J1,2,3) *Globorotalia inflata,* and (K) *Globigerina quinqueloba.* SEM photographs sourced from Kennett & Srinivasan (1983).

Table 6.3 Subantarctic Planktic Foraminiferal Assemblage

*Globigerinita bulloides**	*Globigerina quinqueloba**
Neogloboquadrina pachyderma (sinistral)*	*Neogloboquadrina pachyderma* (dextral)
Globorotalia inflata	*Globorotalia truncatulinoides*
Neogloboquadrina dutertrei	*Globigerina* spp.
Globigerinita spp.	

* indicates the strongest associations.

These assemblages agree with those found at DSDP 594 off eastern South Island by Nelson *et al.* (1993a), where the interglacial biopelagic oozes were dominantly composed of the Subantarctic assemblage and the glacial hemipelagic oozes were dominated by *Neogloboquadrina pachyderma.* Weaver *et al.* (1997) confirm that the northern limit of the Antarctic assemblage roughly coincides with SAF, and that the Subantarctic one is bounded by the SAF in the south and the STF to the north (Figs. 6.2 and 6.3).

6.3.1 Planktic Foraminiferal Trends

Planktic foraminiferal trends are readily identified when comparing mean percentage abundance of planktic foraminifera (Table 6.4) with latitude (Fig. 6.4 A and B) and depth (Fig. 6.5 A and B).

Table 6.4 Mean Planktic Foraminiferal Abundance for NZSSO Cores

Samples	Gg.(spp)	Gg.b	Ga.(spp)	Gr.i	Gr.t	Gg.q	N.d	N.p(d)	N.p(s)
36-42	10	37	3	8	2	20	1	3	16
36-41	2	36	4	7	1	7	x	5	38
16-9	5	40	3	8	2	8	x	3	30
36-40	4	25	3	5	1	17	x	4	39
34-1	4	35	3	5	1	16	3	1	32
36-39	3	23	8	18	2	7	x	6	33
16-8	6	x	x	36	x	x	x	x	20
36-38	2	2	x	x	x	5	x	1	87
50-33	1	6	x	9	x	x	x	x	82

x = represents less than 1% of planktic population.

Watermasses north of the SAF are dominated by a high percentage of subantarctic foraminifera (Table 6.2), whose tests are more susceptible to dissolution

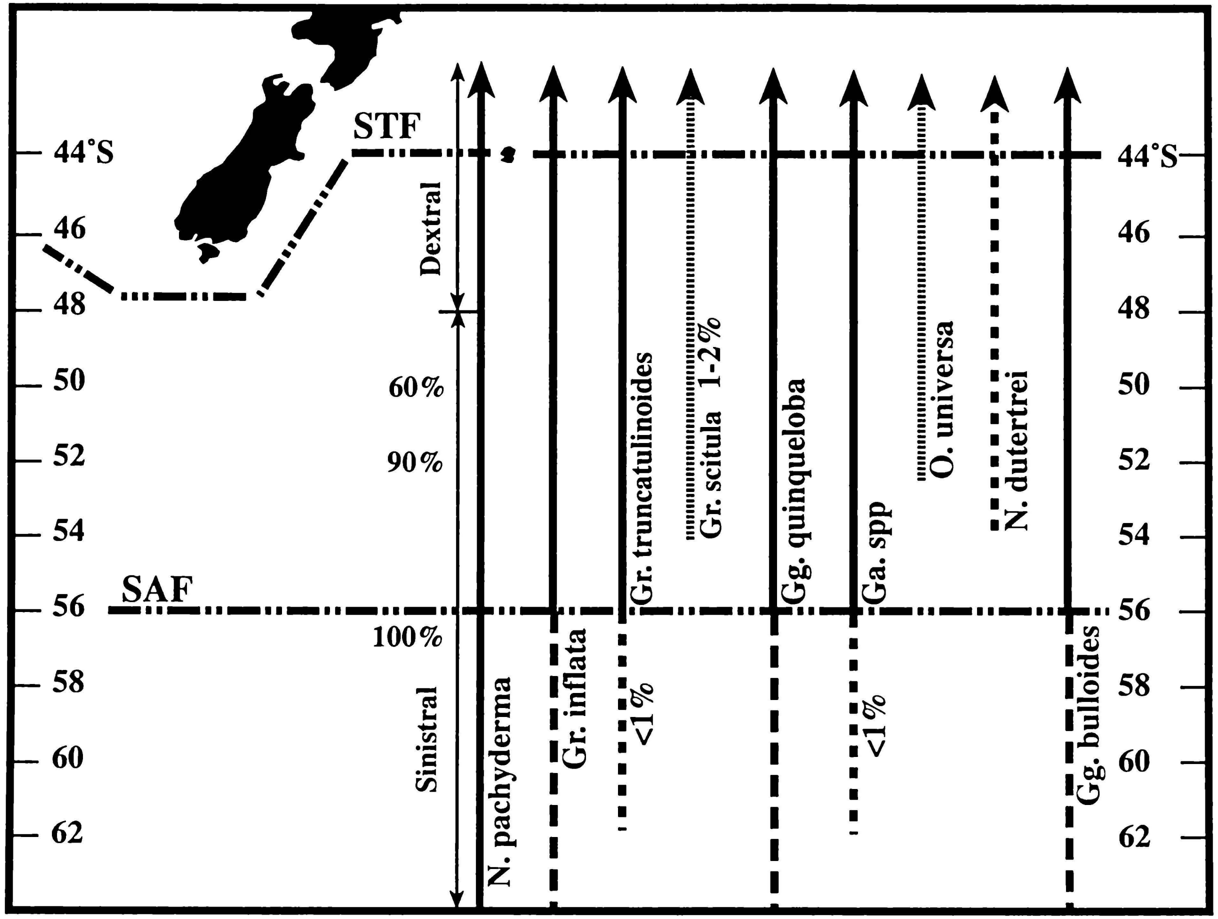

Fig. 6.3 Latitudinal distribution of important planktic foraminifera found within the NZSSO cores of this study. Note the influence of the Subtropical Front (STF) and the Subantarctic Front (SAF). *Neogloboquadrina pachyderma* coiling ratio are seen to change rapidly between 50-52°S, south of the SAF all are sinistrally coiled. The 50% isopleth lies at ~48°S.

and fragmentation (Parker & Berger, 1971). An abrupt faunal change in the subantarctic faunas between 54-56°S occurs as they are replaced by antarctic faunas (Fig. 6.4A).

Neogloboquadrina pachyderma trends also show abrupt changes in coiling ratios at ~56°S (Fig. 6.4B). South of this latitude dextral coiling *Neogloboquadrina pachyderma* are rare or absent in NZSSO cores. Crossing this latitude the percentage of *Neogloboquadrina pachyderma* rises from 20-40% of the planktic foraminifera population to 85%. This agrees with Kennett (1969) who found that *Neogloboquadrina pachyderma* constituted 20-30% of the planktic population of the >125 μm fraction north of ~57°S.

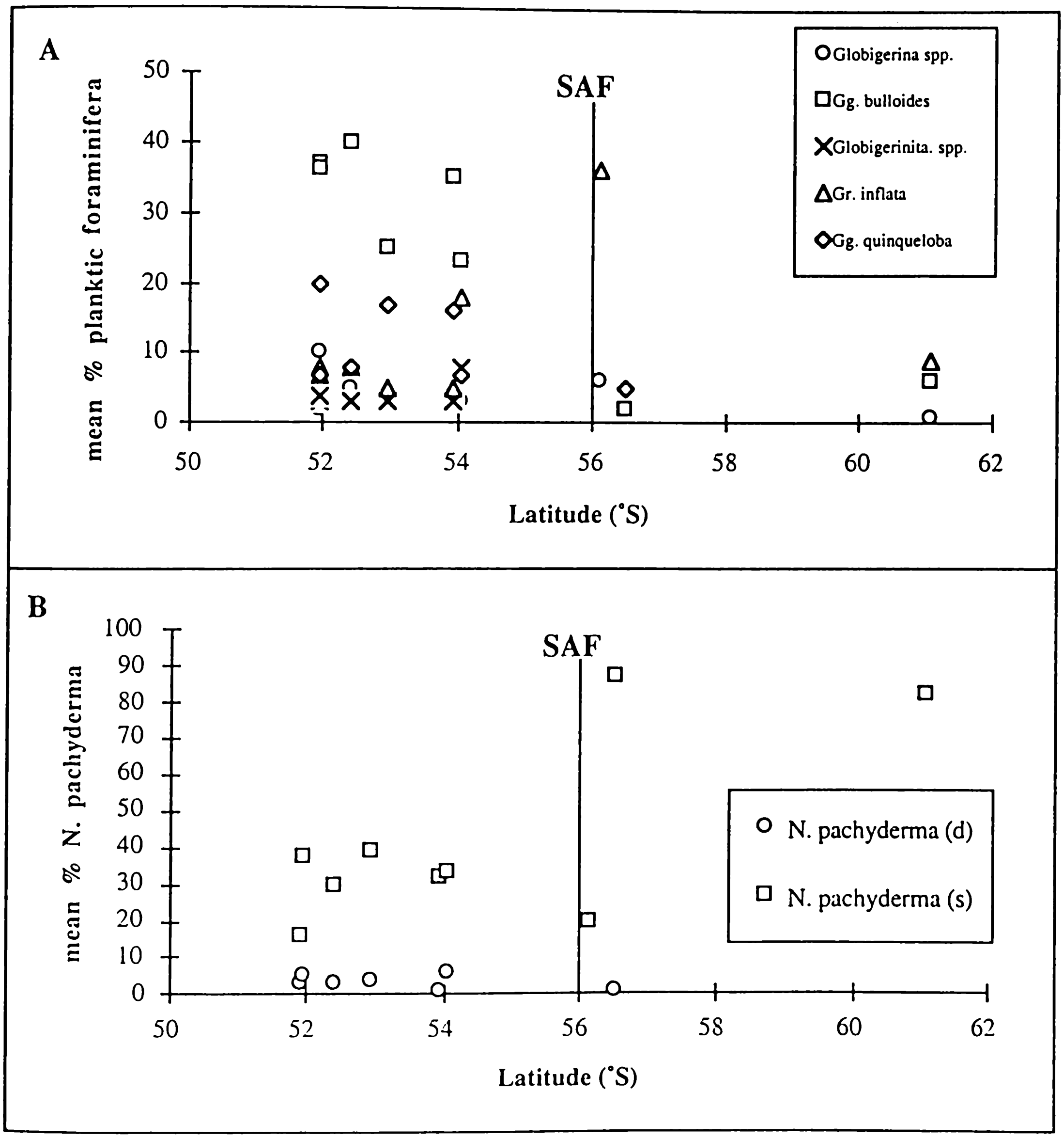

Fig. 6.4 (A) Mean percentage of planktic foraminifera versus latitude for the common foraminifera identified in this study. (B) Mean percentage of *Neogloboquadrina pachyderma* versus latitude. Plots compiled from data in Table 6.4.

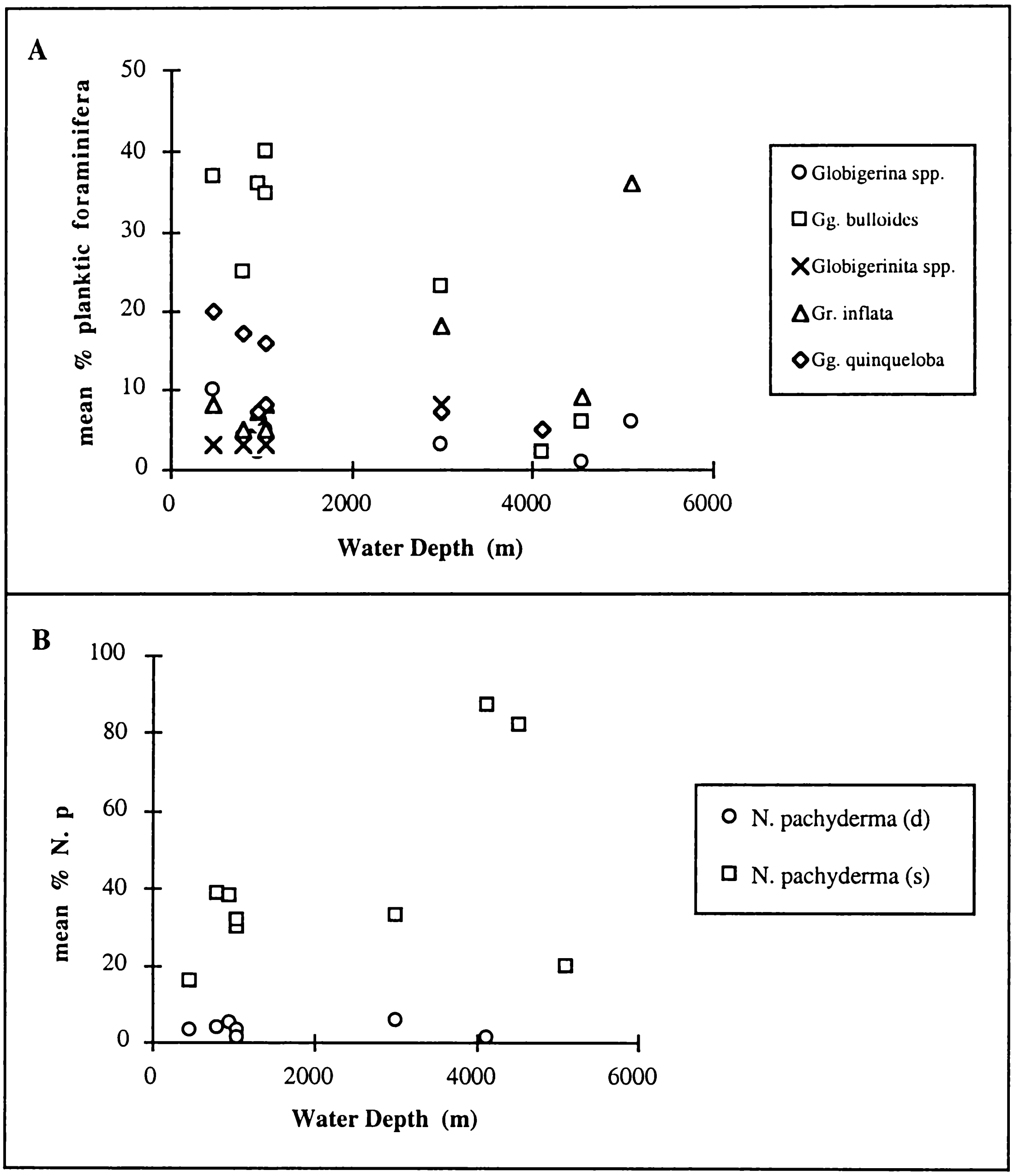

Fig. 6.5 (A) Mean percentage of planktic foraminifera versus water depth for the common foraminifera identified in this study. (B) Mean percentage of *Neogloboquadrina pachyderma* versus depth. Graphs complied from data in Table 6.4.

The habitat ranges of various species can be determined from Fig. 6.4A. *Globigerina bulloides* first appears at ~61°S and shows an increasing abundance northwards into subantarctic waters, where it represents ~33% of the planktic foraminiferal population; these observations are in agreement with Kennett (1969). Another major species, *Globigerina quinqueloba*, first appears at ~56°S representing 5% of the planktic population; north of the SAF the abundance of *Globigerina quinqueloba* ranges from 8-20%.

Kennett (1969, 1970) observed that *Globorotalia inflata* is rarely found south of 58°S, with maximum abundance north of 52°S. This study found *Globorotalia inflata* at 61°S, but the population contained fragments and showed dissolution effects. This indicates that it may represent transported material or be a disproportionate bias of a relic sediment due to the resistance to dissolution of *Globorotalia inflata.* These effects are clearly seen in core 16-8 on the southern margin of the Campbell Drift. Here *Globorotalia inflata* represents 36% of the planktic foraminiferal population. In comparison, in neighbouring cores that are not influenced by the dissolution and transportation effects *Globorotalia inflata* represents only 7% of the planktic population.

Globorotalia truncatulinoides first appears in cores north of the modern SAF at ~56°S, and represents ~2% of the planktic foraminiferal population throughout the core records. Kennett & Srinivasan (1983) state that *Globorotalia truncatulinoides* ranges from warm subtropical to tropical. Kennett (1970) has suggested that *Globorotalia truncatulinoides* has undergone subantarctic adaptation. Specimens found in this study were sinistrally coiled and predominantly smaller and more tightly coiled than subtropical or tropical varieties; tests also appeared to be flattened. Because*Globorotalia truncatulinoides* is a relatively warm water foraminifera, it's total absence could be used to infer cold water intrusion over a site. Since the northern NZSSO cores consistently record *Globorotalia truncatulinoides* downcore at an abundance of ~2%, it is unlikely that any significant cold water intrusion occurred over Campbell Plateau. Consequently, the appearance and abundance of *Globorotalia truncatulinoides* in samples indicate only latitudinal habitat variations.

Comparing the planktic foraminifera in Table 6.4 with water depth demonstrates that below ~3500 m the dominant planktic foraminifera present in the sediment are the more resistant forms, *Globorotalia inflata, Globigerina bulloides* and *Neogloboquadrina pachyderma* (Fig. 6.5A/B). The contribution that planktic foraminifera make to the total foraminiferal population varies, and can be used to characterise the depth at which the sediments accumulated. Using the relationship that

Table 6.5 Common Benthic Foraminifera in NZSSO Cores

Samples	C. spp. %	E. e %	Gc. s %	G. n %	S. b %	O. u %	S. spp. %	B. a %	U. spp. %
36-42									
10	16	4	48	0	0	0	0	0	16
20	0	0	50	0	8	0	0	0	21
30	19	0	38	0	6	6	0	0	6
40	29	14	7	0	21	0	7	0	0
50	8	8	17	17	0	0	8	4	0
60	7	14	7	7	21	0	14	0	14
70	9	0	27	23	0	0	0	5	9
80	8	0	23	0	0	0	15	8	0
90	23	0	29	0	0	6	6	0	0
100	11	11	0	11	0	0	0	0	11
36-41									
0	0	0	0	0	0	13	0	0	0
20	20	0	0	0	0	0	0	0	0
40	0	0	0	0	0	33	0	0	0
100	0	0	0	0	0	0	0	0	50
16-9.									
30	0	33	0	33	0	0	0	0	33
50	0	33	0	0	0	0	0	0	0
90	0	0	0	50	0	0	0	0	50
36-40									
40	0	0	17	0	0	0	0	0	0
80	0	0	10	0	0	0	0	0	0
100	0	0	27	0	0	0	0	0	0
34-1									
10	0	0	25	0	0	0	0	0	0
30	0	100	0	0	0	0	0	0	0
40	0	33	0	33	0	0	0	0	33
80	0	0	0	0	0	0	0	50	0
90	0	0	0	0	0	0	0	50	0
100	0	20	0	0	0	0	0	20	0
36-39									
3	0	0	50	0	0	0	0	0	0
20	0	20	40	0	0	20	0	0	0
16-8.									
10	69	0	0	0	0	19	0	0	0
36-38									
0	0	0	25	0	0	0	25	0	0
10	0	25	25	0	0	0	0	0	0
50	0	20	40	0	0	0	0	0	0
60	0	0	0	50	0	0	0	0	0
70	0	0	25	0	0	0	0	0	0
90	0	0	20	0	0	0	20	0	0
50-33									
0	0	60	10	0	20	10	0	0	0

Common benthic foraminifera species given as a percentage of the benthic population. *Cibicides* species *(C.* spp.*)*, *Epistominella exigua (E.e)*, *Globocassidulina subglobosa (Gc. s)*, *Spheroidina bulloides (S. b)*, *Gyroidina neosolandii (G. n)*, *Oridorsalis umbonatas (O. u)*, *Siphotextularia* species *(Si.* spp.*)*, *Bulimina aculeata (B. a)*, *Uvigerina* species *(U.* spp.*)*.

larger numbers of planktic foraminifera indicate a greater depth of water (Hayward, 1983), the percentage of planktic foraminifera in this study (Appendix 5) indicate water depths ranging from upper to lower bathyal, 500 m to 3000 m. Only cores from north of the SAF could be used for this method; in cores from south of the SAF the planktic foraminifera have been variably lost by dissolution and fragmentation, and indicate water depths far too shallow (i.e. mid-shelf and shallower, 0-100 m).

Cooke (1988) at DSDP 594 states that there was an increase in planktic percentages with increasing water depth, associated with interglacial periods, and a decrease with decreasing water depth, associated with glacial periods. Similar trends might be expected in cores of this study, but none revealed changes in water depth downcore associated with changes in planktic foraminifera.

6.4 Benthic Foraminiferal Assemblages

The benthic foraminiferal assemblage varied considerably both in numbers and species within the twelve NZSSO cores. About 36 benthic foraminiferal species were identified and represent between 0-8% of the microfaunal population in the coarse sand fraction (Fig. 5.9); of the 36 benthic foraminifera 9 species dominate (Table 6.5, Plate 6.2). The remaining benthic foraminifera only occur in one sample and often as only one specimen (Appendix 5). Benthic foraminifera represent a greater percentage of the microfaunal population in the fine sand (63-150 μm) fraction, ranging from 0-15% of the population (Fig. 5.10).

NZSSO core 36-42 had a mean benthic foraminiferal abundance of 5.4% of total foraminiferal population and also contains the greatest variety of benthic foraminifera (Appendix 5.1); other NZSSO cores had benthic foraminiferal abundances ranging from 0.5-3% (Table 6.6). The greatest abundance of benthic foraminifera tends to be in the shallower cores (Fig. 6.6A). The plot shows the rapid decrease in abundance of benthic foraminifera to ~2000 m; after 3000 m water depth benthic abundances increase where dissolution and fragmentation have concentrated the more resistant benthic foraminifera by removal of planktic foraminifera. Factors governing the number of benthic foraminifera present in the sediment are the high current velocities in areas of the NZSSO, the constant movement of the substrate inhibiting benthic colonisation of these regions; and below the lysocline continuous removal of carbonate from benthic foraminiferal tests by dissolution stresses the benthic foraminifera (Echols, 1971; Kennett, 1982).

Table 6.6 Mean Benthic Foraminiferal Percentages

Core	Mean benthic %	Depth m
36-42	5.4	461
36-41	1.0	951
16-9.	1.0	1052
36-40	2.2	783
34-1	0.7	1041
36-39	0.8	2999
16-8.	3.0	5117
36-38	0.9	4129
50-33	0.6	4550

Due to the low percentages of benthic foraminifera present in the NZSSO cores (Table 6.6) statistically accurate conclusions are unable to be drawn. Some broad faunal patterns can be derived from NZSSO core 36-42.

The NZSSO benthic foraminifera in Table 6.5 are commonly associated with intermediate to deep cold water from around the world (Nelson *et al.,* 1993a; McDougall, 1996). The benthic foraminifera *Epistominella exigua* is one of the indices for depths greater than 2000 m in Uchio (1960) and van Morkhoven *et al.* (1986). Uchio (1960) mentions *Epistominella exigua* being present in shallower assemblages also.

This is in agreement with Kurihara and Kennett (1986) who found benthic assemblages at DSDP sites 206 and 590 to be dominated by *Epistominella exigua* . These sites are at depths of 3196 m, and 2131 m respectively and under possible influence of AABW. McDougall (1996) observed *Epistominella exigua* prefers colder waters having temperatures between 1.9-3.9°C, and young oxygenated water masses such as AABW and CPDW. Cooke (1988) found that in the late Quaternary section of core DSDP site 594 (1204 m), *Epistominella exigua* was dominantly restricted to glacial sections. Nelson *et al.* (1993a) at DSDP 594 observed *Epistominella exigua* was rare to absent from the modern and biopelagic sediments, but is abundant in hemipelagic oozes associated with colder bottom water conditions. The presence of *Epistominella exigua* at mid-bathyal depths at DSDP site 594 was attributed to expanded deep cold water upwelling in the Bounty Trough.

Bandy and Echols (1964), in studies from the Gulf of Mexico, Gulf of California and Antarctica, state that 80% of all *Epistominella exigua* present occurred between depths of 500-1000 m, with an upper limit of occurrence of between 200-300 m water depth. NZSSO core 36-42 in 461 m water depth agrees, showing *Epistominella exigua* ranging up to ~10% of the benthic population (Fig. 6.6B, Table 6.5).

Faunal assemblages in the Southeast Indian Ocean suggest *Globocassidulina subglobosa* dominates slightly warmer water bodies (3-5°C) where AABW and Indian Bottom Water (IBW) mix (Corliss, 1979). However van Morkhoven *et al.* (1986) place the *Globocassidulina subglobosa* preferred habitat in upper bathyal depths of 200-300 m. This is in agreement with NZSSO cores where *Globocassidulina subglobosa* is abundant in the shallower cores. The depth habitat for the benthic foraminiferal assemblages in NZSSO core 36-42 (Table 6.5 and Fig. 6.6B) is upper bathyal (van Morkhoven *et al.*, 1986). Core 36-42 has *Epistominella exigua* and *Globocassidulina subglobosa* lying in surface water and possibly upper Subantarctic Mode Water (SAMW). An inverse relationship exists between *Epistominella exigua* (which has a colder water preference) and *Globocassidulina subglobosa* (with a warmer water preference) in the benthic population of NZSSO core 36-42 (Fig. 6.6B). The point at which *Epistominella exigua* increases and *Globocassidulina subglobosa* decreases is ~30 cm downcore. By comparing the benthic record with the oxygen isotopic record for core 36-42 (Section 7.1.1) the increase in abundance of *Epistominella exigua* occurs during warming times (i.e. Stage 3), which seems to contradict its preferred depth and temperature habitat, while *Globocassidulina subglobosa* dominates benthic assemblages during cooler glacial times (i.e. Stages 2 and 4).

To explain these benthic foraminiferal anomalies the benthic habitat changes between glacial and interglacial conditions must be considered taking into account changes in oceanic climate conditions. The southern Campbell Plateau where NZSSO core 36-42 presently lies is in 461 m of water. As sea level dropped by ~120-160 m during the last glacial (Shackleton, 1987), producing a shallow ~300-340 m deep site bounded to the north and east by a shallow relatively warm seas. This shallow relatively warmer sea overlying Campbell Plateau fed warm water over core site 36-42, providing a preferred habitat for *Globocassidulina subglobosa* of 3-5°C at a depth of 200-300 m. As the southern hemisphere temperature began to warm (11-13 ka) the sea level began to rise and an increase in water depth, and possible encroachment of SAMW over the site, created the preferred habitat for *Epistominella exigua*, ~2°C cooler and in the upper depth range for *Epistominella exigua*.

Table 6.7 Percentage Abundances of Radiolaria in the cS Fraction

Samples		A. a %	A. spp. %	L. m %	Sg. spp. %	T. o %	Cc. b %	P. spp. %	S. o %
16-8									
	10	19	32	12	34	0	0	0	0
	30	27	23	5	37	0	0	3	1
	50	26	20	2	41	1	0	6	1
	70	19	15	6	46	0	0	5	0
	90	44	29	0	9	1	2	14	1
36-38									
	0	48	9	4	32	1	1	1	4
	10	45	4	9	35	2	0	3	3
	20	40	5	7	41	1	0	3	3
	30	43	5	10	35	1	0	3	2
	40	32	6	10	42	1	0	1	5
	50	42	4	12	36	1	0	3	2
	60	36	4	10	45	1	0	1	2
	70	57	3	11	24	1	0	2	3
	80	39	3	12	33	1	1	6	4
	90	36	3	16	38	2	0	3	2
50-35									
	0	24	13	3	52	1	0	1	2
	20	54	8	4	19	0	0	14	1
	40	45	11	3	22	0	0	13	1
	60	62	8	1	15	0	0	10	1
	80	42	30	2	14	0	0	10	0
	100	59	18	2	10	0	0	8	0
50-34									
	0	47	10	4	33	0	0	2	2
	10	56	3	4	26	1	0	9	1
	20	64	5	3	20	1	0	7	0
	30	66	4	2	20	1	0	7	0
	40	66	10	0	15	0	0	7	0
	50	72	4	4	11	0	1	8	1
	60	61	13	4	14	0	2	6	0
	70	79	1	1	5	0	8	7	0
	80	61	12	2	12	0	10	2	0
	90	82	1	0	8	0	7	2	0
	100	44	18	1	21	0	10	6	0
34-3									
	0	63	2	5	25	0	0	3	1
	20	64	6	1	18	0	0	6	1
	40	51	9	5	19	0	0	6	0
	60	74	0	3	8	0	0	14	0
	80	50	5	0	24	0	0	16	1
	100	51	6	3	18	0	0	20	0
50-33									
	0	72	2	3	20	0	0	3	0
	20	60	5	7	26	0	0	2	0
	40	53	10	7	23	0	0	3	3
	60	44	9	4	28	0	0	15	0
	80	53	10	4	17	0	0	14	1
	100	49	14	5	17	0	0	15	0

Actinomma antarcticum (A. a), Actinomma species (A. spp.), Lithelius minor (L. m), Spongodiscus species *(Sg. spp.), Tetrapyle octacantha (T. o), Clathrocyclas bicornis (Cc. b), Prunopyle* species *(P. spp.)* and *Spongopyle osculosa (S. o).*

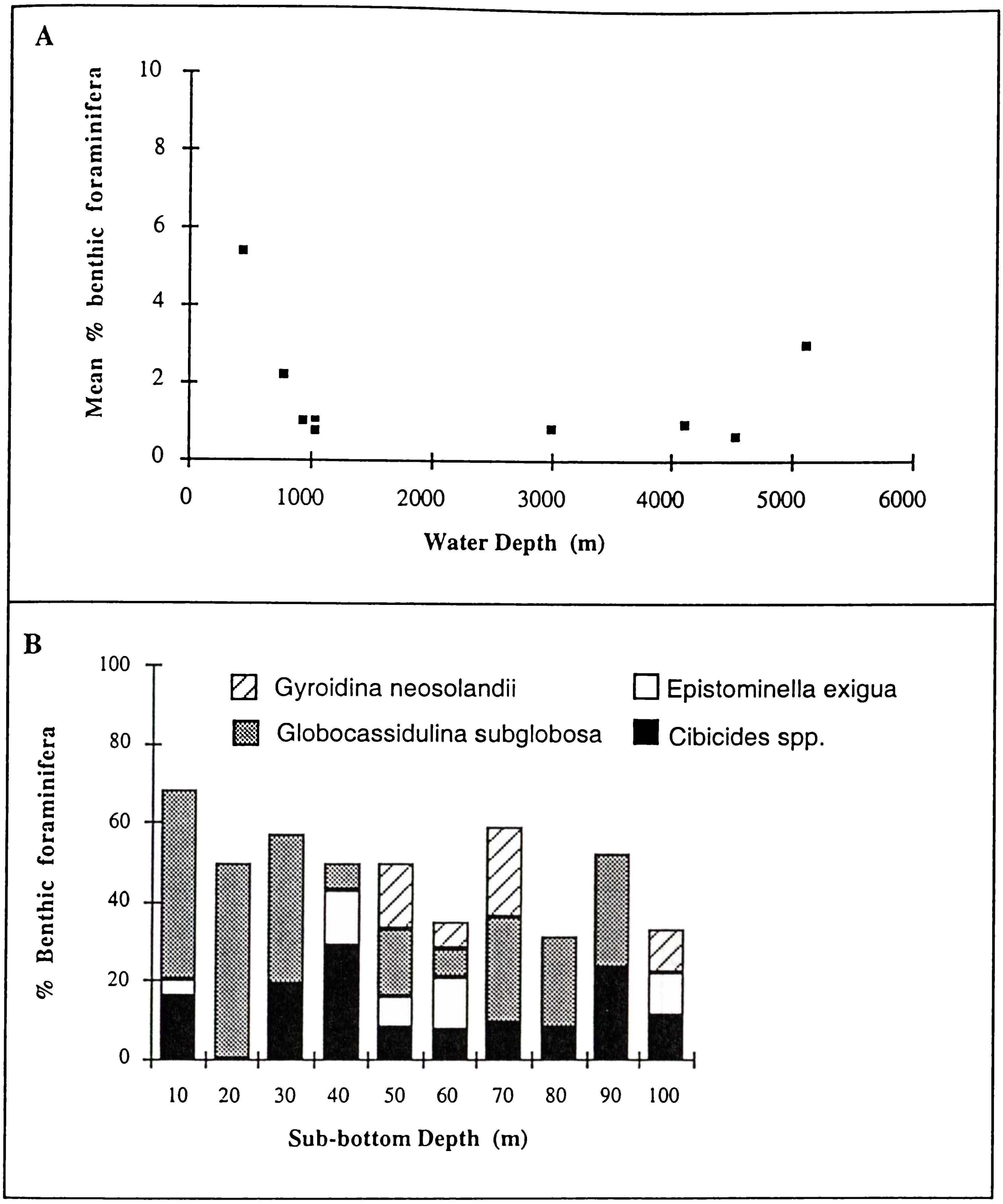

Fig. 6.6 (A) Mean benthic foraminiferal percent versus water depth for the NZSSO cores. (B) Common benthic foraminifera in NZSSO core 36-42, shown as a percentage of the total benthic population. Data from Table 6.5.

6.5 Radiolarian Assemblages

Radiolaria dominate the coarse sand fraction of sediment from south of the SAF. Within the coarse sand fraction 14 radiolarian species are identified, plus a further 7 species in the fine sand fraction. The common radiolaria (Table 6.7; Plate 6.3) in the coarse sand fraction are the suborder Spumellaria, which is dominated by spherical, oval or discoidal forms (i.e. *Actinomma antarcticum*, *Prunopyle* spp. and *Spongodiscus* spp.). These forms have thicker walls and larger test sizes than the

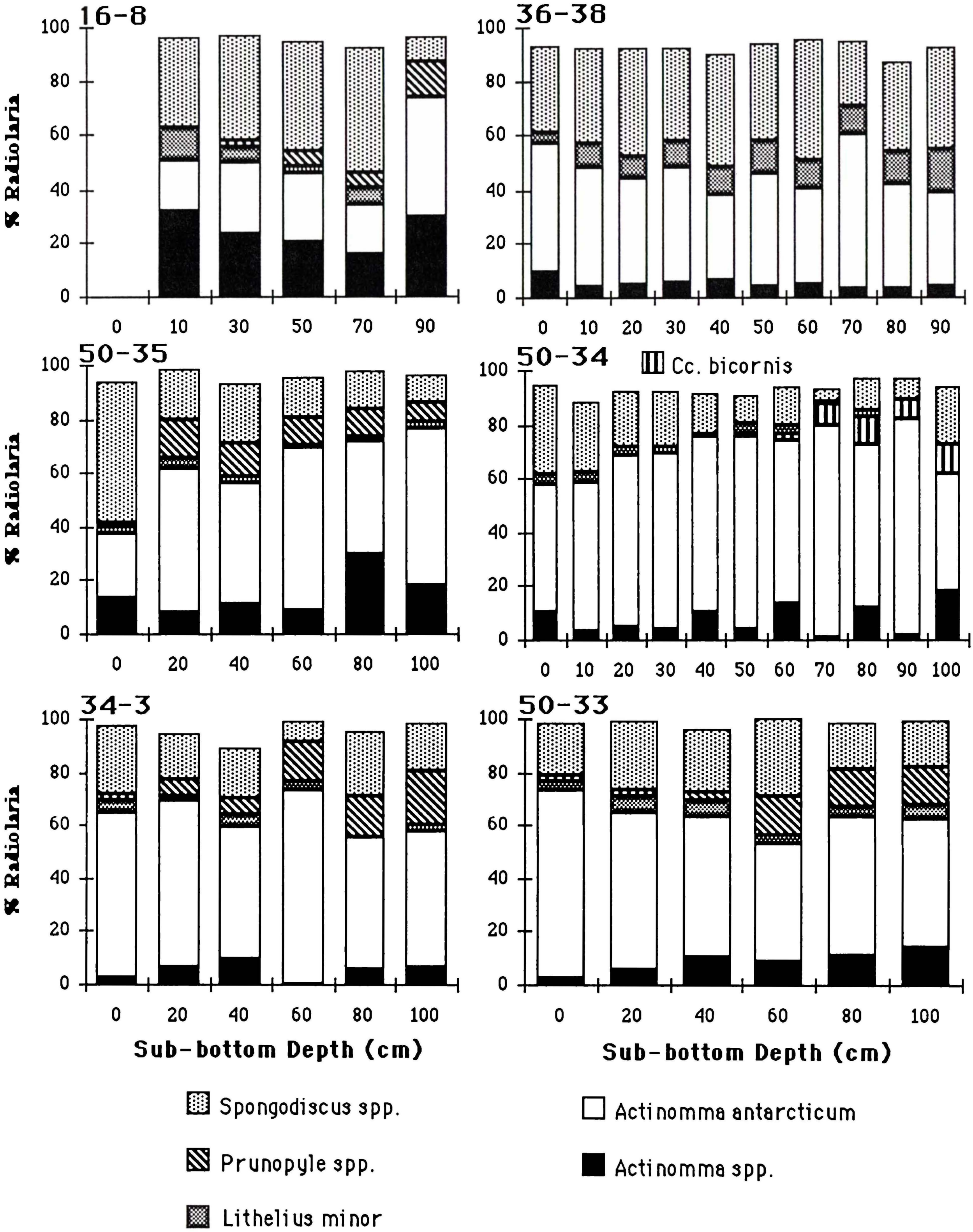

Fig. 6.7 Common radiolaria in the cS fraction of NZSSO core samples, shown as percentages of the total radiolarian population. *Actinomma antarcticum, Actinomma* species, *Lithelius minor, Prunopyle* species, *Clathrocyclas bicornis* and *Spongodiscus* species. Data from Appendix 5.

suborder Nassellaria (Kennett, 1982). The suborder Nassellaria (i.e. *Antarctissa* spp., *Peripyramis* sp. and *Batryocyrtis scutium*) are bell or cap-shaped, with one or more segments uniserially arranged. Nassellaria are smaller, thin shelled and fragile, and are most common in the fine sand fraction of sediment in NZSSO cores south of the SAF (Table 6.8).

By recombining the data from the coarse sand census and the fine sand semi-quantitative census a representative radiolarian assemblage for the NZSSO cores south of the SAF has been established (Table 6.9). The radiolaria presented in Table 6.9 represent a cold water antarctic fauna, characterised by *Actinomma antarcticum, Antarctissa denticulata, Lithelius minor* and *Batryocyrtis scutium* (Hays, 1965). *Actinomma antarcticum* can be used as an indicator of the position of the AAPF, as the greatest abundance of this species occurs ~3° north of the AAPF, and it becomes the dominant radiolarian species (Hays, 1965). Fig. 6.7 shows for cores 50-34, 34-3 and 50-33 that *Actinomma antarcticum* ranging from 55-65% of the radiolarian assemblage, and Fig. 1.4 shows these cores lie ~3° north of the AAPF.

The radiolarians present indicate sediment of a mid-late Quaternary age, corresponding with Petrushevskaya's (1975) Zone A or radiolarian zone NR3+4 of Caulet (1986), which is characterised by the presence of *Antarctissa denticulata* and *Actinomma antarcticum.* This corresponds with Hays (1965) zones ψ and χ (Chen, 1975). The species present in the NZSSO cores represent a typical late Quaternary antarctic radiolarian assemblage. The presence of *Clathrocyclas bicornis*, although rare to absent in most NZSSO cores, represents a significant component of the radiolarian assemblage in core 50-34 from 70 cm downcore. According to Hays (1965), *Clathrocyclas bicornis* represents radiolarian zone Ø of lower Matuyama, late Pliocene age (Keany & Kennett, 1975).

As no other NZSSO core in the region registers this appearance of *Clathrocyclas bicornis,* and the *Clathrocyclas bicornis* do not appear to be transported, indicating it is a true record of core 50-34. This suggests the core has undergone extreme erosion removing ~1.4 million years of sedimentary record, allowing recent sediments to directly lie upon Pliocene sediments. Supporting evidence for the extensive reworking and transporting of material is shown by bedforms at great depth, sediment particles having ferruginous coatings, and paleomagnetic dating of material (Fig. 3.5), showing that some cores have lost Brunhes to upper Matuyama sediments (Goodell & Watkins, 1968; Watkins & Kennett, 1972, 1977; Ledbetter *et al.,* 1983; Osborn *et al.,* 1983).

Table 6.8 Common Radiolaria in the fine sand Fraction

Samples	Ac. sp. %	A. a %	An. spp. %	B. s %	L. m %	Pp. %	P. spp. %	Sg. spp. %	T. o %	Cc. b %
36-38										
0	5	20	29	0	2	13	11	6	6	2
10	3	14	36	0	7	15	9	4	2	1
20	3	15	48	2	0	10	11	8	0	0
30	1	7	34	2	2	19	11	6	2	1
40	3	21	35	3	5	10	8	6	3	0
50	1	8	46	6	3	17	10	4	0	0
60	3	20	41	1	3	16	7	7	0	1
70	2	12	46	3	2	11	9	6	1	1
80	3	15	45	5	5	6	7	6	1	0
90	3	9	46	1	4	10	12	9	3	0
50-34										
0	5	10	43	4	3	7	6	12	3	1
10	2	15	46	4	5	5	10	9	1	0
20	1	16	38	4	3	5	14	13	3	1
30	3	16	35	4	5	5	15	5	5	2
40	2	14	38	2	6	7	12	11	2	3
50	6	17	35	4	5	7	11	10	2	2
60	4	11	38	7	5	6	7	10	1	4
70	2	17	34	0	2	2	10	19	0	9
80	2	15	37	1	3	7	8	10	1	8
90	0	27	22	0	6	8	2	12	2	16
100	1	22	31	0	3	3	11	10	1	8

Common radiolaria as a percentage of the radiolarian population in the fine sand fraction (Appendices 6.3 and 6.4). *Acanthodesmiidae (Ac.* sp.*), Antarctissa* species *(An.* spp.*), Actinomma antarcticum (A. a), Batryocyrtis scutium (B. s), Lithelius minor (L. m), Peripyramis (Pp.), Prunopyle* species *(P.* spp.*), Spongopyle* species *(Sg.* spp.*), Tetrapyle octacantha (T. o)* and *Clathrocyclas bicornis (Cc. b).*

Table 6.9 Radiolarian Assemblage of NZSSO cores

*Actinomma antarcticum**	*Actinomma* spp.
Lithelius minor	*Spongodiscus* spp.*
Prunopyle spp.*	*Spongopyle osculosa*
Antarctissa spp.*	*Peripyramis* spp.*

* Strongest association.

Using the mean radiolarian data for the coarse sand fraction (Table 6.10), and plotting these mean values against latitude (Fig. 6.8) and water depth (Fig. 6.9), reveals some general trends for the radiolarian assemblage.

Table 6.10 Mean Radiolarian Percentages for the coarse sand fraction

Samples	A. a %	A. spp. %	L. m %	Sg. spp. %	T. o %	Cc. b %	P. spp. %	S. o %
16-8.	27	24	5	33	0	0	6	1
36-38	42	5	10	36	1	0	3	3
50-35	48	15	3	22	0	0	9	1
50-34	63	7	2	17	0	3	6	0
34-3	59	5	3	19	0	0	11	1
50-33	55	8	5	22	0	0	9	1

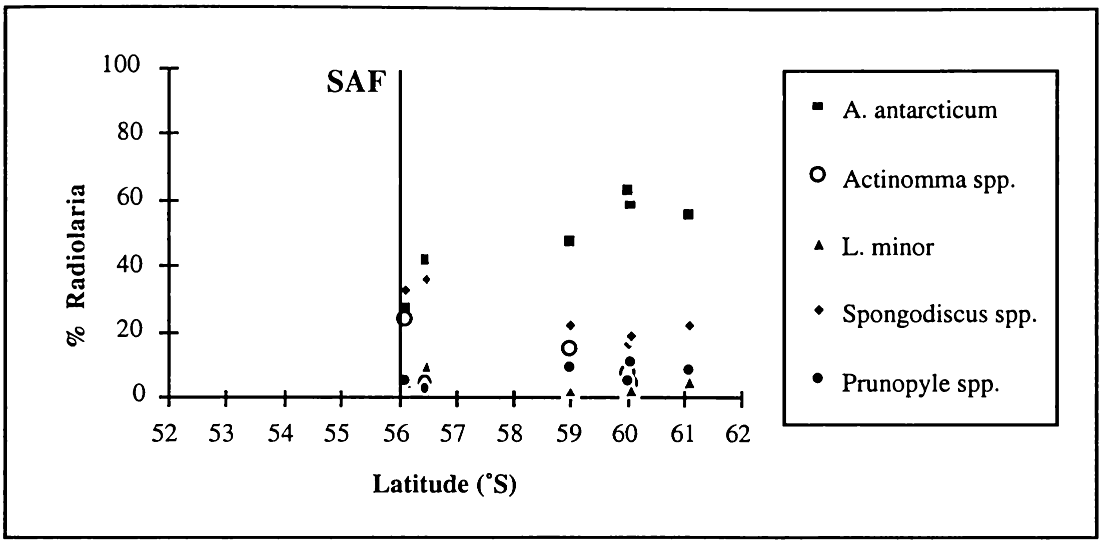

Fig. 6.8 Common radiolarian species found in the coarse sand fraction, shown as percentage of total radiolarian population, plotted against latitude (°S). Data from Appendix 5.

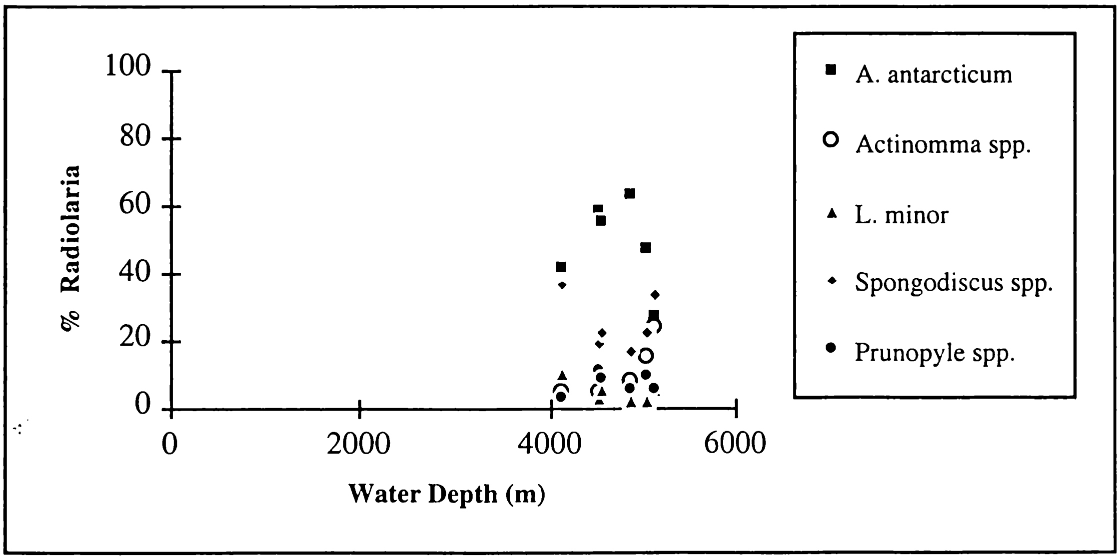

Fig. 6.9 Common radiolarian species found in the coarse sand fraction, shown as percentage of total radiolarian population, plotted against depth (m). Data from Appendix 5.

These trends indicate that the radiolaria do not inhabit subantarctic waters north of the SAF (~56°S; Fig. 6.8) that directly overlie the Campbell Plateau. This is possibly due to a number of factors.

- Aggressive competition with foraminifera, nannofossils and other organisms for habit and nutrients.

- Radiolaria are siliceous biogenic organisms and require the presence of silica for test formation. The absence of free silica within the watermass would render the watermass barren to radiolaria (Vincent *et al.,* 1991).

The main reason for the absence of radiolaria on the Campbell Plateau is probably the absence of free silica in the surface water and AAIW that washes over the southern margins of the Campbell Plateau (Werner, 1977; Vincent *et al.,* 1991). The dominant sources for silica which radiolaria incorporate in their opaline silica test is derived from the continental landmasses of Antarctica and New Zealand and/or from the LCPDW, NADW and NPDW watermasses (Kennett, 1982). Radiolaria are aggressive scavengers of silica: silica derived from Antarctica through weathering is rapidly incorporated into radiolarian tests in the waters surrounding Antarctica, while silicic-rich terrigenous sediment being weathered and eroded off New Zealand is transported away from the Campbell Plateau via the Solander Trough and Bounty Trough. Consequently, silicic terrigenous material is rare to absent on the Campbell Plateau. The deep water bodies LCPDW and NADW that are rich in silica do not wash or upwell on to the Campbell Plateau, but are carried along the southern margin by the coupled ACC-DWBC (Gordon, 1975b; Carter *et al.,* 1996a,b; Carter and McCave, 1997). The lack of free silica in the water masses that lie north of the SAF (~56°) on the Campbell Plateau is the critical factor limiting radiolaria north of the SAF on the Campbell Plateau in the NZSSO cores.

The presence of radiolaria well north of the SAF in the Bounty Trough (45°S) and on the Chatham Rise (43°S) (Fig. 1.4) is likely due to the influence of cold silica-rich LCPDW eddying up the Bounty Trough supplying sufficient silica to build and maintain opaline silica tests (Griggs *et al.,* 1983; Cooke, 1988; Neil, 1991; Nelson *et al.,* 1993a). Griggs *et al.* (1983) attributed the increase in radiolarian abundance during the glacial periods to intensified AABW in the Bounty Trough, which through upwelling introduced silica and cooler more nutrient-rich water over the Bounty Trough region. AABW has been shown not to enter the Southwest Pacific Basin (Rodman & Gordon, 1982; Belkin and Gordon, 1996). The upwelling Griggs *et al.* (1983) mentioned is probably associated with LCPDW rather than AABW.

Dissolution of silicic radiolarian and diatom tests is possible in surface and shallower watermasses such as those present on the Campbell Plateau. Surface waters are undersaturated in silica, and a silica corrosion zone (SCA) lies from 0 to ~1000 m depth (Berger *et al.,* 1989). Between these depths silica is actively dissolved similarly to calcium carbonate below the carbonate compensation depth (CCD). Five of the six NZZSO cores lying on the Campbell Plateau range in depth from 461 m to 1052 m (Fig. 3.1). Any silica present in the sediment is probably being actively corroded, with loss of radiolarian and diatom tests from the northern NZSSO cores if indeed they were ever there in the first place (Berger *et al.,* 1989; Kennett, 1982)

Nutrient supply does not appear to be a critical factor for the absence of radiolaria north of the SAF since the NZSSO is a region of moderate to high productivity (Bradford, 1980a,b). Nannofossils, which can be used as an indicator of paleoproductivity due to their sensitivity to ecological conditions, show high abundance in this study and previous work (Edwards & Perch-Nielsen, 1975; Lohman, 1986). Productivity in the Southwest Pacific is thought to have been enhanced during the glacials, in response to increased iron levels entering the ocean water due to iron-rich terrestrial sediments being blown over the ocean by the intensified weather patterns (Berger *et al.,* 1989; Kumar *et al.,* 1995). However, these weather patterns lie to the north of the southern Campbell Plateau during glacial periods. The lack of iron and limited free silica in the watermasses lying over the southern Campbell Plateau inhibited siliceous biogenic organisms from colonising the surface waters over the Plateau. The radiolarian sediments all occur at depths greater than 4000 m (Fig. 6.9), representing 65-100% of the total biological component of the sediment in the coarse sand and fine sand fractions of sediment south of the SAF; the remaining sediment is composed of diatoms and poorly preserved foraminifera.

6.6 Diatom Assemblages

The dominant biogenic component of the sediment south of the SAF in the NZSSO cores is diatoms. These are mainly limited to the mud fraction, but no quantitative or semi-quantitative study has been undertaken on the diatom assemblages. However, smear slide and SEM analysis has allowed identification of the major types (Table 6.11), which are moderately to well preserved (Plate 6.4).

Table 6.11 Diatom Assemblage in NZSSO Cores South of SAF

Coscinodiscus lentiginous	*Coscinodiscus* spp.
Asteromlampra affinis	*Hemidiscus karstenii*
Rouxia peragalli	*Rouxia antarctia*
Triceratium coscinoides	

This is a Late Quaternary assemblage (0-780 x 10^3 yr) which corresponds with diatom zone NSD 20 (Ciesielski, 1986), or the *Coscinodiscus lentiginous* zone of McCollum (1975). The base of the diatom zone approximately coincides with the base of the Brunhes magnetic epoch (McCollum, 1975).

6.7 Calcareous Nannofossil Assemblages

From SEM analysis of the mud fraction calcareous nannofossils were found to be abundant in NZSSO cores north of the SAF. No quantitative or semi-quantitative study has been carried out on the nannofossil assemblages (Table 6.12). From the identified calcareous nannofossils (Plate 6.5), the assemblage is typical of the late Quaternary, characterised by *Emiliania huxleyi* and assigned to nannofossil zone NN21 (Edwards & Perch-Nielsen, 1975; Lohman, 1986; Martini, 1986; Edwards, pers. commun, 1997).

Table 6.12 Calcareous Nannofossil Assemblage in Northern NZSSO Cores

Emiliania huxleyi (2)	*Coccolithus pelagicus* (3)
Calcidiscus leptoporus (5)	*Coccolithus cf. doronicoides* (4)

(2), (3), (4) & (5) refers to Plate 6.5.

6.8 *Neogloboquadrina pachyderma* Coiling Direction

Many foraminiferal species arrange their chambers in a trochospiral mode in which the coiling direction may be dextral or sinistral. *Neogloboquadrina pachyderma* as a species shows a distinct coiling direction, exhibiting trend four of Bolli (1967) (Hemleben *et al.*, 1989). The coiling preference remains the same worldwide (i.e. the coiling ratio of *Neogloboquadrina pachyderma* dextral to sinistral exhibits the same kind of variation in the southern hemisphere as in the cold waters of the northern hemisphere (Vella *et al.*, 1975; Kohfeld *et al.*, 1996)). Each species within a genera

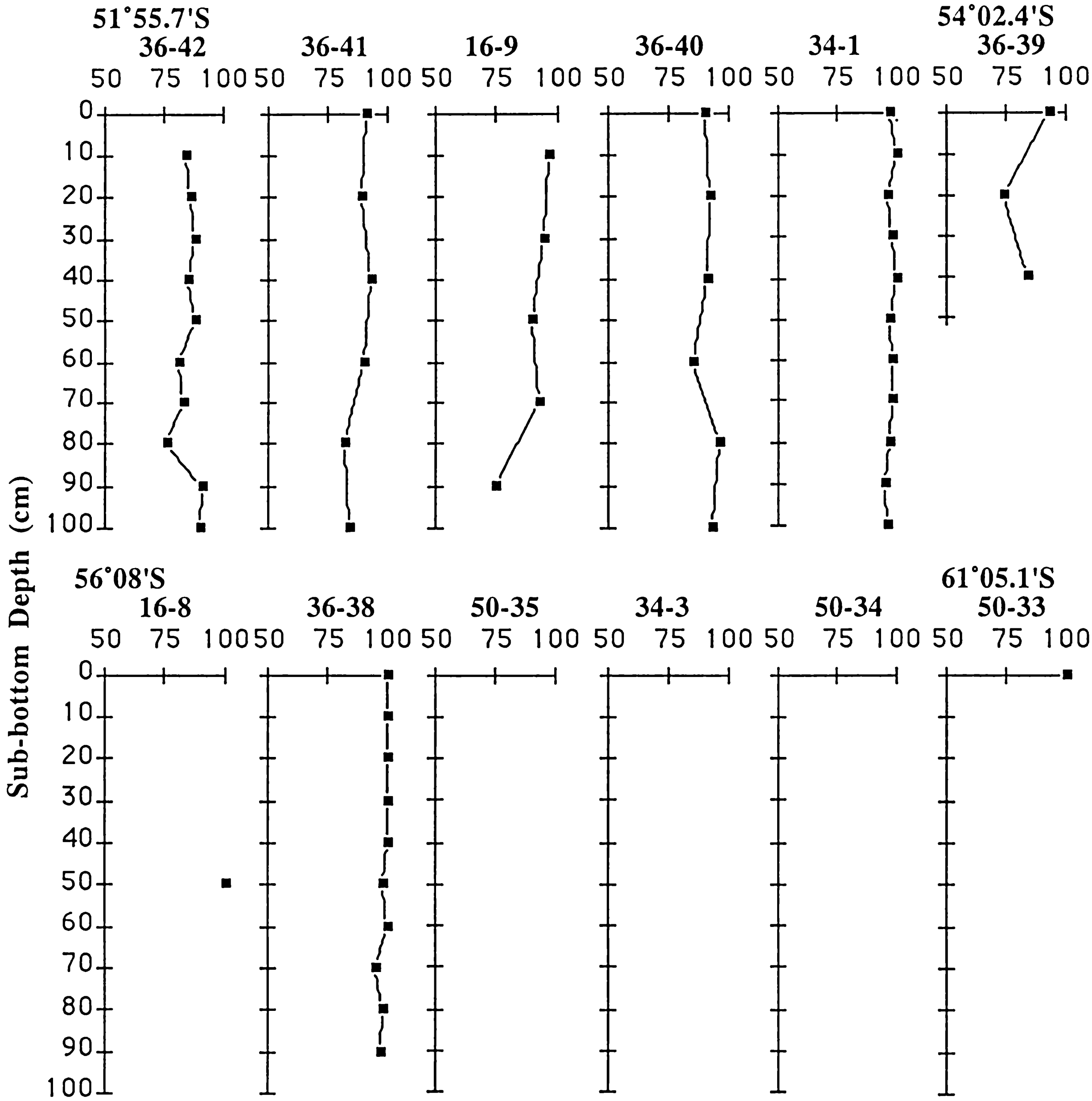

Fig. 6.10 Sintrally coiled *N. pachyderma* percentages for the coarse sand fraction in the NZSSO cores. S = sinistrally coiled, D = dextrally coiled. Data from Appendix 5.

will exhibit a preferred coiling direction, but preferred direction of a given species may be different in different regions at the same time, as with *Neogloboquadrina pachyderma* where preferred coiling is linked to water temperature. *N. pachyderma* exhibits a dominant sinistral coiling direction in cooler water temperatures (0-7°C).

The changes in coiling direction of *Neogloboquadrina pachyderma* have been used as a tool in determining paleoclimatic oscillations of the Quaternary sea-surface temperature (Kennett & Vella, 1975). Vella *et al.* (1975) established that in the coarse sand fraction (> 125 μm) of sediments in the South Pacific the 90% sinistral coiling *Neogloboquadrina pachyderma* isopleth lies a few degrees north of the AAPF, the 50% isopleth varies between 45-50°S, and the 10% sinistrally coiling isopleth lies north of the STF. They devised four groups, Group I lies north of 39°S (i.e. essentially the Subtropical Convergence) representing watermasses warmer than ~12°C. Group II lies between 39°S and 45°S representing a northern subantarctic region of water temperatures ranging from ~8-12°C; neither Groups I or II are observed in the study area and are not discussed further. Group III represents the central subantarctic water masses and lies north of SAF, and indicates sea surface temperatures of ~5-8°C. South of the SAF group IV represents the southern subantarctic and antarctic water masses and arbitrarily designated as having > 90% sinistrally coiled *Neogloboquadrina pachyderma,* occurring where the sea surface temperature is 5°C or less (Fig. 6.3).

The coiling direction for all *Neogloboquadrina pachyderma* populations identified in the coarse sand census were determined and plotted downcore for all NZSSO cores (Fig. 6.10). The *Neogloboquadrina pachyderma* coiling direction was also determined for three selected cores in the fine sand fraction (Fig. 6.11).

The percentage of *Neogloboquadrina pachyderma* sinistral in any core sample was never less than ~65% of the *Neogloboquadrina pachyderma* population. This indicates the NZSSO core sites have remained under Group III and Group IV type water masses as discussed by Vella *et al.* (1975). There is limited variation downcore in the percentages of sinistrally coiled *Neogloboquadrina pachyderma*, indicating that at any one site sea surface temperatures have varied little with time. This lack of downcore variation suggests that sea surface temperature differences between interglacial and glacial periods have been small in higher southern latitudes. Both Cooke (1988) and Neil (1991) off eastern South Island describe dramatic changes in the percentage of sinistral *Neogloboquadrina pachyderma* from low percentages (18-40%) in interglacial periods to percentages of 82-100% during glacial periods. These findings suggest that at lower latitudes the temperature gradient difference between glacial and interglacial periods is much greater than at higher latitudes and more readily observed in the sedimentological record.

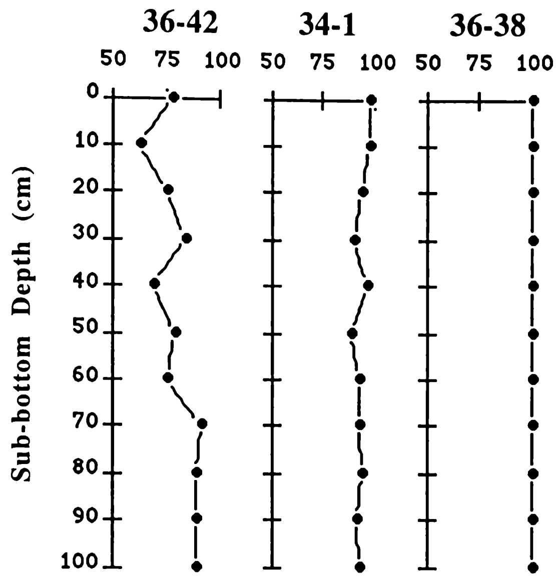

Fig. 6.11 Sinistrally coiled *Neogloboquadrina pachyderma* percentages for the fine sand fraction in selected NZSSO cores. S = sinistrally coiled, D = dextrally coiled. Data from Appendix 6.

The general trends for *Neogloboquadrina pachyderma* are seen in Table 6.13, and associated Fig. 6.12 shows that the higher the southern latitude the greater the percentage of sinistrally coiled *Neogloboquadrina pachyderma* is in the sediment.

Table 6.13 Mean Percentage Sinistrally Coiled *Neogloboquadrina pachyderma* in NZSSO Cores

Core	Depth	Latitude (°S)	N. pachyderma % s coiled
36-42	461	51°55.7'S	86
36-42*	461	51°55.7'S	88
36-41	951	51°56.7'S	89
16-9.	1052	52°25'S	90
36-40	783	52°56.4'S	91
34-1	1041	53°55.4'S	98
34-1*	1041	53°55.4'S	93
36-39	2999	54°02.4'S	84
16-8.	5117	56°08'S	100
36-38	4129	56°28'S	99
36-38*	4129	56°28'S	100
50-33	4550	61°05.1'S	100

* Data from semi-quantitative census of fine sand fraction.

South of the SAF at ~56°S the presence of dextrally coiled *N. pachyderma* is very rare to absent. North of the SAF the percentage of sinistrally coiled *N. pachyderma* decreases slowly to the north. Kennett (1969) observed that the 50% isopleth lies ~47°S; when this study's data (Table 6.13) are extrapolated north they support Kennett's (1969) proposition.

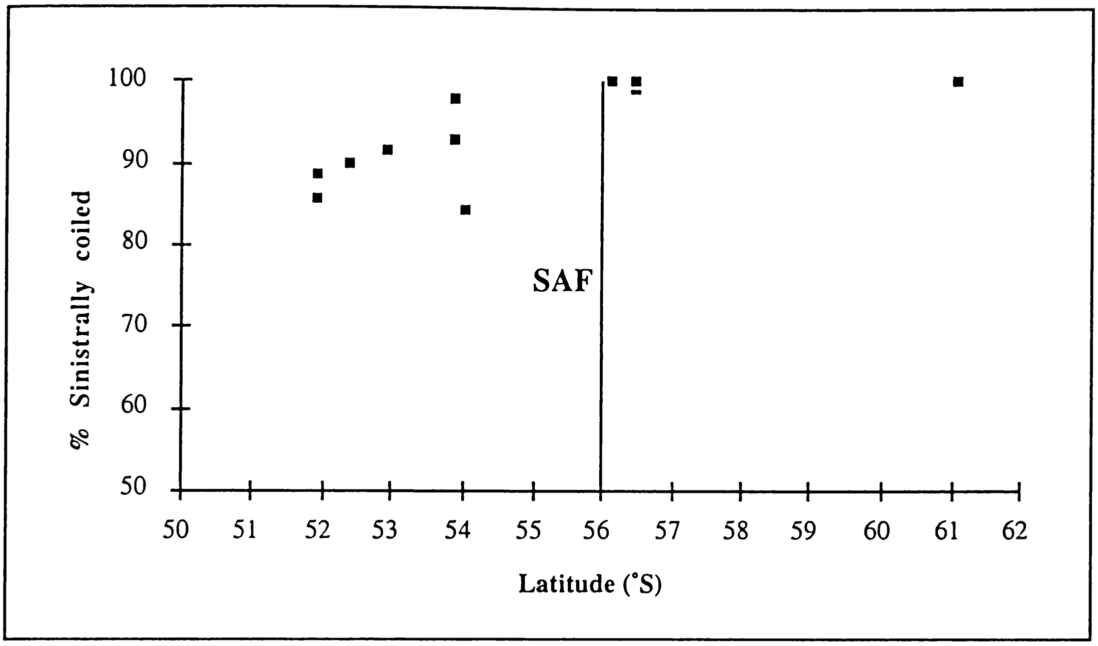

Fig. 6.12 Latitudinal variation in the percentages of *Neogloboquadrina. pachyderma* sinistral in the NZSSO core transect.

In this study the use of *Neogloboquadrina pachyderma* as an indicator of paleoceanographic climatic conditions is limited due to the minor variation that is occurring downcore. The coiling percentages suggest limited past changes in water temperatures over the NZSSO core sites.

6.9 Dissolution of Calcareous Sediments

Carbonate dissolution needs to be considered when undertaking population studies of both planktic and benthic foraminifera, as removal of less resistant forms skews the collected data. Dissolution of calcareous organisms on the sea floor can be considered a function of two factors, the fertility of overlying surface water and the aggressiveness of the bottom water. Carbonate dissolution results from corrosiveness of the water, which increases with the decrease in carbonate ion content, low temperature, high hydrostatic pressure, increased water flow through the sediment and high CO_2 partial pressures. Therefore at greater depth increasing amounts of carbonate are removed from the sediments due to an increase in the above effects (Berger, 1968; Berger *et al.*, 1982; Kennett, 1982; Neil, 1991).

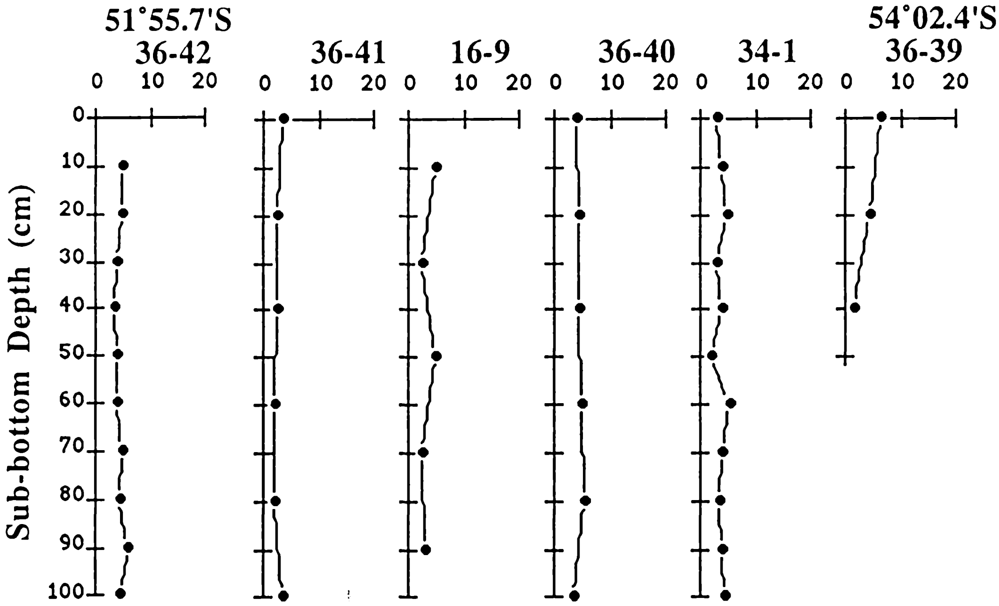

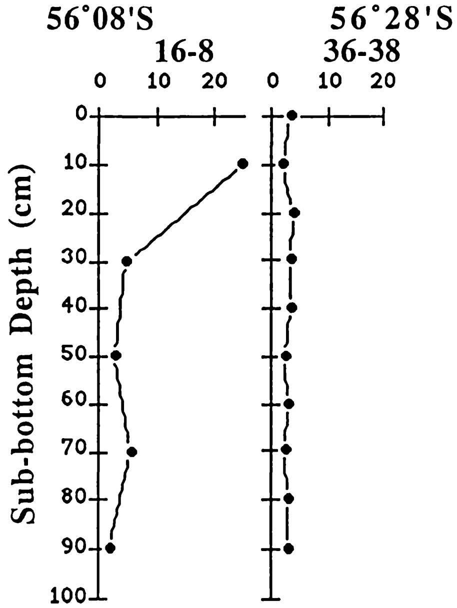

Fig. 6.13 Fragmentation curves of calcareous organism tests in the coarse sand fraction of NZSSO cores. Data from Appendix 5.

Dissolution of calcareous sediments can be estimated by a number of methods, including: (1) ratio of fragments to whole tests; (2) ratio of benthic to planktic foraminifera; and (3) calcium carbonate content of sediment samples (Thunell, 1976; Weaver *et al.,* 1997). Two methods are discussed here, fragmentation and calcium carbonate content. The loss of benthic foraminifera from many of the NZSSO cores from effects other than dissolution, does not allow the use of benthic to planktic ratio accurately in this study.

6.9.1 Fragmentation

Using the fragmentation to whole test ratio approach of Le & Shackleton (1992),

Fragmentation % = 100% x (No. of frags/8) / (No. of frags/8 + No. of whole tests)

From the coarse sand (> 150 μm) census data (Appendix 5), and applying the above calculation, Fig. 6.13 was developed. The NZSSO cores north of the SAF (36-42, 36-41, 16-9, 36-40 and 34-1) show very little change in fragmentation ratio downcore, averaging ~4.5% fragmentation, and indicating limited dissolution. The fragmentation observed may be of mechanical rather than dissolution origin. Certainly the region of the southern Campbell Plateau is swept by strong currents beneath the ACC (Watkins and Kennett, 1972, 1977). Or the fragmentation observed in the northern NZSSO cores may have occurred during hand washing and sieving of samples, reducing the resolution of the index (Volat *et al.,* 1980).

South of the SAF, NZSSO core 16-8 shows strong fragmentation in the top 30 cm of core (Fig. 6.13). This fragmentation is due to water depth and mechanical action. Core 16-8 lies on the southern margin of the Campbell Drift and is directly affected by high current activity under a coupled ACC-DWBC (Carter & McCave, 1994). The dominant species found are *Globorotalia inflata* and sinistral *Neogloboquadrina pachyderma,* both dissolution resistant species. Core 36-38 shows low fragmentation and from the fragmentation ratio alone would appear to show little dissolution. However, when washing planktic foraminifera from the site for isotopic analysis, foraminifera below 20 cm downcore were found to disintegrate, showing severe weakening by dissolution. As a group, fragmentation is seen to decrease with both increasing depth and latitude (Fig. 6.14), with the exception of core 16-8.

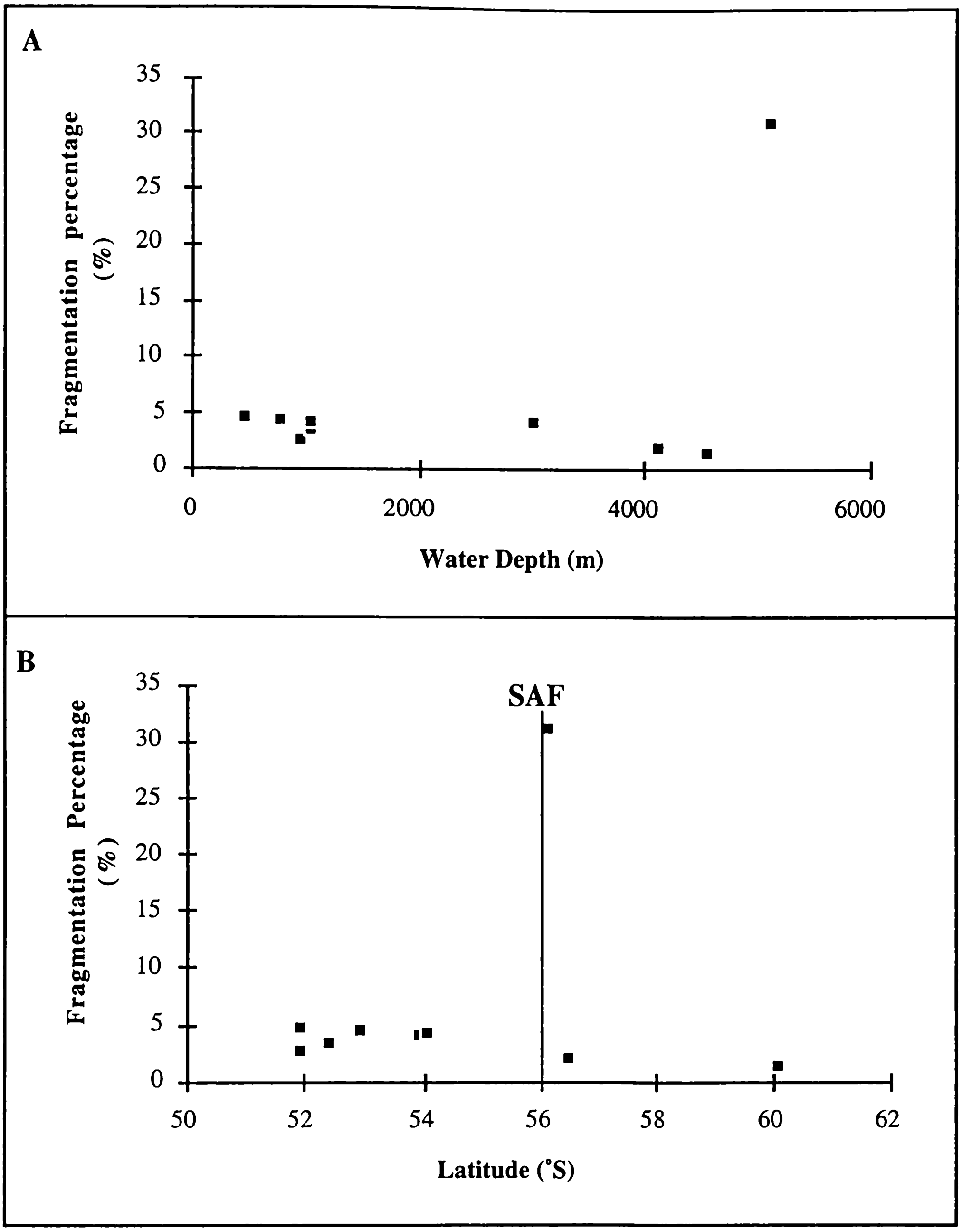

Fig. 6.14 Mean fragmentation ratio versus depth (A) and latitude (B) for the coarse sand fraction of NZSSO cores 36-42, 36-41, 16-9, 36-40, 34-1, 36-39, 16-8 and 36-38. Data from Appendix 5.

An increase in fragmentation is expected with depth, due to the greater influence of dissolution weakening the foraminiferal tests. The decrease in fragmentation may be explained by the removal of fragments into solution by preferential dissolution. The fragmentation of a test exposes greater surface area to dissolution which increases the kinetics of dissolution on fragments. The preferential loss of fragments negatively skews the fragmentation ratio, suggesting less fragmentation at depth than is in fact occurring.

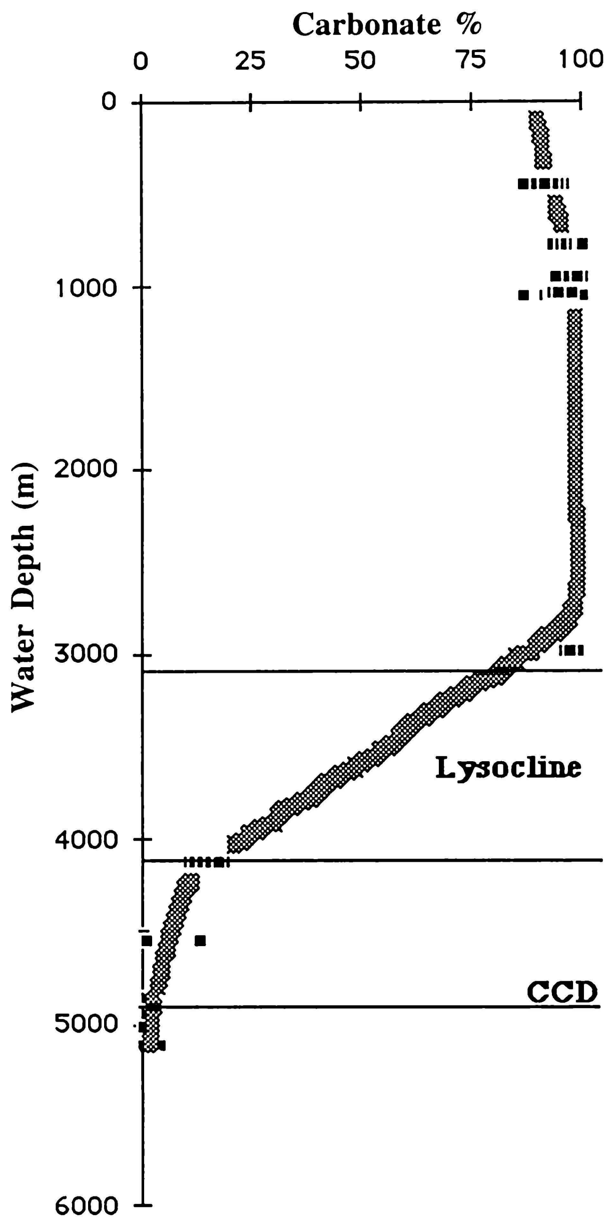

Fig. 6.15 Bulk carbonate for the NZSSO cores against water depth, showing the rapid variation in carbonate composition following ~3000 m depth. Data from Appendix 2.

6.9.2 Calcium Carbonate Dissolution

Another method for determining the influence of dissolution on the sediment is to observe the bulk carbonate curve (Fig. 5.1). These curves indicate there is little to no dissolution occurring in sediment north of the SAF; directly south of the SAF cores show a decrease in carbonate downcore suggesting strong dissolution effects. The exception is core 36-38 which shows little attenuation downcore, although other evidence suggests that it is undergoing similar dissolution effects as other local NZSSO cores south of the SAF.

By comparing bulk calcium carbonate (Fig. 6.15) and mean percentage of planktic and benthic foraminifera (Fig. 6.16) against water depth it is possible to determine the position of the lysocline and the Carbonate Compensation Depth (CCD) within the NZSSO.

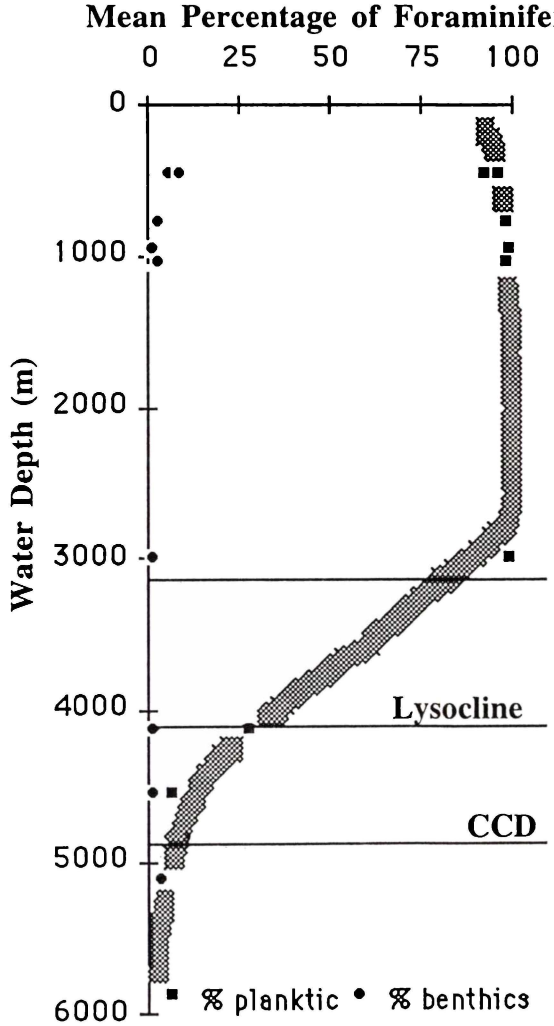

Fig. 6.16 Trend in mean foraminiferal percentages with water depth, showing a rapid shift after ~3000 m depth. Data from Appendix 5.

The lysocline is a depth range over several hundred metres across which the calcium carbonate content (Fig. 6.15) of the sediment changes dramatically (Berger, 1968). Determination of the lysocline point of initiation is based upon the level at which foraminiferal assemblages begin to show obvious solution effects (Berger, 1968; Berger *et al.,* 1982).

Figs. 6.15 and 6.16 suggest that in the NZSSO the lysocline initiates at ~3200 m depth and terminates at ~4100 m, with the CCD the level below which carbonate-free sediment accumulates, lying at ~4800 m. In the NZSSO the lysocline lies in the LCPDW$_{(1)}$ and the CCD within the LCPDW$_{(2)}$. Lisitzin (1972) places the depth at which carbonate begins to rapidly dissolve at between ~3500-~4000 m with the CCD lying at ~4700 m in the Pacific Ocean. Parker & Berger (1971) determined the lysocline to between 4250-4500 m and the CCD at ~4800 m, while Neil (1991) suggested the lysocline within the Bounty Trough lay between 3700-4200 m. Volat *et al.* (1980) suggested the initiation of the lysocline is associated with AABW; however, in the NZSSO AABW is absent due to the mid-ocean ridge barrier (Belkin & Gordon, 1996). Weaver *et al.* (1997) stated that dissolution of sediment increases with depth from about 3500 m and that the CCD lies ~4100 m on the basis of bulk carbonate contents from unpublished McCave & Carter data. There seems little agreement on the depth of initiation of the lysocline and the depth of the CCD. Generally the results of this and other studies are in broad agreement, the depth at which increased dissolution occurs being ~3300 m, and the depth of the CCD at ~4700-~4800 m in the southern Pacific Ocean.

A suggested reason for the greater depths of the lysocline and CCD in the NZSSO could be due to certain water bodies being absent. As Volat *et al.* (1980) suggested the initiation of the lysocline is associated with the AABW. Martinez (1994), with data from the West Tasman Sea, shows the lysocline positioned at ~3600 m which can be associated with AABW flowing northwards into the Tasman Sea Basin. To the east of the Lord Howe Rise, Martinez (1994) found the lysocline to be at ~3100 m, suggesting this was possibly due to the presence of a deep oxygen minimum, high CO_2 corrosive watermass, the North Pacific Deep Water (NPDW). These two water masses are absent from the NZSSO, the AABW being prevented from entering the Southwest Pacific Basin by the mid-ocean ridge (Gordon, 1972, 1977; Belkin & Gordon, 1996) and the NPDW flowing southwards east of the Louisville Seamount Chain to be carried away from the NZSSO by the eastward flowing geostrophic currents (Carter and McCave, 1994). The sediments of the NZSSO lie in watermasses less corrosive than the AABW and NPDW, thereby allowing calcareous sediment to survive to greater depths.

6.9.3 Dissolution of Foraminiferal Assemblages

Previous studies have shown that different species of planktic foraminifera have varying resistance to dissolution. Planktic foraminifera can be ranked on this basis (Table 6.14). A foraminiferal population that contains a greater abundance of dissolution-resistant foraminifera may indicate dissolution effects (Berger, 1968; Parker & Berger, 1971).

As Table 6.14 suggests, the planktic foraminiferal population that contains the greater abundance of high ranked foraminiferal species, the greater the dissolution that the sediment has undergone. Thus poorly preserved sediments contain higher proportions of *Neogloboquadrina pachyderma, Globorotalia inflata*, etc. On this basis the assemblages noted in Section 6.3 and Table 6.1 suggest that foraminifera from south of the SAF, and in deeper water, have undergone strong dissolution.

Table 6.14 Solution Ranking of Planktic Foraminifera

1	*Globigerina quinqueloba*	5	*Globorotalia truncatulinoides*
2	*Globigerina bulloides*	6	*Globorotalia inflata*
3	*Globigerinita spp.*	7	*Neogloboquadrina dutertrei*
4	*Globorotalia scitula*	8	*Neogloboquadrina pachyderma*

The higher the number, the greater the resistance to dissolution (Table adapted from Parker & Berger, 1971).

NZSSO core 16-8 was dominated by kummerform *Neogloboquadrina pachyderma* and *Globorotalia inflata* fragments (over 90% of calcareous fragments could be identified as belonging to *Globorotalia inflata*), suggesting very aggressive dissolution at this site through the entrainment of cold $LCPDW_{(2)}$ over the site and high current velocities below the coupled ACC-DWBC.

6.9.4 Visual Analysis of Dissolution Effects

From SEM analysis of *Neogloboquadrina pachyderma* from NZSSO cores 36-42, 36-38 and 50-34, the effect of dissolution on skeletal structure was noted. The SEM photographs show evidence of progressive dissolution, erosion of surface features, and breakage of chambers (Plate 6.6 1-6). *Neogloboquadrina pachyderma* in Plate 6.6 (1-3) are well preserved, with the classical cubic form. Containing four chambers in the last whorl.

Plate 6.6 (1-3) are *Neogloboquadrina pachyderma* from north of the SAF, and represent typical reticulate forms, with tests having a microcrystalline, well pitted test surface. The aperture lip is well developed in both the sinistral (1, 2) and dextral (3) forms. No evidence of dissolution is present.

South of the SAF in antarctic watermasses the *Neogloboquadrina pachyderma* begin to show evidence of environmental stress and dissolution. Often the final chamber is small giving the foraminifera a more triangular form (Plate 6.6, 5). The crystalline antarctic *Neogloboquadrina pachyderma* from south of the SAF are typified by a thickened crystalline test with distinct euhedral calcite rhombs (4, 5). These southern *Neogloboquadrina pachyderma* in antarctic watermasses begin to show dissolution due to the greater depositional water depth south of the SAF. Plate 6.6 (4, 5) shows loss of surface structure, and loss of definition of the aperture lip. Eventually the surface structure of the tests is weakened to an extent that fragmentation begins (Plate 6.6, 6).

Plate 6.1 Examples of common planktic foraminifera (from Kennett & Srinivasan (1983) found inthe census of NZSSO cores.

1a/b	*Globigerina bulloides,* (1a) x 118, (1b) x 134.
2	*Globigerina quinqueloba,* x 198.
3a/b	*Neogloboquadrina pachyderma,* x 185.
4	*Neogloboquadrina dutertrei,* x 95.
5	*Globorotalia truncatulinoides,* x 90.
6a/b/c	*Globorotalia inflata,* (a) x 113, (b) x 78, (c) x 92.
7	*Globigerinita glutinata,* x 200.
8	*Globigerinita uvula,* x 185.

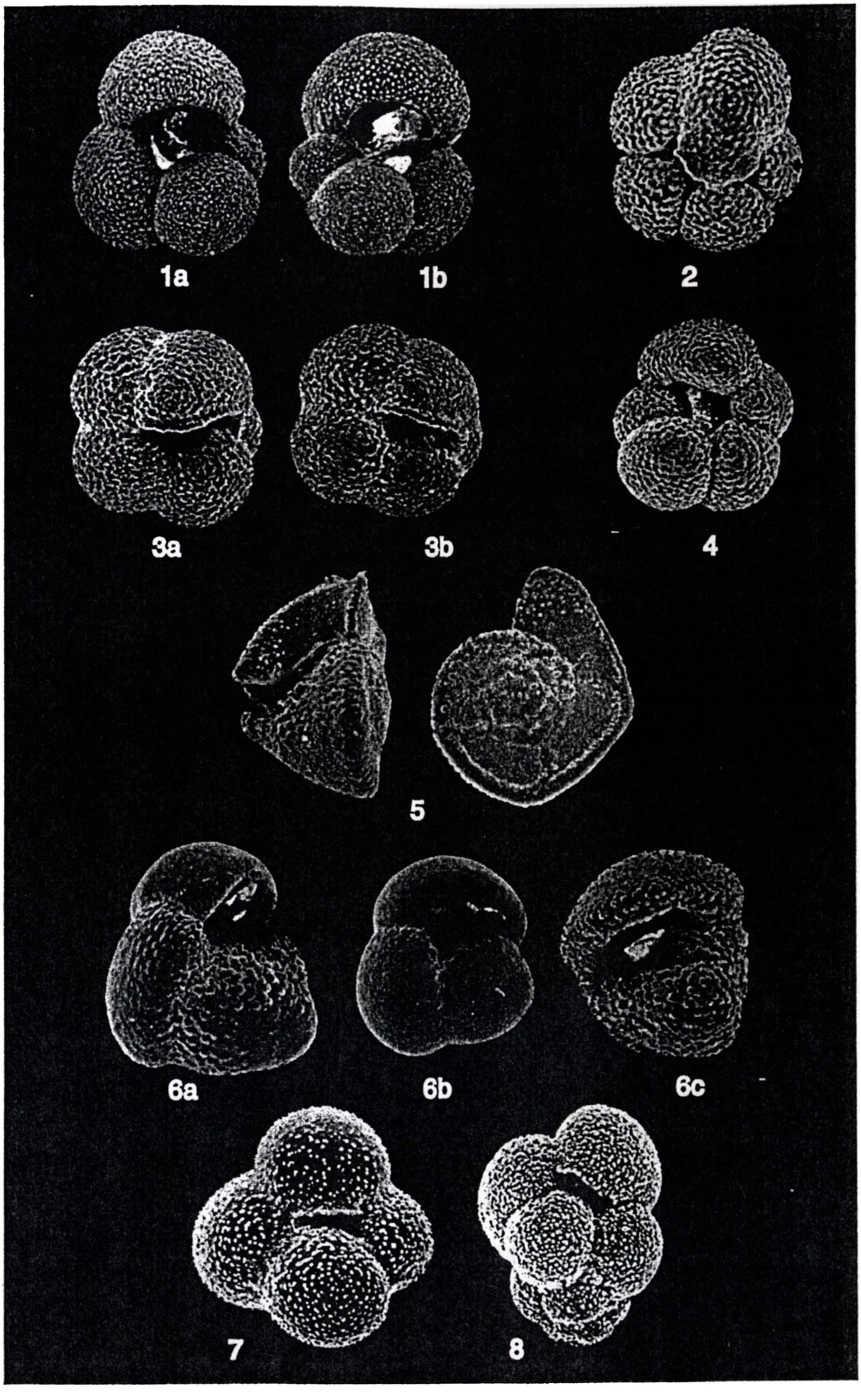
1a
1b
2
3a
3b
4
5
6a
6b
6c
7
8

Plate 6.2 Examples of common benthic foraminifera (from Kurihara & Kennett, 1986) found in the NZSSO core.

1a/b	*Gyroidina neosolandii,* x 160.
2	*Epistominella exigua,* x 227.
3	*Fissurina* sp. x 101.
4	*Bulimina aculeata,* x 120.
5	*Uvigerina peregrina,* x100.
6	*Globocassidulina subglobosa,* x 115.
7	*Ehrenbergina trigona,* x 147.
8	*Cibicides wuellstorfi,* x 70.
9	*Eggerella bradyi,* x 220.
10a/b	*Textularia* sp. x 300.

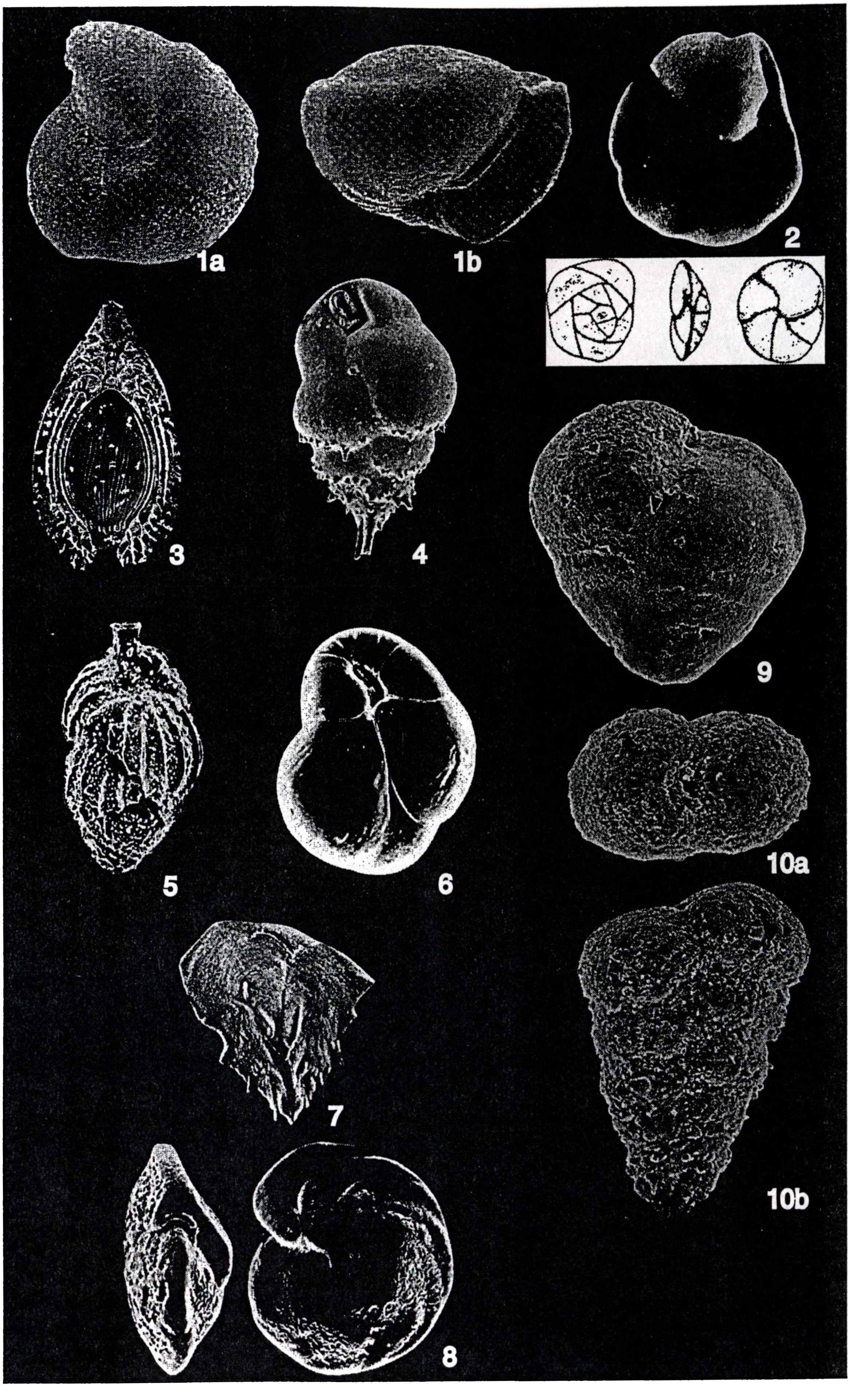
1a
1b
2
3
4
5
6
7
8
9
10a
10b

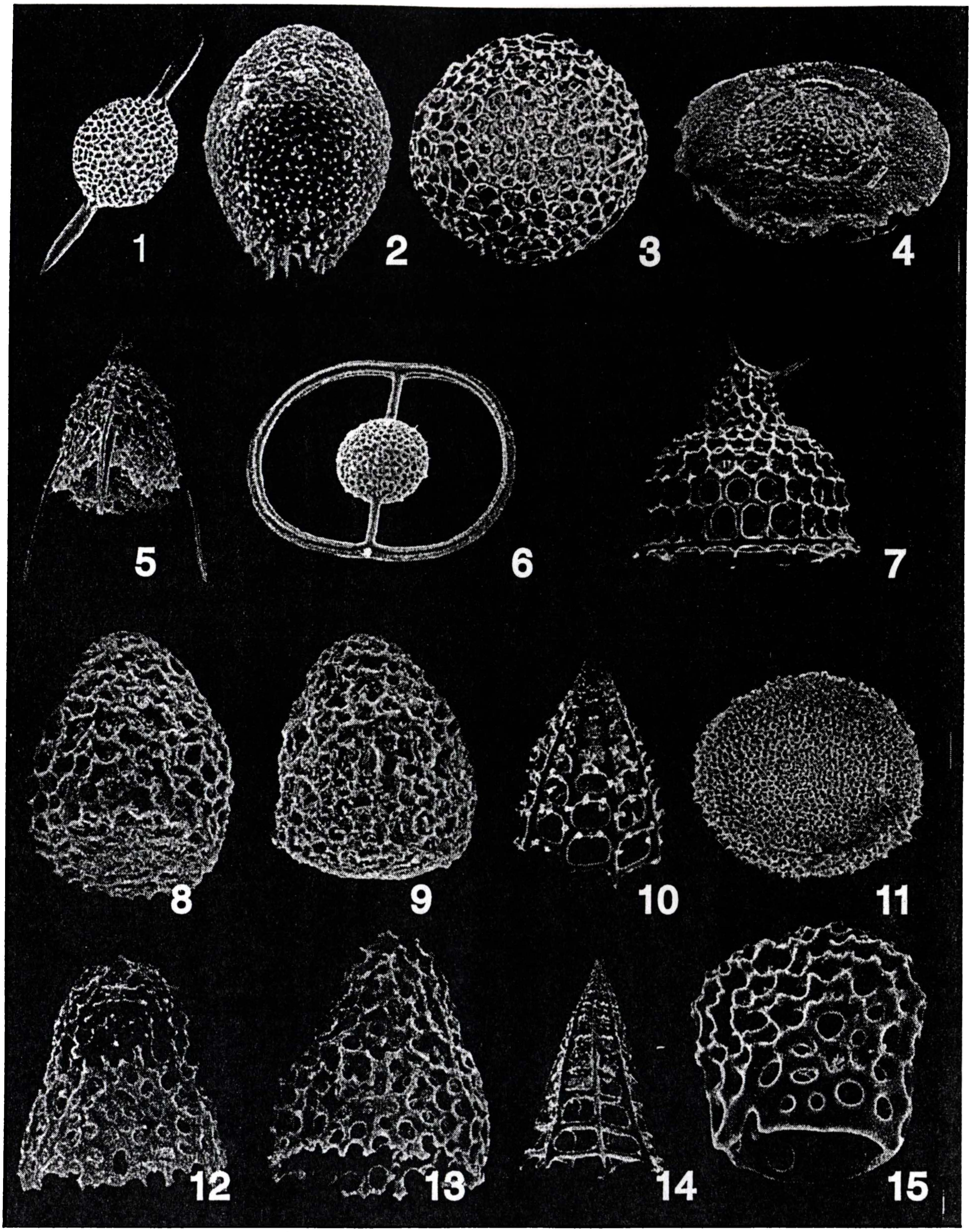

Plate 6.3 Common radiolaria from south of the SAF in the NZSSO. Examples taken from Keany & Kennett (1975). (1) *Stylotracta universa,* x 165; (2) *Prunopyle titan,* x 260; (3) *Actinomma antarcticum,* x 140; (4) *Spongodiscus* sp. x 245; (5) *Pterocanium trilobum,* x 180; (6) *Saturnulus planetes,* x 240; (7) *Clathrocyclas bicornis,* x 245; (8) *Antarctissa denticulata,* x 415; (9) *Antarctissa denticulata,* x 380; (10) *Peripyramis* sp. x 245; (11) *Spongotrochus* sp. x 100; (12) *Antarctissa strelkovi,* x 440; (13) *Antarctissa strelkovi,* x 400; (14) *Plectopyramis* sp. x 140; (15) *Desospyris* sp. x 400.

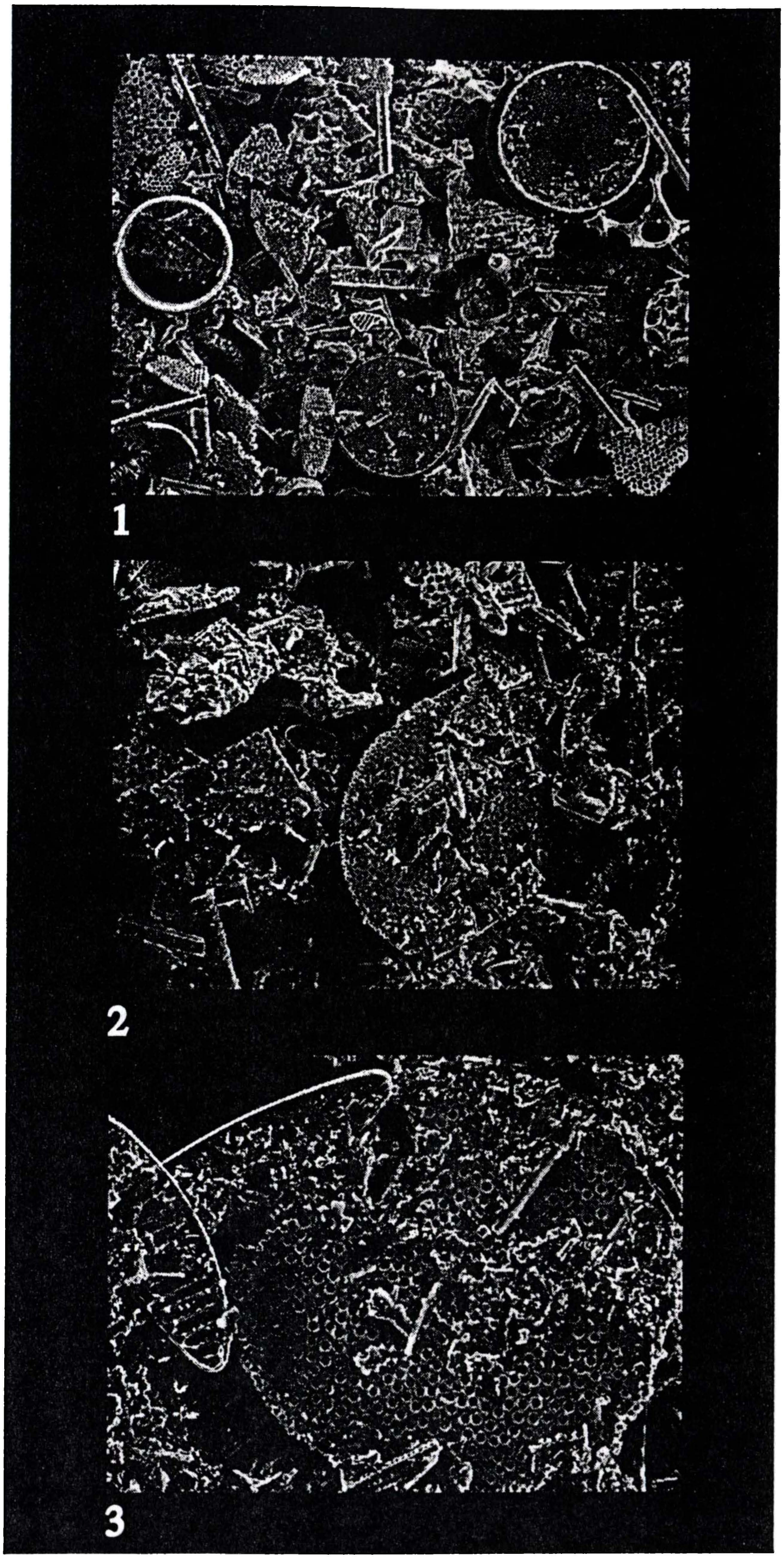

Plate 6.4 (1) NZSSO core 50-34, mud sample from 20 cm downcore, x 400; (2) NZSSO core 50-34, mud sample from 10 cm downcore, x 700; (3) NZSSO core 50-34, mud sample from 10 cm downcore, x 1100. Shows diatoms and radiolarian fragments dominating the mud-size fraction of sediment from south of the SAF.

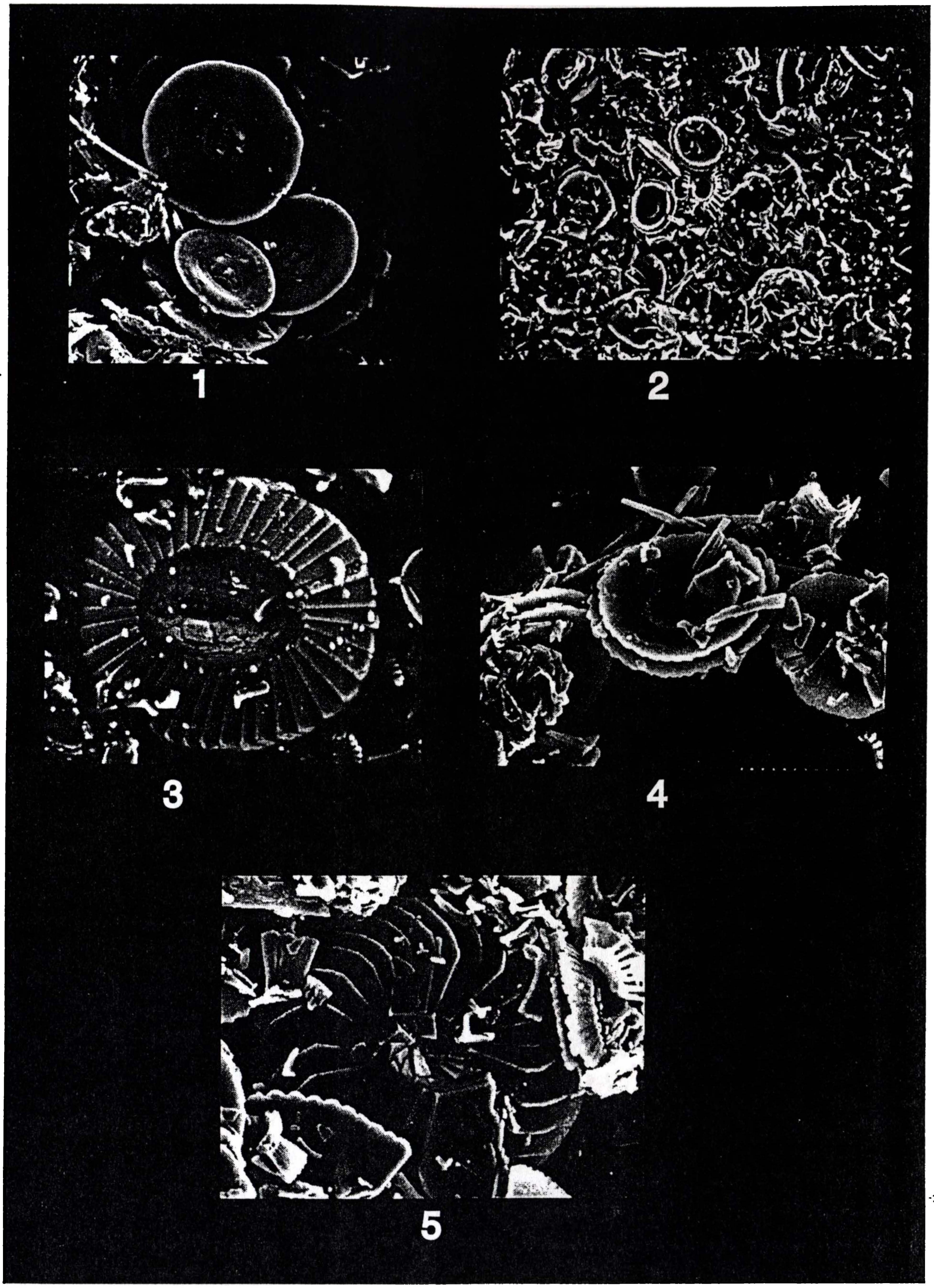

Plate 6.5 Calcareous nannofossils from the mud-sized fraction in NZSSO core 36-42, lying north of the SAF, on the southern margins of the Campbell Plateau. (1) *Coccolithus* sp. x 4500; (2) Calcareous nannofossil ooze, x 3000; (3) *Coccolithus pelagicus,* x 6000; (4) *Coccolithus* cf. *doronicoides,* x 7000; (5) *Calcidiscus leptoporus* x 8000.

Plate 6.6 Foraminiferal dissolution effects shown on *Neogloboquadrina pachyderma.* See Section 6.9.4 for details. (1) x 250,(2) x 180, (3) x 250, (4) x 200, (5) x 180, (6) x 180.

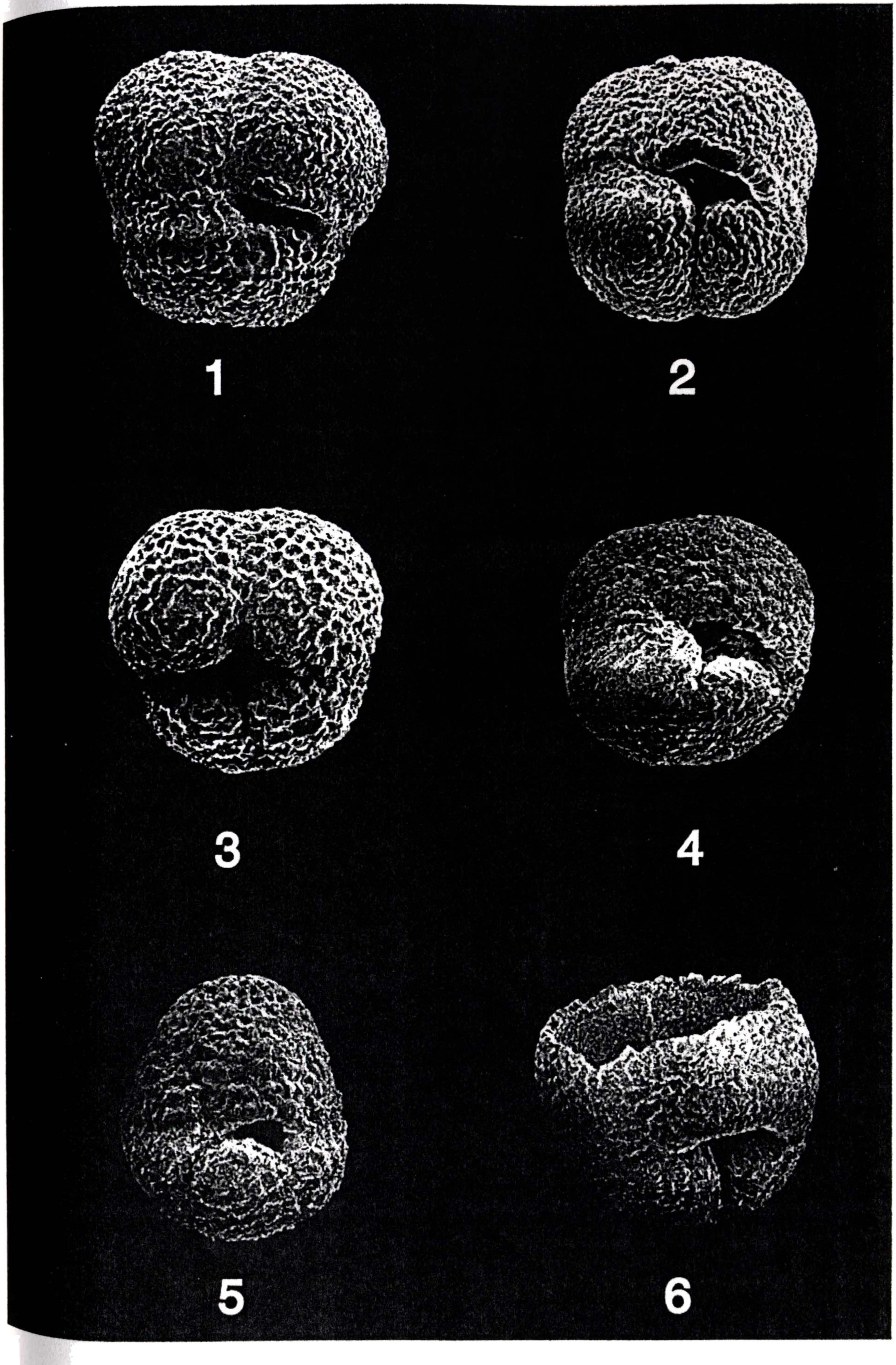
1
2
3
4
5
6

Chapter Seven:

Stable Isotopic Analysis and Radiocarbon Dates

Chapter Seven: ***Table of Contents***

7.1 Stable Isotopic Analysis

In conjunction with the micropaleontological studies, stable isotopic analysis of $\partial^{18}O$ and $\partial^{13}C$ were undertaken on three selected NZSSO cores, 36-42, 34-1, and 36-38, using an Europa 20/20 mass spectrometer. Benthic foraminifera were not used in the stable isotopic studies, as species deemed best suitable for such studies (i.e. *Cibicidoides* and *Uvigerina*) were rare or absent in many of the NZSSO cores. The planktic foraminiferal species selected for stable isotopic analysis was sinistrally coiled *Neogloboquadrina pachyderma* from the coarse sand fraction (>150 µm). This species is abundant throughout the NZSSO and has been shown to be a reliable recorder of $\partial^{18}O$ and $\partial^{13}C$ in surface waters (0-400 m) of the Southern Ocean (e.g. Labeyrie *et al.*, 1987; Charles & Fairbanks, 1990; Hodell & Venz, 1992).

7.1.1 NZSSO Cores 36-42, 34-1 and 36-38 $\partial^{18}O$ Records

The growth of foraminiferal tests through fractionation of $CaCO_3$ from water depends strongly on sea water temperature. The $\partial^{18}O$ of foraminiferal tests is a function of global variations in the isotopic composition of the world's oceans due to changes in the volume of isotopically light ice stored on continents and changes in sea water temperature. For the last deglaciation the ice volume effect is about 1.1-1.4‰ (Emiliani, 1955; Shackleton, 1987; Labracherie *et al.,* 1989; Charles and Fairbanks, 1990). In this study the value of the ice volume effect used is 1.1‰, after Chappell & Shackleton (1986).

None of the analysed cores reveals a 1.1‰ shift in the $\partial^{18}O$ trace downcore, with the largest shift of ~0.8‰ occurring in core 36-42 (Fig. 7.1A). While the stable isotopic records do not show the expected isotopic shift in the oceanic watermass between full glacial and interglacial conditions, the stable oxygen isotopic curves for the individual cores show the expected increase in $\partial^{18}O$ with increasing latitude (Table 7.1)

Table 7.1 Mean $\partial^{18}O$ and $\partial^{13}C$, and Latitude for Selected NZSSO Cores

Core	Depth (m)	Latitude (°S)	Mean ∂18O	Mean ∂13C
36-42	461	51°55.7'S	2.60	0.05
34-1	1041	53°55.4'S	2.94	-0.02
36-38	4129	56°28.0'S	4.09	0.29

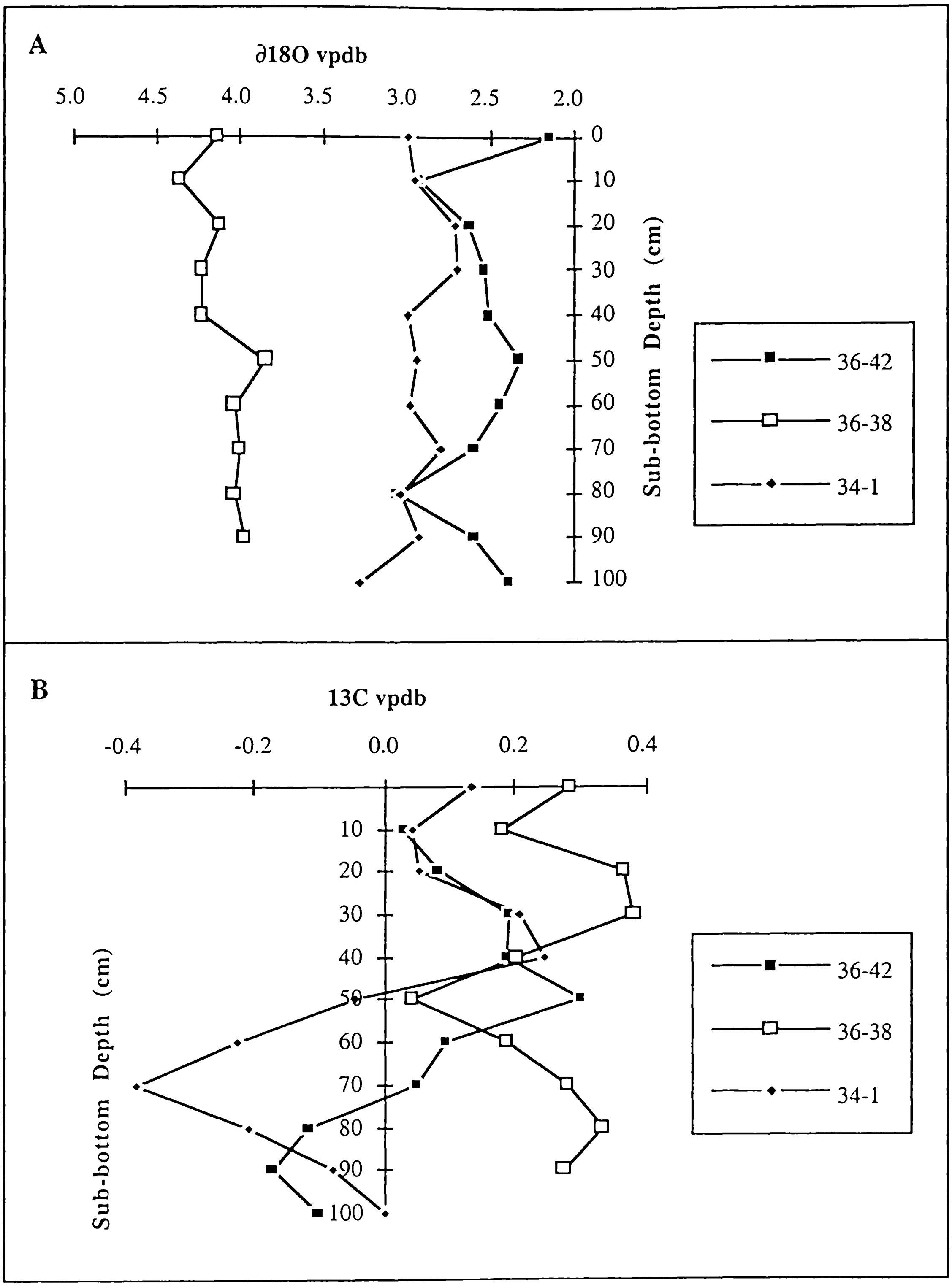

Fig. 7.1 Raw stable isotopic results for $\partial^{18}O$ (A) and $\partial^{13}C$ (B) in NZSSO cores 36-42 (52°S), 34-1(54°S), and 36-38 (56.5°S). Data from Appendix 8.

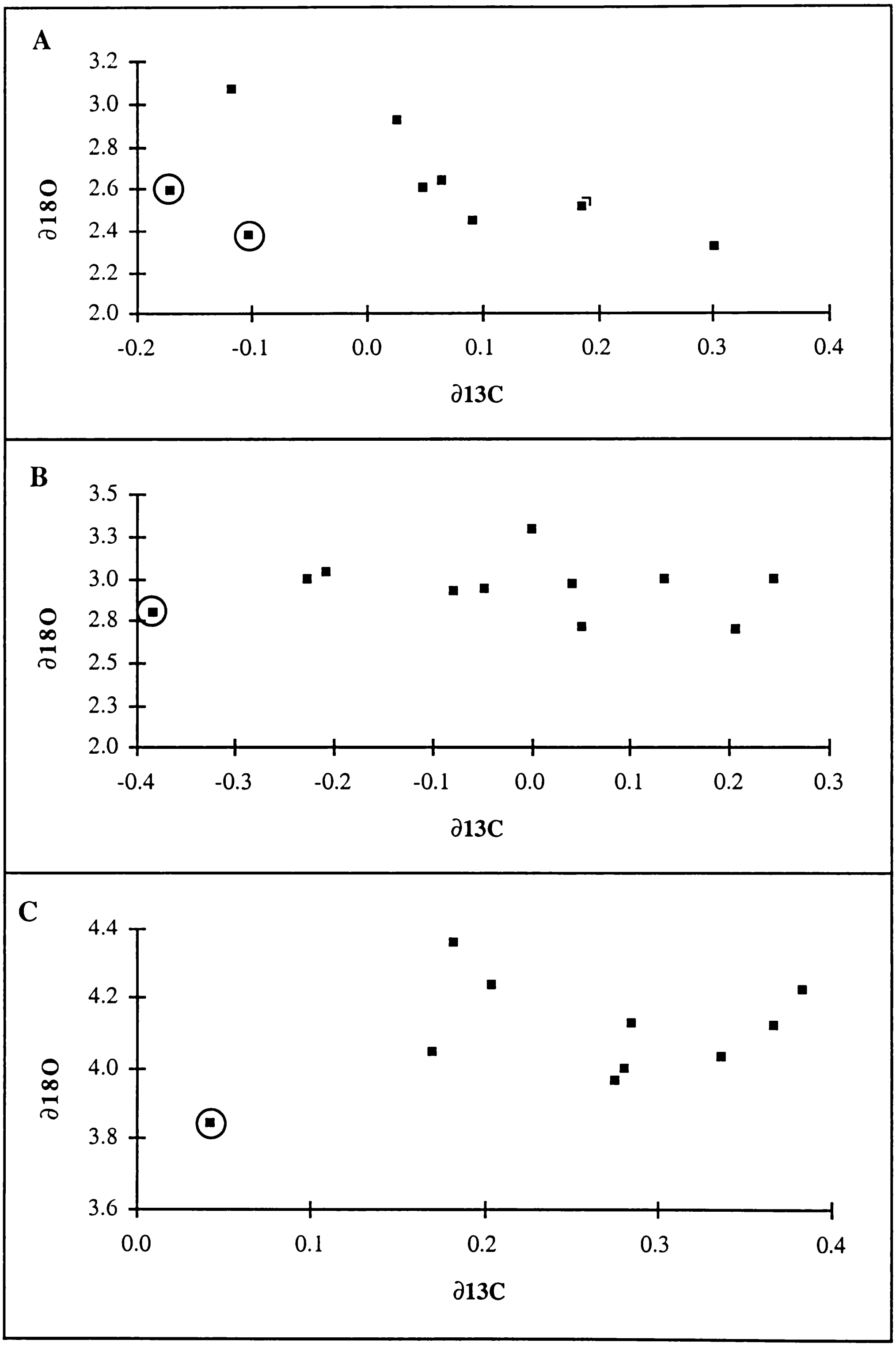

Fig. 7.2 Plots of $\partial^{18}O$ versus $\partial^{13}C$ for selected NZSSO cores: 36-42 (A), 34- 1 (B) and 36-38 (C). The outlying (circled) samples may have undergone limited fractionation. Data from Appendix 8.

To determine the reliability of the stable isotopic data, plots of $\partial^{18}O$ against $\partial^{13}C$ were produced (Fig. 7.2A-C). The scatter plots for the selected NZSSO cores show no negative slopes of an approximately 2:1 ratio which would indicate fractionation (Urey, 1947; Epstein *et al.*, 1953). The plots show outlier samples which may indicate limited fractionation of these samples. Fractionation of the CO_2 gas can occur while passing from the liquid to gaseous phase when exiting the acid in the reaction vessel or when passing the CO_2 gas through the water and CO_2 traps into the mass spectrometer (Cuthbertson, 1988; Hendy, 1995).

Of the selected NZSSO cores, core 36-42 (52°S, 461 m) shows the strongest variations downcore in the stable isotopic trace. The stable isotopic record for NZSSO core 36-42 appears to have been smoothed (i.e. the expected oceanic isotopic shift of 1.1‰ between full glacial and interglacial periods is absent). Two mechanisms may explain this situation in the NZSSO region: reworking by organisms (bioturbation), that can disturb and homogenise the upper 10 cm or more of seafloor, reworking in older sediments; or mechanical reworking of sediment by strong bottom current activity, which is a distinct possibility on the current swept Campbell Plateau (Watkins & Kennett, 1972, 1977; Osborn *et al.*, 1983).

In Fig. 7.3 an attempt has been made to assign oxygen isotope stages in NZSSO core 36-42. The transition between Last Glacial (Stage 2) and the present interglacial Holocene (Stage 1) is ~7 cm downcore, with the Stage 2/3 boundary being indeterminate. The Stage 3/4 boundary occurs ~65 cm downcore. A possible Stage 4/5 boundary is located at ~95 cm downcore. There is doubt on the validity of the Stage 4/5 boundary, as the two outlying samples circled in Fig. 7.2A are points 90 and 100 cm downcore. If these samples were corrected the slope rising out of Stage 4 would lessen, with the effect of pushing the Stage 4/5 boundary downcore.

The record of NZSSO core 36-42 (Fig. 7.3) shows similarities to the stable oxygen isotope curve for the New Zealand Oceanographic Institute core Q585 (49°42.2'S, 177°55.5'W; 4354 m, Fig. 3.3) reported by Nelson *et al.* (1993b)(Fig. 7.4). Core Q585 did register the 1.1‰ oceanic isotopic shift using the planktic foraminifera *Globigerina bulloides* to determine stable isotopic values. Nelson *et al.* (1993b) found in core Q585 that the Stage 1/2 boundary lies ~12 cm downcore with the Stage 4/5 boundary at ~130 cm downcore. No other stable oxygen isotopic records have been found for the NZSSO that have similar sedimentary environments to NZSSO core 36-42. Other isotopic records to the north, on the continental shelf and Chatham Rise off the South Island of New Zealand, or in the Bounty Trough, are

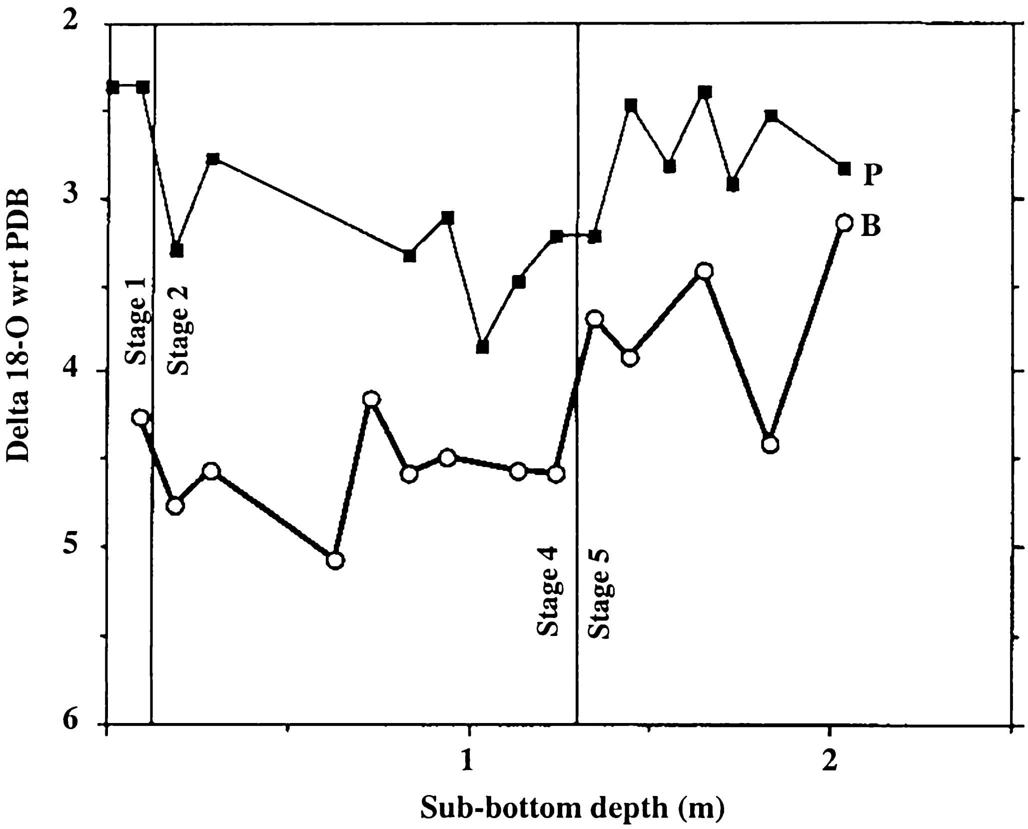

Fig. 7.4 Stable isotopic record of New Zealand Oceanographic Institute core Q585, with assigned oxygen isotope stages. (From Nelson *et al.*, 1993b).

influenced by high terrigenous contents in the glacial hemipelagic sediments and generally high sedimentation rates which have oxygen isotope Stage 1 extending below the 1 m sub-bottom depth (Nelson, 1986; Cooke, 1988; Cuthbertson, 1988; Nelson *et al.*, 1993a). This is the core length limit for the NZSSO cores in this study, so other comparisons cannot be readily made.

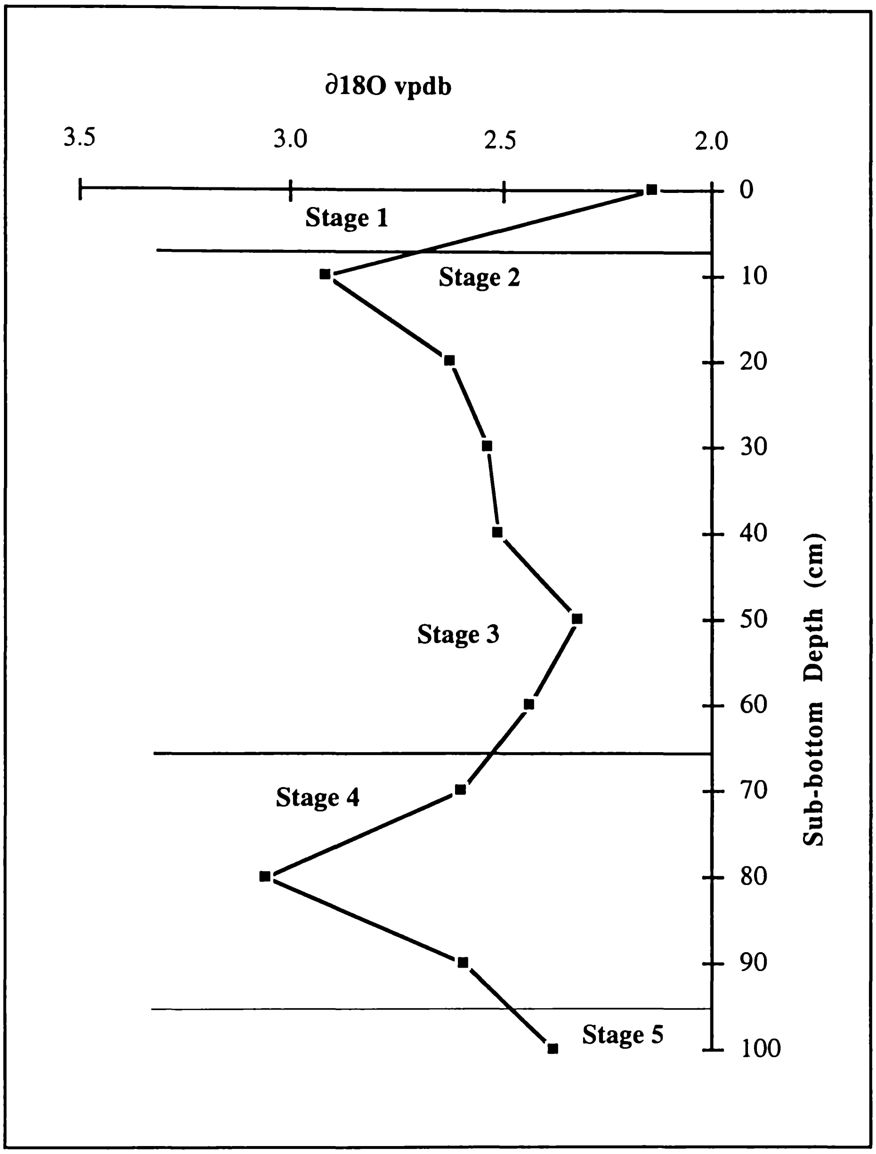

Fig. 7.3 Core 36-42 stable oxygen isotope curve with assigned oxygen isotope stages. Data from Appendix 8.

Paleotemperatures of sea surface waters can be determined using the equation (Shackleton & Kennett, 1975).

$$T(^{\circ}C) = 16.9 - 4.38(\partial_C - \partial_W) + 0.1(\partial_C - \partial_W)^2$$

$\partial_C = \partial^{18}O$ Foraminiferal carbonate ‰

$\partial_W = \partial^{18}O$ Sea-water, taken to be 0‰ for present Holocene and interglacial conditions, and 1.1‰ during the Last Glacial Maximum (Chappell & Shackleton, 1986).

$\partial^{18}O_{seawater}$ can be adjusted for salinity changes by the equation (Craig and Gordon, 1965),

$$\partial^{18}O_{seawater} = 0.5(\text{Salinity} - 35)\ ‰$$

However, for this study the effect of salinity changes is considered to be negligible, and the paleotemperatures are not adjusted for salinity. Using the above equation an attempt is made to plot the two extremes i.e. Holocene / interglacial (using $\partial^{18}O_W$ = 0‰) and Last Glacial Maximum extreme ($\partial^{18}O_w$ = 1.1‰), and then to combine the plots based on the assigned stages in Fig. 7.3.

The plot for $\partial^{18}O_w$ = 0.0‰ (Holocene / interglacial) is shown in Fig. 7.5. When a similar plot was attempted for $\partial^{18}O_w$ = 1.1‰ the results obtained indicated warmer sea surface temperatures during the Last Glacial, with rises of ~4°C. This inaccuracy arises because the change in $\partial^{18}O$between the Last Glacial Maximum and the present interglacial Holocene in the NZSSO cores is too small (i.e. <1.1‰). This may be due: (1) to changes in salinity (less saline water gives lighter $\partial^{18}O$); (2) to core 36-42 missing the Last Glacial Maximum through possible winnowing, creating a condensed record and retention of only a partial ice volume effect (Shackleton & Kennett, 1975; Faure, 1986; Hendy, 1995).

The partial loss of the Last Glacial record from NZSSO core 36-42 is likely due to intensification of oceanic circulation and current patterns about the southern margins of the Campbell Plateau, and enhanced by possible lowering of sea level at the site (Gordon, 1972, 1975b; Shackleton, 1987; Morrow *et al.,* 1992; Nelson *et al.,* 1993a; Carter *et al.,* 1996b). The loss from the records of the isotopic shift from full glacial into interglacial conditions allows no paleotemperatures to be determined for glacial periods in the NZSSO cores.

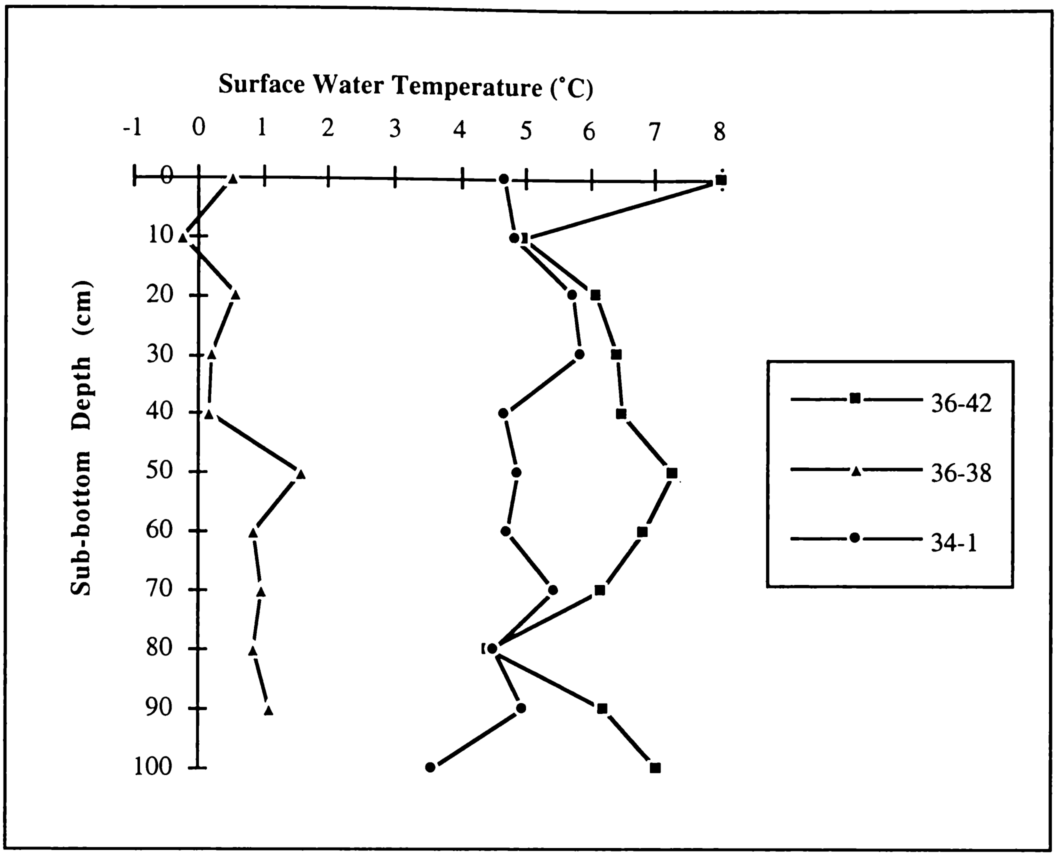

Fig. 7.5 Plot of sea-surface temperature using $\partial^{18}O_w$ = 0‰ (Holocene / Interglacial conditions) for three selected NZSSO cores. Data from Appendix 8.

Using the plot of $\partial^{18}O_w$ = 0‰ (Holocene / Interglacial conditions), the expected trend of warmest sea surface temperatures in the north and coolest in the south is evident (Table 7.2).

Table 7.2 Modern (Interglacial) Sea Surface Temperatures (SST) for Selected NZSSO Cores

Core	Depth (m)	Latitude (°S)	Modern SST (°C)	Stage 3 SST (°C)	Stage 5 SST (°C)
36-42	461	51°55.7'S	~8	6.5-7.25	(~7)
34-1	1041	53°55.4'S	~4.75	*	*
36-38	4129	56°28.0'S	~1	*	*

* Isotope stages indeterminate. (~7) indicates a possible initiation of oxygen isotope stage 5.

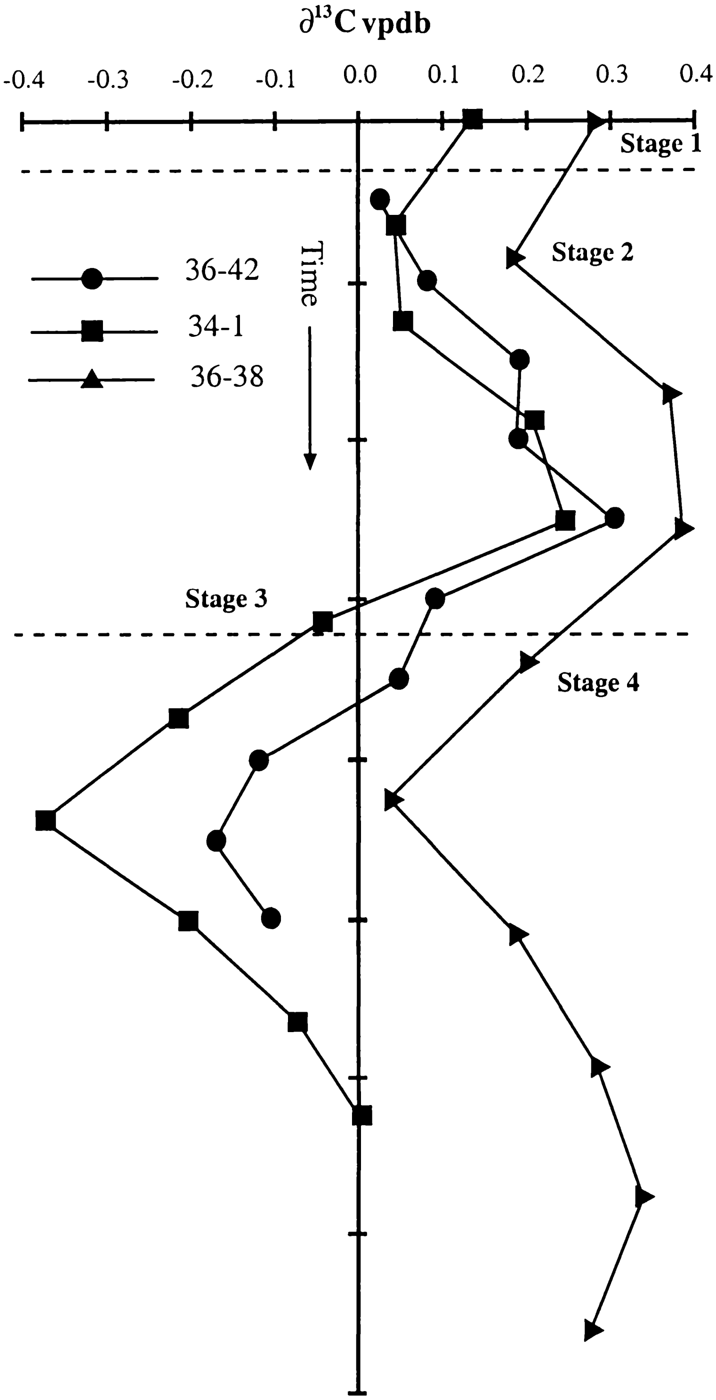

Fig. 7.6 $\partial^{13}C$ records for NZSSO cores 34-1 and 36-38 adjusted to "match" the record for core 36-42 for which oxygen isotope stages have been suggested (Fig. 7.3). Also see Fig. 7.1B. Data from Appendix 8.

Calculated modern sea surface temperatures (SST) from the NZSSO cores 36-42 and 34-1, lying north of the SAF, are ~8°C and ~4.75°C respectively. This is in agreement with previous studies (Vella *et al.,* 1975; Nelson *et al.,* 1993a; Chiswell, 1994; Weaver *et al.,* 1997). Core 36-38, lying south of the SAF shows a marked drop in SST, with a modern SST of ~1°C. This marked temperature drop across the SAF is also noted by Weaver *et al.* (1997); their use of the FA-20 transfer function and the Modern Analogue Technique found the SST drop across the SAF to be 4-5°C. Stable isotopic analysis of selected NZSSO cores shows a drop of 3-6°C across the SAF.

7.1.2 NZSSO Cores 36-42, 34-1 and 36-38 $\partial^{13}C$ Records

The $\partial^{13}C$ records (Fig. 7.1B) show the expected overall increase in $\partial^{13}C$ with increasing latitude (Table 7.1). The $\partial^{13}C$ stable isotopic traces of the three NZSSO cores show some strong variations downcore. Nevertheless, they all show a similar downcore pattern of increase and decreases. Using core 36-42 as the control (since it has the most reliable isotopic record), the $\partial^{13}C$ records for cores 34-1 and 36-38 have been aligned with the features in core 36-42 (Fig. 7.6). What the $\partial^{13}C$ stable isotopic traces indicate is that during glacial periods there is a depletion in the $\partial^{13}C$ values in the surface watermasses of the NZSSO (Fig. 7.6). This was also the case at DSDP Site 594 on the southern Chatham Rise (Nelson *et al.,* 1993a).

Data from Oppo *et al.* (1990) suggest that even small reductions in the North Atlantic Deep Water (NADW) flux during glaciations results in no discernible NADW signal reaching the Southern Ocean. During all glaciations of the past 0.5 million years the Southern Ocean contained an insignificant proportion of NADW relative to North Pacific Deep Water (NPDW) and Indian outflow water (Oppo *et al.,* 1990). The stable isotopic analyses of this study agrees, showing a depletion of $\partial^{13}C$ during glacials and an increase during interglacials when the influx of $\partial^{13}C$-rich NADW again increases (Fig. 7.6). Another source of $\partial^{13}C$-rich water is the NPDW, which increases in volume during glacial periods (Martinez, 1994). However, NPDW flows southward east of the Louisville Seamount Chain, where it is entrained and dispersed within the eastwards flowing ACC. The NPDW entrained in the ACC must circum-navigate the Antarctic continent before reaching the NZSSO. Thus, if there is a NPDW signal in the watermasses of the NZSSO during glacials it is weak, and not readily observed in the NZSSO $\partial^{13}C$ isotope record.

Duplessy *et al.* (1988) state that a poorly ventilated watermass is one which has light $\partial^{13}C$ values, and a well ventilated watermass is heavy in $\partial^{13}C$. Changes in $\partial^{13}C$ values recorded between glacial and interglacial conditions are due to two dominant influences: (1) $\partial^{13}C$ may change with climate, as glacial conditions prevail cold deep water expansion can introduce $\partial^{13}C$-rich watermasses over a core site, as suggested for the northward extension of Southern Ocean fronts during the Last Glacial through the expansion of CDW (Morley, 1989; Charles and Fairbanks, 1990; Nelson *et al.*, 1993a); and (2) $\partial^{13}C$ shifts due to changes in deep water circulation possibly causing upwelling of $\partial^{13}C$-rich watermasses and affecting ventilation.

The interglacial $\partial^{13}C$ values of Stages 1, 3 and possibly 5 from Fig. 7.6 indicate there is strong ventilation of the upper watermasses. The interglacial $\partial^{13}C$ values show positive shifts of ~0.3-0.6‰, indicating ventilation. This suggests upwelling of $\partial^{13}C$-rich waters, presumably Antarctic Circumpolar Deep Water (ACDW), containing a $\partial^{13}C$-rich NADW signal. Weaver *et al.* (1997), using modern (core-top) foraminiferal assemblages, found that off the South Island and south of the Chatham Rise the upwelling assemblage covers most of the Campbell Plateau.

7.2 Radiocarbon Dates for Cores 36-42, 34-1 and 36-38

Three samples from two NZSSO cores (36-42 and 36-38) were sent for dating on an Accelerator Mass Spectrometer (AMS) at the Rafter Radiocarbon Laboratory at the Institute of Geological and Nuclear Sciences (IGNS) in Lower Hutt. Samples of pure *Globigerina bulloides* of >150 µm size were picked for dating from core 36-42 at 10 and 20 cm downcore across a colour boundary which can be correlated to four other of the NZSSO cores. Dating across this colour marked boundary was chosen to determine whether it represents the transition from the Last Glacial to present Holocene. Other factors in the decision to date this core were the excellent preservation of the foraminiferal tests, and that core 36-42 has also been subjected to stable isotopic analysis.

The third sample picked for dating was from 20 cm downcore in NZSSO core 36-38. This core is the southernmost in this study that contains significant calcium carbonate (Fig. 5.1). Nevertheless, all foraminiferal tests from this core were rather poorly preserved, with obvious dissolution effects. To liberate sufficient CO_2, sample weights for AMS analysis are required to be between 8-10 mg. By picking all planktic foraminifera present in the coarse sand fraction, ~5.0 mg was retrieved from core 36-38. Because of this the 20 cm sample from core 36-38 was considered unlikely to produce a particularly reliable result.

The age results (yrs BP) obtained from the Rafter Radiocarbon Laboratory at IGNS are shown in Table 7.2 (Appendix 9), with calculated sedimentation rates for the three samples.

Table 7.3 Radiocarbon Ages and Sedimentation Rates of Samples from NZSSO Cores 36-42 and 36-38

Sample	$\partial^{13}C$	Age yrs BP	Sedimentation Rates
36-42 (10)	0.4 ‰	19120 +/- 110	0.52 cm/ky
36-42 (20)	0.7 ‰	23900 +/- 200	0.83 cm/ky
36-38 (20)	0.4 ‰	1639 +/- 67	12.2 cm/ky

(Data from Appendix 9)

What these ages suggest is that the colour boundary at ~16 cm downcore in NZSSO core 36-42 does not represent the transition between Last Glacial conditions and the present interglacial conditions. This transition is dated by other workers elsewhere as occurring between about 11,000-13,000 yrs BP (Imbrie *et al.*, 1984; Labracherie *et al.*, 1989; Wright *et al.*, 1995). This would place the transition at ~6-7 cm downcore in core 36-42. The colour boundary at ~16 cm in this core may represent a change from a glacial threshold in sedimentation and oceanic climatic conditions to a transitional-interglacial type of sedimentation and oceanic climatic conditions. Wright *et al.* (1995) noted in cores from offshore northern New Zealand that the precise in-phase correlation of biopelagic and hemipelagic sedimentation with interglacial and glacial isotope stages, respectively, is not necessarily global.

As Table 7.3 shows, the sedimentation rate between core top to 10 cm downcore in NZSSO core 36-42 is 0.52 cm/ky and the sedimentation rate for core top to 20 cm downcore is 0.83 cm/ky. However, when the sedimentation rate between 10 to 20 cm downcore is determined, it is 2.09 cm/ky. This shows a rapid increase in sedimentation from 0.52 cm/ky core top and 10 cm downcore (Fig. 7.7). There is no influx of hemipelagic sediment over this interval downcore; the sediment remains biopelagic implying that between 10 and 20 cm downcore the surface waters over NZSSO core site 36-42 became more productive. This is possible through an intensification of oceanic patterns and an increase in upwelling associated with the colder conditions over this period, as recorded in the stable oxygen isotopic curve for NZSSO core 36-42 (Fig. 7.1A). Isotopic studies indicate that at 10 and 20 cm downcore glacial conditions prevailed and greater productivity may be due to wind blown terrestrial sediments introducing iron-rich terrestrial material to oceanic waters east of New Zealand (Kumar *et al.*, 1995).

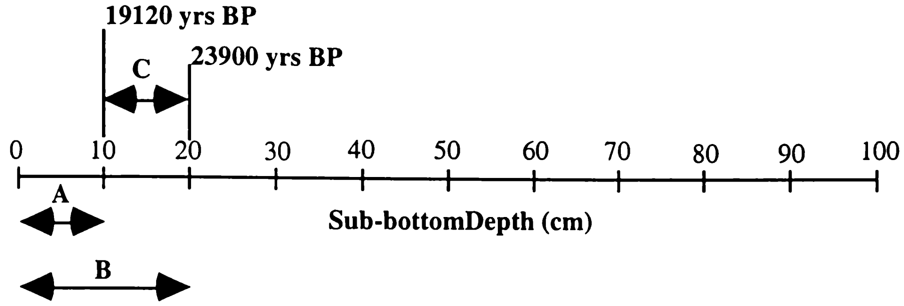

Fig. 7.7 Schematic diagram of Core 36-42, showing positions of radiocarbon dates and determined sedimentation rates (A-C). (A) 0.52 cm/ky; (B) 0.83 cm/ky; and (C) 2.09 cm/ky.

NZSSO core 36-38 has a very young age at 20 cm downcore of only 1639 ± 67 yrs BP, corresponding to a sedimentation rate of 12.2 cm/ky. If the age is reliable it suggests that core 36-38 lies in a sedimentary trap. Fig. 1.4 shows that core 36-38 lies in the southern Emerald Basin, and occupies a depression defined by the 4000 m bathymetric contour. The position of the core also lies across two major sediment transport paths: Solander Trough and the current-swept channels lying north and south of Macquarie Island. Other evidence of rapid sedimentation rate in core 36-38 is from paleomagnetic stratigraphy; the full 12 m length of core 36-38 does not penetrate the Brunhes/Matuyama boundary (0.78 million yrs BP). This suggests a high sedimentation rate and/or low degree of erosion in the vicinity of core 36-38. Despite this, the reliability of the young age remains uncertain.

7.3 Discussion of Combined Stable Isotopic Records and Radiometric Dating

The dates and stable isotopic results achieved for NZSSO core 36-42 are in good agreement. The dates of 19 ky and 23.9 ky are located at 10 and 20 cm downcore, respectively. This position on the stable isotopic record lies within the section assigned to oxygen isotope stage 2 (Fig. 7.3). Imbrie *et al.* (1984) assigned the stage 1/2 boundary an age of 12 ky, suggesting a Last Glacial / interglacial transition occurs at ~6 cm downcore. This shows strong agreement with the assigned oxygen isotope stages in Fig. 7.3. The stage 2/3 boundary has been assigned an age of 24 ky, which places the boundary ~21 cm downcore, in agreement with the stable oxygen isotopic curve (Fig. 7.3). Using the sedimentation rates (Table 7.3) determined from the radiometric age and the date of 59 ky assigned to the stage 3/4 boundary by Imbrie *et al.* (1984), the calculated oxygen isotope stage 3/4 boundary for core 36-42 lies at ~63 cm downcore. This agrees well with an assigned stage 3/4 boundary at ~65 cm using the stable oxygen isotopic record alone (Fig. 7.3). Fig 3.1A (core 36-42 lithostratigraphy) shows that this depth corresponds with a gradational colour marked boundary.

The date obtained in core 36-38 is treated with caution. This is because the $\partial^{13}C$ record agrees well with the other selected NZSSO cores (Fig. 7.6), yet that date appears far too young. The radiocarbon date at 20 cm downcore suggests a very recent age (1639 ± 67 yrs BP). However, 20 cm downcore on the basis of the matched $\partial^{13}C$ records places this point within oxygen isotope stage 3.

Chapter Eight:

Summary and Conclusions

Chapter Eight: Table of Contents

8.1 Lithologies

The NZSSO lies in a highly dynamic region that registers signals from all the world's major oceans and is the access pathway to the Pacific Ocean for the world's largest deep-water current which passes around the base of the Campbell Plateau before heading north (Fig. 1.4). The twelve *USNS Eltanin* cores used in this study form a north-south transect across this dynamic region. Sedimentological indices, micropaleontological census studies, stable oxygen and carbon isotopic analysis, and radiocarbon dating have shown the cores of the NZSSO must be viewed as two subsets. The NZSSO cores are clearly divided on the basis of sedimentary lithologies, textures, composition and depositional histories, associated with oceanic circulation patterns and topographical influences. The NZSSO cores are subdivided into a northern and southern subgroup, the main characteristics of which are given in Table 8.1 and 8.2.

The foraminiferal oozes of the northern subgroup are composed predominantly of a Subantarctic microfossil assemblage (Table 6.3). The main species are *Globigerina bulloides, Neogloboquadrina pachyderma* (both dextrally and sinistrally coiled), *Globigerinita* spp., *Globorotalia inflata,* and *Globorotalia truncatulinoides.* The mud fraction of the northern foraminiferal oozes is composed of calcareous nannofossils, characterised by *Emiliania huxley, Coccolithus* spp. and *Calcidiscus* spp. (Table 6.12). These calcareous flora represent a Late Quaternary assemblage. Where foraminifera exist in the siliceous dominated southern subgroup, they form an Antarctic (polar) microfossil assemblage composed of *Neogloboquadrina pachyderma* (sinistrally coiled), *Globigerina bulloides, Globigerina quinqueloba* and *Globorotalia inflata. Neogloboquadrina pachyderma* (sinistrally coiled) is by far the dominant species (Table 6.2).

The change in microfaunal assemblages is reflected in the change of textural facies. In the northern cores biogenic siliceous and terrigenous material are absent. Therefore, calcareous biogenic organisms govern the textural facies changes. Textural facies A, a muddy sand, is dominated by planktic and benthic foraminifera with a matrix of calcareous nannofossils (Table 4.1). Textural facies B is dominated by calcareous nannofossils with varying amounts of sand-sized foraminifera, giving the sediment a sandy mud texture. The southern subgroup comprises sandy silt of textural facies C, and is dominated by silt-sized frustules of diatoms and nassellaria radiolaria, and terrigenous material.

Table 8.1 Sedimentary Characteristics of Northern NZSSO Cores

Cores	Latitude (°S)	Depth (m)	Dominant lithology	$CaCO_3$ %	*N. pachyderma* (sin coiled) %	Terrig %	Facies
36-42	51°55.7'S	461	Foraminiferal ooze	86-95	87	<0.5	A & B
36-41	51°56.7'S	951	Foraminiferal ooze	94-100	89	0	A & B
16-9	52°25'S	1052	Foraminiferal ooze	87-100	90	<0.5	A & B
36-40	52°56.4'S	783	Foraminiferal ooze	93-100	91	0	A & B
34-1	53°55.4'S	1041	Foraminiferal ooze	93-98	98	0	A & B
36-39	54°02.4'S	2999	Foraminiferal ooze	95-99	84	<1.5	A & B
mean		1215	Foraminiferal ooze	91-99	90	<0.5	A & B

Table 8.2 Sedimentary Characteristics of Southern NZSSO Cores

Cores	Latitude (°S)	Depth (m)	Dominant lithology	$CaCO_3$ %	*N. pachyderma* (sin coiled) %	Terrig %	Facies
16-8	56°08'S	5117	Diatom sandy mud	0-4	100	40-80	C
36-38	56°28'S	4129	Muddy spicule ooze	10-18	99	5-11	C
50-35	58°59.3'S	5024	Sandy diatom ooze	<1	absent	8-12	C
50-34	60°00'S	4863	Diatom ooze	<1	absent	6-21	C
34-1	60°01.5'S	4517	Radiolarian ooze	0.5-1.5	absent	5-13	C
36-39	61°05.1'S	4550	Muddy diatom ooze	0-13	100	4-27	C
mean		4700	Rad/Diatom ooze	<1.0	100	11-27	C

The northern and southern subgroups are divided by the SAF, and associated changes in topography and watermasses. The northern subgroup predominantly lie beneath average water depths of ~1200 m on the southern margin of the Campbell Plateau washed by ASW and possibly SAMW in the deeper cores (Fig. 3.1). The southern cores lie in colder surface waters south of the SAF, with an average water depth dramatically increasing to ~4700 m. This water depth is well below the water depth determined for the lysocline in this study of ~3200-4100 m, with the CCD at ~4800 m (Fig. 6.15). Therefore, calcareous material is certain to be affected by dissolution, which biases the sedimentary record towards dissolution resistant siliceous organisms (diatoms and radiolaria) and terrigenous material.

8.2 Glacial - Interglacial Transitions

The position of the transition between the Last Glacial and the Holocene can be determined in the northern subset of cores through a number of factors. The stable isotopic record for NZSSO core 36-42 has been shown to have the cleanest stable isotopic

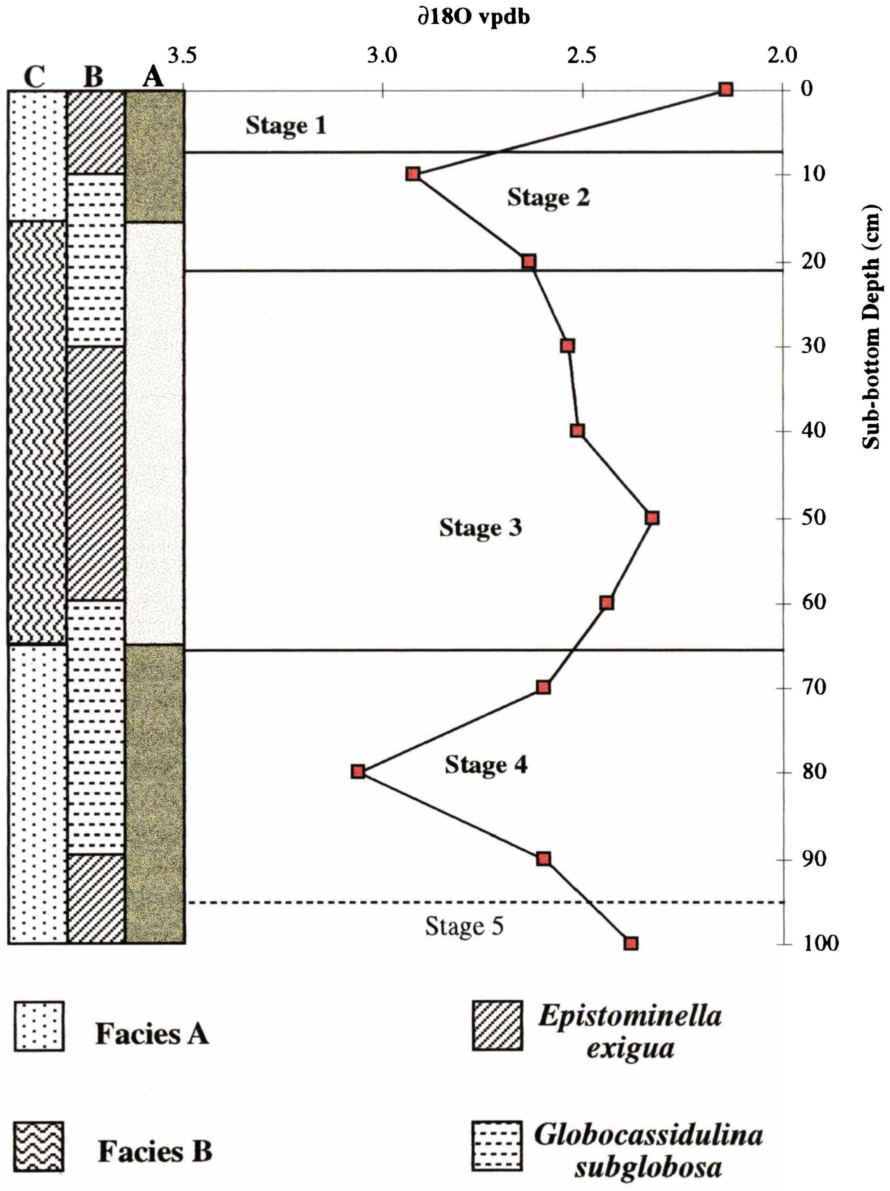

Fig. 8.1 Summary of the evidence for the transitions between glacial and interglacial conditions in NZSSO core 36-42. (A) colour changes downcore, colours approximate colour values as listed in the core discriptions (B) benthic faunal changes between *Epistominella exigua* and *Globocassidulina subglobosa* ; and (C) textural facies changes downcore.

signal, though it is a smoothed record and does not show the expected ~1.1-1.4‰ oceanic isotopic shift between glacial and interglacial conditions (Emiliani, 1955; Shackleton, 1987; Charles and Fairbanks, 1990). The isotopic curve suggests the transition is at ~7 cm downcore. This hypothesis is confirmed by the radiocarbon ages obtained from 36-42 in samples at 10 and 20 cm downcore, which gave ages of 19,120 ± 110 and 23,900 ± 200 yrs, respectively. The transition between the Last Glacial and the Holocene has been assigned an age of between 11-13000 yrs BP in the southern hemisphere (Imbrie *et al.*, 1984; Labracherie *et al.*, 1989), which using determined sedimentation rates places the transition just above 10 cm in core 36-42, in agreement with the isotopic record (Fig. 8.1).

Micropaleontological evidence also registers a transition in oceanic paleoenvironmental conditions. The sinistrally coiled *Neogloboquadrina pachyderma* percentage curve for core 36-42 indicates a warming between 10 cm downcore and core top. Other northern NZSSO cores show little variation downcore in the *Neogloboquadrina pachyderma* percentage curves. The benthic foraminiferal record for 36-42 shows faunal changes in the vicinity of the stable oxygen isotopic stage boundaries assigned to core 36-42. *Epistominella exigua* is associated more with interglacial periods, an uncharacteristic trend due to depth and temperature variables (Uchio, 1960; van Morkhoven *et al.*, 1986). During interglacial periods deeper water occurs and possible intrusion of Subantarctic Mode Water (SAMW) over core site 36-42 allows *Epistominella exigua* to inhabit the site, suggestive of a ~2°C temperature drop. During glacial periods when sealevel drops ~120 m a very shallow environment is produced with relatively warmer surface water washing in from the Campbell Plateau, and *Globocassidulina subglobosa* dominates (Fig. 8.1). Other micropaleontological evidence for the NZSSO cores is unable to be used to determine the transition.

Textural and associated colour changes downcore in core 36-42 indicate a transition at ~16 cm. This colour change does not indicate the exact transition from Last Glacial to Holocene (cf. Wright *et al.*, 1995) (Fig. 8.1). This colour and textural change is suggested to indicate a change from a glacial threshold in sedimentation and oceanic circulation conditions to a transitional-interglacial set of sedimentation and oceanic conditions. A similar colour marked boundary near 20 cm downcore occurs in several of the northern NZSSO cores, allowing the position of the transition to be correlated.

The transition out of the Last Glacial cannot be determined in the southern group of NZSSO cores. From paleomagnetic stratigraphies (Fig. 3.4) most of the southern NZSSO cores have had extensive erosion and reworking, losing up to 0.6 million years of sediment (Watkins & Kennett, 1972; Osborn *et al.*, 1983). Two cores, 16-8 and 36-

38, retain sediments of Brunhes age (0-0.78 Ma). In both cores no sedimentary or micropaleontological indices register a transition that could be specifically assigned to the Last Glacial or to the Holocene. Core 36-38 had a radiocarbon date of 1639 ± 67 yrs at 20 cm downcore. This yields a sedimentation rate of 12.2 cm/ky which, extrapolated downcore, would place the Last Glacial-Holocene transition at 146 cm sub-bottom depth. However, there is some doubt over the reliability of carbonate-derived data from the core, both in the stable isotopic and radiocarbon analysis, because of dissolution effects and limited carbonate material to evolve recommended volumes of gas in the radiocarbon and isotopic analyses. A high sedimentation rate for this core is expected. Core 36-38 has a total length of 1209 cm; this core length does not penetrate the Brunhes/Matuyama magnetic reversal, suggesting a high sedimentation rate and/or that the erosion suffered by other southern NZSSO cores was not experienced at this core site.

8.3 Oceanic Front Positions in the NZSSO and Shifts During the Last Glacial-Holocene Transition

The north-south transect developed from the twelve NZSSO cores crosses one major oceanographic front, the SAF. The southern point of the transect lies ~3° north of the AAPF. Any shifts that occurred in these fronts should be recorded in the NZSSO cores. The SAF can be clearly delineated on the basis of sedimentological indices and micropaleontological data ((Fig. . 8.2). Gordon (1975b), using salinity and temperature data in a transect along 170°E, located the SAF at ~56-57°S in the modern watermasses. In the modern oceanic conditions the SAF is currently topographically constrained by the edge of the Campbell Plateau which forces the SAF ~10°S southward around the plateau margins (Heath, 1985; Belkin & Gordon, 1996).

The change in planktic foraminiferal faunal assemblages positions the SAF at ~56°S. North of this latitude a Subantarctic assemblage dominates (Table 6.3), while south of ~56°S an Antarctic assemblage dominates the calcareous sediments (Table 6.2; Fig. 6.4). The percentage curves for *Neogloboquadrina pachyderma* indicate that north of the SAF sinistrally coiled *Neogloboquadrina pachyderma* ranges in abundance between 70-93%. South of the SAF sinistral *Neogloboquadrina pachyderma* constitutes 99-100% of the *Neogloboquadrina pachyderma* population (Figs. 6.4 and 6.12).

Associated with the substitution of the Subantarctic assemblage for the Antarctic assemblage across the SAF, there is an introduction of siliceous components (diatoms and radiolarians) to the sediments south of SAF. The trend across the SAF is a dramatic one, from calcareous-rich sediments in the north to siliceous sediments in the south (Fig. 8.2). The absence of siliceous sediments north of the SAF on the Campbell Plateau is likely due to the concentration of free silica in the surface waters being below some critical threshold.

Due to the faunal changes across the SAF, there is a corresponding shift in the textural facies. North of the SAF, Facies A and B dominate as the main biogenic contributors to the sediment are of sand (foraminifera) and clay (nannofossils) size. South of the SAF, Facies C dominates (diatoms and radiolarians and terrigenous material (quartz, plagioclase feldspars and mica)).

	(North, 1215 m)	**SAF**	**(South, 4700 m)**
Average % $CaCO_3$	95%		<1.0%
Dominant composition	Foraminifera Nannofossils		Diatoms & Radiolaria Terrigenous material
Foraminiferal assemblages	Subantarctic		Antarctic
% *N. pachyderma* (s)	70-93%		99-100%
Textural facies	A and B		C
Average terrigenous %	<1.0%		11-27%
		~56°S	

Fig 8.2 Summary of the distinguishing sedimentological features either side of the SAF in the NZSSO.

Extensive erosion and reworking is experienced by many of the cores south of the SAF (50-33, 50-34, 34-3 and 50-35 lying ~3° north of the AAPF). The loss of the upper Brunhes sedimentary record is confirmed from previous paleomagnetic stratigraphies and from biostratigraphies of diatoms and radiolaria. Due to the loss of the sediment from the southern cores the position of the AAPF is unable to be placed in the sedimentary record.

The SAF does not appear to have shown any northward shift during the Last Glacial. Micropaleontogical evidence indicates no northward shift of an Antarctic planktic foraminiferal assemblage into the Subantarctic record. Nor is there evidence of radiolaria or diatoms north of the present SAF in the stratigraphic record from NZSSO cores on the Campbell Plateau. Radiolaria found north of this study's cores (e.g. DSDP site 594) during glacial periods have been attributed to the expansion of colder deep water upwelling, usually up a topographical feature (e.g. Bounty Trough). *Neogloboquadrina*

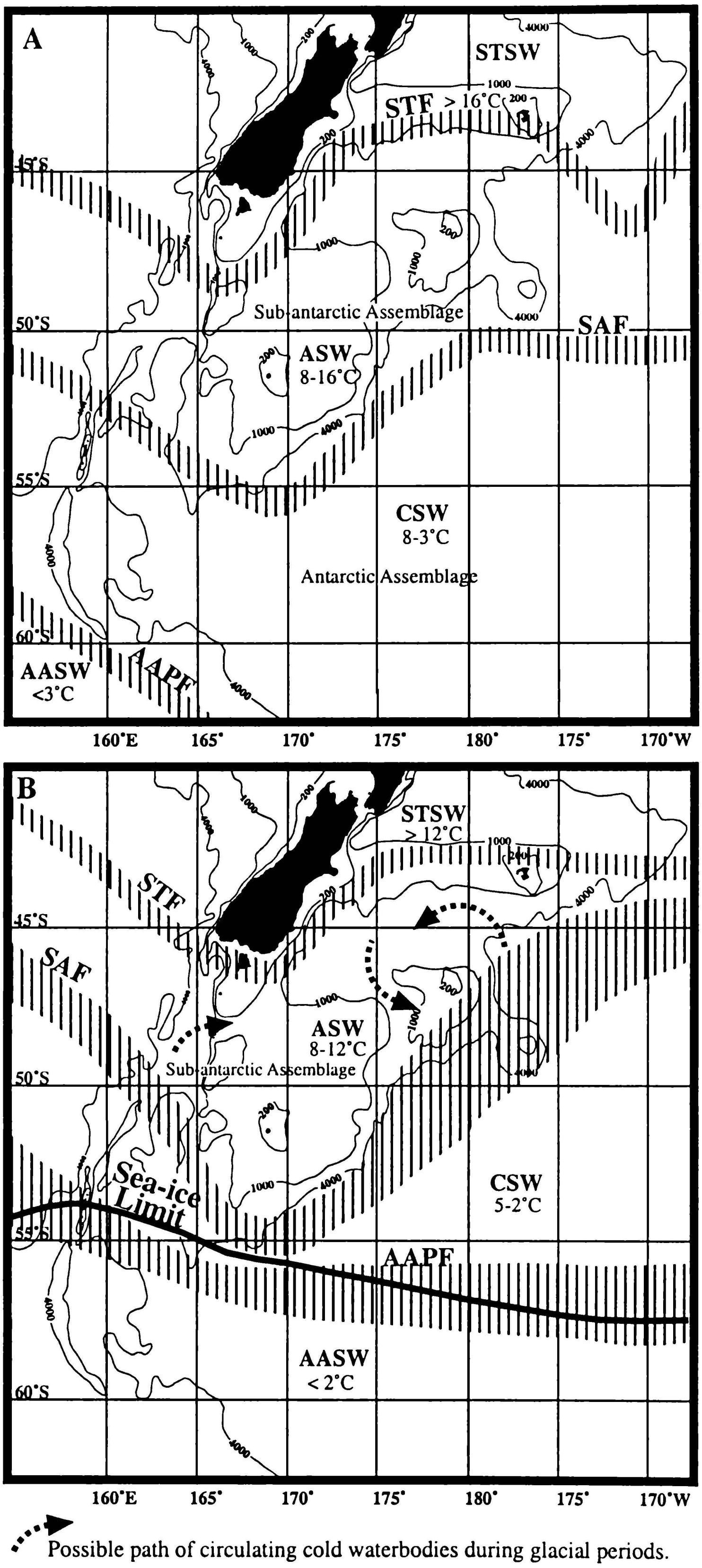

Fig. 8.3 (A) The modern surface water masses and fronts in the NZSSO contrasted in (B) with their inferred distribution during the Last Glacial Maximum. Note, in particular, the suggestion arising from this study that the SAF remained essentially fixed about the southern edge of Campbell Plateau despite at least >7° of latitude northward shift in the AAPF. During the Last Glacial Maximum the AAPF and SAF zones probably became more intense, wider and dynamic, with strong eddying off their margins. Possible gyres of cold water are shown extending up the Solander Trough and into the Bounty Trough, bringing Antarctic-like assemblages to southern Chatham Rise, but leaving a possibly isolated mass of relatively warmer waters over the southern Campbell Plateau. Last Glacial Maximum sea-ice limit from Climap Project Members (1981) and Heusser (1989)

pachyderma sinistrally coiled percentage curves of cores north of the SAF range between about 70-95%, or Groups III and IV of Vella *et al.* (1975). The limited variation in their abundance downcore suggests only small variations in the watermass temperatures that have bathed the southern Campbell Plateau in the past. The benthic foraminiferal record from core 36-42 shows faunal changes associated with differing stable isotopic stages; however, this is probably due to water depth changes between glacial and interglacial conditions and not to colder deep-water bodies expanding and intruding northwards over the Campbell Plateau.

Collectively, the data suggest there has not been any significant change in oceanic paleoenvironmental conditions at the seafloor north of the SAF, immediately south of New Zealand, between recent past glacial and interglacial periods. This suggests that the topographic high marking the southern edge of the Campbell Plateau has essentially fixed the SAF, irrespective of oceanic climatic conditions. The topographic lock is further enhanced by sealevel drops of ~120 m during glacial periods. East and west of New Zealand in open water conditions evidence from other studies indicates major northward shifts in the position of both the SAF and the AAPF. For example, shifts of the AAPF of at least 5° are suggested to have occurred during the Last Glacial (Morley & Hays, 1979; Heusser, 1989; Morley, 1989; Charles & Fairbanks, 1990; Nelson *et al.,* 1993a).

Due to the position of the New Zealand continental landmass extending southwards into high latitudes (~56°S), this effectively deflects the SAF and associated watermasses some 10° of latitude south of it's open oceanic position. The SAF is effectively locked in this southern position. During the Last Glacial the position of the AAPF has been suggested to have expanded northwards by 5-7° latitude. In the NZSSO, the SAF and AAPF may have more or less merged to form a "composite" front directly south of New Zealand off the Campbell Plateau; the fronts would again diverge in open ocean conditions east of the continental landmass. Any such convergence of the SAF and AAPF would have set up a very steep temperature gradient south of New Zealand (Fig. 8.3).

8.4 Latitudinal Temperature Gradients and Glacial-Interglacial Records

The limited variation downcore in the abundances of sinistrally coiled *Neogloboquadrina pachyderma,* the stable oxygen isotope record having minimal shifts in the $\partial^{18}O$ values, and the downcore lack of change in faunal assemblages suggest that at higher latitudes the gradients in sea surface temperature between glacial and interglacial periods were perhaps not so severe (e.g. a 4°C change in sea-surface temperature in temperate latitudes might translate into only a 1°C equivalent at higher latitudes). Because of rather smaller absolute temperature changes between glacial and interglacial conditions at higher latitudes the faunal and isotopic indicators tend to record only the extreme events. Faunal and possibly textural facies shifts are likely to last for shorter periods than at lower latitudes. This effect may be seen in textural facies for some of the northern cores (Table 4.2), which show textural changes occurring over shorter periods of the sedimentary record with increasing latitude.

8.5 Epilogue

The micropaleontological and compositional, textural and isotopic characteristics of sediment cores can provide important information and evidence for changes in the oceanic climatic state affecting the NZSSO. Downcore evidence from a transect of cores south of New Zealand suggests that although there was intensification of oceanic circulation patterns associated with global cooling during glacial periods, the SAF remained locked to the southern edge of the Campbell Plateau. This allowed minimal variation in the sea surface temperatures north of the SAF on the Campbell Plateau, and there was no intrusion of cold water over the Plateau. No faunal assemblage changes occur in the cores from the southern margins of the Plateau. The temperature drop across the SAF during the Last Glacial may have been enhanced by the AAPF expanding northwards by 5-7°. Much of the Late Quaternary is lost in the sedimentary records south of the SAF due to intensification of oceanic circulation patterns causing significant erosion and/or reworking of sediments in the southern Emerald Basin and Southwest Pacific Basin.

The important special aspects when considering the NZSSO are: (1) extension of the New Zealand continental landmass southwards, which deflects oceanic circulation patterns some 10° of latitude south of their open oceanic positions; and (2) the volumetrically large and dynamic DWBC. These features set up the NZSSO's unique position which will allow workers to study oceanic patterns which are registered globally in the sedimentary records. The NZSSO's position is unique, at present is poorly represented in paleoceanographic studies, because of inadequate exploration and sampling. The effect the New Zealand continental landmass has on oceanic circulation and it's contribution to global oceanic climate change should be addressed in further studies.

References

Abbot, W.H. 1973: Investigation of Diatoms in Southern Ocean Deep Sea Cores. *Antarctic Journal,* Vol. 8 (5). pp.287-288.

Admiralty Charts 1994: A Planning Chart for South Pacific Ocean (4007). Hydrographic Office, British Navy.

Bandy, O.L.; Casey, R.E. and Wright, R.L. 1971: Late Neogene Planktonic Zonation, Magnetic Reversals and Radiometric Dates, Antarctica to the Tropics. In. *Antarctic Oceanology I,* Reid, J.L. (ed.) *Antarctic Research Series,* Vol. 15. pp. 1-26.

Bandy, O.L. and Echols, R.J. 1964: Antarctica Foraminiferal Zonations. In: Biology of Antarctic Seas. Lee, M.O. (ed.). *Antarctic Research Series,* Vol.1. pp. 73-91.

Barker, R. W. 1960: Taxonomic Notes on the Species Figured By H.B. Brady in his Report on the Foraminifera Dredge by H.M.S. Challenger, During the Years 1873 - 1876. *Society of Economic Paleontologists and Mineralogists, Special Publication No 9.*

Belkin, I.M. and Gordon, A.L. 1996: Southern Ocean Fronts from the Greenwich Meridian to Tasmania.*Journal of Geophysical Research,* Vol. 101 (C2), pp. 3675-3696.

Berger, W.H. 1968: Planktonic Foraminifera: Selective Solution and Paleoclimatic Interpretation. *Deep-Sea Research,* Vol. 15, pp. 31-43.

Berger, W.H.; Bonneau, M.C. and Parker, F.L. 1982: Foraminifera on the Deep-Sea Floor: Lysocline and Dissolution Rate. *Oceanologica Alta,* Vol. 5. pp. 249-258.

Berger, W.H.; Smetacek, V.S. and Wefer, G. 1989: Ocean Productivity and Paleoproductivity - an overview. pp. 1-34. In: Productivity of the Ocean: Present and Past. Berger, W.H.; Smetacek, V.S. and Wefer, G. (eds.). Wiley and Son, New York.

Bolli, H.M. 1967: The Direction of Coiling in Planktonic Foraminifera. pp. 639-648. In: The Micropaleontology of Oceans. Funnell, B.M. and Riedel, W.R. (eds.). Cambridge University Press.

Bradford, J.M. 1980a: Primary Productivity - Intergrated, 1:6,000,000 at Latitude 46°S. *New Zealand Oceanographic Institute Chart, Miscellaneous Series 43, DSIR.*

Bradford, J.M. 1980b: Surface Chlorophyll A, 1:6,000,000 at Latitude 46°S. *New Zealand Oceanographic Institute Chart, Miscellaneous Series 44, DSIR.*

Bryden, H.L. and Heath, R.A. 1985: Energetic Eddies at the Northern Edge of the Antarctic Circumpolar Current in the Southwest Pacific. *Progress in Oceanology,* Vol. 14, pp. 65-87.

Carter, L. 1997: NZOI Cruise Report - Cruise 3034. Pacific Gateway - Paleoceanography. Wellington 10 Feb 1997 - Dunedin 18 Feb 1997.

Carter, L.; Carter, R.M.; McCave, I.N. and Gamble, J. 1996a: Regional Sediment Recycling in the Abyssal Southwest Pacific Ocean. *Geology,* Vol. 24 (8), pp. 735-738.

Carter, R.M.; Carter, L. and McCave, I.N. 1996b: Current Controlled Sediment Deposition from the Shelf to the Deep Ocean: The Cenozoic Evolution of Circulation through the Southwest Pacific Gateway. *Geol Rundsch,* Vol. 85. pp. 438-451.

Carter, L. and McCave, I.N. 1994: Development of Sediment Drifts Approaching and Active Plate Margin Under the SW Pacific Deep Western Boundary Current. *Paleoceanography,* Vol. 9 (6), pp. 1061-1085.

Carter, L. and McCave, I.N. 1997: The sedimentary Regime Beneath the Deep Western Boundary Current Inflow to the Southwest Pacific Ocean. *Journal of Sedimentary Research..*

Caulet, J.P. 1986: Radiolarians from the Southwest Pacific.pp. 835-861. In: Initial Reports of the Deep-Sea Drilling Project, Vol. 90, Part 2. Blakeslee, J.H. (ed.). National Science Foundation, Washington (U.S. Government Printing Office).

Ciesielski, P.F. 1986: Middle Miocene to Quaternary Diatom Biostratigraphy of Deep-Sea Drilling Project Site 594, Chatham Rise, Southwest Pacific. pp. 863-885. In: Initial Reports of the Deep-Sea Drilling Project, Vol. 90, Part 2. Blakeslee, J.H. (ed.). National Science Foundation, Washington (U.S. Government Printing Office).

CLIMAP Project Members, 1981: Seasonal Reconstructionsof the Earth'sSurfaceat the Last Glacial Maximum. In: *Geological Society of America Map and Chart Series 36.*

Chappel, J. and Shackleton, N.J. 1986: Oxygen Isotopes and Sea Level. *Nature,* Vol. 324. pp. 137-140

Charles, C.D. and Fairbanks, R.G. 1990: Glacial to Interglacial Changes in the Isotopic Gradient of the Southern Ocean Surface Water. pp. 519-538. In: Geological History of Polar Oceans: Arctic Vs Antarctica. Bleil, U. and Thiede, J. (eds.). Kluwer, Amsterdam.

Chen, P. 1975: Antarctic Radiolaria. pp.437-514. In: Initial Reports of the Deep-Sea Drilling Project, Vol. 28. Kaneps, A.G. (ed.). National Science Foundation, Washington (U.S. Government Printing Office).

Chiswell, S.A. 1994: Variability in Sea Surface Temperature Around New Zealand From AVHRR Images. *New Zealand Journal of Marine and Freshwater Research,* Vol. 28. pp. 179-192.

Collen, J. 1995: Micropaleontology Laboratory Manual. Department of Geology & Research School of Earth Sciences, Victoria University,Wellington, New Zealand.

Cooke, P.J. 1988: The Late Quaternary Stratigraphy & Micropaleontology of DSDP Site 594 Southwest Pacific. M.Sc Thesis, Department of Earth Sciences, University of Waikato, Hamilton, New Zealand.

Corliss, B.H. 1979: Taxonomy of Recent Deep-Sea Benthonic Foraminifera from Southeast Indian Ocean. *Micropaleontology,* Vol. 25 (1). pp. 1-19.

Craig, H. and Gordon, L.I. 1965: Deuterium and Oxygen-18 Variations in the Ocean and MarineAtmosphere. pp. 9-130. In: Stable Isotopes in Oceanographic Studies and Paleotemperatures. Tongiogi, E. (ed.). Consiglio Nazionale delle Richerche, Laboratorio di Geologia Nucleare, Pisa.

Cuthbertson, A.M. 1988: Stable Isotope Stratigraphy of Deep-Sea Cores from the Southwest Pacific Regions Aspects of Late Quaternary Paleoceanography. D.Phil Thesis. University of Waikato, Hamilton, New Zealand.

Duplessy, J.C.; Shackleton, N.J.; Fairbanks, R.G.; Labeyrie, L.; Oppo, D. and Kallel, N. 1988: Deepwater source variations during the Last Climatic Cycle and their Impact on the Global Deepwater Circulation. *Paleoceanography,* Vol. 3 (3). pp 343-360.

Echols, R.J. 1971: Distribution of Foraminifera in Sediments of the Scotia Sea Area, Antarctic Waters. pp. 93-168. In. *Antarctic Oceanology I,* Reid, J.L. (ed.) *Antarctic Research Series,* Vol. 15.

Edwards, A.R. 1997: Personal communication, Geological Society of New Zealand National Conference. Wellington.

Edwards, A.R. and Perch-Nielsen, R. 1975: Calcareous Nannofossils from Southern Southwest Pacific Deep-Sea Drilling Project Leg 29. pp. 469-541. In: Initial Reports of the Deep-Sea Drilling Project, Vol. 29. White, S.M. (ed.). National Science Foundation, Washington (U.S. Government Printing Office).

Emilianii, C. 1955: Pliestocene Temperatures.*Journal of Geology,* Vol. 63. pp. 538-578.

Epstein, S.; Buchsbaum, R.; Lowenstein, H.A. and Urey, H.C. 1953: Revised Carbonate-water Isotopic Temperature Scale. *Geological Society of America Bulletin,* Vol. 64. pp. 1315-1325.

Faure, G. 1986: Principles of Isotope Geology, 2nd Ed. John Wiley and Sons, New York

Fenner, J.; Carter, L. and Stewart R. 1992: Late Quaternary Paleoclimatic and Paleoceanographic Change Over Northern Chatham Rise, New Zealand. *Marine Geology,* Vol. 108. pp. 383-404.

Florida State University - Cruises 32-45, 1971: *Antarctic Core Facility Contribution 33*. Frakes, L. (ed.). Antarctic Research Facility, Florida State University.

Florida State University - Cruises 4-54, 1973: *Antarctic Core Facility Contribution 37*. Frakes, L. (ed.). Antarctic Reseach Facility, Florida State University.

Folk, R.L. 1968: Petrology of Sedimentary Rocks. University of Texas.

Geitzenauer, K.R. 1969: The Pliestocene Calcareous Nannoplankton of the Subantarctic, Pacific Ocean. Department of Geology, Florida State University Contribution No.32.

Glasby, G.P. 1976: Surface Densities of Manganese Nodules in the Sothern Sector of the South Pacific. *New Zealand Journal of Geology and Geophysics,* Vol. 19 (6), pp. 771-790.

Goodell, H.G. 1968: Marine Geology - USNS Eltanin Core Descriptions, Cruises 16-27. Antarctic Core Facility Contribution 25. Florida State University.

Goodell, H.G. and Watkins, N.D. 1968: The Paleomagnetic Stratigraphy of the Southern Ocean 20° West to 160° E Longitude. *Deep-Sea Research,* Vol. 15. pp. 89-112.

Goodell, H.G.; Houtz, R.; Ewing, M.; Hayes, D.; Naini, B.; Echols, R.J.; Kennett, J.P. and Donahue, J.G. 1973: Marine Sediments of Southern Ocean. *Antarctic Map Folio Series,* Folio 17, American Geographical Society, pp.1-5.

Gordon, A.L. 1971: Recent Physical Oceanographic Studies of Antarctic Waters. pp. 609-629. In: Research in the Antarctic; Symposium (Dallas) December, 1968, Quam, L.Q. (ed.). American Association for the Advancement of Science Publication No. 93.

Gordon, A.L. 1972: On the Interaction of the Antarctic Circumpolar Current and the Macquarie Ridge. *Antarctic Oceanology: Antarctic Research Series,* Vol. 19. pp. 71-78.

Gordon, A.L. 1975a: General Ocean Circulation, "Numerical Models of Ocean Circulation". Symposium 17-20 Oct 1972 . *National Association for Science Publication.* Durham, N.H. (ed.), pp. 39-53.

Gordon, A.L. 1975b: An Antarctic Oceanographic Section Along 170°E. *Deep -Sea Research,* Vol. 22, pp. 357-377.

Gordon, A.L. 1977: Antarctic Oceanographic Zonation. pp. 45-76 In: Polar Oceans. Dunbar, M.J. (ed.). Arctic Institute of North America.

Gordon, A.L. 1988: Spatial and Temporal Variability Within the Southern Ocean. pp. 41-56. In: Antarctic Ocean and Resources Variability, Sahrage, D. (ed.). Springer-Verlag.

Gordon, A.L. and Goldberg, R.D. 1970: Circumpolar Characteristics of Antarctic Waters. *Antarctic Map Folio Series,* Folio 13, American Geographical Society. pp.1-5.

Gordon, A.L.; Molinelli, E. and Baker, T. 1978: Large-Scale Relative Dynamic Topography of the Southern Ocean. *Journal of Geophysical Research,* Vol. 83 (C6). pp. 3023-3032.

Gordon, A.L.; Molinelli, E.J. and Baker, T.N. 1982: Southern Ocean Atlas. Columbia University Press.

Gordon, A.L.; Taylor, H.W. and Georgi, D.T. 1977: Antarctic Oceanographic Zonation. pp. 45-76. In: Polar Oceans, Dunbar, M.J. (ed.).

Griggs, G.B.; Carter, L.; Kennett, J.P. and Carter, R.M. 1983: Late Quaternary Marine Stratigraphy Southeast of New Zealand. *Geological Society of America Bulletin.* Vol. 94. pp. 791-797.

Hays. J.D. 1965: Radiolaria and Late Tertiary and Quaternary History of Antarctic Seas. *American Geophysical Union Antarctic Research Series,* Vol. 5. pp. 125-184.

Hayward, B.W. 1983: Planktic Foraminifera (Protozoa) in New Zealand Waters: A Taxonomic Review. *New Zealand Journal of Zoology,* Vol. 10. pp. 63-74.

Heath, R.A. 1981: Oceanic Fronts around Southern New Zealand. *Deep-Sea Reseach,* Vol.28a (6). pp. 547-560.

Heath, R.A. 1985: A Review of the Physical Oceanography of the Seas Around New Zealand. *New Zealand Journal of Marine and Freshwater Research,* Vol.19. pp 79-124.

Heezen, B.C. and Hollister, C. 1964: Deep-Sea Current Evidence from Abyssal Sediments. *Marine Geology,* Vol. 1. pp. 117-140

Hemleben, Ch.; Spindler, M. and Anderson, O.R. 1989: Modern Planktonic Foraminifera. Springer-Verlag, New York.

Hendy, I.L. 1995: Paleoceanography of the Glacial-Holocene Transition in the Waters Surrounding New Zealand. M.Sc thesis, University of Waikato.

Hodell, D.A. and Venz, K. 1992: Toward a High Resolution Stable Isotopic Record of the South Ocean During the Pliocene-Pliestocene (4.8 to 0.8 Ma). In: The Antarctic Paleoenvironment: A perspective on Global Change. *Antarctic Research Series,* Vol. 56. pp. 265-310.

Houlton, Th. J. 1967: Water Masses and Fronts in the Southern Ocean South of New Zealand. *New Zealand Department of Scientific and Industrial Research. Bulletin, No. 174.*

Heusser, C.J. 1989: Polar Perspective of Late-Quarternary Climates in the Southern Hemisphere. *Quarternary Research,* Vol. 32. pp. 60-71.

Imbrie, J.; Hays, J.D.; Martinson, D.G.; McIntyre, A.; Mix, A.C.; Morley, J.J.; Pisias, N.G.; Prell, W.L. and Shackleton, N.J. 1984: The Orbital Theory of Pleistocene Climate: Support from a Revised Chronology of the Marine $\partial^{18}O$ Record. pp. 269-305. In: Milankovitch and Climate, Part 1. Berger, A.; Imbrie, J.; Hays, J.; Kukla, G. and Saltzman, B (eds.). Riedel, Dordrecht, The Netherlands; NATO ASI series: Advanced Science Institutes series.

Jacobs, S.S.; Bruchhausen, P.M. and Bauer, E.B. 1970: Eltanin Reports, Cruises 32-36, 1968. Hydrographic Stations, Bottom Photographs, Current Measurements. *Lamont-Doherty Geological Observatory of Columbia University, Technical Report.*

Jenkins, D.G. and Srinivasan, M.S. 1986: Cenozoic Planktonic Foraminifera from the Equator to the Subantarctic of the Southwest Pacific. pp 795-834. In: Initial Reports of the Deep-Sea Drilling Project, Vol 90, Part 2. Blakeslee, J.H. (ed.). National Science Foundation, Washington (U.S. Government Printing Office).

Keany, J. and Kennett, J.P. 1975: Plioecene-Pliestocene Radiolarian Biostratigraphy and Paleoclimatology at DSDP Site 278 on the Antarctic Convergence. pp. 757-760. In: Initial Reports of the Deep-Sea Drilling Project, Vol. 29. White, S.M. (ed.). National Science Foundation, Washington (U.S. Government Printing Office).

Kennett, J.P. 1969: Distribution of Planktonic Foraminifera in Surface Sediments Southeast of New Zealand. Proceeding of the First International Conference on Planktic Microfossils (Geneva 1967), Vol. 2. pp. 307-322.

Kennett, J.P. 1970: Pleistocene Paleoclimates and Foraminiferal Biostratigraphy in Subantarctic Deep-Sea Cores. *Deep-Sea Research,* Vol.17. pp.125-140.

Kennett, J.P. 1982: Marine Geology. Prentice-Hall inc, Englewood Cliffs.

Kennett, J.P. and Srinivasan, M.S. 1983: Neogene Planktonic Foraminifera, A Phylogenetic Atlas. Hutchinson Ross Publishing Company,Stroudsburg, Pennsylvania.

Kennett, J.P. and Vella, P. 1975: Late Cenozoic Planktic Foraminifera and Paleoceanography at DSDP Site 284 in the Cool Subtropical South Pacific. pp. 769-800. In: Initial Reports of the Deep-Sea Drilling Project, Vol. 29. White, S.M. (ed.). National Science Foundation, Washington (U.S. Government Printing Office).

Kohfeld, K.E.; Fairbanks, R.G.; Smith, S.L. and Walsh, I.D. 1996: *Neogloboquadrina pachyderma* (sinistral coiling) as Paleoceanographic Tracers in Polar Oceans: Evidence from Northeast Water Polynya Plankton Tows, Sediment Traps, and Surface Sediments. *Paleoceanography,* Vol. 11 (6). pp. 679-699.

Krinsley, D.H. and Takahashi, T. 1962: Applications of Electron Microcopy to Geology. *New York Academy of Science Transactions,* Vol. 25. pp. 3-22.

Kumar, N.; Anderson, R.F.; Mortlock, R.A.; Froelich, P.N.; Kubik, P.; Dittrich-Hannen, B. and Suter, M. 1995: Increased Biological Productivity and Export Production in the Glacial Southern Ocean. *Nature,* Vol. 378.

Kurihara, K. and Kennett, J.P. 1986: Neogene Benthic Foraminifera: Distribution in a Depth Traverse, Southwest Pacific. pp.1037-1077. In: Initial Reports of the Deep-Sea Drilling Project, Vol 90, Part 2. Blakeslee, J.H. (ed.). National Science Foundation, Washington (U.S. Government Printing Office).

Labeyrie, L.D.; Duplessy, J.C. and Blanc, P.L. 1987: Variations in Mode of Formation and Temperature of Oceanic Deep Waters Over the Past 125,000 Years. *Nature,* Vol. 327. pp. 477-482.

Labracherie, M.; Labeyrie, L.D.; Duprat, J.; Bard, E.; Arnold, M.; Pichon, J.J. and Duplessy, J.C. 1989: The Last Deglaciation in the Southern Ocean. *Paleoceanography,* Vol. 4 (6). pp. 629-638.

Le, J. and Shackleton, N.J. 1992: Carbonate Dissolution Flucuations in the Western Equatorial Pacific during the Late Quaternary. *Paleoceanography,* Vol. 7 (1). pp. 21-42.

Ledbetter, M.T.; Ciesielski, P.F.; Osbourne, N.I. and Allison, E.T. 1983: Bottom-Current Erosion in the Southerneast Indian and Southwest Pacific Oceans During the Last 5.4 Million Years. In: Antarctic Earth Science. Oliver, R.L.; ames, P.R and Jago, J.B. (eds.). Cambridge University Press, Cambridge. pp. 379-383.

Lewis, D.W. and McConchie, D.M. 1994: Practicle Sedimentology (2nd ed). Chapman and Hall, New York.

Lisitzin, A.P. 1972: Sedimentation in the World Oceans. *Society of Economic Paleontologists and Mineralogists, Special Publication No. 17.*

Lohman, W.H. 1986: Calcareous Nannoplankton Biostratigraphy of the Southern Coral Sea, Tasman Sea and Southwest Pacific Ocean. pp. 763-793. In: Initial Reports of the Deep-Sea Drilling Project, Vol 90, Part 2. Blakeslee, J.H. (ed.). National Science Foundation, Washington (U.S. Government Printing Office).

Lombari, G. and Boden, G. 1985: Modern Radiolarian Distributions. *Cushman Foundation for Foraminiferal Research; Special Publication No. 16A.*

McCartney, M.S. 1977: Subantarctic Mode Water. pp 103-119. In: A Voyage of Discovery. Angel, M. (ed.). *Deep Sea Research*, Vol. 24. George Deacon Fourth Anniversary Volume.

McCave, I.N.; Bryant, R.J.; Cook, H.F. and Coughanover, C.A. 1986: Evaluation of a Laser-Diffraction-Size Analyzer for use with Natural Sediments. *Journal of Sedimentary Petrology* .Vol. 56. pp.561-564.

McCollum, D.W. 1975: Diatom Stratigraphy of the Southern Ocean. pp. 515-573. In: Initial Reports of the Deep-Sea Drilling Project, Vol 28. Kaneps, A.G. (ed.). National Science Foundation, Washington (U.S. Government Printing Office).

McDougall, K. 1996: Benthic Foraminiferal Response to the Emergence of the Isthmus of Panama and Coincident Paleoceanographic Changes. *Marine Micropaleontology,* Vol. 28. pp 133-139.

McGlone, M.S.; Salinger, M.J. and Moar, N.T. 1994: Paleovegetation studies of the New Zealand Climate since the Last Glacial Maximum. pp 294-317. In: Global Climates since the Last Glacial Maximum. Wright, H.E.; Kutzbach, J.E.; Webb, T.; Ruddiman, W.F.; Street-Perrott, F.A. and Bartlein, P.J. (eds.). University of Minnesota Press, Minneapolis.

Margolis, S.V. and Kennett, J.P. 1971: Cenozoic Paleoglacial History of Antarctica Recorded in Subantarctic Deep-Sea Cores. *American Journal of Science,* Vol. 271. pp. 1-36.

Margolis, S.V. and Krinsley, D.H. 1971: Submicroscopic Frosting on Eolian and Subaqueous Quartz Sand Grains. *Geological Society of America Bulletin,* Vol. 5. pp. 3395-3406.

Martinez, J.I. 1994: Late Pliestocene Carbonate Dissolution Patterns in the Tasman Sea. pp. 215-228. In: Evolution of the Tasman Sea Basin. van der Lingen, G.J.; Swanson, K.M. and Muir, R.J. (eds.).

Martini, E. 1986: Paleogene Calcareous Nannoplankton From Southwest Pacific Ocean, Deep-Sea Drilling Project, Leg 90. pp. 747-761. In: Initial Reports of the Deep-Deep-Sea Drilling Project, Vol. 90, Part 2. Blakeslee, J.H. (ed.). National Science Foundation, Washington (U.S. Government Printing Office).

Morley, J.J. 1989: Variations in High-Latitude Oceanographic Fronts in the Southern Indian Ocean: An Estimation Based on Faunal Changes. *Paleoceanography,* Vol. 4 (5). pp. 547-554.

Morley, J.J. and Hays, J.D. 1979: Comparison of Glacial and Interglacial Oceanographic Conditions in the South Atlantic from Variations in Calcium Carbonate and Radiolarian Distributions. *Quaternary Research,* Vol. 12. pp. 396-408.

Morrow, R.; Church, J.; Coleman, R.; Chelton, D. and White, N. 1992: Eddy Momentum Flux and it's Contribution to the Southern Ocean Momentum Balance. *Nature,* Vol. 357. pp. 482-484.

Neil, H.L. 1991: Late Quaternary Stratigraphy, Sedimentology and Evolution of Bounty Fan System, Bounty Trough, Southwest Pacific. M.Sc Thesis, Department of Earth Sciences, University of Waikato, Hamilton, New Zealand.

Nelson, C.S. 1986: Lithostratigraphy of Deep Sea Drilling Project Leg 90 Drill Sites in the Southwest Pacific: An Overview. pp. 1471-1491 In: Initial Reports of the Deep Sea Drilling Project, Vol. 90, Part 1 & 2. National Science Foundation, Washington (U.S. Government Printing Office).

Nelson, C.S.; Keane, S.L and Head, P.S. 1988: Nontropical Carbonate Deposits on the Modern New Zealand Shelf.*Sedimentary Geology,* Vol. 60. pp. 71-94.

Nelson, C.S.; Cooke, P.J.; Hendy, C.H. and Cuthbertson, A.M. 1993a: Ocenanographic And Climatic Changes Over The Past 160,000 Years At Deep Sea Drilling Project Site 594 Off Southeastern New Zealand, Southwest Pacific. *Paleoceanography,* Vol. 8 (4). pp. 435-458.

Nelson, C.S.; Hendy, C.H. and Cuthbertson, A.M. 1993b: Compendium of Stable Oxygen and Carbon Isotope Data for the Late Quaternary Interval of Deep-Sea Cores from the New Zealand Sector of the Tasman Sea and Southwest Pacific Ocean. Ocassional Report No. 16. Departemnt of Earth Science, University of Waikato, Hamilton, New Zealand.

Nelson, C.S.; Hendy, C.H. and Cuthbertson, A.M. 1994: Oxygen Isotope Evidence for Climatic Contrasts Between Tasman sea and Southwest Pacific Ocean during the Late Quaternary. pp. 181-196. In: Evolution of the Tasman Sea Basin. van der Lingen, G.J.; Swanson, M. and Muir, R.J. (eds.). A.A. Balkems, Rotterdam.

Nigirini, C. and Moore, T.C. 1979: A Guide to Modern Radiolaria. *Cushman Foundation for Foraminiferal Research; Special Publication No. 16.*

Orsi, A.H.; Whitworth, T. and Worth N.D. 1995: On the Meridional Extent and Fronts of the Antarctic Circumpolar Current. *Deep-Sea Research I,* Vol. 42 (5). pp. 641-673.

Osborn, N.I.; Ciesielski, P.F. and Ledbetter, M.T. 1983: Disconformities and Paleoceanography in the Southeast Indian Ocean During the Past 5.4 Million Years. *Geological Society of America Bulletin,* Vol. 94. pp. 1345-1358.

Oppo, D.W.; Fairbanks, R.G. and Gordon, A.L. 1990: Late Pliestocene Southern Ocean Delta 13C Variability. *Paleoceanography,* Vol. 5 (3). pp. 43-54.

Ovenshine, A.T., Margolis, S.V. and Larson, R.R. 1973: Bottom Water Conditions Indicated by Surface Features of Detrital Silicate Grains at Site 276. pp. 1065-1069. In: Initial Reports of the Deep Sea Drilling Project, Vol. 29. White, S.M. (ed.). National Science Foundation, Washington (U.S. Government Printing Office).

Parker, F.L. and Berger, W.H. 1971: Faunal and Solution Patterns of Planktonic Foraminifera in Surface Sediments of the South Pacific. *Deep-Sea Research,* Vol. 18. pp. 73-107.

Petrushevskaya, M.G. 1975: Cenozoic Radiolarians of the Antarctic, Leg 29, DSDP. pp. 541-675. In: Initial Reports of the Deep Sea Drilling Project, Vol. 29. White, S.M. (ed.). National Science Foundation, Washington (U.S. Government Printing Office).

Rawle, A. 1994: The Basic Principles of Particle Size Analysis. Malvern Instruments Ltd.

Rodman, M.R. and Gordon, A.L. 1982: Southern Ocean Bottom Water of the Australian-New Zealand Sector.*Journal of Geophysical Research,* Vol. 87 (C8). pp. 5771-5778.

Schmitz, W.; Mangini, A.; Stoffers, P.; Glasby, G.P. and Plugger, W.L. 1986: Sediment Accumulation Rates in the Southwestern Pacific Basin and Aitutaki Passage. *Marine Geology,* Vol. 73. pp. 181-190.

Singer, J.K.; Anderson, J.B.; Ledbetter, M.T.; McCave, N.I; Jones K.P.N. and Wright, R. 1988: *Journal of Sedimentary Petrology,* Vol. 58 (3). pp. 534-543.

Shackleton, N.J. 1987: Oxygen Isotopes, Ice Volume and Sea Level. *Quaternary Science Reviews,* Vol. 6. pp. 183-190.

Shackleton, N.J. and Kennett, J.P. 1975: Paleotemperature History of the Cenozoic and the Initiation of Antarctic Glaciation: Oxygen and Carbon Isotope Analyses in DSDP Sites 277, 279 and 281. In: Initial Reports of the Deep Sea Drilling Project, Vol. 29. White, S.M. (ed.). National Science Foundation, Washington (U.S. Government Printing Office).

Summerhayes, C.P. 1969: Marine Geology of the New Zealand Subantarctic Sea Floor. *New Zealand Department of Scientific and Industrial Research, Bulletin No. 190.*

Thunell, R,C. 1976: Optimum Indices of Calcium Carbonate Dissolution in Deep-Sea Sediments. *Geology,* Vol, 4. pp. 525-528.

Uchio, T. 1960: Benthonic Foraminifera of the Antarctic Ocean. *Seto Marine Biology Laboratory, Special Publication No. 12.* pp. 3-20.

Urey, H.C. 1947: The Thermodynamic Properties of Isotopic Substances. J*ournal of Chemistry Society*. pp 562-581.

van Morkhoven, F.P.; Berggren, W.A. and Edwards, A.S. 1986: Cenozoic Cosmopolitan Deep-Water Benthic Foraminifera. Oertli, H.J. (ed.). *Bulletin Des Centres De Research Exploration-Production Elf-Aquitaine,* Memoir 11.

Vella, P.; Ellwood, B.B. and Watkins N.D. 1975: Surface-water Temperature Changes in the Southern Ocean Southwest of Australia During the Last One Million Years.*Quaternary Studies Royal Society of New Zealand Bulletin 13.* pp. 297-310.

Vincent, W.F.; Howard-William, C.; Tildesley, P. and Butler, E. 1991: Distribution and Biological Properties of Oceanic Water Masses Around the South Island, New Zealand. *New Zealand Journal of Marine and Freshwater Research,* Vol. 25. pp. 21-42.

Volat, J.L.; Pastouret, L. and Vergnaud-Grazzini, C. 1980: Dissolution and Carbonate Flucuation in Pliestocene Deep-Sea Cores: A Review. *Marine Geology,* Vol. 34. pp. 1-28.

Warren, B.A 1981: Deep Circulation of the World Oceand. pp. 6-41. In: Evolution of Physical Oceanography. Warren, B.A. and Wunsch, C. (eds.). MIT Press, Cambridge, Massachusetts.

Watkins, N.D. and Kennett, J.P. 1971: Antarctic Bottom Water: Mayor Change in Velocity During the Late Conozoic Between Australia and Antarctica. *Science,* Vol. 173. pp. 813-818.

Watkins, N.D. and Kennett, J.P. 1972: Regional Sedimentary Disconformities and Upper Cenozoic Changes in Bottom Water Velocities Between Australasia and Antarctica. *Antarctic Oceanology II: The Australian-New Zealand Sector;* Hayes, D.E. (ed.), *Antarctic Research Series,* Vol. 19. pp.273-293

Watkins, N.D. and Kennett, J.P. 1977: Erosion of Deep-Sea Sediments in the Southern Ocean Between Longitudes 70°E and 190°E and Contrasts in Maganese Nodule Development. *Marine Geology,* Vol. 23. pp.103-111.

Weaver, P.P.E.; Neil, H. and Carter, L. 1997: Sea Surface Temperature Estimates from the SW Pacific based on Planktonic Foraminifera and Oxygen Isotopes. *Paleogeography, Paleoclimatology, Paleoecology*, Vol. 131 (3-4). pp. 241-256.

Werner, D. 1977: Silicate Metabolism. pp.110-149. In: The Biology of Diatoms, Botanical Monographs, Vol. 13. Werner, D. (ed.). Blackwell Scientific Publications.

Williams, M.A.J.; Dunkerley, D.L.; Kershaw, A.P. and Stokes, T.J. 1993: Quaternary Environments. Edward Arnold, Hodder & Stoughton, London.

World.Wide.Web 1997: Http://www.arf.fsu.edu.

Wright, I.C.; McGlone, M.S.; Nelson, C.S. and Pillans, B.J. 1995: An Intergrated Latest Quaternary (Stage 3 to Present) Paleoclimatic and Paleoceanographic Record from Offshore Northern New Zealand. *Quaternary Research,* Vol. 44. pp. 283-293.

Appendices

Appendix 1

NZOI Research Cruise 3034 Report

RESEARCH CRUISE 3034, REPORT

Cruise Designation : Pacific Gateway - Palaeoceanography

Departure: Wellington, 1800h, 10 February, 1997.

Arrival: Dunedin, 1000h, 28 February, 1997.

Personnel: Lionel Carter (leader)

John Hunt

John Mitchell

Helen Neil

Rick Pridmore

Steve Wilcox

Visiting Scientists

Prof. Bob Carter (James Cook University, Townsville)

Prof. Nick McCave (Cambridge University)

Jonathan Mackie (Waikato University).

Acknowledgments.

Research cruise 3034 was a successful venture that was in part due to the professionalism and enthusiasm of the captain, officers and crew of the *Tangaroa*.. The other major factor affecting the outcome of the voyage was the invaluable contributions made by the science party, and I express my thanks to (in reverse alphabetical order):

Steve Wilcox for his efforts in commissioning the multi-channel seismic system, often in trying circumstances, as well as servicing other electronic equipment;

Rick Pridmore who, on his first research cruise, readily acclimatised to working at sea to produce an extensive set of chlorophyll data in addition to instigating development of a new "high speed" water sampler;
Helen Neil who had a major input to the cruise including the onshore preparation, setting up of lab facilities and the onboard sampling, initial analysis and preliminary interpretation of cores;
John Mitchell for his willing assistance and professional manner in which he carried out watch-keeping duties and the processing of the navigational, depth and side-scan sonar data.;
Nick McCave for his enthusiasm, expertise and assistance in all facets of the survey, in particular the core sampling and description;
Jonathan Mackie, another "first timer" who came through with flying colours by contributing to the watchkeeping and coring programme;
John Hunt for the pre-cruise efforts in preparing much of the heavy equipment and his onboard efforts in helping to keep equipment operational.
Bob Carter, firstly for the enormous personal effort put into getting the Ocean Drilling Programme to NZ waters - ODP site surveys being a main part of 3034 - and secondly for his all-round contribution to the shipboard operations (ship's printer aside).

A final debt is owed to the Southern Ocean which against all expectations turned on a benign sea for much of the voyage, making the work that much easier.

Objectives.

- Survey sites scheduled in Leg 181 of the Ocean Drilling Programme (ODP) as a necessary precursor to the drilling of these sites in the winter of 1997. Each site was to be subjected to a series of passes with the 12kHz and 3.5 kHz sounders and a seismic reflection system. The sites were also to be cored where necessary. Leg 181 has been designed to evaluate:

  1. the development of the Antarctic Circum - Polar Current (ACC) and deep western boundary current (DWBC) since their inception;

  2. the supply of Circum - Pacific Deep Water (CDW) into the Pacific, in particular the roles played by Weddell and North Atlantic Deep Water in CDW formation;

3. derive the past flow velocities of intermediate and deep waters and therefore determine their transport;

4. establish the AAIW history along the NZ margin and its relationship to terrestrial climatic change;

5. productivity change at the Subtropical Convergence;

6. past changes in the locations of oceanic fronts including the Subtropical, Subantarctic and Antarctic fronts;

7. correlations between variability in the ACC and Milankovitch cyclicity;

8. timing of northern and southern hemisphere climatic and oceanic events.

- To collect a latitudinal transect of cores which will be analysed to evaluate the northward transport of Australasian Subantarctic Water and Antarctic Intermediate Water (AAIW) across the Campbell Plateau together with migration of Circumpolar Deep Water along the plateau-rise margins since the Last Glacial Maximum or earlier.

- To ascertain the impact of oyster dredging and natural oceanographic processes on the seabed of Foveaux Strait through a side-scan sonar and seismic (3.5 kHz) survey supplemented by photographic transects of pristine and dredged sites.

- Provide field measurements of the concentration of chlorophyll in oceanic surface waters for comparison with data collected by the Ocean Colour Temperature Sensor on the ADEOS satellite. Samples to be collected while on station and during the ships passage particularly during sunny mornings.

- Investigate seabed conditions in the vicinity of a methane plume on the continental slope off Palliser Bay.

- Run sea trials for the multichannel seismic system, ADCP and Benthos camera system..

Operations

1. Kasten Corer. The coring retrieval/deployment system worked well under the calm to gale-force sea conditions experienced on the cruise. The corer itself regularly retrieved c. 2-3m of sediment although failed in sandy and/or consolidated substrates as determined from the acoustical character of the 3.5kHz record. Onboard processing was labour intensive and took 3 people 4-5 hrs to describe, subsample a ≈3m core into conduits, x-ray slabs, bags, and wet bulk density tubes, and to set the corer up for the next sample site. Magnetic susceptibility measurements at 2-4 cm intervals downcore, took Helen Neil a further 2-4 hours.

2. Multi-Channel System. On its first outing, the MCS appears to have produced very good results going by the EPC record from one channel. This result was not possible without considerable effort from Steve Wilcox who worked through a series of "bedding-down" problems that will become fewer as we accustom ourselves to using the equipment. Problems included, (a) water leakage at the array distal termination (poor manufacturing), (b) evaluating the correct depressor angle for array "birds" (c) determination of deployment procedure with the best method being to have the ship moving at 4 knts into the sea followed by playing out of the array and, when steaming straight behind the vessel, deploy the airgun, (d) failure of the new compressor to perform to expectations and eventually become inoperable because of burning out of the Vee belts. Reliance placed on the old William and James compressor for the rest of the voyage.

3. Multicorer. Time permitted only three deployments of the Multicorer which was armed with 4 core barrels. One deployment failed to trip, whereas the other 2 collected a small amount of surficial foraminiferal sediment and overlying water in one core barrel only; the remaining barrels having only a centimetre of sediment that was too thin to seal the tube thereby allowing water to escape with the inevitable washing of the sediment. The corer may be better suited to soft material but nevertheless, it has to be tested further with concentration on the closure of the bottom flap which appears to be sealing incorrectly.

4. Benthos Camera. Worked well in its one and only deployment, but the flash still needs adjustment to the remove a hot-spot on the negatives.

5. 12kHz Echo and 3.5kHz Sounding. The ORE 3.5kHz sounder provided a mix of results, the most disappointing aspect being its exposure to bubbles resulting in a loss of record. This was prevalent in moderate to rough seas especially when the vessel was heading directly into a sea or with the wind on the port or starboard bow in which cases the vessel tended to heel with the wind presumable exposing the hull to aeration. The 12 kHz sounder provided a better and more continuous record in moderate seas and was only subject to minor aeration and partial loss of record when heading into a sea under strong gale to storm force conditions.

5. Acoustic Doppler Current Profiler (ADCP) was used in a test capacity over a deep water transect across the Campbell Drift at 51^{0}S, and over shallow water tracks within Foveaux Strait. The preliminary results look encouraging in that the direction and strength of the flow are logical. Further analysis, e.g., comparison of the Foveaux Strait data with the tidal regime at the time of measurements will provide a better check on ADCP performance. However, the ultimate test must be made against moored current meters recording at the same time as the ADCP pass. This will be a small objective of future research voyages.

Results

Palliser Gas Plume (Station Y1). A plume of acoustically opaque water, rising 350 m above the 1050 m-deep seabed off Cape Palliser, was discovered by Patrick Cordhu in 1996. Our initial interpretation was that the feature was a gas plume formed by the escape of shallow gas within the accretionary prism. The plume was still present when revisited on 10.2.97. Dimensions were 300 m high and approximately 300 m wide. A camera transect revealed a pock-marked, muddy substrate, the pocks being tell-tale indicators of gas escape. Some fauna are evident in the negatives but until enlarged photographic prints are made, the nature of the fauna cannot be established. A total of 15 photographs of the seabed within the plume, were collected along with 3.5 kHz and 28 kHz soundings - the latter displaying the plume outline as well as the substrate.

ODP Sites SWPAC 2A, 5A, 6A, 7A, 8A. SWPAC 2A was surveyed by 3.5k Hz and Multi-Channel Seismics (MCS) to supplement the single industry line from this site. Surficial sediment samples and the 3.5kHz records indicated the seabed is mainly acoustically reflective, foram sand, whereas the unprocessed output from MCS confirmed the structure seen in the industry profile, namely a thin Plio-Pleistocene uppermost Unit B,

ADCP Vectors

Cruise 3034

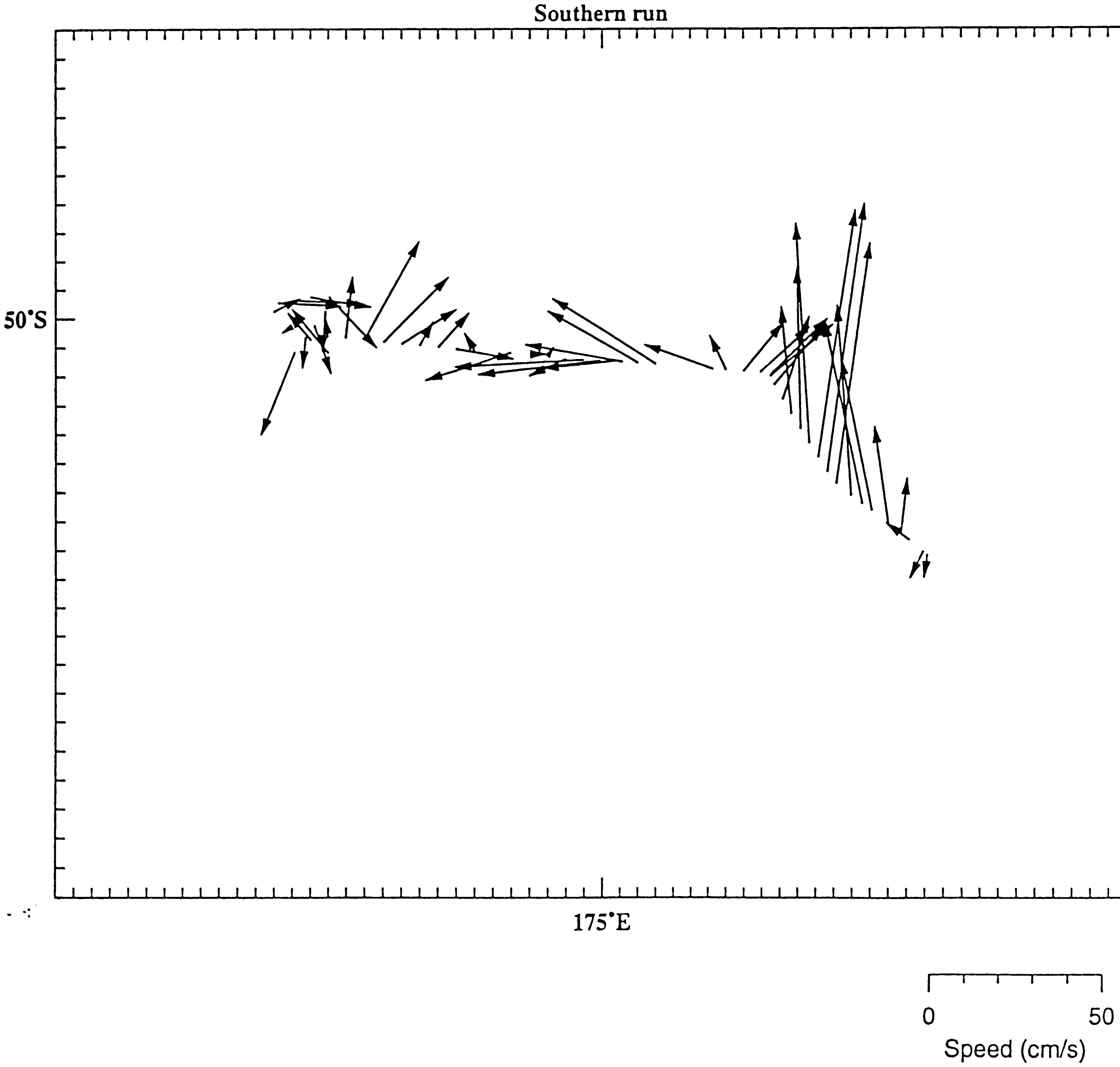

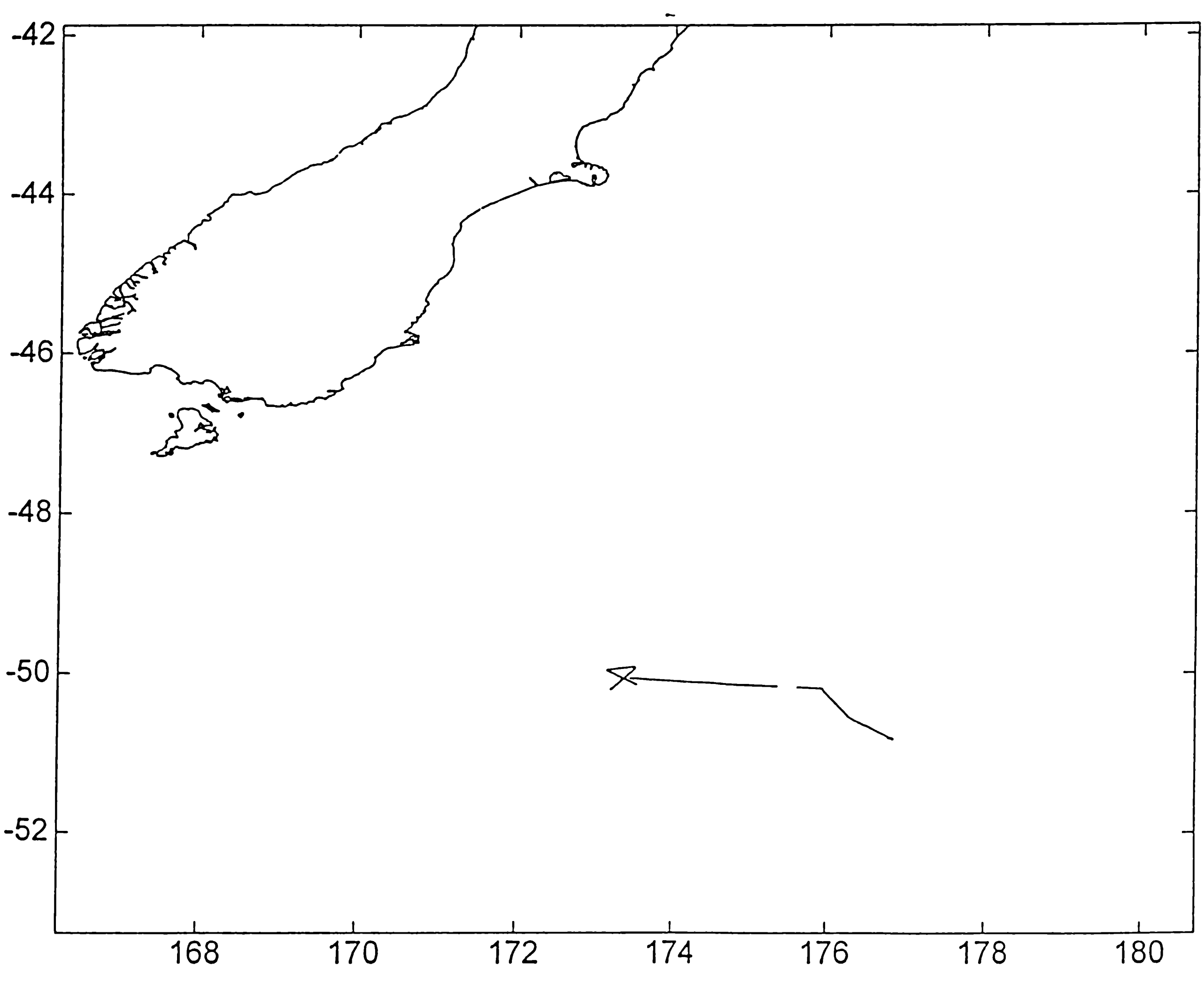

-42
-44
-46
-48
-50
-52
168
170
172
174
176
178
180

ADCP Vectors

Cruise 3034

Strait run

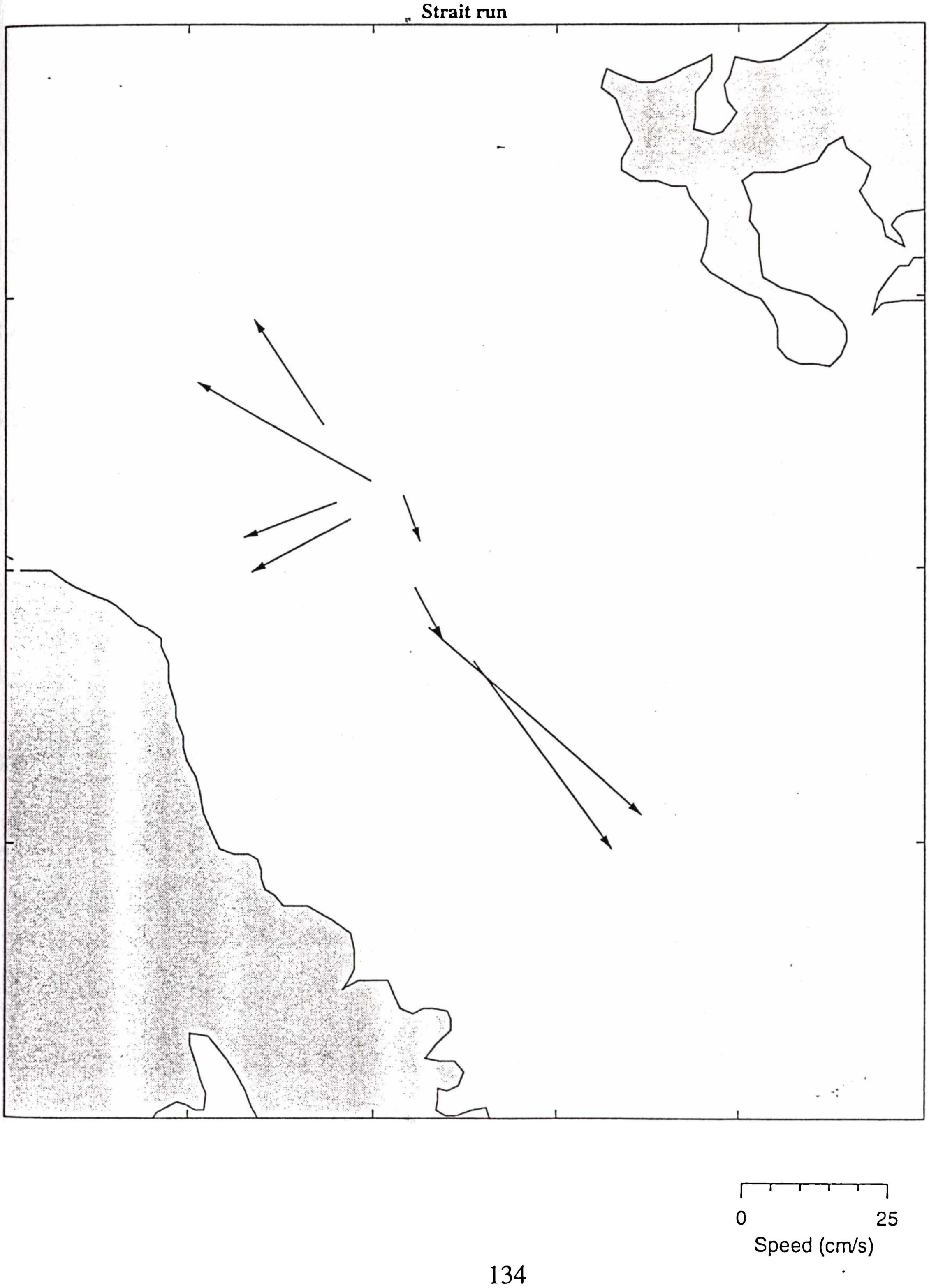

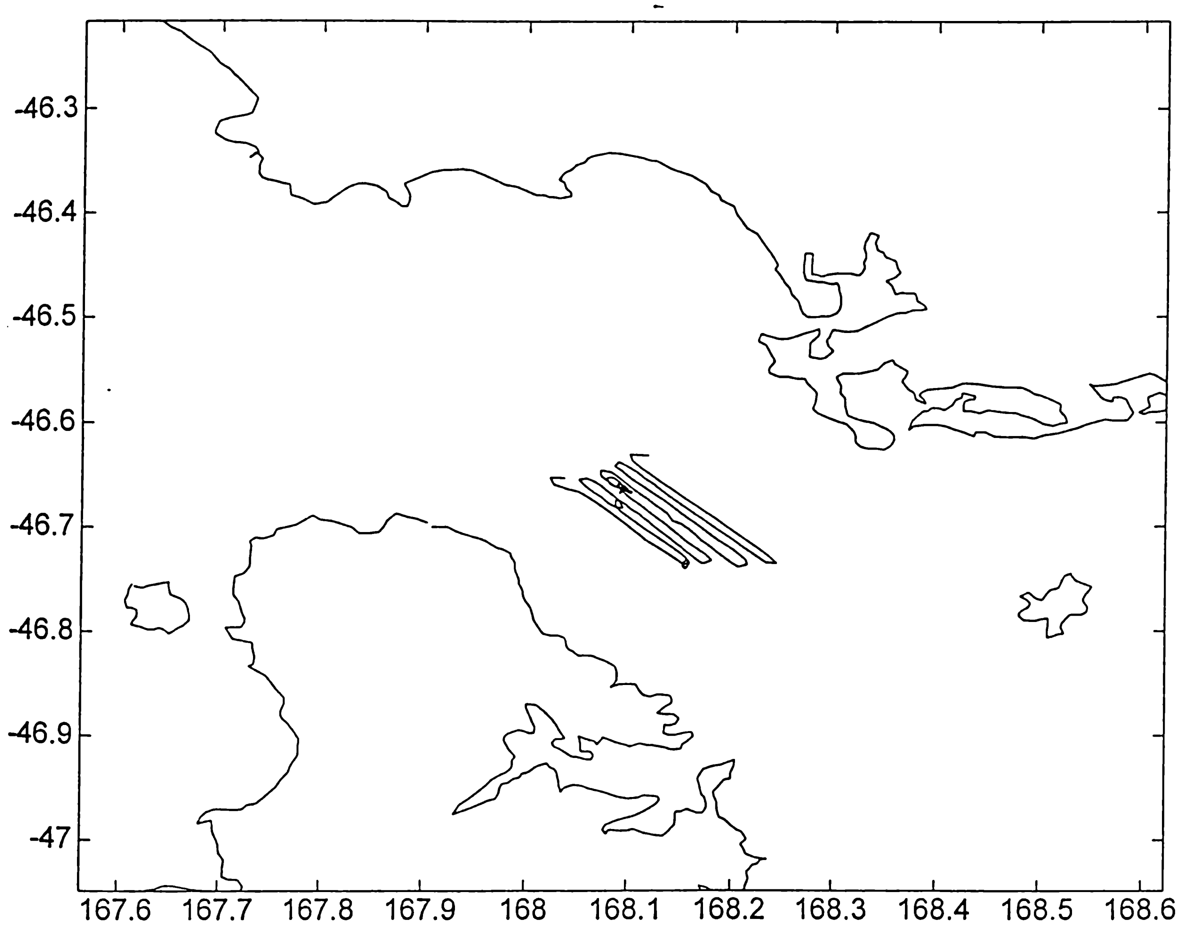
-46.3
-46.4
-46.5
-46.6
-46.7
-46.8
-46.9
-47
167.6
167.7
167.8
167.9
168
168.1
168.2
168.3
168.4
168.5
168.6

underlain unconformably by a semi-transparent, massive Unit B of probable Miocene age, followed by a series of strong reflectors belonging to probable Oligocene Unit C.

SWPAC 5A. MCS Line 7 was run perpendicular to existing NIWA line from Cruise 2050. The 1.2 sec. unprocessed section outlined a northward thinning Unit A (max. 0.2 sec.) unconformably above a fairly uniform thickness of Unit B (0.45 sec) with strong reflectors that become acoustically transparent with depth apart from a ill-defined intraformational unconformity X_1 and a basal unconformity X which is part of the strong reflecting Unit C.

Site SWPAC 6B is a new site at 548 m depth, initially positioned on the basis of isopachs constructed from single channel seismic records collected by the *Eltanin*. The new seismic data collected on CR 3034, confirm a substantial thickness of sediment exceeding 1 sec. (two way travel time). The uppermost 0.3 sec. of record comprises a well ordered set of parallel and continuous reflectors that rest on an apparent unconformity marking the top of a less ordered succession of layered sediments ($\approx$ 0.2 sec.) with discontinuous, undulating reflectors sometimes with small scale hyperbolae. The base of this sequence is also marked by an unconformity which is the top of $\approx$ 0.25 sec. of strong, continuous reflectors. Kasten core Y12 from the site retrieved calcareous biopelagites.

Site SWPAC 7A occupies the crest of the Campbell Drift at 4490 m. The MCS Lines 16 and 17 readily penetrated to ocean basement approximately 0.6 - 0.8 sec. below the ocean floor along Line 16. East of the proposed ODP site, in depths > 4960 m and 100 km from the foot of the Campbell Plateau, the drift is covered by a drape which overlies a hummocky, erosional surface as outlined on 3.5 kHz records. This surface becomes more reflective towards the western boundary - a trend that is accompanied by an increase in the scale of the hummocky topography. The presence of the buried hummocky surface implies the ancestral boundary current was either wider and/or more meandering that at present. In the MCS section, the upper $\approx$0.08 sec. is strong contorted reflectors often with hyperbolae that probably represent a series of buried erosional surfaces as evinced by the accompanying 3.5 kHz profiles. An unconformity separates the upper sequence from a more ordered succession of continuous closely spaced reflectors ($\approx$0.15 sec. thick) and a basal massive, acoustically transparent layer. The succession rests on a prominent, widespread reflector that may be Oligocene reflector X .

SWPAC 8A, at the crest of the left bank (north) Bounty Channel levee, was surveyed along MCS Line 12 which revealed in some detail the migrating sediment wave field of Unit A (0.45 sec.). This sequence rests on continuous, closely spaced reflectors (0.2 sec. max.) which are locally but not exclusively conformable with Unit A and have a similar acoustical signature, and therefore are ascribed to the Plio-Pleistocene. The widespread underlying unconformity, marked by strong discontinuous reflectors, is probably reflector Y of late Miocene age. It is followed by Unit C and possibly D to a rugged Cretaceous basement about 1.6 sec. below the seabed.

AAIW-CDW Palaeoceanography. Kasten core Y4 from the eastern end of Chatham Rise penetrated 2.74 m of foram mud of which the upper 0.5m were Stg 1, 0.5-2.70 m were Stg 2-4 and 2.6-2.7 m Stg 5. The Kawakawa Tephra (22,590 C14yrs) provided some chronostratigraphic control along with other tephra one of which may be the 28,000 yr Omataroa Tephra. A series of glauconite layers were located in Stg 2-4 and may be the product of redeposition from the Chatham Rise crest during sea-level lowstands.

Core Y6 retrieved 3.15 m of foram ooze and mud from the deep terrace drift on the south side of Chatham Rise. Colour zonation suggest a stratigraphy back to isotope Stage 5 with some control provided by the presence of the Kawakawa Tephra centred on c.0.75 m and possibly the Omataroa Tephra at 0.11-0.16m . Magnetic susceptibility also offers some stratigraphic control by providing a magnetic signature of Stage 5 that potentially includes differentiation of substages 5a-e.

Cores Y8 from a terrace on the south side of Bounty trough and Y9 from south of Bounty Platform, have similar lithological and magnetic susceptibility stratigraphies, namely a 0.4-0.5 biopelagic Stage 1; a condensed (0.4m) slightly terrigenous biopelagic Stages 2-4; a thick (1.50-1.55m) Stage 5 with substages, followed by a thin (0.3m) Stage 6 and in the case of Y8, by Stages 7 and 8. A salient feature of these cores is the apparent high productivity of the interglacial vs the glacial periods as manifested in the marked differences in sedimentation rates, e.g. Stage 1 $\approx$ 3.4 - 4..2 cm/1000y compared to Stages 2-4 combined $\approx$ 0.7 cm/1000y.

Core Y8

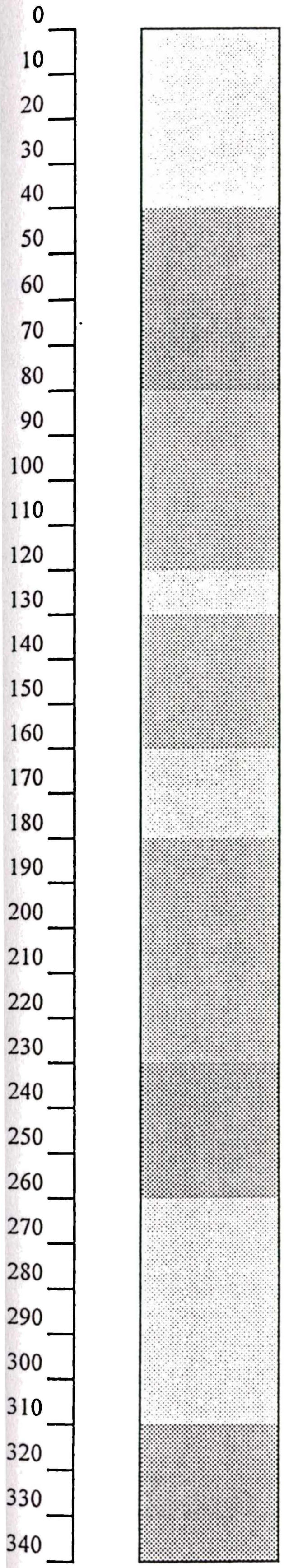

1 0-42 cm 2.5 Y 7/2 light grey foram mud, oxidised, sloppy, bioturbation blebs and mottles (~10%). Large planolites-like 2.5Y 8/2 white burrow at 16-18cm.

35-42 cm transition zone, significant oxidised bioturbation

2 42-84 cm 2.5 Y 5/2 light olive brown foram mud, many bioturbation blebs and mottles increasing to base of unit (~30%). Large white bleb at 55-57cm.

50-51 cm Tephra blebs and streaks, ? Kawakawa

67 & 73 cm distinct burrows

3/4

5a 84 - 123 cm 5Y 8/1 white foram ooze, bioturbation blebs and planolites-like burrows ~5%. Increases at top and base of unit (~10%)

92-97 cm ?core disturbance introducing dark green mud

117 cm oxidised planolites-like burrow

5b 123-131 cm 5Y 8/2 white foram ooze, significant bioturbation mottles and blebs, oxidised planolites-like burrow at 124 cm

5c 131-160 cm 5Y 8/1 white foram ooze, planolites-like burrows at 134 & 148 c

5d 160-183 cm 5Y 8/2 white foram ooze, minor bioturbation blebs and mottles

5e 183-230 cm 2.5Y 8/2 white (yellow hue) foram ooze, minor bioturbation

6 230-266 cm 5Y 5/2 olive grey foram mud with ~ 20% bioturbation blebs and mottles, increased at top and base of unit

243-250 cm significant bioturbation blebs

254 cm light planolites-like burrow

7 266-314 cm 2.5 Y 8/2 white (yellow hue) foram ooze with many bioturbation mottles and blebs (~30-40%) down to 279cm, decreases to ~ 10% till base

279-288 cm 5Y 6/2 light olive grey band with light bioturbation

8 314-333 cm 5Y 4/2 olive grey foram mud with significant bioturbation blebs and planolites-like oxidised burrows till 324cm

end of core 333cm

338-339 cm tephra blebs and streaks ? Mt Curl

end of catcher 344cm

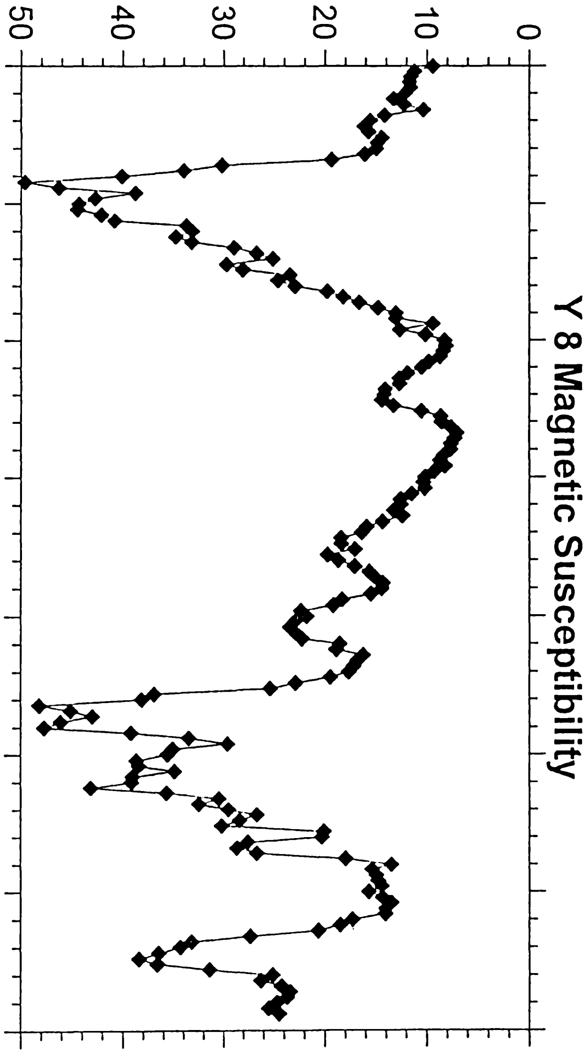
Y 8 Magnetic Susceptibility
0
10
20
30
40
50
0
50
100
150
200
250
300
350

The Campbell Drift was cored for the first time at 1247hr on 21 February, 199? - an historic occasion for one of the globe's largest drift deposits. Core Y11 contained 1.94m of muddy sand with bedding distinguished by varying quantities of Mn-coated grains and foram tests. A layer of ferromanganese nodules occurred at 1.12 m subsurface depth suggesting that this layer at least had been buried by younger sediment. However, other Mn-rich sand layers may not be old deposits but a function of the source material.

Cores Y12 -Y17 were from a latitudinal transect of the Campbell Plateau. despite the wide geographical extent and the variability of core length, the lithostratigraphy was consistent across over the Plateau. Our initial interpretation based on lithology and magnetic susceptibility suggest a thin (≈0.2m), calcareous biopelagic Stg. 1 overlying foram. mud belonging to Stg. 2-4 (≈ 0.5m) which in turn rests on a distinctive white ooze of a well developed Stg. 5 up to 1.1m thick. In the longest core (Y16), the white ooze rests on an alternating grey foram mud and white foram mud that may extend the stratigraphy back to St. 8.

Foveaux Strait Side-Scan Sonar Survey. A total of 8 lines were run NW-SE along a sector of the bryozoan and oyster beds that were either pristine or recently dredged. The resultant sonographs clearly outlined the sections of seabed disrupted by the dredges and together with the concomitant ADCP data, 3.5kHz seismic profiles and 12 kHz soundings provide a base chart for sampling exploited and unexploited areas. The sonographs also revealed a plethora of bedforms and acoustically distinct substrates that will go a long way in determining the hydraulic interactions on the seabed.

Samples and Records

Station	Latitude	Longitude	Depth (m)	Remarks
Y1	41o47.13'S	175o25.10E	1050	Gas plume off Cape Palliser; 15 bottom photos
Y2	42o56.68'S	177o33.37W	595	North side, central Chatham Rise; Multicorer; 0.105m foram sand

Y3	42o56.69'S	177o33.43'W	595	North side, central Chatham Rise; 3 Kasten attempts; no sample.
Y4	42o05.00'S	172o39.14'W	2405	Eastern Chatham Rise in apron drift; Kasten, 2.70m foram. mud; Stg 1-5?
Y5	41o09.14'S	170o37.53'W	4073	Deep apron drift N.Chatham Rise;3 Kasten attempts; 0.3m foram. mud
Y6	44o33.16'S	173o18.75'W	3678	Deep terrace drift, S Chatham Rise, Kasten, 3.15m foram mud; Stg 1-5?
Y7	46o36.56'S	177o23.78'W	4452	Bounty N levee; Kasten; only sample (hemipelagite) in core head.
Y8	46o58.25'S	178o39.40'W	3751	Terrace south Bounty Trough; Kasten 3.43 m alternate pelagite/hemipelagite; Stg 1-8?
Y9	48o14.21'S	177o20.67'E	1267	Campbell Plateau; Kasten, 3.13m alternate biopelagite/foram mud; Stg 1-7?
Y10	48o14.42'S	177o21.01'E	1265	Campbell Plateau; Multicorer; 6 cm pelagite with surface water.
Y11	50o51.21'S	177o04.82'E	4527	Campbell Drift; Kasten; 1.94 m muddy sand (foram, qz/feld, Mn nod.
Y12	50o04.16'S	173o22.67'E	548	E.Campbell Plateau; Kasten, 0.6m calcareous biopelagic mud.
Y13	50o11.87'S	173o12.44'E	550	E. Campbell Plateau, Kasten 0.74m (tot) brown biopelagite above white ooze.

Y14	51o20.11'S	171o54.20'E	523	S. Campbell Plateau; Kasten, biopelagite.
Y15	52o43.33'S	167o40.23'E	990	S.Campbell Plateau; Kasten, biopelagite
Y16	50o35.43"S	169o45.33'E	600	W. Campbell Plateau; Kasten, 2.99m (tot) br. biopelagite, gr. foram mud, white ooze.
Y17	48o23.31"S	169o31.73'E	691	W. Campbell Plateau, Kasten, 2.25 m (tot) br. biopelagite, gr. foram. mud, white ooze.

Records

3.5kHz Lines 1 - 25
12.kHz Lines 1 - 25
Multichannel seismic Lines 4, 7, 12, 16, 17, 18, 21.
Side-scan sonar lines (Foveaux Strait) 1- 8

Core Y16

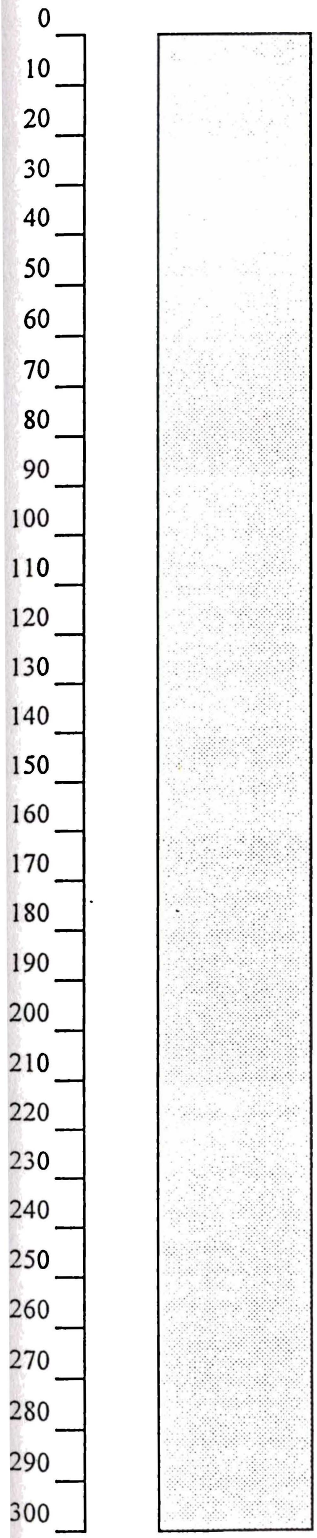

0-4 cm 5Y 8/2 white foram mud, oxidised, sloppy

4-25 cm 5Y 8/1 white (grey hue) foram mud, firm, minor bioturbation blebs

25-43 cm 5Y 7/1 light grey foram mud, significant bioturbation blebs and mottles, pyrite blebs and streaks

43-67 cm N 8/1 white (grey hue) foram mud, bioturbation blebs ~ 10% especially at top and base of unit, pyrite blebs and streaks

67-173 cm N 8/1 white foram mud ? siliceous component, minor bioturbation at top and base of unit, pyrite blebs and streaks especially at 110-120, 140, 158 cm

173-208 cm N 8/1 whote (grey hue) foram mud bioturbation blebs ~15% especially at base

203 cm large planolites-like burrow of N8/1 white

208-235 cm 5Y 7/2 light grey (green hue) foram mud, bioturbation blebs ~20%, pyrite blebs and streaks

209, 217 cm planolites-like burrows of N 8/1 white

235-289 cm N 8/1 white (grey hue) foram mud, bioturbation blebs ~20% at top and base of units, pyrite blebs and streaks

283 cm bioturbation blebs N8/1 white

end of core 289 cm

end of catcher 299 cm

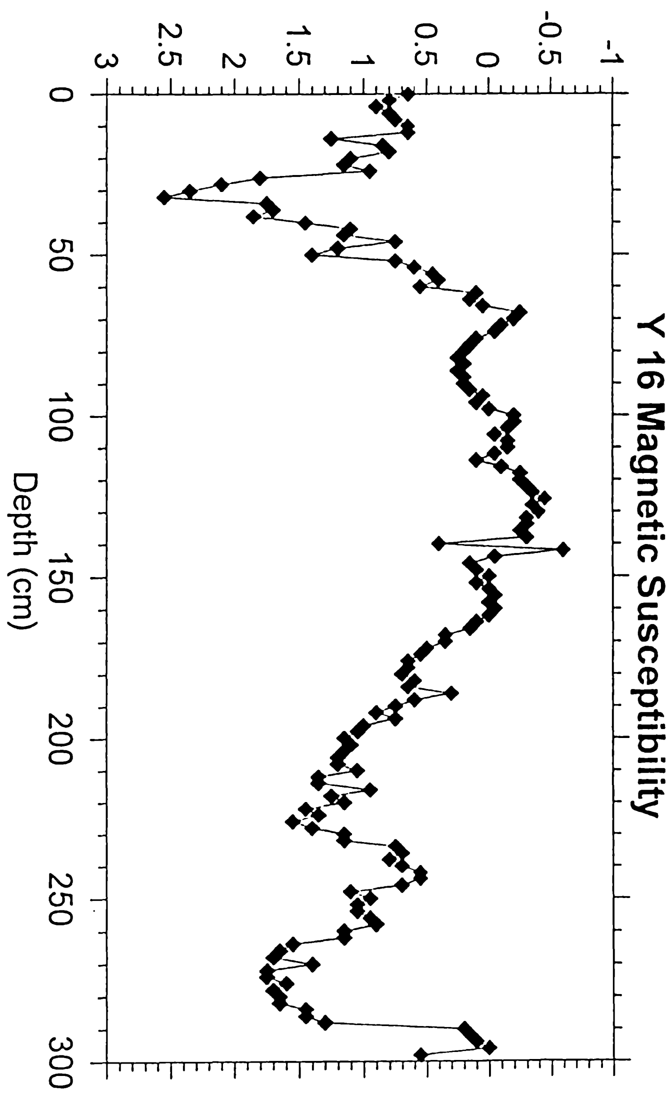
Y 16 Magnetic Susceptibility
Depth (cm)
0
50
100
150
200
250
300
-1
-0.5
0
0.5
1
1.5
2
2.5
3

Appendix 2

Sieving and $CaCO_3$ Data NZSSO Cores

Depth	wt total	wt mud	wt cS	wt fS	%cS	%fS	%M	%CaCO3
36-42								
0	1.018	1.480	1.341	1.267	32.80	30.99	36.20	86.69
10	1.018	1.275	1.701	1.183	40.90	28.44	30.66	86.67
20	1.007	1.913	1.543	1.377	31.93	28.50	39.58	90.38
30	1.007	2.720	1.319	1.421	24.16	26.03	49.82	95.61
40	1.040	2.890	1.352	1.185	24.91	21.84	53.25	93.12
50	1.054	2.555	1.315	1.295	25.46	25.07	49.47	94.78
60	1.007	1.725	1.213	1.220	29.17	29.34	41.49	94.32
70	0.990	1.763	1.427	1.387	31.18	30.31	38.51	92.38
80	1.019	1.613	1.349	1.369	31.15	31.61	37.24	89.51
90	1.006	1.540	1.643	1.361	36.16	29.95	33.89	93.17
100	0.999	1.575	1.633	1.664	33.52	34.15	32.33	91.67
36-41								
0	1.016	0.595	2.587	0.596	68.48	15.78	15.75	97.00
10	0.974	0.525	2.509	0.578	69.46	16.00	14.54	99.50
20	1.024	1.235	2.281	0.859	52.50	19.08	28.42	99.80
30	1.032	2.625	1.848	1.105	33.13	19.81	47.06	96.16
40	1.018	1.295	2.331	0.910	51.39	20.06	28.55	99.80
50	0.995	1.785	2.250	0.912	45.48	18.43	36.08	99.80
60	0.996	1.890	2.111	1.239	40.29	23.65	36.07	96.28
70	1.009	3.788	2.472	1.031	33.91	14.14	51.95	94.15
80	0.970	1.050	2.249	0.881	53.80	21.08	25.12	99.80
90	0.989	1.350	2.215	0.876	49.88	19.73	30.40	96.79
100	0.992	0.525	2.629	0.449	72.97	12.46	14.57	98.56
16-9								
10	1.026	0.585	1.683	0.611	58.46	21.22	20.32	86.83
20	1.075	2.375	0.299	0.123	10.69	4.40	84.91	91.27
30	1.052	1.760	0.921	0.366	30.23	12.01	57.76	97.03
40	1.008	1.435	1.056	0.435	36.09	14.87	49.04	98.90
50	1.051	1.645	1.304	0.501	37.80	14.52	47.68	97.56
60	1.037	1.330	1.093	0.439	38.19	15.34	46.47	96.77
70	1.071	1.100	1.216	0.561	42.27	19.50	38.23	99.88
80	1.050	1.170	1.281	0.543	42.79	18.14	39.08	99.90
90	1.043	1.505	0.894	0.639	29.43	21.03	49.54	96.66
100	1.041	1.105	1.287	0.708	41.52	22.84	35.65	96.08
36-40								
0	1.011	0.375	1.943	0.959	59.29	29.27	11.44	93.26
10	0.972	0.300	2.082	1.161	58.76	32.77	8.47	97.08
20	0.953	0.275	2.369	1.018	64.69	27.80	7.51	97.69
30	0.993	0.125	2.440	0.851	71.43	24.91	3.66	95.17
40	0.994	0.200	2.988	0.960	72.04	23.14	4.82	97.72
50	0.963	0.250	1.943	0.967	61.49	30.60	7.91	97.81
60	1.000	0.325	1.862	1.220	54.65	35.81	9.54	96.59
70	0.995	0.475	1.992	1.104	55.78	30.92	13.30	98.32
80	0.955	0.250	3.163	0.537	80.08	13.60	6.33	99.12
90	0.965	0.150	3.169	0.526	82.42	13.68	3.90	99.80
100	0.944	0.175	3.102	0.486	82.43	12.92	4.65	99.80

Depth	wt total	wt mud	wt cS	wt fS	%cS	%fS	%M	%CaCO3
34 -1								
0	1.011	0.070	2.732	0.609	80.09	17.85	2.05	93.41
10	1.007	0.130	2.754	0.419	83.38	12.69	3.94	96.12
20	1.029	0.675	2.893	0.608	69.28	14.56	16.16	92.73
30	1.016	0.490	2.974	0.403	76.91	10.42	12.67	92.63
40	1.029	0.595	2.846	0.596	70.50	14.76	14.74	94.69
50	1.006	0.595	2.740	0.824	65.88	19.81	14.31	93.33
60	0.996	0.293	2.784	0.818	71.49	21.00	7.51	94.87
70	1.030	0.330	2.361	0.778	68.06	22.43	9.51	96.14
80	1.030	0.315	2.486	0.893	67.30	24.17	8.53	97.24
90	1.034	0.563	2.303	0.948	60.39	24.86	14.75	94.35
100	1.000	0.425	2.025	1.069	57.55	30.38	12.08	97.38
36 -39								
3	1.010	3.200	0.485	0.679	11.11	15.56	73.33	95.24
10	1.046	3.575	0.284	0.479	6.55	11.04	82.41	98.87
20	1.056	3.088	0.474	0.932	10.55	20.74	68.71	95.83
30	1.026	2.763	0.374	0.899	9.27	22.28	68.46	95.76
40	1.011	2.200	0.542	0.701	15.74	20.36	63.90	97.25
16 - 8								
10	1.036	2.300	0.276	0.464	9.08	15.26	75.66	3.75
20	1.030	2.375	0.441	0.736	12.42	20.72	66.86	0.24
30	1.053	2.125	0.367	0.495	12.29	16.57	71.14	0.05
40	1.060	1.920	1.466	0.451	38.21	11.75	50.04	0.25
50	1.057	2.400	0.852	0.452	23.00	12.20	64.80	0.47
60	1.043	2.200	1.060	0.379	29.13	10.42	60.46	0.96
70	1.040	1.615	0.911	0.311	32.11	10.96	56.93	0.15
80	1.043	1.445	1.134	0.333	38.94	11.44	49.62	0.43
90	1.042	2.200	0.944	0.310	27.33	8.98	63.69	0.35
100	1.023	2.253	0.652	0.443	19.48	13.23	67.29	0.25
36 - 38								
0	1.084	2.663	0.107	0.459	3.31	14.21	82.47	13.82
10	1.103	2.520	0.034	0.306	1.19	10.70	88.11	10.40
20	1.059	2.625	0.049	0.558	1.52	17.26	81.22	11.55
30	1.088	2.835	0.086	0.728	2.36	19.95	77.69	13.94
40	1.079	2.850	0.098	0.828	2.60	21.93	75.48	13.31
50	1.094	3.000	0.088	0.772	2.28	20.00	77.72	15.80
60	1.061	1.890	0.057	0.492	2.34	20.17	77.49	15.33
70	1.069	2.063	0.113	0.661	3.98	23.30	72.72	18.22
80	1.047	2.438	0.121	0.888	3.51	25.76	70.73	18.20
90	1.037	2.738	0.061	0.673	1.76	19.38	78.86	17.23

Depth	wt total	wt mud	wt cS	wt fS	%cS	%fS	%M	%CaCO3
50 - 35								
0	1.018	2.593	0.957	1.018	20.95	22.29	56.76	0.60
10	1.028	3.113	0.945	1.028	18.58	20.21	61.20	0.08
20	1.021	2.840	0.950	1.021	19.75	21.22	59.03	0.48
30	1.047	2.765	0.968	1.047	20.25	21.90	57.85	0.50
40	1.032	2.848	0.965	1.032	19.92	21.30	58.78	0.80
50	1.033	3.443	0.952	1.033	17.54	19.03	63.43	0.48
60	1.055	3.600	0.965	1.055	17.17	18.77	64.06	0.32
70	1.066	3.360	0.982	1.066	18.16	19.71	62.13	0.59
80	1.045	3.160	0.966	1.045	18.68	20.21	61.11	0.06
90	1.067	3.300	0.979	1.067	18.31	19.96	61.73	0.52
100	1.069	2.835	0.988	1.069	20.20	21.85	57.95	0.31
34 - 3								
0	1.043	1.063	0.347	0.284	20.49	16.77	62.74	1.28
10	1.066	1.350	0.448	0.348	20.88	16.22	62.91	1.01
20	1.067	1.750	0.457	0.344	17.92	13.49	68.60	0.55
30	1.055	1.063	0.225	0.197	15.16	13.27	71.57	1.03
40	1.053	1.755	0.488	0.341	18.89	13.20	67.92	0.86
50	1.028	1.305	0.369	0.337	18.35	16.76	64.89	0.64
60	1.041	1.080	0.410	0.334	22.48	18.31	59.21	0.75
70	1.034	0.808	0.292	0.248	21.67	18.40	59.93	0.99
80	1.051	1.318	0.257	0.292	13.77	15.64	70.59	0.56
90	1.018	1.445	0.133	0.188	7.53	10.65	81.82	0.64
100	1.049	1.540	0.203	0.248	10.20	12.46	77.35	0.44
50 - 34								
0	1.029	2.465	0.240	0.376	7.79	12.20	80.01	1.00
10	1.024	2.438	0.641	0.591	17.47	16.11	66.43	0.63
20	1.016	1.760	0.539	0.569	18.79	19.84	61.37	0.40
29	1.033	1.880	0.516	0.476	17.97	16.57	65.46	0.39
40	0.994	1.880	0.403	0.450	14.75	16.47	68.79	0.30
50	0.999	1.980	0.378	0.325	14.09	12.11	73.80	0.41
60	1.023	2.200	0.451	0.411	14.73	13.42	71.85	0.10
70	1.039	2.338	0.303	0.384	10.02	12.70	77.29	0.41
80	1.029	3.038	0.184	0.262	5.28	7.52	87.20	0.43
90	1.027	3.188	0.416	0.261	10.77	6.75	82.48	0.18
100	1.056	4.005	0.097	1.056	1.87	20.47	77.65	0.49
50 - 33								
0	0.968	2.100	0.301	0.227	11.45	8.64	79.91	12.79
10	0.996	2.040	0.474	0.237	17.23	8.62	74.16	1.05
20	1.015	1.665	0.285	0.211	13.19	9.76	77.05	0.76
30	1.006	1.960	1.911	0.327	45.52	7.79	46.69	1.28
40	0.995	1.880	1.096	0.355	32.90	10.66	56.44	0.66
50	1.034	2.040	0.457	0.242	16.69	8.84	74.48	0.75
60	0.990	1.840	0.478	0.243	18.67	9.49	71.85	0.65
70	1.010	2.083	0.236	0.171	9.48	6.87	83.65	0.67
80	1.017	1.828	0.300	0.214	12.81	9.14	78.05	0.59
90	0.985	2.160	0.272	0.188	10.38	7.18	82.44	0.35
100	0.986	1.725	0.247	0.273	11.00	12.16	76.84	0.66

Appendix 3

Resieved Data NZSSO Cores

Depth	wt mud	wt of cS (reseived)	wt of fS (reseived)	%M (reseived)	% cS (reseived)	% fS (reseived)
36-42						
0	1.480					
10	1.275	1.514	1.370	30.66	36.41	32.94
20	1.913	1.315	1.605	39.59	27.21	33.21
30	2.720	1.105	1.635	49.81	20.24	29.95
40	2.890	1.147	1.388	53.28	21.14	25.58
50	2.555	1.109	1.499	49.48	21.49	29.03
60	1.725	1.034	1.397	41.51	24.88	33.62
70	1.763	1.212	1.601	38.52	26.49	34.99
80	1.613	1.173	1.542	37.27	27.09	35.64
90	1.540	1.408	1.593	33.92	31.01	35.08
100	1.575	1.373	1.922	32.34	28.18	39.47
36-41						
0	0.595	1.026	0.680	25.86	44.60	29.54
10	0.525	2.297	0.790	14.53	63.60	21.86
20	1.235	2.033	1.106	28.24	46.49	25.27
30	2.625	1.589	1.360	47.09	28.51	24.40
40	1.295	2.077	1.165	28.55	45.78	25.68
50	1.785	2.022	1.139	36.09	40.88	23.03
60	1.890	1.848	1.504	36.06	35.25	28.69
70	3.788	2.200	1.302	51.96	30.17	17.86
80	1.050	1.989	1.140	25.13	47.60	27.28
90	1.350	2.002	1.087	30.42	45.10	24.48
100	0.525	2.453	0.627	14.56	68.04	17.40
16-9						
10	0.585	0.766	0.686	28.72	37.61	33.67
20	2.375	0.274	0.150	84.86	9.78	5.36
30	1.760	0.852	0.436	57.75	27.95	14.30
40	1.435	0.971	0.519	49.06	33.19	17.76
50	1.645	1.204	0.601	47.68	34.90	17.42
60	1.330	0.989	0.542	46.48	34.57	18.95
70	1.100	1.097	0.680	38.24	38.15	23.62
80	1.170	1.154	0.671	39.07	38.53	22.40
90	1.505	0.781	0.751	49.56	25.72	24.72
100	1.105	1.115	0.881	35.64	35.96	28.41
36-40						
0	0.375	0.721	1.105	17.04	32.75	50.21
10	0.300	1.682	1.561	8.47	47.47	44.06
20	0.275	2.018	1.368	7.51	55.13	37.35
30	0.125	2.105	1.194	3.65	61.48	34.87
40	0.200	2.538	1.409	4.82	61.21	33.97
50	0.250	1.591	1.321	7.91	50.32	41.78
60	0.325	1.458	1.624	9.54	42.79	47.67
70	0.475	1.795	1.301	13.30	50.27	36.42
80	0.250	2.906	0.792	6.33	73.60	20.07
90	0.150	3.002	0.693	3.90	78.07	18.03
100	0.175	2.892	0.696	4.65	76.85	18.50

Depth	wt mud	wt of cS (reseived)	wt of fS (reseived)	%M (reseived)	% cS (reseived)	% fS (reseived)
34 -1						
0	0.070	1.293	0.710	3.38	62.36	34.27
10	0.130	2.622	0.547	3.94	79.48	16.58
20	0.675	2.693	0.805	16.18	64.53	19.30
30	0.490	2.832	0.540	12.69	73.32	13.99
40	0.595	2.683	0.757	14.75	66.48	18.77
50	0.595	2.262	1.129	14.93	56.75	28.33
60	0.293	2.466	1.129	7.53	63.43	29.04
70	0.330	2.080	1.055	9.52	60.02	30.45
80	0.315	2.191	1.182	8.54	59.40	32.05
90	0.563	1.928	1.317	14.79	50.63	34.58
100	0.425	1.742	1.348	12.09	49.55	38.36
36 -39						
3	3.200	0.219	0.718	77.35	5.30	17.36
10	3.575	0.244	0.519	82.41	5.63	11.97
20	3.088	0.410	0.995	68.73	9.13	22.14
30	2.763	0.322	0.952	68.45	7.97	23.58
40	2.200	0.464	0.780	63.88	13.48	22.65
16 - 8						
10	2.300	0.257	0.482	75.70	8.44	15.86
20	2.375	0.426	0.752	66.86	11.98	21.16
30	2.125	0.352	0.508	71.19	11.81	17.01
40	1.920	1.511	0.463	49.31	38.80	11.89
50	2.400	0.839	0.469	64.72	22.63	12.66
60	2.200	1.050	0.393	60.40	28.82	10.78
70	1.615	0.897	0.326	56.92	31.60	11.48
80	1.445	1.122	0.351	49.52	38.44	12.04
90	2.200	0.930	0.329	63.60	26.89	9.50
100	2.253	0.636	0.458	67.32	18.99	13.69
36 - 38						
0	2.663	0.069	0.476	83.01	2.15	14.84
10	2.520	0.028	0.314	88.08	0.96	10.96
20	2.625	0.045	0.573	80.96	1.38	17.66
30	2.835	0.068	0.745	77.70	1.87	20.43
40	2.850	0.070	0.858	75.45	1.84	22.71
50	3.000	0.074	0.789	77.67	1.92	20.42
60	1.890	0.046	0.504	77.47	1.89	20.65
70	2.063	0.096	0.680	72.68	3.39	23.94
80	2.438	0.097	0.914	70.69	2.80	26.51
90	2.738	0.046	0.689	78.85	1.31	19.84

Depth	wt mud	wt of cS (reseived)	wt of fS (reseived)	%M (reseived)	% cS (reseived)	% fS (reseived)
50 - 35						
0	2.593	0.147	1.028	68.81	3.90	27.29
10	3.113	0.168	1.042	72.00	3.89	24.11
20	2.840	0.231	1.039	69.11	5.61	25.28
30	2.765	0.233	1.067	68.01	5.73	26.26
40	2.848	0.130	1.047	70.76	3.23	26.01
50	3.443	0.154	1.047	74.15	3.31	22.55
60	3.600	0.193	1.076	73.95	3.96	22.10
70	3.360	0.091	1.076	74.22	2.01	23.77
80	3.160	0.099	1.061	73.16	2.29	24.55
90	3.300	0.230	1.083	71.54	4.99	23.47
100	2.835	0.109	1.079	70.47	2.72	26.81
34 - 3						
0	1.063	0.338	0.300	62.49	19.88	17.63
10	1.350	0.434	0.370	62.68	20.14	17.18
20	1.750	0.431	0.371	68.58	16.88	14.54
30	1.063	0.219	0.208	71.39	14.67	13.94
40	1.755	0.457	0.373	67.89	17.69	14.42
50	1.305	0.349	0.357	64.89	17.35	17.76
60	1.080	0.387	0.359	59.16	21.21	19.64
70	0.808	0.278	0.263	59.88	20.61	19.51
80	1.318	0.240	0.306	70.75	12.86	16.40
90	1.445	0.123	0.197	81.84	6.98	11.18
100	1.540	0.191	0.260	77.36	9.60	13.05
50 - 34						
0	2.465	0.227	0.390	79.99	7.37	12.65
10	2.438	0.605	0.621	66.55	16.50	16.95
20	1.760	0.509	0.599	61.37	17.74	20.89
29	1.880	0.485	0.505	65.51	16.91	17.58
40	1.880	0.381	0.471	68.81	13.96	17.24
50	1.980	0.360	0.341	73.84	13.43	12.73
60	2.200	0.429	0.432	71.85	14.02	14.12
70	2.338	0.290	0.405	77.10	9.55	13.35
80	3.038	0.174	0.273	87.17	4.99	7.84
90	3.188	0.404	0.273	82.49	10.44	7.07
100	4.005	0.084	1.066	77.71	1.62	20.67
50 - 33						
0	2.100	0.268	0.252	80.16	10.22	9.61
10	2.040	0.445	0.269	74.08	16.17	9.75
20	1.665	0.265	0.232	77.00	12.26	10.74
30	1.960	1.843	0.398	46.66	43.87	9.47
40	1.880	1.042	0.412	56.40	31.26	12.34
50	2.040	0.434	0.267	74.43	15.82	9.75
60	1.840	0.455	0.265	71.86	17.78	10.36
70	2.083	0.222	0.186	83.64	8.89	7.46
80	1.828	0.281	0.233	78.06	11.99	9.95
90	2.160	0.257	0.204	82.43	9.81	7.77
100	1.725	0.231	0.289	76.84	10.31	12.86

Sample	Weight Vial (no lid) (g)	Weight Empty Vial (g)	Weight Sample (g)	Weight of >150 m (g)	Weight Diff (g)
36-41					
0 - 1	11.9186	10.8089	1.1097	1.0260	0.0837
10 - 11	13.3215	10.8124	2.5091	2.2974	0.2117
20 - 21	13.1557	10.8758	2.2799	2.0334	0.2465
30 - 31	12.6271	10.7828	1.8443	1.5892	0.2551
40 - 41	12.9711	10.6395	2.3316	2.0768	0.2548
50 - 51	12.9139	10.6651	2.2488	2.0216	0.2272
60 - 61	12.9591	10.8469	2.1122	1.8475	0.2647
70 - 71	13.2578	10.7871	2.4707	2.1995	0.2712
80 - 81	13.0550	10.8069	2.2481	1.9891	0.2590
90 - 91	12.8818	10.6694	2.2124	2.0017	0.2107
100 - 101	13.5622	10.9315	2.6307	2.4526	0.1781
36-42					
10 - 11	12.6536	10.9526	1.7010	1.5141	0.1869
20 - 21	12.3293	10.7867	1.5426	1.3148	0.2278
30 - 31	12.0033	10.6838	1.3195	1.1053	0.2142
40 - 41	12.2489	10.8997	1.3492	1.1466	0.2026
50 - 51	12.1367	10.8234	1.3133	1.1094	0.2039
60 - 61	11.7598	10.5487	1.2111	1.0339	0.1772
70 - 71	12.2645	10.8382	1.4263	1.2122	0.2141
80 - 81	12.0641	10.7181	1.3460	1.1726	0.1734
90 - 91	12.4257	10.7863	1.6394	1.4078	0.2316
100 - 101	12.3498	10.7191	1.6307	1.3725	0.2582
36-40					
0 - 1	11.7885	10.9223	0.8662	0.7205	0.1457
10 - 11	12.7135	10.6315	2.0820	1.6820	0.4000
20 - 21	12.9753	10.6074	2.3679	2.0184	0.3495
30 - 31	12.9942	10.5464	2.4478	2.1048	0.3430
40 - 41	13.7362	10.7494	2.9868	2.5382	0.4486
50 - 51	12.6465	10.7023	1.9442	1.5906	0.3536
60 - 61	12.4551	10.5929	1.8622	1.4580	0.4042
70 - 71	12.8218	10.8296	1.9922	1.7954	0.1968
80 - 81	14.0066	10.8451	3.1615	2.9062	0.2553
90 - 91	13.8466	10.6777	3.1689	3.0017	0.1672
100 - 101	13.7443	10.6422	3.1021	2.8920	0.2101
36-39					
3 - 4	11.0848	10.8267	0.2581	0.2191	0.0390
10 - 11	11.1331	10.8488	0.2843	0.2441	0.0402
20 - 21	11.1832	10.7102	0.4730	0.4103	0.0627
30 - 31	11.0391	10.6648	0.3743	0.3215	0.0528
40 - 41	11.0619	10.5188	0.5431	0.4641	0.0790

Sample	Weight Vial (no lid) (g)	Weight Empty Vial (g)	Weight Sample (g)	Weight of >150 m (g)	Weight Diff (g)
16 - 9					
10 - 11	11.7839	10.9429	0.8410	0.7662	0.0748
20 - 21	11.0824	10.7818	0.3006	0.2736	0.0270
30 - 31	11.5957	10.6743	0.9214	0.8517	0.0697
40 - 41	11.9605	10.9054	1.0551	0.9707	0.0844
50 - 51	12.0778	10.7737	1.3041	1.2041	0.1000
60 - 61	12.0228	10.9306	1.0922	0.9891	0.1031
70 - 71	11.9094	10.6935	1.2159	1.0974	0.1185
80 - 81	12.1733	10.8917	1.2816	1.1537	0.1279
90 - 91	11.4939	10.6014	0.8925	0.7809	0.1116
100 - 101	11.9891	10.7013	1.2878	1.1150	0.1728
34-3					
0 - 2	11.1907	10.8367	0.3540	0.3381	0.0159
10 - 12	11.0593	10.6036	0.4557	0.4338	0.0219
20 - 21	11.2090	10.7513	0.4577	0.4308	0.0269
30 - 31	10.9960	10.7670	0.2290	0.2185	0.0105
40 - 41	11.2661	10.7771	0.4890	0.4573	0.0317
50 - 51	11.1877	10.8186	0.3691	0.3489	0.0202
60 - 61	11.2534	10.8417	0.4117	0.3872	0.0245
70 - 71	11.2127	10.9194	0.2933	0.2781	0.0152
80 - 81	10.8700	10.6170	0.2530	0.2395	0.0135
90 - 91	10.8767	10.7441	0.1326	0.1232	0.0094
100 - 101	10.8532	10.6504	0.2028	0.1911	0.0117
50-35					
0 - 2	10.9149	10.7575	0.1574	0.1471	0.0103
10 - 11	10.7614	10.5789	0.1825	0.1683	0.0142
20 - 21	11.0100	10.7615	0.2485	0.2306	0.0179
30 - 31	11.0825	10.8290	0.2535	0.2331	0.0204
40 - 41	11.0534	10.9085	0.1449	0.1300	0.0149
50 - 51	10.9824	10.8149	0.1675	0.1536	0.0139
60 - 61	10.8054	10.5920	0.2134	0.1926	0.0208
70 - 71	10.9122	10.8111	0.1011	0.0911	0.0100
80 - 81	10.9710	10.8565	0.1145	0.0989	0.0156
90 - 91	10.9979	10.7521	0.2458	0.2303	0.0155
100 - 101	10.6622	10.5430	0.1192	0.1094	0.0098
16-8					
10 - 11	11.0117	10.7372	0.2745	0.2565	0.0180
20 - 21	11.1689	10.7276	0.4413	0.4255	0.0158
30 - 31	11.0613	10.6962	0.3651	0.3524	0.0127
40 - 41	12.3934	10.8710	1.5224	1.5106	0.0118
50 - 51	11.5917	10.7353	0.8564	0.8391	0.0173
60 - 61	11.8253	10.7618	1.0635	1.0499	0.0136
70 - 71	11.7106	10.7993	0.9113	0.8966	0.0147
80 - 81	11.8908	10.7508	1.1400	1.1218	0.0182
90 - 91	11.5986	10.6497	0.9489	0.9302	0.0187
100 - 101	11.4832	10.8325	0.6507	0.6356	0.0151

Sample	Weight Vial (no lid) (g)	Weight Empty Vial (g)	Weight Sample (g)	Weight of >150 m (g)	Weight Diff (g)
36-38					
0 - 1	10.8631	10.7770	0.0861	0.0691	0.0170
10 - 11	10.7196	10.6845	0.0351	0.0275	0.0076
20 - 21	10.6483	10.5890	0.0593	0.0446	0.0147
30 - 31	10.7679	10.6822	0.0857	0.0684	0.0173
40 - 41	10.8718	10.7724	0.0994	0.0696	0.0298
50 - 51	10.6774	10.5868	0.0906	0.0740	0.0166
60 - 61	10.5566	10.4988	0.0578	0.0461	0.0117
70 - 71	10.8912	10.7766	0.1146	0.0961	0.0185
80 - 81	10.9624	10.8393	0.1231	0.0967	0.0264
90 - 91	10.7193	10.6577	0.0616	0.0456	0.0160
34-1					
0 - 1	12.1499	10.7558	1.3941	1.2927	0.1014
10 - 11	13.5532	10.8038	2.7494	2.6215	0.1279
20 - 21	13.6597	10.7699	2.8898	2.6926	0.1972
30 - 31	13.6552	10.6866	2.9686	2.8315	0.1371
40 - 41	13.7441	10.9002	2.8439	2.6826	0.1613
50 - 51	13.1699	10.6024	2.5675	2.2622	0.3053
60 - 61	13.4890	10.7114	2.7776	2.4664	0.3112
70 - 71	13.1257	10.7691	2.3566	2.0795	0.2771
80 - 81	13.0912	10.6117	2.4795	2.1905	0.2890
90 - 91	13.0747	10.7785	2.2962	1.9275	0.3687
100 - 101	12.6791	10.6584	2.0207	1.7415	0.2792
50-33					
0 - 2	11.1769	10.8843	0.2926	0.2678	0.0248
10 - 11	11.4208	10.9439	0.4769	0.4453	0.0316
20 - 21	10.9733	10.6870	0.2863	0.2651	0.0212
30 - 31	12.6631	10.7498	1.9133	1.8426	0.0707
40 - 41	11.7009	10.6024	1.0985	1.0420	0.0565
50 - 51	11.3526	10.8939	0.4587	0.4336	0.0251
60 - 61	11.4320	10.9545	0.4775	0.4553	0.0222
70 - 71	11.0320	10.7957	0.2363	0.2215	0.0148
80 - 81	11.2012	10.9014	0.2998	0.2808	0.0190
90 - 91	11.0682	10.7957	0.2725	0.2570	0.0155
100 - 101	11.0054	10.7584	0.2470	0.2314	0.0156
50-34					
0 - 2	10.8615	10.6207	0.2408	0.2271	0.0137
10 - 11	11.1240	10.4894	0.6346	0.6046	0.0300
20 - 21	11.2230	10.6841	0.5389	0.5089	0.0300
29 - 31	11.1123	10.5984	0.5139	0.4853	0.0286
40 - 42	11.1801	10.7779	0.4022	0.3813	0.0209
50 - 52	11.0837	10.7073	0.3764	0.3601	0.0163
60 - 61	11.2779	10.8271	0.4508	0.4294	0.0214
70 - 71	11.1098	10.7994	0.3104	0.2895	0.0209
80 - 82	10.8976	10.7124	0.1852	0.1739	0.0113
90 - 92	11.3340	10.9181	0.4159	0.4036	0.0123
100 - 102	10.7166	10.6235	0.0931	0.0835	0.0096

Appendix 4

Other Regional Core Descriptions

Core	Reference	Location	Depth (m)	Lithostratigraphy	Remarks
Elt 25-11	Goodell, (1968) Margolis & Kennett, (1971)	50°02'S, 127°38'W	3949	Lt grey foraminiferal ooze	Quartz ~25% @ 0 cm drops to ~ 15% @ 65 cm, rapidly increasing to 75% @ 1 m. N. pachyderma ~60% @ core top to ~35% @ 30 cm, rising to ~55% @ 60 cm and continuing down core at this value. A few manganese micronodules present.
Elt 52-12	Florida State University, (1973) ODP Proposal 441, (1997)	51°37.2'S, 175°08.5'E	1348	Lt grey foraminiferal ooze	Glauconite present.
Elt 43-6	Florida State University, (1973) ODP Proposal 441, (1997)	50°29.4'S, 176°18.6'E	2955	Lt grey to greyish olive ooze, sand > radiolaria > sponge spicules	Heavy minerals, mottling and laminated colour banding.
Elt 16-1	Goodell & Watkins, (1968) Goodell, (1968)	44°12'S, 162°01'E	4755	0-5 cm grey clayey silt 5-21 cm greenish grey fine sand 21-35 cm grey clayey silt 35-78 cm greenish grey silty clay 78cm -> olive grey clay	Gradational lower boundary. Gradational lower boundary. sharp lower boundary.
Elt 16-2	Goodell & Watkins, (1968) Goodell, (1968)	47°08'S, 162°07'E	4466	0-3 cm greyish yellow brown fine silt 3 cm -> grey fine silt	Diatomaceous. minor foraminifera abundances.
Elt 16-4	Goodell & Watkins, (1968) Goodell, 1968	55°36'S, 162°12'E	4151	0-6 cm grey sand, foraminifera 6 cm -> dull reddish brown clayey silt	Pebbles at 4 & 10 cm Diatoms.
Elt 16-6	Goodell & Watkins, (1968) Goodell, (1968)	58°59'S, 161°55'E	4636	0-32 cm greyish brown ooze, diatoms 32-62 cm dk reddish brown ooze, diatoms 62-74 cm lt grey ooze, diatoms 74 cm -> dk reddish brown ooze, diatoms	Mottled. Burrows, mottled. Burrows. Burrows, mottling.
Elt 36-36	Watkins & Kennett, (1972) Florida State University, (1971)	60°23.3'S, 157°32.0'E	2816	0-67 cm ooze sponge spicules > diatoms > foraminifera > radiolaria 67-81 cm ooze sponge spicules > diatoms > diatoms > radiolaria 81 cm --> olive yellow ooze foraminifera > radiolaria > diatoms > sponge spicules	Mottling between dull yellowish brown and dull yellow orange. Sharp base bounds the unit. Mottling between dull yellowish brown and brownish black.

Table continues

Elt 36-37	Florida State University, (1971) Watkins & Kennett, (1972)	58°40.0'S, 159°31.0'E	3877	0-47 cm greyish olive sand, foraminifera > radiolaria 47-86 cm olive mud, radiolaria > sandy 86 cm --> greyish olive mud, radiolaria > sand > diatoms	Ice-rafted pebbles, manganese nodules, bounded by sharp base. Manganese nodules.
Elt 27-22	Florida State University, (1971) Watkins & Kennett, (1972)	64°58.2'S, 160°37.4'E	2944	Dull yellowish brown foraminiferal ooze	Manganese present 0-3 cm.
DSDP 276	Init Rep DSDP Vol. 29	50°48.11'S, 176°48.40'E	4671	Detrital gravelly-sandy silty	Manganese and glauconite bearing.
DSDP 277	Init Rep DSDP Vol. 29	52°13.43'S, 166°11.48'E	1214	Foraminiferal ooze, abundant nannofossils	Mottling between lt grey (10%) and white. Unit contains glauconite.
DSDP 278	Init Rep DSDP Vol. 29	56°33.42'S, 160°04.29'E	3675	Greyish yellow foram bearing, radiolarian, diatom ooze	Increase in detritals amd mica down core.
Y11 SWPAC 7B	ODP Proposal 441	50°51.21'S, 177°04.82'E	4527	0-37 cm dull yellowish brown sandy mud, foraminifera rich 37-45 cm pale brown sandy mud 45-52 cm dk brown sandy mud 52 cm --> pale brown sandy mud	Stage 1. Manganese sand grains. Mottled lt brown to dk brown and lt olive green (~20%). Bounded at base by a gradational boundary, marked by colour change Stage 2. Bioturbation blebs ~10%. Manganese grains At base a gradational boundary marked by a colour change. Stage 3/4. Bioturbation blebs and manganese grains ~30%. At a gradational boundary marked by color change. Stage 5. ~10% bioturbation blebs and manganese sandy mottles~40%, increase in Mn grains @ 80-91 cm.
Y12 SWPAC 6B	ODP Proposal 441	50°04.16'S, 173°24.67'E	548	0-24 cm white foraminiferal mud 24-40 cm lt yellow foraminiferal mud 40-60 cm white ooze, possible siliceous components.	Stage 1. Bioturbation ~5%, some shell hash. Gradational boundary marked by colour change. Some bioturbation blebs, shell hash. Brachiopods in situ @ 25 cm. Stage 2 at top of unit stages 3/4 at base. Stage 5. Bioturbation blebs.

Appendix 5

Census Data, Coarse Sand Fraction (> 150 μm)

Planktonic Foraminifera	**Core 36-42**									
	10-11	**20-21**	**30-31**	**40-41**	**50-51**	**60-61**	**70-71**	**80-81**	**90-91**	**100**
Globigerina spp.	50	23	54	22	32	24	30	40	23	19
Globigerina bulloides	122	144	112	182	81	142	84	111	118	110
Globogerinita spp.	7	6	7	13	10	12	6	8	3	10
Globorotalia cf. scitula	3			3	2	2	5	4		
Globorotalia inflata	21	34	16	45	24	30	22	25	17	23
Globorotalia spp.		1			2	1				1
Globorotalia truncatulinoides	8	9	5	18	5	6	2	5	4	5
Globigerina quinqueloba	30	69	67	95	73	84	63	80	59	70
Neogloboquadrina dutertrei			1	2	6	2	3	3	2	1
N. pachyderma (d)	6	9	5	9	4	14	8	20	7	5
N. pachyderma (s)	33	59	39	54	29	60	41	64	69	47
Orbulina universa					1			3	1	
Unknown spp.			1	1						
Total Planktics	280	354	307	444	269	377	264	363	303	291
Benthonic Foraminifera										
Angulogerina spp.						1				
Anomalinoides spp.	1						1			
Biloculina spp.					2	1				
Bolivina spp.								1		
Bulimina aculeata					1		1	1		
Bulimina spp.									2	2
Cassidulina neocarinata			1		1					
Cibicidoides wuellstorfi			1						2	2
Cibicides spp.	4		3	4	2	1	2	1	4	1
Eggerella bradyi			1	1						
Epistominella exigua	1			2	2	2				1
Epistominella spp.			1							
Eu Uvigerina cf. peregrina	3									1
Eu Uvigerina cf. pliozea	1	4					1			
Eu Uvigerina spp.		1	1			2	1			
Fissurina spp.	1	1			3		1	2		
Globocassidulina carinata									1	
Globocassidulina subglobosa	12	12	6	1	4	1	6	3	5	
Gyroidina neosolandii						1	5			1
Gyroidinoides spp.					4					
Gyroidinoides zealandicus	1						1			
Lagena spp.		1					1			
Oolina spp.	1									
Oridulsalis spp.									1	
Oridulsalis umbonatas			1							
Planulina cf. wuellerstorfi		1						2		
Planulinoides spp.							1			
Pyrgo spp.				1					1	
Siphotextularia spp.				1	2	2		2	1	
Spheroidina bulloides		2	1	3	2	3				
Textularia spp.					1					
Trifarina spp.							1			
Unknown spp.		2		1		1		1		1
Total Benthics	25	24	16	14	24	14	22	13	17	9
Others										
Terrigenous		2	1				1			1
Calcic fragments	131	154	103	124	100	135	120	140	165	124
Sponge spicules						1	1	1		
Echinoderm spines		2		1	1	1		5	3	2
Aggregates		2				3				
Glauconite pellets		4	2	3		3		3	4	
Total Mounted	436	542	429	586	394	535	408	525	492	427
N. Pachyderma (s) %	84.62	86.76	88.64	85.71	87.88	81.08	83.67	76.19	90.79	90.38
Benthics %	8.20	6.35	4.95	3.06	8.19	3.58	7.69	3.46	5.31	3.00
Terrigenous %	0.00	0.37	0.23	0.00	0.00	0.00	0.25	0.00	0.00	0.23
Total Fragmentation %	5.10	4.85	3.83	3.27	4.09	4.14	4.98	4.45	6.06	4.91
Planktic %	91.80	93.65	95.05	96.94	91.81	96.42	92.31	96.54	94.69	97.00

Planktonic Foraminifera	**Core 36-41**					
	0-1	**20-21**	**40-41**	**60-61**	**80-81**	**100-101**
Globigerina spp.	3	4	7	8	4	3
Globigerinita spp.	10	15	13	18	10	5
Globigerina bulloides	180	146	100	128	91	109
Globorotalia cf. scitula	2	1		1	1	
Globorotalia inflata	28	24	19	30	15	30
Globorotalia truncatulinoides	15	6	3	5	2	
Globigerina quinqueloba	18	41	23	24	25	13
Neogloboquadrina dutertrei	1	1	2		1	
N. pachyderma (d)	17	22	7	17	21	16
N. pachyderma (s)	186	184	102	152	98	86
Unknown sp.		1	2		1	
Aberant sp.				1		
Total Planktics	460	445	278	384	269	262
Benthonic Foraminifera						
Angulogerina angulosa		1				
Astrononion spp.	2	1				
Cibicides spp.		1				
Ehrenbergina spp.	2			4		
Ehrenbergina trigona			1			
Epistominella exigua				2		
Eu Uvigerina spp.						1
Gyroidinoides spp.						1
Gyroidinoides zealandicus		1				
Largena spp.	1	1				
Nodosaria spp.	1					
Oridulsalis spp.			1			
Oridulsalis umbonatas	1					
Spheroidina bulloides			1			
Trifarina spp.	1					
Total Benthic	8	5	3	6	0	2
Others						
Calcic fragments	131	88	59	63	40	74
Echinoderm spines					1	2
Glauconite pellets	1					1
Ostocods		1				
Total Mounted	600	539	340	453	310	341
N. pachyderma (s) %	91.63	89.32	93.58	89.94	82.35	84.31
Benthics %	1.71	1.11	1.07	1.54	0.00	0.76
Planktic %	98.29	98.89	98.93	98.46	100.00	99.24
Total fragmentation %	3.38	2.39	2.56	1.98	1.82	3.39

Planktonic Foraminifera	**Core 16-9**				
	10-11	**30-31**	**50-51**	**70-71**	**90-91**
Globigerina spp.	17	17	10	17	19
Globigerina bulloides	100	183	114	140	77
Globogerinita spp.	8	5	10	12	11
Globorotalia cf. scitula		1			2
Globorotalia inflata	11	25	20	35	31
Globorotalia truncatulinoides		11	6	11	4
Globigerina quinqueloba	28	27	26	24	19
Neogloboquadrina pachyderma (d)	5	5	6	8	25
Neogloboquadrina pachyderma (s)	150	84	51	105	75
Orbulina universa					1
Unknown sp					1
Aberant sp.				1	
Total Planktic	319	358	243	353	265
Benthonic Foraminifera					
Astrononion spp.				1	
Biloculina spp.			1		
Cassidulina neocarinata	1				
Cibicidoides wuellstorfi	1			1	
Eggerella bradyi	1				
Ehrenbergina spp.				1	
Epistominella exigua		1	1		
Eu Uvigerina spp.		1			1
Gyroidina neosolandii		1			1
Pullenia spp.			1		
Trifarina spp.	2				
Total Benthic	5	3	3	3	2
Others					
Terrigenous		1			
Calcic fragments	133	73	96	73	60
Echinoderm spines	1				
Glauconite pellets					1
Total Mounted	458	435	342	429	328
N. pachyderma (s) %	96.77	94.38	89.47	92.92	75.00
Benthics %	1.54	0.83	1.22	0.84	0.75
Planktics %	98.46	99.17	98.78	99.16	99.25
Terrigenous %	0.00	0.23	0.00	0.00	0.00
Total fragmentation %	4.88	2.47	4.65	2.50	2.73

Planktonic Foraminifera	**Core 36-40**					
	0-1	**20-21**	**40-41**	**60-61**	**80-81**	**100-101**
Globigerina spp.	15	21	16	21	1	
Globigerina bulloides	61	62	90	49	85	100
Globogerinita spp.	20	15	8	10	5	4
Globorotalia cf. scitula			1	1		
Globorotalia inflata	13	7	12	11	16	37
Globorotalia spp.			1	1		1
Globorotalia truncatulinoides	2	5	4	3	5	5
Globigerina quinqueloba	84	77	44	63	29	27
N. pachyderma (d)	14	13	15	18	3	8
N. pachyderma (s)	126	148	161	105	78	115
Unknown sp	1	1		1	1	1
Aberant sp.						3
Total Planktics	336	349	352	283	223	301
Benthonic Foraminifera						
Astrononion spp.			1			
Anomalinoides spp.		1				
Biloculina spp.						1
Cassidulina spp.			1		1	4
Cassidulinoides spp.						2
Eggerella bradyi			1	1		
Ehrenbergina spp.	1		3		4	1
Fissurina spp.			1			
Globocassidulina subglobosa			2		1	3
Planulinoides spp.	1		1			
Pullenia spp.						
Pyrgo spp.			2		1	
Quinqueloculina spp.	1	1		1	1	
Trifarina spp.					1	
Unknown					1	
Total Benthics	3	2	12	2	10	11
Others						
Calcic fragments	110	131	138	119	103	86
Echinoderm spines	1	3		1	3	2
Gastropods	2	1		2		
Worm tubes			3	3	1	
Byrozoa			1	12		5
Total Mounted	452	486	506	422	340	405
N. pachyderma (s) %	90.00	91.93	91.48	85.37	96.30	93.50
Benthics %	0.88	0.57	3.30	0.70	4.29	3.53
Planktic %	99.12	99.43	96.70	99.30	95.71	96.47
Total fragmentation %	3.90	4.46	4.52	4.96	5.24	3.33

Planktonic Foraminifera	**Core 34-1**										
	0	**10**	**20**	**30**	**40**	**50**	**60**	**70**	**80**	**90**	**100**
Globigerina spp.	5	7	5	6	7	25	11	24	25	22	19
Globigerina bulloides	101	183	145	198	102	109	84	81	88	110	94
Globogerinita spp.	6	6	2	12	4	10	7	18	13	9	12
Globorotalia cf. scitula		2		1		2	1	1	1	1	2
Globorotalia inflata	10	19	32	31	14	19	7	16	11	20	18
Globorotalia spp.	1	1		1	1						1
Gr. truncatulinoides		5	3	7	4	1		2	2	3	1
Globigerina quinqueloba	27	58	9	61	26	107	28	119	35	117	50
N. pachyderma (d)	4		2	1		3	3	2	5	4	7
N. pachyderma (s)	156	89	57	55	60	108	137	114	162	87	201
Neogloboquadrina spp.	10	7	6	1	6	21	11	9	14	14	18
Unknown sp	4										
Aberant sp.					1						2
Total Planktics	324	377	261	374	225	405	289	386	356	387	425
Benthonic Foraminifera											
Angulogerina spp.		2						1			
Biloculina spp.							1			1	
Bulimina aculeata									1	1	1
Cassidulina spp.	1										
Cibicidoides wuellstorfi							1				
Eggerella bradyi							1				
Ehrenbergina cf. pacifica											1
Epistominella exigua				1	1						1
Eu Uvigerina spp.					1						
G. subglobosa		1									
Gyroidina neosolandii					1						
Largena spp.									1		1
Planulina cf. wuellerstorfi		1									
Pullenia spp.											1
Pyrgo spp.						1					
Unknown	2							1		1	
Total Benthics	3	4	0	1	3	1	3	2	2	3	5
Radiolaria											
Lithelius minor	1										
Total Radiolaria	1	0	0	0	0	0	0		0	0	0
Others											
Calcic fragments	80	120	104	88	72	72	136	126	99	120	160
Echinoderm spines	1	1	1					1			
Aggregates					1						
Glauconite pellets					1			1		1	
Worm tubes								1			
Total Mounted	409	502	366	463	302	478	428	517	457	511	590
N. pachyderma (s %)	97.5	100.0	96.6	98.2	100.0	97.3	97.9	98.3	97.0	95.6	96.6
Benthics %	0.9	1.0	0.0	0.3	1.3	0.2	1.0	0.5	0.6	0.8	1.2
Terrigenous %	0.0	0.0	0.0	0.0	0.0	0.0	0.0	0.0	0.0	0.0	0.0
Fragmentation %	3.0	3.8	4.7	2.8	3.8	2.2	5.5	3.9	3.3	3.7	4.4
Planktics %	98.8	99.0	100.0	99.7	98.7	99.8	99.0	99.5	99.4	99.2	98.8
Radiolaria %	0.3	0.0	0.0	0.0	0.0	0.0	0.0	0.0	0.0	0.0	0.0

Planktonic Foraminifera	**Core 36-39**		
	3-4	**20-21**	**40-41**
Globigerina spp.	13	17	9
Globigerina bulloides	92	100	84
Globogerinita spp.	23	48	26
Globorotalia cf. scitula	1		
Globorotalia inflata	46	120	50
Globorotalia spp.	1	1	5
Globorotalia truncatulinoides	8	9	4
Globigerina quinqueloba	17	20	41
Neogloboquadrina pachyderma (d)	12	28	26
Neogloboquadrina pachyderma (s)	174	83	138
Unknown sp	1		
Total Planktics	388	426	383
Benthonic Foraminifera			
Biloculina spp.	1		
Ehrenbergina spp.			1
Epistominella exigua		1	
Globocassidulina subglobosa	1	2	
Gyroidinoides zealandicus			1
Oridulsalis spp.		1	
Spiroloculina spp.			1
Unknown		1	
Total Benthics	2	5	3
Radiolaria			
Actinomma spp.	1		
Antarctissa spp.			1
Total Radiolaria	1	0	1
Others			
Terrigenous	3	1	6
Calcic fragments	216	165	50
Aggregates		2	
Total Mounted	610	599	443
N. pachyderma (s) %	93.55	74.77	84.15
Benthics %	0.51	1.16	0.78
Planktic %	99.23	98.84	98.97
Radiolaria %	0.26	0.00	0.26
Terrigenous %	0.49	0.17	1.35
Fragmentation (c) %	6.47	4.57	1.59
Total fragmentation %	6.46	4.57	1.59

Planktonic Foraminifera			**Core 16-8**		
	10-11	**30-31**	**50-51**	**70-71**	**90-91**
Globigerina spp.	2				
Globorotalia inflata	7				
Globorotalia spp.					1
Neogloboquadrina pachyderma (s)			2		
Total Planktics	9	0	2	0	1
Benthonic Foraminifera					
Cibicides spp.	11				
Fissurina annectens	2				
Oridulsalis umbonatas	3				
Total Benthics	16	0	0	0	0
Radiolaria					
Actinomma spp.	27	18	16	14	30
Actinomma antarcticum	16	21	21	18	45
Antarctissa spp.	2	2	2	5	0
Bathrapyramis spp.	0	0	0	1	0
Clathrocyclas bicornis	0	0	0	0	2
Lithelius minor	10	4	2	6	0
Prunopyle spp.	0	2	5	5	14
Spongodiscus spp.	29	29	33	43	9
Spongopyle osculosa	0	1	1	0	1
Stylatractus spp.	1	1	0	1	0
Tetrapyle octacantha	0	0	1	0	1
Total Radiolarian	85	78	81	93	102
Others					
Terrigenous	255	348	225	228	500
Calcic fragments	250	3			
Silicic fragments	37	28	18	41	15
Aggregates		2		2	4
Total Mounted	652	459	326	364	622
N. pachyderma (s) %			100		
Benthics %	14.55	0.00	0.00	0.00	0.00
Planktic %	8.18	0.00	2.41	0.00	0.97
Radiolaria %	77.27	100.00	97.59	100.00	99.03
Terrigenous %	39.11	75.82	69.02	62.64	80.39
Fragmentation (s) %	5.16	4.29	2.70	5.22	1.81
Fragmentation (c) %	55.56	100.00	0.00	0.00	0.00
Total fragmentation %	24.59	4.73	2.64	5.22	1.79

Planktonic Foraminifera	Core 36-38									
	0	**10**	**20**	**30**	**40**	**50**	**60**	**70**	**80**	**90**
Globigerina spp.	2		2	2	4		1	2	3	2
Globigerina bulloides	1	5	5	3					4	2
Globogerinita spp.									1	
Globorotalia inflata		2								
Globorotalia spp.						1				2
Gr. truncatulinoides										1
Globigerina quinqueloba	3	11	6	6			2	6	6	5
Neoglogoquadrina dutertrei		2								
N. pachyderma (d)						1		5	3	3
N. pachyderma (s)	75	33	49	125	103	62	68	113	134	119
Unknown sp									1	1
Aberrant sp.		1								
Total Planktics	81	54	62	136	107	64	71	126	152	135
Benthonic Foraminifera										
Astrononion spp.		1		1		1				
Cyclammina spp.	1									
Epistominella exigua		1				1				
Eponides cf bradyi				1						
Globocassidulina spp.		1								
G. subglobosa	1					2		1		1
Gyroidina neosolandii							1			
Gyroidinoides spp.	1			2	1					
Nonion spp.						1				1
Oolina spp.					1					
Pullenia spp.		1		1	1			2		
Siphotextuluria spp.	1									1
Spiroloculina spp.							1			
Trifarina spp.								1		
Unknown				1	1					2
Total Benthics	4	4	0	6	4	5	2	4	0	5
Radiolaria										
Actinomma spp.	14	13	14	16	14	12	14	11	5	9
Actinomma antarcticum	76	154	123	129	75	143	126	199	63	94
Antarctissa spp.					4					
Bathypyramis spp.		1		1		1	2		1	
Clathrocyclas bicornis	1								1	1
Lithelius minor	6	30	23	29	23	39	35	37	19	41
Lynchnocanium grande					1					
Prunopyle spp.	1	9	8	9	3	9	2	6	10	9
Saturnulus plantetes				1						
Spongodiscus spp.	51	122	125	104	98	122	155	84	53	100
Spongopyle osculosa	7	10	10	7	12	7	8	9	7	4
Stylatractus spp.			1							
Tetrapyle octacantha	2	6	3	4	3	4	4	4	2	5
Unknown		1	1	1	1		4	1	1	1
Total Radiolaria	158	345	307	300	233	337	346	350	161	263
Others										
Terrigenous	18	4	44	71	56	25	26	12	27	32
Calcic fragments	11	10	12	19	12	17	8	17	27	23
Silicic fragments	55	50	105	101	88	70	95	84	42	67
Sponge spicules		4		2		6		1		2
Echinoderm spines								1	1	
Aggregates	6	8	3	8		3	4	4	9	3
Glauconite pellets				1						
Total Mounted	333	480	534	645	501	527	556	600	420	531
N. pachyderma (s) %	100.0	100.0	100.0	100.0	100.0	98.4	100.0	95.8	97.8	97.5
Benthics %	1.65	0.99	0.00	1.36	1.16	1.23	0.48	0.83	0.00	1.24
% Terrigenous	5.41	0.83	8.24	11.01	11.18	4.74	4.68	2.00	6.43	6.03
Fragmentation % (silicic)	4.17	1.78	4.10	4.04	4.51	2.53	3.32	2.91	3.16	3.09
Fragmentation % (calcic)	1.59	2.11	2.36	1.65	1.33	2.99	1.35	1.61	2.17	2.01
Total Fragmentation %	3.28	1.83	3.81	3.28	3.51	2.61	2.98	2.56	2.68	2.72
% Planktic	33.33	13.40	16.80	30.77	31.10	15.76	16.95	26.25	48.56	33.50
% Radiolaria	65.02	85.61	83.20	67.87	67.73	83.00	82.58	72.92	51.44	65.26

Planktonic Foraminifera	**Core 50-35**					
	0-1	**20-21**	**40-41**	**60-61**	**80-81**	**100-101**
Total Planktics	0	0	0	0	0	0
Benthonic Foraminifera						
Total Benthics	0	0	0	0	0	0
Radiolaria						
Actinomma spp.	48	26	30	24	67	50
Actinomma antarcticum	89	185	126	181	94	164
Antarctissa strelkovi	2					
Bathypyramis spp.	2	1			1	
Lithelius minor	10	15	7	3	4	6
Prunopyle spp.	5	49	35	29	23	21
Saturnulus planetes					2	
Spongodiscus spp.	192	65	62	45	32	29
Spongopyle osculosa	7	2	4	2		
Spongotrochus spp.	9					
Stylatractus spp.			1	1		1
Tetrapyle octacantha	2			1	1	
Unknown	1		13	8		8
Total Radiolaria	367	343	278	294	224	279
Others						
Terrigenous	45	59	49	40	32	32
Calcic fragments			1			
Silicic fragments	121	110	107	111	98	60
Sponge spicules	1					
Aggregates			3	7	4	4
Worm tubes						1
Shrimp tail				1		
Total Mounted	534	512	438	453	358	376
Terrigenous %	8.43	11.52	11.19	8.83	8.94	8.51
Total fragmentation %	3.96	3.85	4.59	4.51	5.19	2.62
Radiolaria %	100	100	100	100	100	100

Planktonic Foraminifera	**Core 50-34**										
	0	**10**	**20**	**29**	**40**	**50**	**60**	**70**	**80**	**90**	**100**
Globigerina quinqueloba								1			
Total Planktics	0	0	0	0	0	0	0	1	0	0	0
Benthonic Foraminifera											
Planulinas cf wuellerstorfi										1	
Unknown	1										
Total Benthics	1	0	0	0	0	0	0	0	0	1	0
Radiolaria											
Actinomma spp.	43	10	14	15	23	15	32	3	27	3	54
Actinomma antarcticum	198	190	191	253	155	273	147	302	142	268	131
Antarctissa strelkovi		4									
Bathypyramis spp.				1							
Clathrocyclas bicornis		1			1	2	5	30	23	23	31
Dictyocryne profunda	1										
Lithelius minor	17	12	10	8	1	15	9	2	5	0	2
Phormostichoartus spp.		1									
Plectopyramis spp.											1
Prunopyle spp.	10	30	20	25	17	32	15	25	5	8	17
Saturnulus planetes					3				1		
Spongodiscus spp.	139	89	59	78	34	40	33	18	27	26	62
Spogopyle osculosa	10	2				2		1	1		
Tetrapyle octacantha	1	2	3	4							
Unknown					1				1	1	
Total Radiolaria	419	341	297	384	234	379	241	381	231	328	298
Others											
Terrigenous	44	27	39	27	19	38	25	50	46	69	106
Calcic fragments		1		2		1					
Silicic fragments	126	96	123	172	60	65	63	73	92	165	94
Sponge spicules		1				1					
Echinoderm spines						3					
Aggregates		5		7		4		5	5	12	5
Total Mounted	590	471	459	592	314	491	329	510	375	576	503
% Benthics	0.24	0.00	0.00	0.00	0.00	0.00	0.00	0.00	0.00	0.30	0.00
% Terrigenous	7.46	5.73	8.50	4.56	6.05	7.74	7.60	9.80	12.27	11.98	21.07
Fragmentation % (silicic)	3.62	3.40	4.92	5.30	3.11	2.10	3.16	2.34	4.74	5.92	3.79
Total Fragmentation	3.61	3.43	4.92	5.36	3.11	2.13	3.16	2.33	4.74	5.90	3.79
% *N. pachyderma (s)*	0.00	0.00	0.00	0.00	0.00	0.00	0.00	0.00	0.00	0.00	0.00
% Planktics	0.00	0.00	0.00	0.00	0.00	0.00	0.00	0.26	0.00	0.00	0.00
%Radiolaria	100	100	100	100	100	.100	100	100	100	100	100

Planktonic Foraminifera	**Core 34-3**					
	0-1	**20-21**	**40-41**	**60-61**	**80-81**	**100-101**
Total Planktics	0	0	0	0	0	0
Benthonic Foraminifera						
Total Benthics	0	0	0	0	0	0
Radiolaria						
Actinomma spp.	7	17	22	0	10	13
Actinomma antarcticum	218	179	122	209	102	106
Antarctissa spp.	2	11	24	0	1	2
Batryocyrtis scutium	0	1	0	0	0	0
Clathrocyclas bicornis	1	0	1	0	0	0
Lithelius minor	16	3	11	9	0	6
Prunopyle spp.	9	17	15	41	32	42
Pterocanium spp.	0	0	0	0	3	0
Saturnulus planetes	0	0	0	0	1	1
Spongodiscus spp.	88	50	45	23	49	37
Spongopyle osculosa	4	2	0	0	3	0
Tetrapyle octacantha	1	0	1	0	0	0
Unknown				1	1	
Total Radiolaria	346	280	241	283	202	207
Others						
Terrigenous	27	20	52	30	15	28
Silicic fragments	114	67	102	69	114	81
Aggregates			18	4		8
Worm tubes						1
Total Mounted	487	367	413	386	331	325
Terrigenous %	5.54	5.45	12.59	7.77	4.53	8.62
Total fragmentation %	3.96	2.90	5.02	2.96	6.59	4.66
Radiolaria %	100.00	100.00	100.00	100.00	100.00	100.00

Planktonic Foraminifera	**Core 50-33**					
	0-2	**20-21**	**40-41**	**60-61**	**80-81**	**100-101**
Globigerina spp.	1					
Globigerinia bulloides	5					
Globorotalia inflata	8					
N. pachyderma (s)	72					
Unknown sp	2					
Total Planktics	88	0	0	0	0	0
Benthonic Foraminifera						
Epistominella spp.	6					
Globocassidulina subglobosa	1					
Oridulsalis umbonatas	1					
Spheroidina bulloides	2					
Total Benthics	10	0	0	0	0	0
Radiolaria						
Actinomma spp.	4	11	26	22	35	48
Actinomma antarcticum	157	127	138	114	178	168
Antarctissa spp.			1			
Bathypyramis spp.					1	
Dictyocryne profunda			1			
Lithelius minor	6	14	18	9	15	17
Prunopyle spp.	6	4	7	39	47	51
Spongodiscus spp.	43	56	61	73	59	59
Spongopyle osculosa	1	1	7		3	
Stylatractus spp.						1
Tetrapyle octacantha	1		1			
Total Radiolaria	218	213	260	257	338	344
Others						
Terrigenous	87	55	115	44	45	16
Calcic fragments	63					
Silicic fragments	103	78	56	124	63	64
Aggregates	1				3	2
Total Mounted	570	346	431	425	449	426
N. pachyderma (s) %	100					
Benthics %	3.16					
Terrigenous %	15.26	15.90	26.68	10.35	10.02	3.76
Fragmentation (s) %	5.58	4.38	2.62	5.69	2.28	2.27
Fragmentation (c) %	7.44					
Total fragmentation %	6.16	4.38	2.62	5.69	2.28	2.27
Planktic %	27.85	0	0	0	0	0
Radiolaria %	68.99	100.00	100.00	100.00	100.00	100.00

Appendix 6

Semiquantitative Analysis of the Fine Sand Fraction (63-150 μm)

Planktonic Foraminifera	**Core 36-42**										
	0	**10**	**20**	**30**	**40**	**50**	**60**	**70**	**80**	**90**	**100**
Globigerina spp.	18	19	26	30	39	33	20	29	27	20	19
Globigerina bulloides	6	12	10	14	23	20	22	13	20	16	16
Globogerinita spp.	4	4	3	6	6	4	8	4	1	4	5
Globorotalia cf scitula						1	1	1		1	
Globorotalia inflata	1		1	2	1					2	1
Globorotalia spp.		1	3		3	5	3	3	4	3	2
Gr. truncatulinoides		1		2	1	2	1			1	1
Globigerina quinqueloba	19	19	17	25	24	25	20	27	20	25	36
N. pachyderma (d)	6	7	5	3	9	5	3	1	2	2	2
N. pachyderma (s)	20	12	15	16	20	19	9	10	16	17	17
Unknown sp	2								1		
Aberant sp.									1		
Total Planktics	76	75	80	98	126	114	87	88	92	91	99
Benthonic Foraminifera											
Astrononion spp.	1		1	1							
Bolivina spp.	1			1		1		1			
Bulimina aculeata						2					1
Bulimina spp.						1					
Cassidulina spp.					2		3	2	2		
Cibicidoides wuellstorfi		1								1	1
Cibicides spp.			1								
Eggerella bradyi								1			
Ehrenbergina spp.			1								
Epistominella exigua	1	1	1	3	2	3	3				
Epistominella spp.					1						
Eu Uvigerina cf. peregrina			1	2		2			2		
Eu Uvigerina spp.							1				
G. subglobosa	4	2	1	1		2	1	1	1		
Gyroidina neosolandii						1					
Gyroidinoides spp.							2				
Nodosaria spp.			2		2	1					1
Oridulsalis spp.				1							
Oridulsalis umbonatas		1									
Planulinoides spp.				1							
Pyrgo spp.						1					
Q. cf. larmarckiana		1									
Textularia spp.			3					1			
Globular cone	1	2	2	1	3		2	2			
Unknown			1	1							
Total Benthics	8	8	14	12	10	14	12	8	5	1	3
Others											
Terrigenous	1	1	1								
Calcic fragments	62	63	96	90	70	91	68	87	71	76	52
Sponge spicules		1	2	1		2	2		2		
Echinoderm spines	1	1	1	1	1		2	2	3	1	2
Glauconite pellets	3	1	1		1	1	2	2	1	5	3
Worm tubes					1						
Total Mounted	151	150	195	202	209	222	173	187	174	174	159
N. pachyderma (s) %	77	63.2	75	84.2	69	79.2	75	90.9	88.9	89.5	89.5
Benthic %	9.5	9.64	14.9	10.9	7.35	10.9	12.1	8.33	5.15	1.09	2.94
Planktic %	90	90.4	85.1	89.1	92.6	89.1	87.9	91.7	94.8	98.9	97.1
Radiolaria %	0	0	0	0	0	0	0	0	0	0	0
Terrigenous %	0.7	0.67	0.51	0	0	0	0	0	0	0	0
Total fragmentation %	8.4	8.67	11.3	9.28	6.04	8.16	7.91	10.2	8.38	9.36	5.99

Planktonic Foraminifera	**Core 34-1**										
	0	**10**	**20**	**30**	**40**	**50**	**60**	**70**	**80**	**90**	**100**
Globigerina spp.	15	19	25	22	28	34	27	20	22	25	26
Globigerina bulloides	5	8	14	9	9	12	5	5	7	7	7
Globogerinita spp.	6	3	10	7	13	16	14	5	9	8	7
Globorotalia cf scitula			2	1	2				3	1	
Globorotalia inflata		7	3	3	2			3	2	1	
Globorotalia spp.	1	11	6	3	5	1	2	2	2	1	4
Gr. truncatulinoides	1		1	1		1	2			1	
Globigerina quinqueloba	25	17	20	26	29	52	35	30	27	38	39
N. pachyderma (d)	1	1	2	3	1	4	3	2	2	4	3
N. pachyderma (s)	30	29	25	27	27	29	35	23	28	41	35
Unknown sp		1									
Aberant sp.			1		1			1			
Total Planktic	84	96	109	102	117	149	123	91	102	127	121
Benthonic Foraminifera											
Cibicidoides wuellstorfi							1				1
Epistominella spp.				1			1	1	1		
Eu Uvigerina spp.		1									1
G. subglobosa				1	2			1	2		1
Gyroidinoides spp.	1										
Nodosaria spp.					1						3
Pyrgo spp.					1	1					
Textularia spp.				1							
Unknown											1
Total Benthics	1	1	0	3	4	1	2	2	3	0	7
Others											
Calcic fragments	140	125	119	153	220	52	107	128	91	65	134
Sponge spicules			1		4		1				
Echinoderm spines					1				1		1
Glauconite pellets	1				1			1			1
Total Mounted	226	222	229	258	347	202	233	222	197	192	264
N. pachyderma (s) %	97	96.7	92.6	90	96.4	87.9	92.1	92	93.3	91.1	92.1
Benthics %	1.2	1.03	0	2.86	3.31	0.67	1.6	2.15	2.86	0	5.47
Planktics %	99	99	100	97.1	96.7	99.3	98.4	97.8	97.1	100	94.5
Total Fragmentation %	17	13.9	12	15.4	18.5	4.15	9.67	14.7	9.77	6.01	11.6

Planktonic Foraminifera	**Core 36-38**									
	0	**10**	**20**	**30**	**40**	**50**	**60**	**70**	**80**	**90**
N. pachyderma (s)		1		1				2		1
Unknown sp								1		
Total Planktics	0	1	0	1	0	0	0	3	0	1
Benthonic Foraminifera										
Globocassidulina subglobosa					1				2	
Gyroidinoides spp.						2	1			1
Nodoseria spp.				1						
Unknown					1		1			
Total Benthics	0	0	0	1	2	2	2	0	2	1
Radiolaria										
Acanthodesmiidae	4	3	2	1	2	1	2	2	3	2
Actinomma antarcticum	13	13	9	5	9	5	10	8	12	2
Actinomma spp.	4	2		1	4	1	5	3	1	4
Antarctissa spp.	25	40	30	29	22	33	30	41	40	31
Bathypyramis spp.		1		1	2			1		
Batryocyrtis scutium			1	2	2	4	1	3	4	1
Clathrocyclas bicornis	2	1		1			1	1		
Dictyocryne profunda					1					
Eucyrtidium cf calvertense		1		1					2	
Lamprocyclas spp	1									
Lithelius minor	2	8		2	3	2	2	2	4	3
Lithomelissa spp		1		2						
Peripyramis spp	11	17	6	16	6	12	12	10	5	7
Phormostichoartus spp	2	2				1	1	1	1	
Plectopyramis spp.		1								
Prunopyle spp.	9	10	7	9	5	7	5	8	6	8
Pterocanium cf trilobum		2		1					1	
Spongodiscus spp.	5	4	5	5	4	3	5	5	5	6
Spongopyle osculosa	1		1	2		1		1		2
Stylatractus spp.				3		1		2	1	
Tetrapyle octacantha	5	2		2	2			1	1	2
Unknown	1	2	1	2					2	
Total Radiolaria	85	110	62	85	62	71	74	89	88	68
Others										
Terrigenous	22	39	23	66	60	85	73	28	18	84
Calcic Fragments	2	3	6	13	9	35	31	40	18	37
Silicic Fragments	68	55	67	50	69	40	70	70	55	73
Sponge Spicules	11	5	17	7	12	10	14	6	3	14
Echinoderm Spines	1									
Glauconite Pellets	1					2				
Unknown diatom	40	25	26	18	18	19	26	16	39	37
Rings	3	2	2	1	1		6			1
Total Mounted	233	240	203	242	233	264	296	252	223	316
N. pachyderma (s) %		100		100				100		100
Benthic %	0	0	0	0.95	2.44	2.17	1.96	0	1.55	0.93
Planktic %	0	0.74	0	0.95	0	0	0	2.78	0	0.93
Radiolaria %	68	80.9	70.5	81	75.6	77.2	72.5	82.4	68.2	63.6
Diatom %	32	18.4	29.5	17.1	22	20.7	25.5	14.8	30.2	34.6
Terrigenous %	9.44	16.3	11.3	27.3	25.8	32.2	24.7	11.1	8.07	26.6
Fragmentation (s) %	6.37	4.85	8.69	5.72	9.73	5.26	8.05	7.69	5.14	8
Fragmentation (c) %	100	27.3	100	44.8	36	68.6	66	62.5	52.9	69.8
Total Fragmentation %	8.92	5.84	12.1	7.84	12.7	10.6	13.8	12.5	8.85	15.9

Radiolaria	**Core 50-34**										
	0	**10**	**20**	**30**	**40**	**50**	**60**	**70**	**80**	**90**	**100**
Acanthodesmiidae	8	3	1	3	2	8	6	3	2		1
Actinomma antarcticum	12	21	12	12	14	15	14	14	14	8	20
Actinomma spp.	3	2	7	6	1	6	2	7	1	6	6
Antarctissa spp.	63	70	45	38	39	44	56	41	37	11	37
Bathypyramis spp.		1									
Batryocyrtis scutium	6	6	4	4	2	5	10		1		
Clathrocyclas bicornis	1		1	2	3	2	6	11	8	8	9
Eucyrtidium cf. calvertense	2			1	1				2		3
Lithelius minor	5	7	3	5	6	6	8	3	3	3	6
Lithomelissa spp							2		1		
Peripyramis spp	10	8	6	6	7	8	9	2	7	4	4
Phormostichoartus spp		1			2	1		3	2	2	
Plectopyramis spp.	1					1	1	1			
Prunopyle spp.	9	15	16	16	12	14	11	12	8	1	13
Pterocanium spp.		1	1	1			1				1
Spongodiscus spp.	17	13	15	6	11	13	15	23	10	6	11
Spongopyle osculosa	1	1		2	1	1					2
Stylatractus spp.	2	1	2	2		1	4	1		1	2
Tetrapyle octacantha	4	2	4	5	2	2	2		1	1	1
Unknown	2			1	1				2		3
Total Radiolaria	146	152	117	110	104	127	147	121	99	51	119
Others											
Terrigenous	19	23	121	18	48	48	58	72	68	125	99
Silicic fragments	100	108	122	110	91	154	145	122	92	74	89
Sponge spicules	9	9	8	21	21	15	21	18	22	9	15
Echinoderm spines		1									
Aggregates						1		1			
Worm tubes							1	1			
Unknown diatom	19	8	7	17	11	13	20	12	15	1	22
Total Mounted	293	301	375	276	275	358	392	347	296	260	344
Terrigenous %	6.5	7.64	32.3	6.52	17.5	13.4	14.8	20.7	23	48	28.8
Total Fragmentation %	7.9	8.16	11.5	11.1	9.86	13.2	11	11.2	10.4	15	8.55
Diatom %	12	5	5.65	13.4	9.57	9.29	12	9.02	13.2	1.9	15.6
Radiolaria %	88	95	94.4	86.6	90.4	90.7	88	91	86.8	98	84.4

Appendix 7

XRD Analysis Records

D I F I L E :

Sample identification: Jon Mackie 34-1 @ 30 cm

DI file name: JM__1_30.
Input file name: JM__1_30

Start angle [°2_θ]: 5.010
End angle [°2_θ]: 39.990
Start d-value [Å]: 17.62392
End d-value [Å]: 2.25269
Maximum number of counts: 9293

Anode material: Cu
$_\alpha$1 Wavelength [Å]: 1.54056
$_\alpha$2 Wavelength [Å]: 1.54439

Intensities for FIXED slit

Peak positions defined by: Minimum of 2nd derivative of peak
Minimum peak tip width: 0.00
Maximum peak tip width: 1.00
Maximum peak base width: 2.00
Minimum significance: 0.75
Number of peaks: 5

D I F F R A C T I O N L I N E S :

Angle [°2_θ]	d-value $_\alpha$1 [Å]	d-value $_\alpha$2 [Å]	T.width [°2_θ]	Height [counts]	Backgr. [counts]	Rel.int. [%]	Signific
23.070	3.85205	3.86162	0.120	847	102	9.1	2.62
29.420	3.03348	3.04101	0.180	9293	142	100.0	25.93
31.445	2.84259	2.84965	0.120	635	132	6.8	2.39
35.970	2.49469	2.50089	0.140	1232	106	13.3	4.98
39.420	2.28394	2.28962	0.120	1552	90	16.7	4.34

Sample identification Jon Mackie 34-1 @ 30 cm

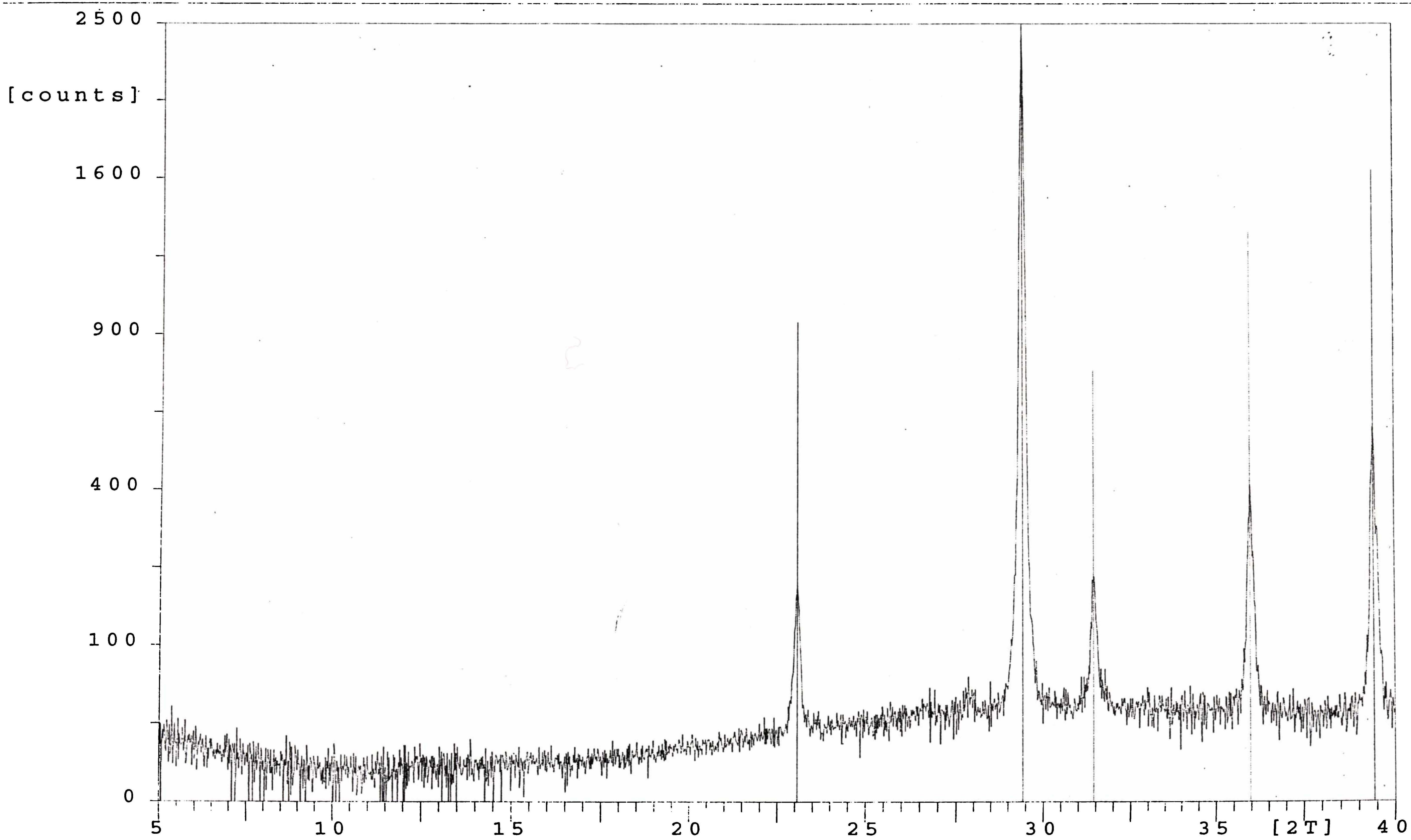

D I F I L E :

Sample identification: Jon Mackie 34-1 @ 90 cm

DI file name: JM__1_90.
Input file name: JM__1_90

Start angle [°2θ]: 5.010
End angle [°2θ]: 39.990
Start d-value [Å]: 17.62392
End d-value [Å]: 2.25269
Maximum number of counts: 9860

Anode material: Cu
α1 Wavelength [Å]: 1.54056
α2 Wavelength [Å]: 1.54439

Intensities for FIXED slit

Peak positions defined by: Minimum of 2nd derivative of peak
Minimum peak tip width: 0.00
Maximum peak tip width: 1.00
Maximum peak base width: 2.00
Minimum significance: 0.75
Number of peaks: 6

D I F F R A C T I O N L I N E S :

Angle [°2θ]	d-value α1 [Å]	d-value α2 [Å]	T.width [°2θ]	Height [counts]	Backgr. [counts]	Rel.int. [%]	Signific
23.050	3.85535	3.86493	0.160	571	69	5.8	3.95
27.935	3.19127	3.19920	0.480	62	92	0.6	1.07
29.350	3.04055	3.04811	0.180	9860	86	100.0	23.88
31.430	2.84391	2.85098	0.140	713	85	7.2	2.89
35.915	2.49839	2.50459	0.120	894	77	9.1	2.82
39.375	2.28645	2.29213	0.100	1369	62	13.9	2.05

Sample identification Jon Mackie 34-1 @ 90 cm

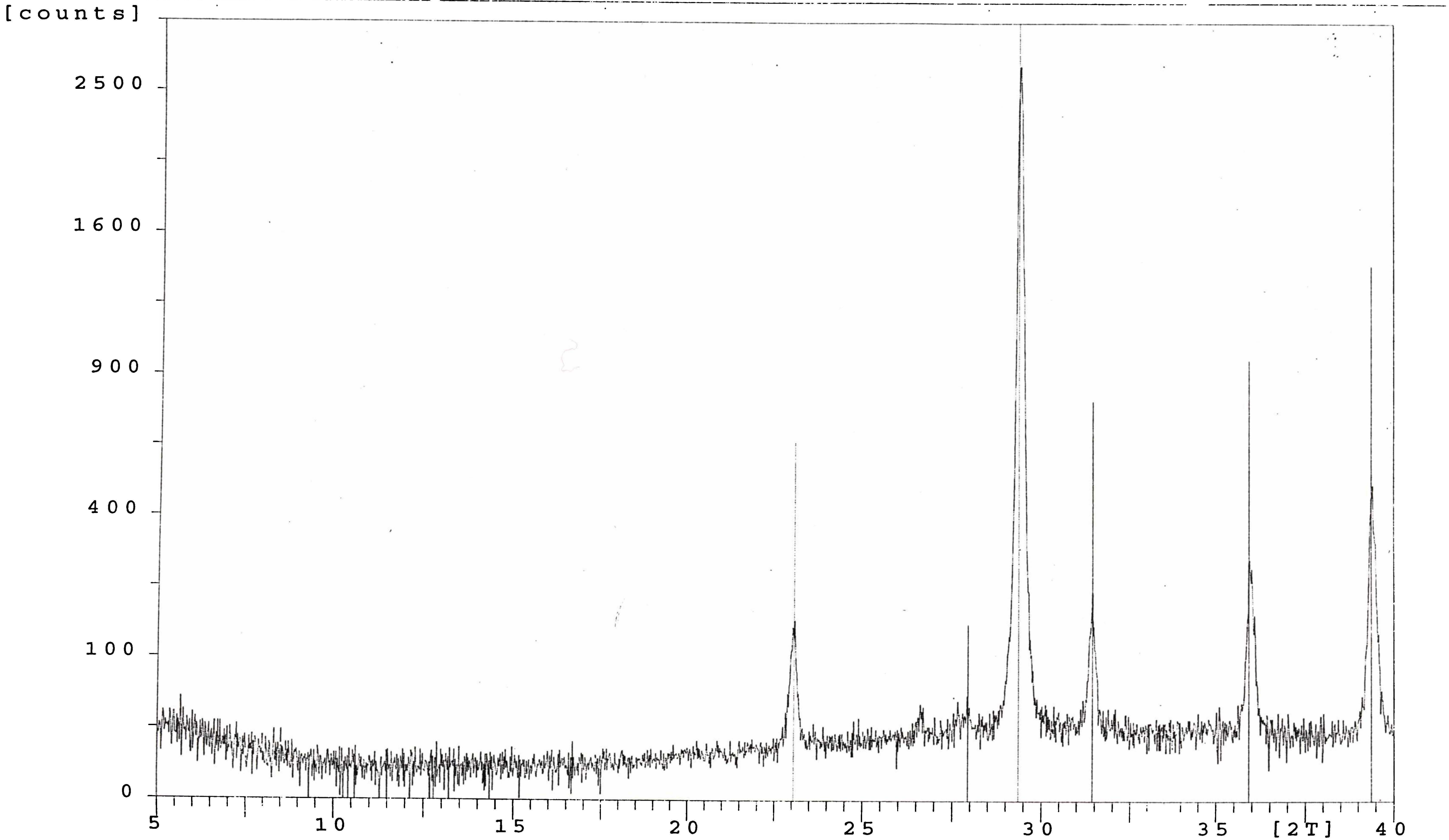

D I F I L E :

Sample identification: Jon Mackie 50-34 @ 10 cm

DI file name: JM_34_10.
Input file name: JM_34_10

Start angle [°2_θ]: 5.010
End angle [°2_θ]: 39.990
Start d-value [Å]: 17.62392
End d-value [Å]: 2.25269
Maximum number of counts: 2372

Anode material: Cu
$_\alpha$1 Wavelength [Å]: 1.54056
$_\alpha$2 Wavelength [Å]: 1.54439

Intensities for FIXED slit

Peak positions defined by: Minimum of 2nd derivative of peak
Minimum peak tip width: 0.00
Maximum peak tip width: 1.00
Maximum peak base width: 2.00
Minimum significance: 0.75
Number of peaks: 14

D I F F R A C T I O N L I N E S :

Angle [°2_θ]	d-value $_\alpha$1 [Å]	d-value $_\alpha$2 [Å]	T.width [°2_θ]	Height [counts]	Backgr. [counts]	Rel.int. [%]	Signific
6.975	12.66269	12.69415	0.640	480	718	20.2	0.77
8.795	10.04598	10.07095	0.240	734	353	31.0	1.02
12.500	7.07544	7.09302	0.200	269	139	11.3	0.87
19.755	4.49033	4.50149	0.480	169	225	7.1	1.14
20.855	4.25590	4.26648	0.240	372	225	15.7	1.42
21.970	4.04237	4.05241	0.200	353	228	14.9	1.12
23.580	3.76988	3.77924	0.200	346	234	14.6	1.14
24.270	3.66424	3.67334	0.240	328	234	13.8	1.40
26.650	3.34216	3.35046	0.140	2372	237	100.0	5.02
27.970	3.18735	3.19527	0.160	1225	240	51.7	1.36
30.370	2.94072	2.94802	0.240	225	243	9.5	1.22
34.900	2.56869	2.57507	0.960	149	202	6.3	1.81

Sample identification Jon Mackie 50-34 @ 10 cm

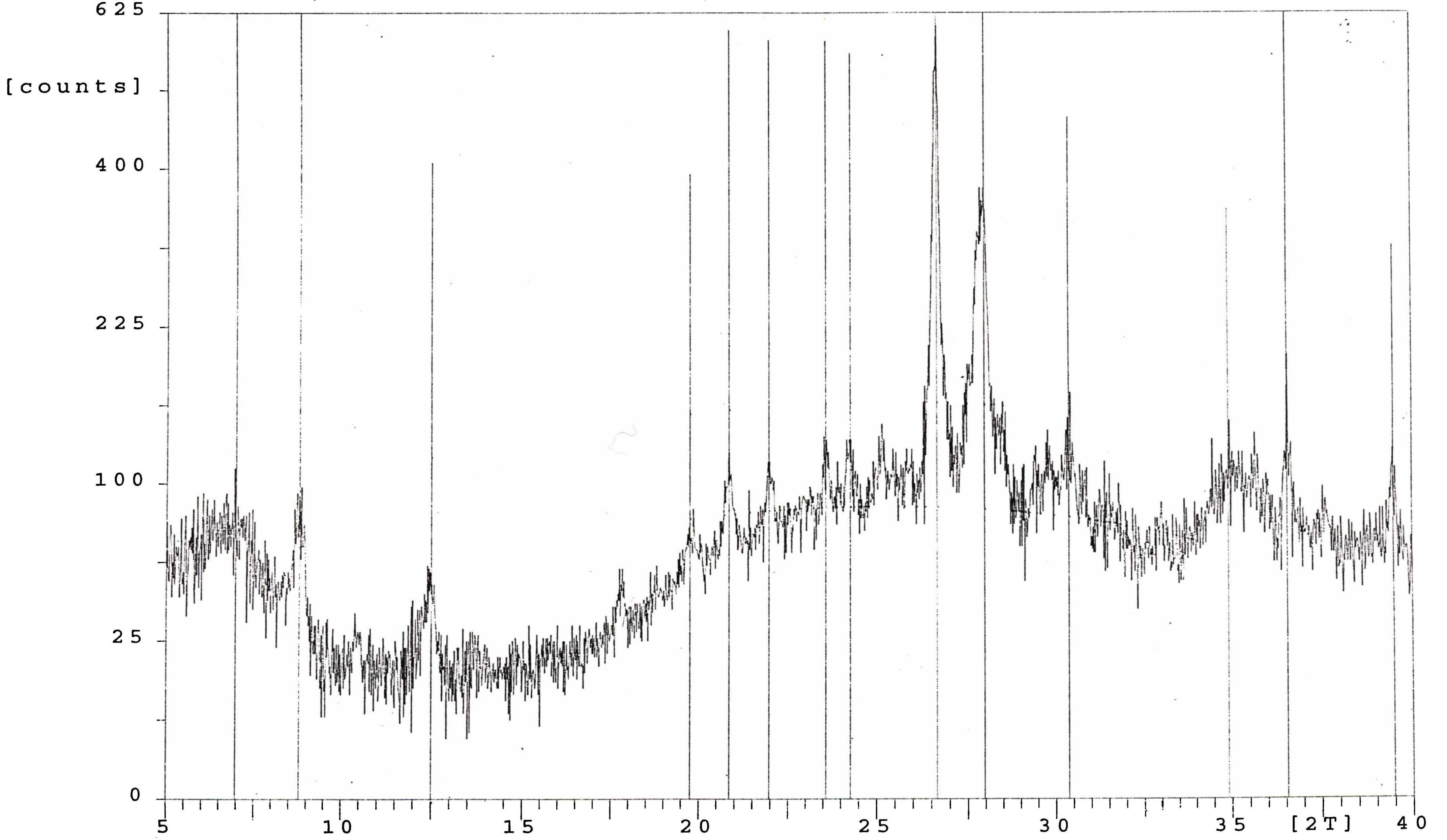

D I F I L E :

Sample identification: Jon Mackie 50-34 @ 70 cm

DI file name: JM_34_70.
Input file name: JM_34_70

Start angle [°2θ]: 5.010
End angle [°2θ]: 39.990
Start d-value [Å]: 17.62392
End d-value [Å]: 2.25269
Maximum number of counts: 3215

Anode material: Cu
α1 Wavelength [Å]: 1.54056
α2 Wavelength [Å]: 1.54439

Intensities for FIXED slit

Peak positions defined by: Minimum of 2nd derivative of peak
Minimum peak tip width: 0.00
Maximum peak tip width: 1.00
Maximum peak base width: 2.00
Minimum significance: 0.75
Number of peaks: 19

D I F F R A C T I O N L I N E S :

Angle [°2θ]	d-value α1 [Å]	d-value α2 [Å]	T.width [°2θ]	Height [counts]	Backgr. [counts]	Rel.int. [%]	Signific
7.265	12.15786	12.18807	0.560	216	708	6.7	0.94
8.840	9.99494	10.01978	0.200	961	350	29.9	1.46
10.415	8.48673	8.50782	0.200	92	166	2.9	0.96
12.505	7.07262	7.09020	0.240	240	125	7.5	2.22
13.850	6.38866	6.40454	0.480	71	108	2.2	0.99
19.740	4.49371	4.50487	0.640	146	177	4.6	1.11
20.780	4.27109	4.28171	0.140	488	169	15.2	1.60
21.935	4.04874	4.05880	0.240	445	159	13.8	1.89
23.565	3.77224	3.78162	0.160	433	149	13.5	0.95
24.325	3.65608	3.66516	0.120	502	144	15.6	1.34
25.305	3.51666	3.52540	0.480	331	139	10.3	1.43
26.650	3.34216	3.35046	0.220	3215	132	100.0	14.97

50-34 @ 70 cm

Angle [°2θ]	d-value α1 [Å]	d-value α2 [Å]	T.width [°2θ]	Height [counts]	Backgr. [counts]	Rel.int. [%]	Signific
27.965	3.18791	3.19583	0.120	2209	125	68.7	2.51
30.390	2.93883	2.94613	0.240	339	114	10.5	1.70
32.980	2.71371	2.72045	0.120	250	106	7.8	1.19
34.820	2.57441	2.58080	0.960	207	102	6.4	1.74
36.555	2.45610	2.46220	0.120	331	96	10.3	2.01
37.530	2.39450	2.40045	0.400	151	94	4.7	0.90
39.515	2.27867	2.28433	0.160	225	90	7.0	0.79

Sample identification Jon Mackie 50-34 @ 70 cm

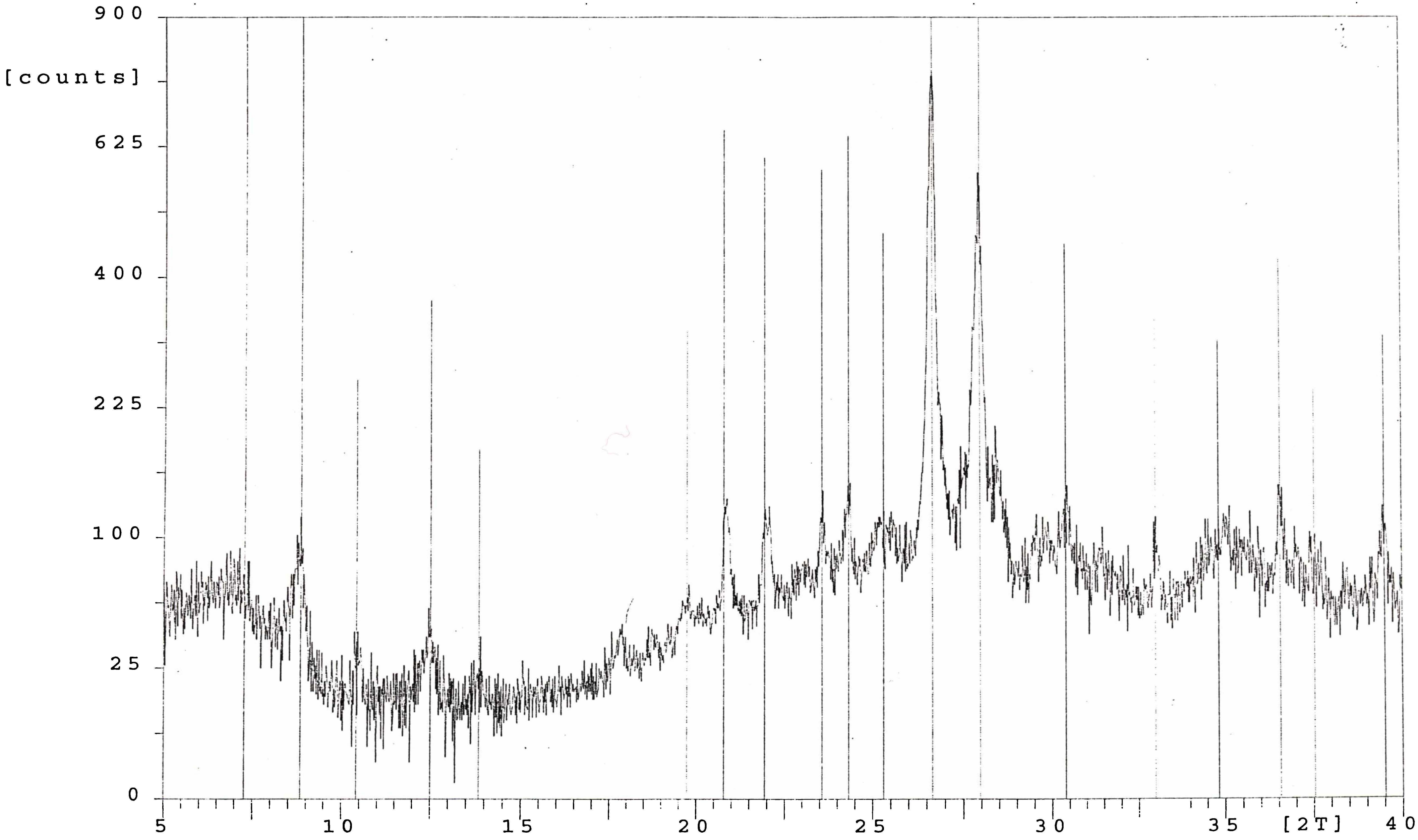

D I F I L E :

Sample identification: Jon Mackie 36-42 @ 60 cm

DI file name: JM_42_60.
Input file name: JM_42_60

Start angle [°2θ]: 5.010
End angle [°2θ]: 39.990
Start d-value [Å]: 17.62392
End d-value [Å]: 2.25269
Maximum number of counts: 9312

Anode material: Cu
α1 Wavelength [Å]: 1.54056
α2 Wavelength [Å]: 1.54439

Intensities for FIXED slit

Peak positions defined by: Minimum of 2nd derivative of peak
Minimum peak tip width: 0.00
Maximum peak tip width: 1.00
Maximum peak base width: 2.00
Minimum significance: 0.75
Number of peaks: 9

D I F F R A C T I O N L I N E S :

Angle [°2θ]	d-value α1 [Å]	d-value α2 [Å]	T.width [°2θ]	Height [counts]	Backgr. [counts]	Rel.int. [%]	Signific
12.460	7.09806	7.11570	0.240	77	49	0.8	0.92
23.035	3.85782	3.86741	0.120	708	106	7.6	1.98
26.640	3.34339	3.35169	0.120	117	121	1.3	0.92
27.720	3.21553	3.22352	0.240	369	117	4.0	1.26
29.405	3.03499	3.04253	0.180	9312	114	100.0	24.63
31.420	2.84480	2.85186	0.200	408	112	4.4	3.51
33.085	2.70534	2.71206	0.160	92	110	1.0	0.94
35.975	2.49436	2.50055	0.120	1260	108	13.5	3.26
39.390	2.28561	2.29129	0.120	1513	106	16.2	4.52

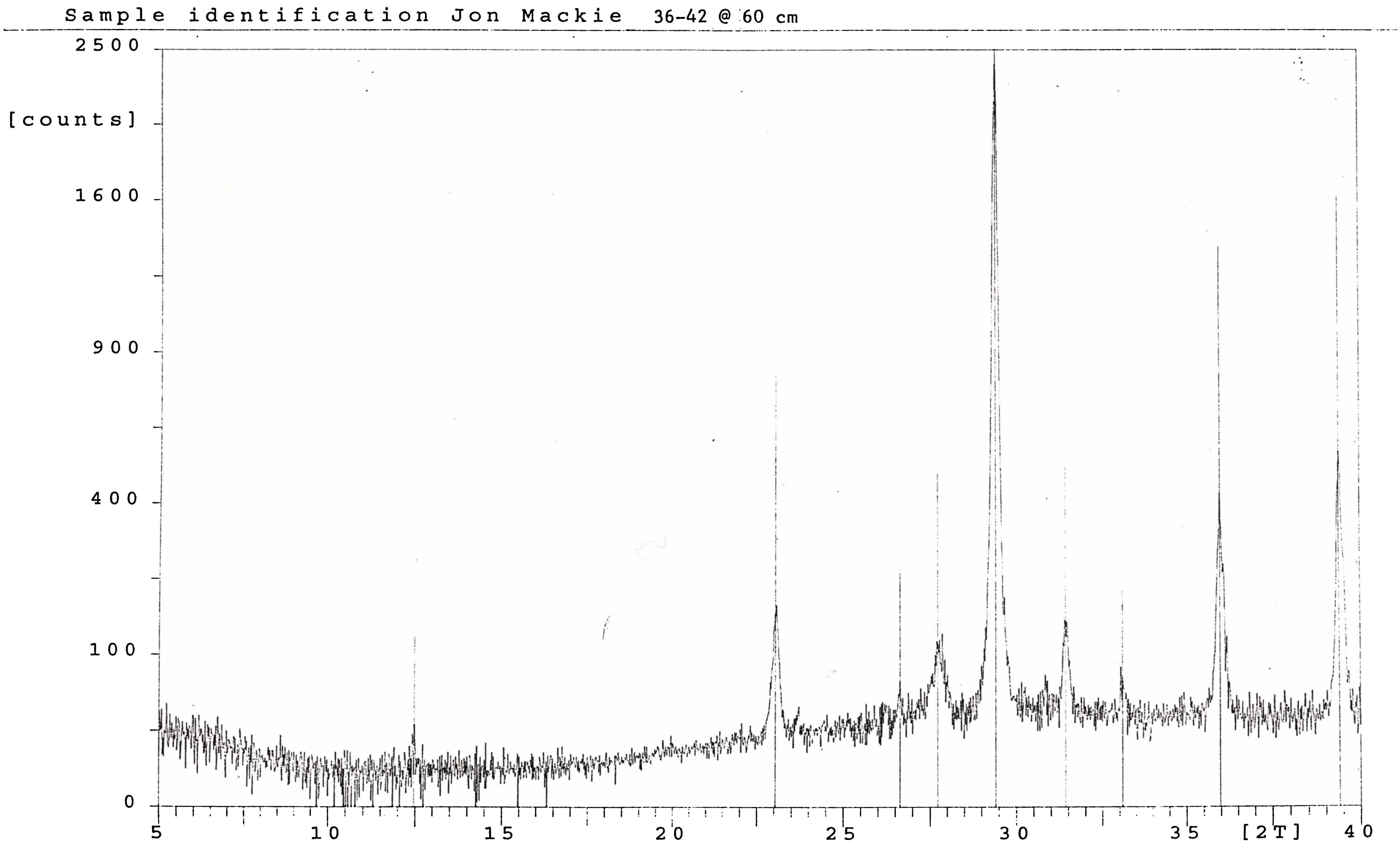
Sample identification Jon Mackie 36-42 @ 60 cm
2500
[counts]
1600
900
400
100
0
5
10
15
20
25
30
35
[2T]
40

D I F I L E :

Sample identification: Jon Mackie 36-38 @ 0 cm

DI file name: JM__38_0.
Input file name: JM__38_0

Start angle [°2θ]: 5.010
End angle [°2θ]: 39.990
Start d-value [Å]: 17.62392
End d-value [Å]: 2.25269
Maximum number of counts: 2777

Anode material: Cu
α1 Wavelength [Å]: 1.54056
α2 Wavelength [Å]: 1.54439

Intensities for FIXED slit

Peak positions defined by: Minimum of 2nd derivative of peak
Minimum peak tip width: 0.00
Maximum peak tip width: 1.00
Maximum peak base width: 2.00
Minimum significance: 0.75
Number of peaks: 22

D I F F R A C T I O N L I N E S :

Angle [°2θ]	d-value α1 [Å]	d-value α2 [Å]	T.width [°2θ]	Height [counts]	Backgr. [counts]	Rel.int. [%]	Signific
7.015	12.59057	12.62186	0.480	408	692	14.7	0.78
8.745	10.10331	10.12841	0.240	369	342	13.3	1.40
10.400	8.49894	8.52006	0.200	144	177	5.2	0.99
12.415	7.12369	7.14139	0.200	467	142	16.8	1.25
13.795	6.41401	6.42995	0.240	121	121	4.4	0.90
18.720	4.73619	4.74796	0.240	166	130	6.0	0.84
20.800	4.26703	4.27763	0.160	502	117	18.1	1.00
22.010	4.03511	4.04514	0.240	388	110	14.0	1.48
22.985	3.86610	3.87571	0.240	353	106	12.7	1.02
23.540	3.77619	3.78558	0.240	396	104	14.3	1.68
25.130	3.54076	3.54955	0.160	548	98	19.7	1.02
26.655	3.34154	3.34984	0.100	2777	92	100.0	2.28

36-38 @ 0 cm

Angle [°2θ]	d-value α1 [Å]	d-value α2 [Å]	T.width [°2θ]	Height [counts]	Backgr. [counts]	Rel.int. [%]	Signific
27.395	3.25293	3.26102	0.120	745	90	26.8	0.92
27.890	3.19631	3.20426	0.100	2490	88	89.7	1.70
28.485	3.13089	3.13867	0.160	502	86	18.1	0.88
29.395	3.03600	3.04354	0.100	1756	83	63.2	2.14
30.480	2.93035	2.93763	0.320	282	81	10.2	0.95
31.360	2.85010	2.85718	0.200	328	77	11.8	1.05
33.030	2.70972	2.71645	0.120	204	74	7.4	0.76
35.990	2.49335	2.49955	0.160	317	69	11.4	0.99
36.565	2.45545	2.46155	0.200	331	67	11.9	1.55
39.445	2.28255	2.28822	0.100	384	62	13.8	0.86

Sample identification Jon Mackie 36-38 @ 0 cm

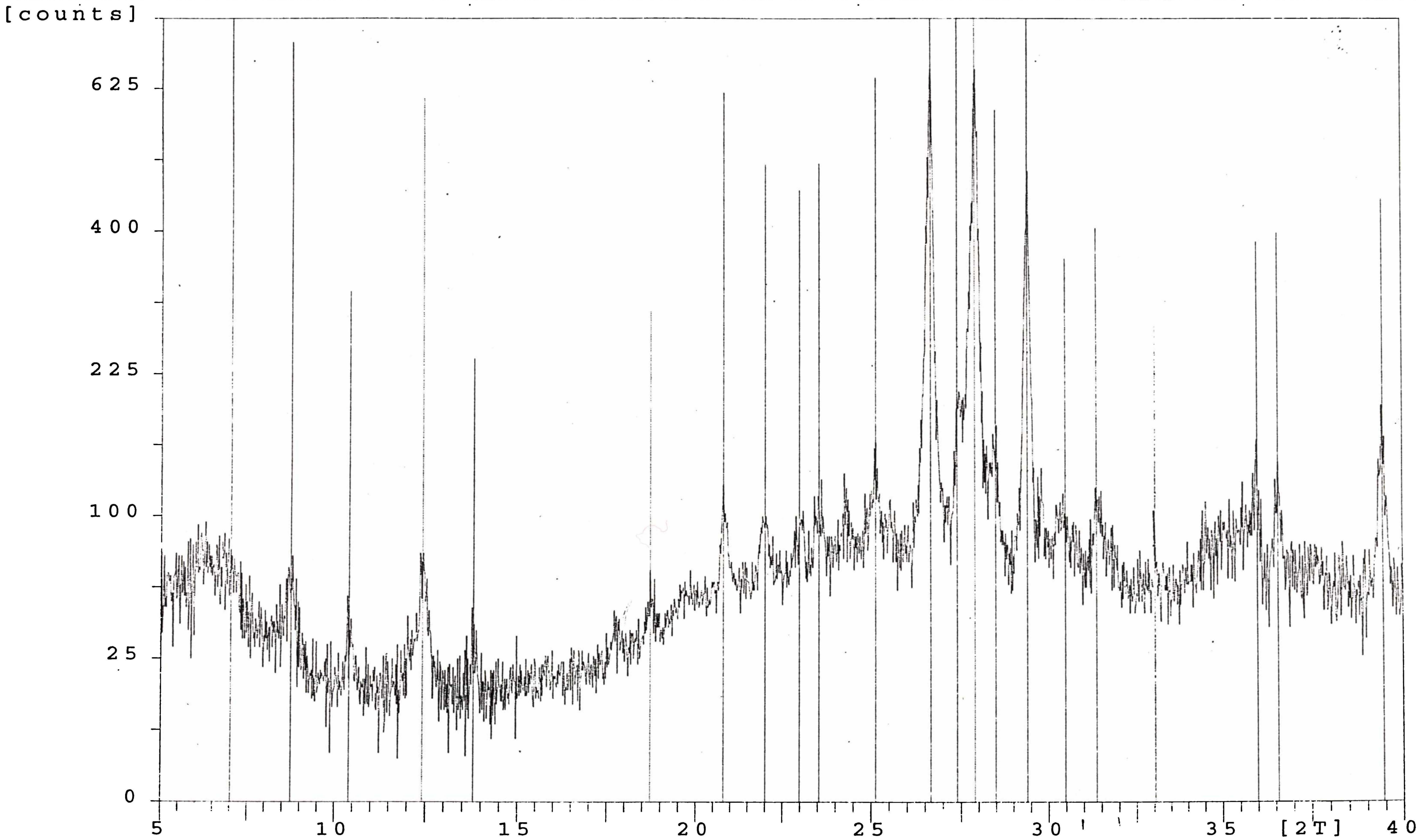

D I F I L E :

Sample identification: Jon Mackie 36-38 @ 90 cm

DI file name: JM_38_90.
Input file name: JM_38_90

Start angle [°2θ]: 5.010
End angle [°2θ]: 39.990
Start d-value [Å]: 17.62392
End d-value [Å]: 2.25269
Maximum number of counts: 2725

Anode material: Cu
α1 Wavelength [Å]: 1.54056
α2 Wavelength [Å]: 1.54439

Intensities for FIXED slit

Peak positions defined by: Minimum of 2nd derivative of peak
Minimum peak tip width: 0.00
Maximum peak tip width: 1.00
Maximum peak base width: 2.00
Minimum significance: 0.75
Number of peaks: 20

D I F F R A C T I O N L I N E S :

Angle [°2θ]	d-value α1 [Å]	d-value α2 [Å]	T.width [°2θ]	Height [counts]	Backgr. [counts]	Rel.int. [%]	Signific
8.860	9.97243	9.99721	0.200	169	250	6.2	0.94
10.485	8.43023	8.45118	0.120	185	142	6.8	1.08
12.520	7.06418	7.08174	0.160	376	119	13.8	1.00
20.895	4.24785	4.25840	0.120	310	279	11.4	0.90
21.915	4.05239	4.06246	0.120	353	266	13.0	1.15
23.055	3.85452	3.86410	0.200	282	253	10.4	1.28
23.605	3.76594	3.77530	0.200	296	246	10.9	1.07
24.400	3.64501	3.65407	0.240	317	237	11.6	1.10
25.535	3.48551	3.49417	0.120	384	228	14.1	2.07
26.660	3.34092	3.34923	0.120	2237	219	82.1	4.46
28.025	3.18122	3.18913	0.140	1823	207	66.9	3.56
28.540	3.12498	3.13274	0.160	458	204	16.8	1.23

36-38 @ 90 cm

Angle [°2θ]	d-value α1 [Å]	d-value α2 [Å]	T.width [°2θ]	Height [counts]	Backgr. [counts]	Rel.int. [%]	Signific
29.415	3.03398	3.04152	0.140	2725	199	100.0	7.68
30.835	2.89742	2.90462	0.060	615	185	22.6	2.42
31.455	2.84171	2.84877	0.120	353	180	13.0	3.53
32.990	2.71291	2.71965	0.040	219	172	8.0	1.11
34.450	2.60120	2.60767	0.240	92	166	3.4	0.82
35.970	2.49469	2.50089	0.060	515	159	18.9	1.58
36.595	2.45351	2.45960	0.240	114	156	4.2	1.13
39.425	2.28366	2.28934	0.100	605	146	22.2	1.39

Sample identification Jon Mackie 36-88 @ 90 cm

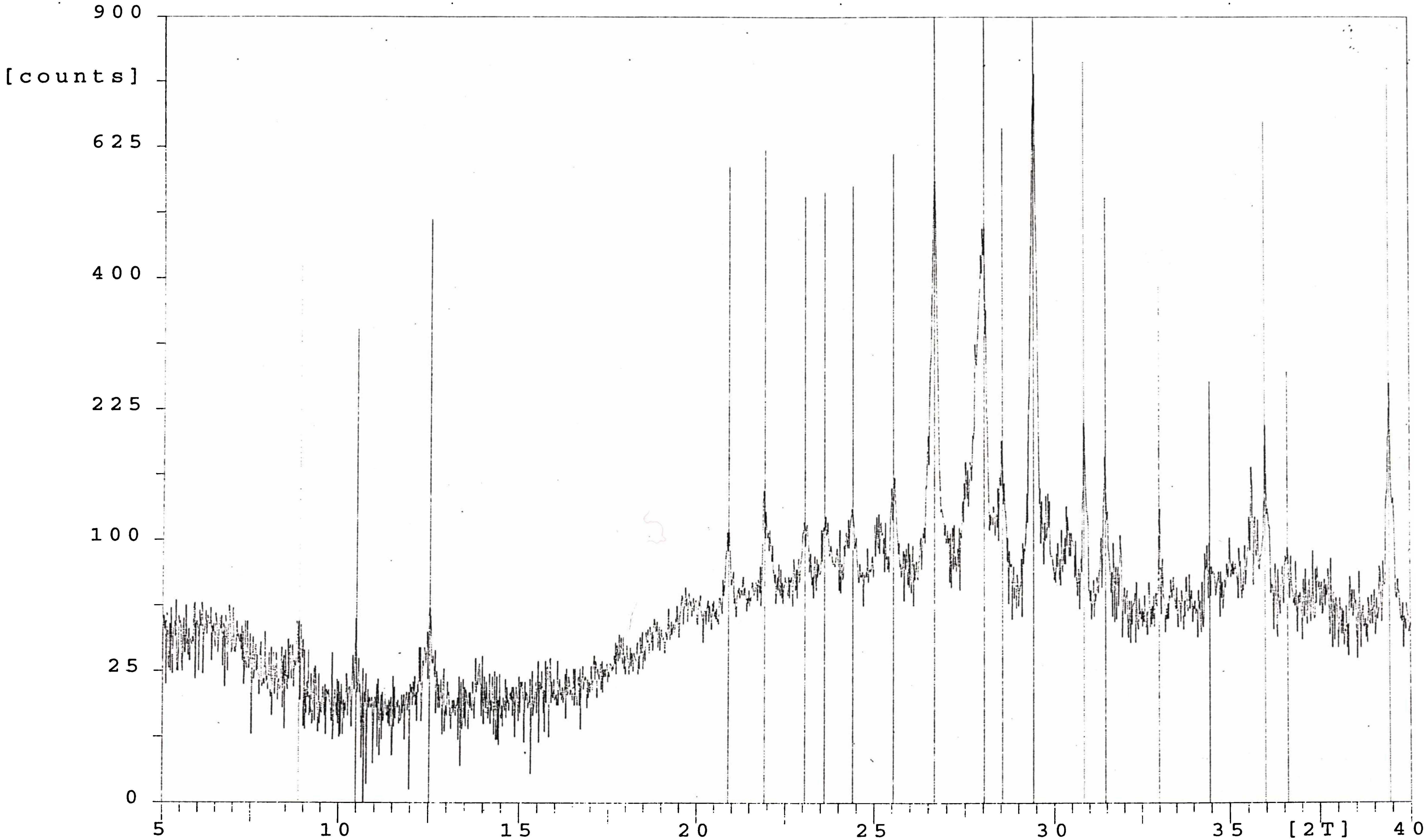

Appendix 8

Stable Oxygen and Carbon Isotope Data

Isotopes of Cores 34-1, 36-42 and 36-38
Europa Scientific Geo 20-20

Date	Sample	Depth (cm	D-45	D-46	d-C13	d-O18	C13 vpdb	O18 vpdb
14-7-97	TSS-201M		0.371	-4.744	1.991	-2.175		
	TSS-202M		0.364	-4.766	1.984	-2.197		
	TSS-203M		0.375	-4.662	1.992	-2.093		
	mean		0.370	-4.724	1.989	-2.155	1.950	-2.200
	34-1	0-1			0.173	3.042	0.134	2.997
		10-11	5 delta values only		0.081	3.004	0.042	2.959
		20-21	Repicked					
		30-31	Repicked					
15-7-97	TSS-204M		0.337	-4.703	1.953	-2.134		
	TSS-205M		0.372	-4.679	1.989	-2.110		
	TSS-206M		0.379	-4.616	1.995	-2.047		
	mean		0.363	-4.666	1.979	-2.097	1.950	-2.200
		40-41			0.275	3.100	0.246	2.997
		50-51			-0.018	3.047	-0.047	2.944
		60-61			-0.197	3.091	-0.226	2.988
		70-71			-0.354	2.896	-0.383	2.793
		80-81			-0.179	3.145	-0.208	3.042
		90-91			-0.049	3.031	-0.078	2.928
		100-101			0.030	3.394	0.001	3.291
16/7/97	TSS-207M		0.367	-4.656	1.983	-2.087		
	TSS-208M		0.395	-4.693	2.014	-2.124		
	TSS-209M		0.344	-4.690	1.960	-2.121		
	mean		0.369	-4.680	1.986	-0.211	1.950	-2.200
	36-42	10-11			0.063	3.011	0.027	2.922
		20-21	Repicked					
		30-31			0.227	2.626	0.191	2.537
		40-41			0.223	2.604	0.187	2.515
		50-51			0.337	2.413	0.301	2.324
		60-61			0.128	2.528	0.092	2.439
		70-71			0.084	2.688	0.048	2.599
		80-81			-0.141	3.150	-0.117	3.061
		90-91			-0.134	2.686	-0.170	2.597
		100-101			-0.067	2.469	-0.103	2.380
17-7-97	TSS-210M		0.373	-4.678	1.990	-2.109		
	TSS-211M		3.630	-4.685	1.980	-2.116		
	TSS-212M		0.355	-4.646	1.970	-2.076		
	mean		0.364	-4.670	1.980	-2.100	1.950	-2.200
	36-38	0-1			0.315	4.228	0.285	4.128
		10-11			0.213	4.454	0.183	4.354
		20-21			0.397	4.219	0.367	4.119
		30-31			0.413	4.325	0.383	4.225
		40-41			0.234	4.337	0.204	4.237
		50-51			0.072	3.940	0.042	3.840
		60-61			-0.083	3.834	-0.113	3.734
		70-71			0.311	4.101	0.281	4.001
		80-81			0.367	4.134	0.337	4.034
		90-91			0.306	4.067	0.276	3.967

Repicked Samples

25.7.97	TSS-223M		0.339	-4.780	1.957	-2.211		
	TSS-224M		0.349	-4.757	1.967	-2.188		
	TSS-225M		0.361	-4.796	1.981	-2.227		
	mean		0.350	-4.778	1.968	-2.209	1.950	-2.200
	34-1-20X	20-21			0.069	2.707	0.051	2.716
	34-1-30X	30-31			0.225	2.681	0.207	2.690
	36-38-X	60-61			0.189	4.036	0.171	4.045
	36-42-X	20-21			0.083	2.630	0.065	2.639

Appendix 9

Radiocarbon Data

Institute of
Geological &
Nuclear Sciences
Limited

Rafter Radiocarbon Laboratory

Accelerator Mass Spectrometry Result

R 21934/1	**Job** 12630
Description	Forams from a core (Globigerina bulloides)
Sample ID	36-42 @ 10cm
Submitter	Campbell Nelson Department of Earth Sciences

Radiocarbon Laboratory Reference	NZA 8096
Date measured	20-Nov-97
$\delta^{13}C$	.4 ‰

* **Radiocarbon Age**	19120 ± 110 BP
$\delta^{14}C$	-903.1 ± 1.3 ‰
$\Delta^{14}C$	-908 ± 1.3 ‰
** **Per cent modern**	9.2 ± .13

Issued 22/11/97

* Reported age is the conventional radiocarbon age before present (BP)

** Per cent modern means absolute per cent modern relative to the NBS I oxalic acid standard, corrected for decay since 1950.

Age, $\Delta^{14}C$, $\delta^{14}C$ and absolute per cent modern are as defined by Stuiver and Polach, Radiocarbon 19:355-363 (1977)

The reported errors comprise statistical errors in sample and standard determinations, combined in quadrature with a system error component that is based on the analysis of an ongoing series of measurements on ANU sucrose secondary standard. For the present result the system error component is conservatively estimated as .6% (= ± 48 radiocarbon years).

Nuclear Sciences Group, Institute of Geological and Nuclear Sciences Ltd., PO Box 31-312, Lower Hutt, New Zealand
Fax +64 4 570 4657 Phone +64 4 570 4671

Institute of
Geological &
Nuclear Sciences
Limited

Rafter Radiocarbon Laboratory

Accelerator Mass Spectrometry Result

R 21934/2	**Job** 12631
Description	Forams from a core (Globigerina bulloides)
Sample ID	36-42 @ 20cm
Submitter	Campbell Nelson
	Department of Earth Sciences

Radiocarbon Laboratory Reference	NZA 8097
Date measured	20-Nov-97
$\delta^{13}C$	.7 ‰

* **Radiocarbon Age**	23900 ± 200 BP
$\delta^{14}C$	-946.5 ± 1.3 ‰
$\Delta^{14}C$	-949.2 ± 1.2 ‰
** **Per cent modern**	5.08 ± .12

Issued 22/11/97

* Reported age is the conventional radiocarbon age before present (BP)

** Per cent modern means absolute per cent modern relative to the NBS I oxalic acid standard, corrected for decay since 1950.

Age, $\Delta^{14}C$, $\delta^{14}C$ and absolute per cent modern are as defined by Stuiver and Polach, Radiocarbon 19:355-363 (1977)

The reported errors comprise statistical errors in sample and standard determinations, combined in quadrature with a system error component that is based on the analysis of an ongoing series of measurements on ANU sucrose secondary standard. For the present result the system error component is conservatively estimated as .6% (= ± 48 radiocarbon years).

Nuclear Sciences Group, Institute of Geological and Nuclear Sciences Ltd., PO Box 31-312, Lower Hutt, New Zealand
Fax +64 4 570 4657 Phone +64 4 570 4671

Institute of
Geological &
Nuclear Sciences
Limited

Rafter Radiocarbon Laboratory

Accelerator Mass Spectrometry Result

R 21934/3	**Job** 12632
Description	Mixed species planktic foram sample from a core
Sample ID	36-38 @ 20cm
Submitter	Campbell Nelson
	Department of Earth Sciences

Radiocarbon Laboratory Reference	NZA 8098
Date measured	20-Nov-97
$\delta^{13}C$	.4 ‰

* **Radiocarbon Age**	1639 ± 67 BP
$\delta^{14}C$	-146.3 ± 7 ‰
$\Delta^{14}C$	-189.2 ± 6.7 ‰
** **Per cent modern**	81.08 ± .67

Issued 22/11/97

* Reported age is the conventional radiocarbon age before present (BP)

** Per cent modern means absolute per cent modern relative to the NBS I oxalic acid standard, corrected for decay since 1950.

Age, $\Delta^{14}C$, $\delta^{14}C$ and absolute per cent modern are as defined by Stuiver and Polach, Radiocarbon 19:355-363 (1977)

The reported errors comprise statistical errors in sample and standard determinations, combined in quadrature with a system error component that is based on the analysis of an ongoing series of measurements on ANU sucrose secondary standard. For the present result the system error component is conservatively estimated as .6% (= ± 48 radiocarbon years).

Nuclear Sciences Group, Institute of Geological and Nuclear Sciences Ltd., PO Box 31-312, Lower Hutt, New Zealand
Fax +64 4 570 4657 Phone +64 4 570 4671